1-1-1989

A spectroscopic analysis of phase separation and deformation behavior of model polyurethanes/

Han Sup Lee
University of Massachusetts Amherst

A SPECTROSCOPIC ANALYSIS OF PHASE SEPARATION AND DEFORMATION BEHAVIOR OF MODEL POLYURETHANES

A Dissertation Presented

By

HAN SUP LEE

Submitted to the Graduate School of the
University of Massachusetts in partial fulfillment
of the requirements for the degree of

DOCTOR OF PHILOSOPHY

September 1989

Department of Polymer Science and Engineering

A SPECTROSCOPIC ANALYSIS OF PHASE SEPARATION AND DEFORMATION BEHAVIOR OF MODEL POLYURETHANES

A Dissertation Presented

by

HAN SUP LEE

Approved as to style and content by:

Shaw L. Hsu, Chairman of Committee

William J. MacKnight, Member

Howard D. Stidham, Member

Matthew A. Harthcock, Member

William J. MacKnight, Department Head
Polymer Science and Engineering

To my parents.

ACKNOWLEDGEMENTS

I wish to acknowledge the guidance and encouragement given to me by my advisor, Professor Shaw Ling Hsu, through the entire course of this research. It has been truly rewarding experience to have the opportunity to work with him. I would also like to thank the other members of my committee, Professor William J. MacKnight, Professor Howard D. Stidham and Dr. Matthew A. Harthcock for their helpful suggestions.

I want to thank many other people who made this endeavor more enjoyable by their help and friendship. In particular I would like to express my appreciation to Dave Waldman, Nick Reynolds, Cun Feng Fan and Dr. Steve Pollack for their assistance and, more importantly, for their many helpful discussion. The experimental assistance of Dr. D.S.Lee and many thoughtful discussion of Dr.K.J.Kim are also recognized.

Finally, the love, patience, support, sacrifice and understanding from my wife, Ji Eun and my two sons, Jay and Jeff, and the assistance, teaching me of the importance of hard work and the encouragement from my father and mother during all my life are acknowledged with much love and appreciation.

ABSTRACT

A SPECTROSCOPIC ANALYSIS OF PHASE SEPARATION AND DEFORMATION BEHAVIOR OF MODEL POLYURETHANES

SEPTEMBER 1989

HAN SUP LEE, B.S., SEOUL NATIONAL UNIVERSITY

M.S., NORTH CAROLINA STATE UNIVERSTY

Ph.D., UNIVERSITY OF MASSACHUSETTS

Directed by: Professor Shaw Ling Hsu

Model polyurethanes having monodisperse hard and soft segments have been characterized for phase separation, miscibility and molecular orientation behavior.

Phase separation kinetics has been observed to be strongly dependent upon temperature. The phase separation rate at temperatures between the soft segment T_g and the hard domain dissociation temperature exhibits a functional dependence that is quite similar to the well known "bell shaped" function pertaining to crystal growth theory. The extended soft segment conformation in the phase separated state appears to be an additional effect contributing to the slow high temperature phase separation rate.

Domain miscibility is shown to be significantly affected by the chemical nature of the hard and soft segments. Increased hard segment length not only increases the domain

dissociation temperature but also strongly hinders the domain mixing behavior even above the melting temperature. The polybutadiene based polyurethane, which does not have strong secondary interaction, i.e. hydrogen bonding, is shown to exist as a phase separated structure even well above the melting transition.

The miscibility behavior of the two polyurethanes having hard segments of different segmental length has been investigated with both infrared and thermal methods. The limited solubility of one of the hard segments in the other hard domain has been clearly observed in samples with various blend compositions. The melting temperature of domains containing mainly long hard segments is depressed by the small amount of the short hard segments dissolved. The melting temperature depression relationship obtained from Scott's equation describing the thermodynamic mixing behavior of two polymers has been utilized for the quantitative analysis. The transition temperature of the short hard segment domain is shown to be insensitive to the blend composition. It appears to indicate that the incorporation of the long hard segments in the domain of the short hard segments significantly increases the free energy of mixing.

Segmental orientation and domain deformation behavior has been studied at different temperatures. Even though the stress and orientation relaxation is observed to be extremely fast initially, qualitative correlation between two parameters has been observed. By applying the elastic

network theory to the heterogeneous phase system, it is found that the hard domain of polyurethane may not be approximated as rigid junction points as in cross-linked elastomers.

TABLE OF CONTENTS

	Page
ACKNOWLEDGEMENT	v
ABSTRACT	vi
LIST OF TABLES	xi
LIST OF FIGURES	xii
Chapter	
I. INTRODUCTION	1
Overview of Dissertation	1
Polyurethane As a Thermoplastic Elastomer	3
Chemistry and Morphology of Polyurethanes	4
Infrared Characterization of the Hydrogen Bond	7
Phase Separation Kinetics	10
Segmental Orientation Studies by Infrared Dichroism	12
References	14
II. SPECTROSCOPIC ANALYSIS OF PHASE SEPARATION BEHAVIOR	16
Introduction	16
Experimental	20
Results and Discussion	26
Spectroscopic Features Sensitive to Structural Changes	26
Spectral Observations	33
Discussion	45
Conclusion	48
References	50
III. PHASE SEPARATION KINETICS OF MODEL POLYURETHANES	52
Introduction	52
Theory of Phase Separation Kinetics	55
Nucleation and Growth	56
Spinodal Decomposition	59
Experimental	60
Infrared Spectroscopic Studies	61
Thermal Analysis	66
Results and Discussion	67
Spectroscopic Study of Phase Separation Kinetics	67

Phase Separation Mechanism. 91
Thermal Analysis of Phase Separation Kinetics 100
Conclusion. 110
References. 113

IV. A SPECTROSCOPIC STUDY ON THE DOMAIN MISCIBILITY OF THE VARIOUS POLYURETHANES. 115

Introduction. 115
Experimental. 117
Results and Discussion. 119
Conclusion. 136
References. 139

V. MISCIBILITY BEHAVIOR OF MODEL POLYURETHANES INCORPORATING DIFFERENT LENGTH OF HARD SEGMENTS . . 141

Introduction. 141
Experimental. 145
Results and Discussion. 148
SAXS Studies. 148
Infrared Spectroscopic Studies. 158
Differential Scanning Calorimetric Studies. 167
Conclusion. 185
References. 190

VI. INVESTIGATION OF THE MOLECULAR ORIENTATION BY THE METHOD OF INFRARED DICHROISM 192

Introduction. 192
Overview of the Orientation Theory. 194
Orientation Function Measurements by Infrared Dichroism. 194
Deformation Theory of Elastic Network . . . 197
Experimental. 201
Results and Discussion. 206
Orientation Behavior of Each Segment. . . . 206
Domain Change during Deformation. 217
Orientation and Stress Relaxation 228
Theoretical Dichroism for Morphology Characterization. 240
Conclusion. 249
References. 252

VII. RECOMMENDATIONS FOR FUTURE WORKS. 255

Phase Separation of Polyurethanes 255
Compatibility of the Hard Segments. 257
Molecular Orientation Behavior. 258

LIST OF TABLES

		Page
2.1	Elemental Analysis Results	23
5.1	Interdomain Spacings	157
5.2	Assignments for the Bands Shown in Figure 5.3. . .	159
5.3	Weight Fraction of Soft Segment and Hard (B2 and B4) Segments	170
5.4	Parameter Values Used for Equation 5.12.	183

LIST OF FIGURES

		Page
1.1	Four vibrational modes mostly affected by the hydrogen bond; -A-H and B- correspond to proton donor and acceptor, respectively.	9
2.1	Schematic representations of polyurethane structures at various temperatures; (a) ambient temperature phase separated morphology; (b) most disassociated structures at high temperature; (c) dispersed phase "trapped" at extremely low temperature	19
2.2	Schematic drawings of the model polyurethanes (n=2,4 corresponds to B2 and B4 polyurethanes respectively); (a) polymer; (b) hard-segment; (c) soft segment.	22
2.3	The variable temperature cell used for infrared experiments	25
2.4	Temperature cycles during experiment.	27
2.5	Infrared spectra obtained for the B2 polyurethanes; $2cm^{-1}$ resolution; 200 scans; ambient temperature. .	28
2.6	Infrared spectra obtained for the B2 polyurethane; $2cm^{-1}$ resolution; 200 scans; $-40^{o}C$.	29
2.7	Variation of the N-H stretching region during temperature cycle shown in Figure 2.4	36
2.8	Variation of the C=O stretching vibration during temperature cycle shown in Figure 2.4	41
3.1	Temperature dependence of the crystal growth rate	58
3.2	Schematic drawing for the isothermal temperature set-up using both hot and cold nitrogen gas	62
3.3	Temperature variations during (a) high temperature phase separation experiments (FTIR and DSC) (b) low temperature phase separation experiments (FTIR)	64

3.4 Changes observed as a function of low temperature isothermal phase separation time for the C=O stretching region of B2 polyurethane; Spectrum obtained at t=0 has low absorbance at 1700cm^{-1} and high absorbance at 1730cm^{-1} 70

3.5 Changes observed as a function of high temperature (65°C) isothermal phase separation time for the C=O stretching region of B2 polyurethane; Spectrum obtained at t=0 has low absorbance at 1700cm^{-1} and high absorbance at 1730cm^{-1} 74

3.6 The total integrated intensity of the C=O stretching bands around the 1700cm^{-1} region as a function of time during isothermal phase separation at 10°C (top) and 20°C (bottom) 76

3.7 Decrease of the 1730cm^{-1} (increase of 1700cm^{-1}) component as a function of time; $\phi(t)$ denotes the fractional degree of phase separation and is calculated as $\frac{I(t)-I(0)}{I(\infty)-I(0)}$ where I(0), I(t), I(∞) being intensity of 1730cm^{-1} component at phase separation time zero (just after quenching), t, infinity (extrapolated), respectively 79

3.8 Changes observed in the N-H stretching region of B2 polyurethanes as a function of isothermal phase separation time at low and high temperature; Spectrum obtained at t=0 has the lowest absorbance at 3330cm^{-1}. 82

3.9 Changes of the integrated N-H stretching band during isothermal phase separation at 25°C; The intensity change of the free C=O peak is included for comparison. 87

3.10 Phase separation rate of B2 polyurethane as a function of temperature; $t_{1/2}$ is the time for 50% phase separation. 89

3.11 Concentration modulation at time t due to the β_m component during spinodal decomposition 92

3.12 Integrated hard segment depletion (log Q) vs time t during spinodal decomposition 95

3.13 Avrami plot of the intensity observed for the decrease of the 1735cm^{-1} component as a function of time and temperature. The lines drawn are fitted to the data shown. 99

3.14 Schematic drawing of the growing hard segment domain associated with a nucleation and growth mechanism 101

3.15 DSC traces for two (B2 and B4) polyurethanes during isothermal (55°C) phase separation; t=0 corresponds to time just after quenching to phase separation temperature; Transient state after quenching is observed for both samples. 103

3.16 DSC traces for B2 polyurethanes during isothermal phase separation at different temperatures 107

3.17 Fractional phase separation, $\phi(t)$, as a function of isothermal (70°C) phase separation time; $\phi(t)$ is obtained as $\frac{I(t)-I(0)}{I(\infty)-I(0)}$ where I(t) is the absorbance of 1730 cm^{-1} component for the FTIR data and exothermic energy evolved up to time t for the DSC data. 109

4.1 Schematic drawings of the hard and soft segments of the butadiene based polyurethanes. 118

4.2 N-H stretching regions of four different samples at high and quenched states; (a) B2 (b) B4 quenched from 185°C (c) B4 quenched from 210°C (d) Polybutadiene and TDI based polyurethane; Dotted spectra are obtained at room temperature and used as reference 122

4.3 C=O stretching regions of Figure 4.2; Dotted spectra are obtained at room temperature and used as reference 127

4.4 N-H stretching regions during phase separation as a increasing function of temperature from a quenched state; Samples are same as Figure 4.2; Dotted spectra are obtained at room temperature and used as reference 130

4.5 N-H stretching frequency change during phase separation from the quenched state; Linear data points are obtained by slowly cooling the sample from the room temperature 133

5.1 Schematic drawing of the B2 and B4 polyurethanes denoting the hard segment length difference 146

5.2 Small angle x-ray scattering profiles for B2, B4, and 50/50 blend sample. 149

5.3 Small angle x-ray scattering profiles corrected for lamellar geometry 150

5.4 Infrared spectra of the polyurethanes obtained with $2cm^{-1}$ resolution, 200 scans, at room temperature 152

5.5 Infrared spectra between 1850 and $1400cm^{-1}$ at temperatures shown in the spectra 161

5.6 Absorbance ratio of the two C=O stretching peaks, i.e. $A(1702cm^{-1})/A(1730cm^{-1})$, of three samples as a function of temperature; Blend compositions are indicated in the figure; The top two samples are shifted vertically for clarity; The ratio values at ambient temperatures before shifting were approximately 1.55 for all three samples. 165

5.7 N-H stretching regions of the 50/50 (B2/B4) blend sample as a function of temperature 166

5.8 Intensity changes of two spectral regions of 99/1 (B2/B4) sample as a function of temperature (a) $1702cm^{-1}$ peak height (b) integrated area of N-H stretching peak 169

5.9 DSC thermograms of the samples with various blend compositions; Samples were annealed at (a) 60°C and 85°C. 173

5.10 Composition and transition temperatures diagram; Annealing temperatures are indicated with the legends; T(B2) and T(B4) in the legend indicate the transition temperatures of the corresponding domains 177

5.11 Melting temperature depression of the samples annealed at 60°C; Experimental data points are with the lower abscissa (blend composition) and the calculated lines are with the upper abscissa ("true" ϕ_1). 182

5.12 Schematic drawing of the internal phase structure of the B2/B4 blend; Two types of hard domains containing the different hard segments are shown; "A" denotes the short hard segments dissolved in the hard domains of the long hard segments. 187

6.1 Schematic representation of relationship between transition moment (**M**) and chain axis of perfectly ordered sample. 196

6.2 Schematic representation of relationship between transition moment (**M**), chain axis and stretching direction 198

6.3 Survey spectra of B4 polyurethanes with two polarizations at 300% strain; Spectra without strain are shown in dotted line; Thickness change due to stretching has been corrected; Stretching direction is vertical and polarizations of each peak are shown in the figure. 204

6.4 Carbonyl stretching region at different strain; Relative orientations of the polarizer to the stretching direction are indicated in the figure. . 209

6.5 Orientation function of two carbonyl peaks plotted as a function of full cycle of strain 211

6.6 Orientation function of integrated C-H stretching region plotted as a function of strain. 214

6.7 Orientation function of carbonyl peaks at three different temperatures plotted as a function of strain; (a) free peak (b) hydrogen bonded peak. . . 216

6.8 Carbonyl stretching region at different strain; Relative orientations of polarization directions to stretching direction are shown in the figure . . 219

6.9 Intensity ratio of bonded to free C=O peak, $A_T(b)/A_T(f)$, plotted as a function of strain; One sample has been annealed at 150°C for a day . . 221

6.10 Schematic representation of two possible modes of hydrogen bonding; (a) between hard segments (b) between hard and soft segment 224

6.11 Expanded scale spectra of N-H stretching region at 300% strain; Relative polarization directions to stretching direction are indicated on the spectra; Spectrum without strain is in dotted line; Intensity change due to strain has been corrected. 226

6.12 Band width of N-H stretching peak plotted as a function of strain. 227

6.13 Intensity ratio of bonded to free C=O peak, $A_T(b)/A_T(f)$, at three different temperatures plotted as a function of full cycle of strain; Squares obtained during increasing strain and crosses obtained during decreasing strain 230

6.14 Stress relaxation of the B4 polyurethane; Sample has been step strained for 100%. 233

6.15 Carbonyl stretching region before and after relaxation; Solid and dotted spectra are obtained with perpendicular and parallel polarization respectively. 235

6.16 Orientation function relaxation of two carbonyl peaks plotted as a function of relaxation time at (a) 25°C and (b) 0°C. 238

6.17 Survey spectrum of polybutadiene based polyurethane. 241

6.18 Dichroic ratio of two peaks plotted as a function of strain; Vinyl-1,2 and trans-1,4 are at 910cm^{-1} and 965cm^{-1} respectively 242

6.19 Ratio of Equation 6.14 plotted as a function of strain 244

6.20 Orientation function of two peaks plotted as a function of strain. 246

6.21 Dichroic ratio for vinyl-1,2 peak as a function estimated soft segment strain; Three lines obtained with Equation 6.12 are included; Numbers on each line are N values of Equation 6.12 248

CHAPTER I

INTRODUCTION

Overview of Dissertation

Polyurethanes have extremely complicated phase separated structures. The formation of such structure and the resultant properties depend on numerous factors such as nature of hard and soft segments, molecular weight and its distribution, synthetic methods, amount of each component, and morphology of the material. In order to clarify how each parameter affects the properties of polyurethanes, it is important to study well defined samples to eliminate some of the physical and chemical factors which may prevent a direct correlation of structural aspects to mechanical properties. The polydispersity effect on the material properties is very difficult to define. However, this problem is minimized by using model polyurethane samples carefully synthesized with monodisperse hard and soft segments in order to achieve well defined micro and macrostructures. With well defined samples used in most of the chapters of this work, it is expected that the role of each of the parameters on properties can be better assessed.

This dissertation is presented in seven chapters. After the general introduction in Chapter I, the second chapter concentrates on the spectroscopic characterization of the

phase separation behavior. The characteristic phase structure at various environments are studied through their effects on the infrared spectra.

In Chapter III, phase separation kinetics is described. Even though scattering methods are extensively used in many phase separation kinetic studies, the applicability of infrared spectroscopy to analyze the phase separation kinetics of the polyurethanes has been demonstrated. The spectroscopic method gives the information at the segmental level during the phase separation process which is not readily available with the scattering methods. A separate, independent analysis of the phase separation kinetics is carried out with the thermal method. Since the free energy of the phase separated structure is different from that of the phase mixed state, the isothermal phase separation is accompanied with the heat flow that can be detected by the thermal method. The data obtained by two methods have been compared.

In Chapter IV, the domain miscibility of the three different polyurethanes is studied. The mixing of the hard segment and soft segment at the elevated temperatures is found to be very dependent on the nature and specificity of the interaction between hard and soft segment. The dependence of the interurethane interaction on the hard segment length is also investigated. The miscibility of the hard segments with same chemical structure and with different segmental length is studied by the infrared spectroscopy and

thermal method in Chapter V. Since the commercial polyurethanes contain hard segments with broad segmental length distribution, the results in this chapter will be useful to understand the miscibility behavior between the hard segments with different length.

The segmental orientation studies are presented in Chapter VI. The orientation of the hard and soft segment during uniaxial deformation is determined by the infrared dichroism. From the relaxation experiment, the close correlation between stress and orientation relaxation is demonstrated. The effect of the temperature on the different domains is also investigated. By approximating the soft chains which are interconnected to each other through the hard domain as a crosslinked elastic network, the experimental dichroic data are evaluated with the theoretical prediction. The results are utilized for the evaluation of the domain morphology. The final chapter proposes work for future studies.

Polyurethane As a Thermoplastic Elastomer

Polyurethanes are segmented copolymers which consist of hard and soft segment units. Due to incompatibility between the two types of structural units, it is generally agreed that the polymers formed undergo microphase separation resulting in hard segment-rich hard domains, soft segment-rich soft matrix, and interphase between them. Since the

glass transition temperatures (T_g) of soft segments and hard segments are well below and higher than the usual service temperature, i.e. ambient temperature, respectively, polyurethanes are thermoplastic elastomers with wide range of mechanical properties depending on the ratio of the two structural components.

Before the polyurethanes were introduced, elastomers were made exclusively from rubber. Since the fluid state (melt or solution) is required for shaping polymers into objects, conventional rubbers which require crosslinking (vulcanization) to obtain acceptable properties present a number of processing difficulties. The hard domain of the polyurethane has been speculated as a junction point of the cross-linked rubber which prevents permanent deformation. Since polyurethanes are non-crosslinked, linear polymers which can be easily processed at high temperature, the desired structure can be obtained by cooling the high temperature shape to low temperature.

Chemistry and Morphology of Polyurethanes

Polyurethanes are segmented block copolymers with blocks of different character defined as "soft" and "hard" segments. Several different diisocyanates such as methylene bis(p-phenyl isocyanate) (MDI),[1,2] 2,4-, and 2,6-toluene diisocyanate (TDI)[3,4] are preferred as hard segments. A wide variety of prepolymers have been studied as soft segments. Some of the widely used prepolymers are polyesters,

polytetramethylene oxide (PTMO), and polypropylene oxide (PPO).[5,6] Diamine or dihydroxyl short chain hydrocarbons also have to be used as a chain extender.[7,8] By changing the stoichiometric ratio of the chain extender to the prepolymer, the average hard segment length can be controlled which in turn affects the physical properties of the polyurethane.

The phase separated structure of polyurethanes are due to incompatibility between the two components. It has been shown that there is a large difference in the solubility parameter between the two components.[9] Even though polyurethanes are known to be heterophase, the degree of phase separation is dependent on the various factors such as chemical structure of soft and hard segment, stoichiometric ratio,[10] molecular weights and molecular weight distribution of each component.[11-13]

The properties of polyurethanes are dependent not only on the chemical nature of the component but also on the synthetic procedures.[14] If all three components are allowed to react at the same time, it is called a "one step" process. During a "two step" process, the prepolymer is end-capped with diisocyanates and a chain extender is added to connect the end-capped prepolymer. It has been found that the properties of the resultant polymer is significantly dependent upon the synthetic methods. When the all hydrocarbon soft segment (polybutadiene, for example) are used, the polymerization is usually carried out in solution to ensure the homogeneous mixing of the reactants.[15,16]

Since the urethane formation reaction does not produce any by-product to remove, polymerization can be carried out during the structure forming process similar to reaction injection molding (RIM).[17,18] During RIM processing, all three components are injected into the mold and reacted at appropriate temperatures. This process can reduce production costs significantly.

The existence of a heterogeneous phase morphology in polyurethanes has been suggested based on the data from viscoelastic measurements.[19] For homogeneous polymer mixtures, the absolute value of the plateau modulus of the modulus-temperature plot does not change with temperature even through the glass transition temperature changes significantly by varying the amount of each component. For the polyurethanes initially investigated, the plateau modulus value was observed to change by varying the content of each component.

The individual domain structure is quite dependent on the specific polyurethane system. For polyurethanes having high hard segment content, the regular packing of the hard segment has been observed and characterized by wide angle x-ray scattering (WAXS) extensively.[20,21] The structure of the hard segment inside the hard domain has been shown to be mainly trans in conformation especially when stretched or annealed.[22,23] The spherulitic superstructure of hard segment has also been determined with TEM and light microscopy.[24,25] If 2,4 TDI is used, the hard domain does not show any

crystallinity due to the lack of symmetry in the molecule. Soft domains can also have a variety of morphologies depending on the nature of the molecules and molecular weight. Semicrystalline structure can be obtained by deforming the high molecular weight soft segment.[26]

Infrared Characterization of the Hydrogen Bond

Even though the formation of strong hydrogen bonds between hard segments is not a necessary condition for phase separated morphologies,[11,27] hard domains are generally believed to be stabilized by the hydrogen bonding. When polyesters or polyethers are used as soft segments, hydrogen bonding between hard segment and soft segment is also possible.[28,29]

A hydrogen bond is formed between a functional group A-H, the proton donor, and an atom or group of atoms B, proton acceptor, in the same molecule or a different molecule. In most cases, the proton is donated by a carboxyl, hydroxyl, amine or amide group. The usual electron contributing parts of the molecule are the oxygen in carbonyl, ether, hydroxyl groups and the nitrogen in amines.[30] In the case of polyurethanes, urethane functional groups have both proton donor (N-H group) and acceptor (carbonyl). Polyether and polyester soft segments can also be a proton acceptor.

Infrared spectroscopy has been extensively used to investigate the hydrogen bonding characteristics because many

vibrational modes are significantly perturbed by the formation of the hydrogen bond. The vibrational modes which are mostly affected by the hydrogen bond are shown in Figure 1.1.[30] In case of A-H stretching mode (Figure 1.1a), the frequency shift due to the hydrogen bonding is linearly related to the hydrogen bonding distance. The strength of the hydrogen bond can be, therefore, easily inferred from the frequency shift of the N-H stretching infrared band.

The N-H stretching band was shown to be shifted by ca. 100 - 1000cm^{-1} depending on the proton acceptor group of the polyurethane. The N-H stretching peak is appreciably broad due to the distribution of the hydrogen bond distance over all molecules. Since the intensity of N-H stretching band is also strongly dependent on the frequency shift, the overall absorbance can be a function of the extent of hydrogen bonding.[31]

For polyurethanes, the effect of hydrogen bonding on the infrared spectrum can be characterized from a few different bands. In addition to the N-H stretching and N-H bending modes (Figure 1.1a and b), the C=O stretching region has been extensively studied.[32,33] The carbonyl stretching region gives important information about the hydrogen bonding. Even though the frequency shift due to hydrogen bonding is not as large as that of the N-H stretching component, the small effect of hydrogen bonding on the overall absorbance makes quantitative analysis possible.[34]

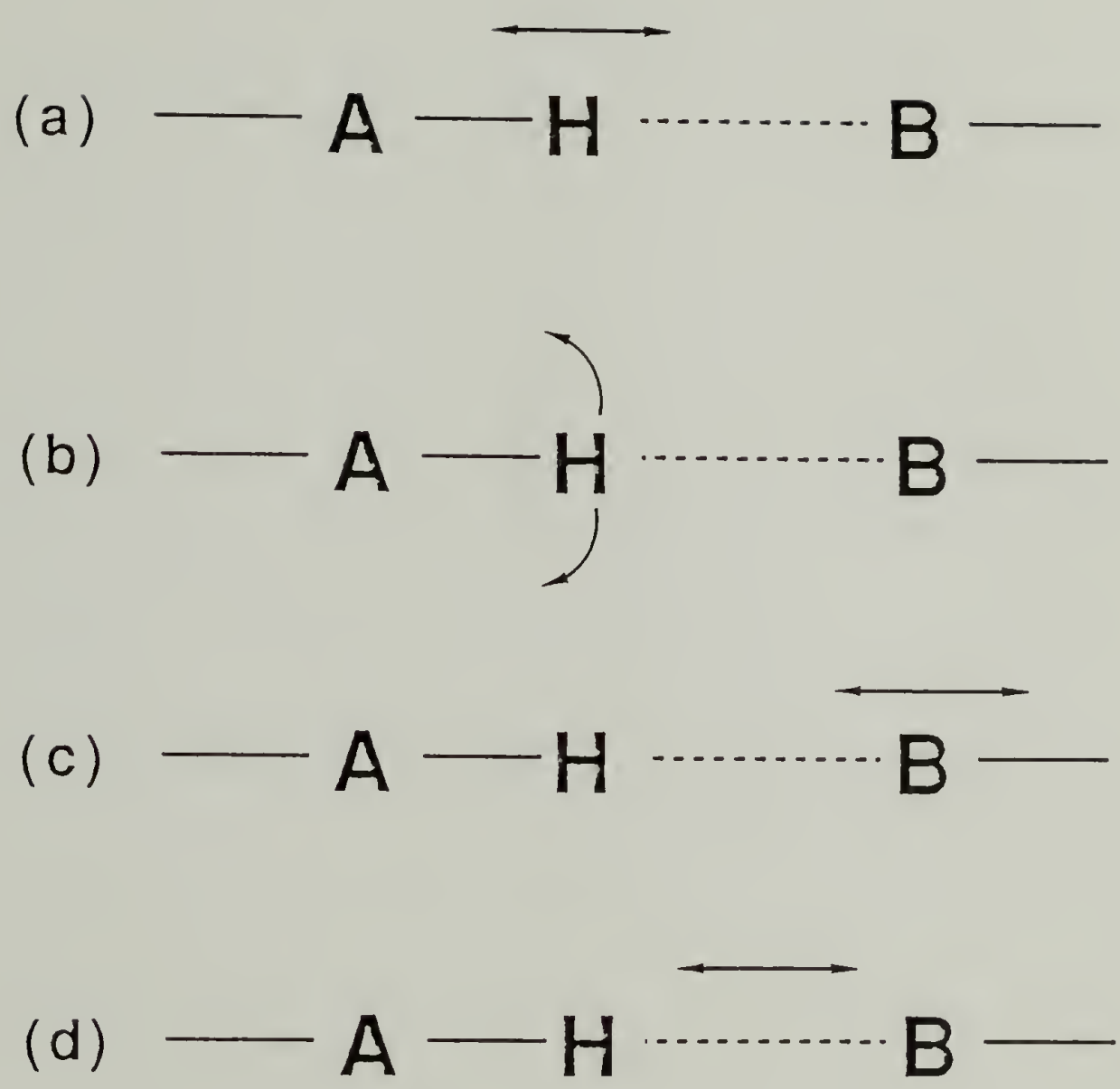

FIGURE 1.1 Four vibrational modes mostly affected by the hydrogen bond; -A-H and B- correspond to proton donor and acceptor, respectively.

The frequency of the N-H bending component is shifted to higher wavenumber upon hydrogen bonding in contrast with the two previous stretching components, which show a shift to lower frequency. The effect of hydrogen bonding on the spectrum can also be found on a few different spectral regions, but the analysis is not straightforward due to the coupling of the hydrogen bonded functional group with the backbone vibrations.

Phase Separation Kinetics

The heterogeneous phase separated structure of the polyurethane is not obtained instantaneously after the chemical reaction between the two segments. The reaction product approaches the equilibrium structure at a rate which depend on the phase separation kinetics. Since the mechanical properties are determined largely by the phase separated structure, the phase separation kinetics has to be understood to monitor the time variation of the material's properties.

Even though the phase separation kinetics of the polymeric blends has been investigated extensively, the experimental studies to characterize the microphase separation kinetics of the segmented polyurethanes are scarce and the theoretical development is far from complete. Phase separation kinetics has been traditionally investigated with scattering methods, of the appropriate wavelength of electromagnetic radiation, to probe the domain size. In the

case of segmented polyurethanes, the microphase separation kinetics has not been widely investigated because the average domain size is in the range of a hundred Angstroms which is not easily accessible by the traditional source of the electromagnetic radiation.

The phase separation kinetics of the polyurethanes has generally been studied indirectly. Since the glass transition temperature (T_g) of the soft matrix is dependent on the amount of the hard segment dissolved in it, the relative purity of the soft matrix can be assessed by measuring the T_g as a function of phase separation.[35] The mechanical properties can also be related to the degree of phase separation. The modulus of the material is found to change with the degree of phase separation.[36] Therefore, the observation of changes in the mechanical properties as a function of time gives information which can be related to the degree of phase separation. Most of the kinetic methods used have determined the properties of the sample of which the phase separation process has been frozen. The direct investigation of the phase separation kinetics can only be achieved when the experimental observation is made on the samples undergoing phase separation during measurement. The major focus of the kinetic study of this work will be on the direct application of Fourier transform infrared spectroscopy to the phase separation kinetic study. The differential scanning calorimetric method can also be used to follow the phase separation kinetics by monitoring the heat flow.

Segmental Orientation Studies by Infrared Dichroism

Infrared spectroscopy is a very useful technique to study the orientational behavior of the complicated polyurethane structure. The orientational response of the each segment of the chain can be investigated independently, in general, from the same set of experiments. When polyurethanes are strained macroscopically, the individual segment orients and deforms in a manner which is characteristic to the morphological state of the material. In order to understand the internal structure and also the relationship between structure and properties, the deformation behavior of the separate components must be characterized.

The deformation behavior of the soft segment has been found to be very different from that of the hard segment. Since the glass transition temperature of the soft matrix is well below ambient temperature, the soft segment shows fairly good elastic properties. It recovers to the initial state upon the removal of the applied stress, whereas the hard domain was found to undergo plastic deformation especially at high strain.[37] Therefore, the hard domain shows residual orientation when subjected to stresses higher than a certain critical stress level at which point plastic deformation of the hard domain starts to occur.

The initial strain is mostly developed on the soft segment due to its relatively low modulus. The stress is

then subsequently transferred to the hard segment at both ends of the soft segment while the soft segment relaxes. The strain transfer from the soft segment to the hard segment will be studied by the stress relaxation experiment in Chapter 6. The deformation behavior of the flexible soft chain, i.e. butadiene based polyurethane, will also be investigated by applying a theoretical prediction of the infrared dichroism to the experimental values.

References

1. Christenson,C.P.; Harthcock,M.A.; Meadows,M.D.; Spell,H.L.; Howard,W.L.; Creswick,M.W.; Guerra,R.E.; Turner,R.B. *J.Polym.Sci.-Phys.* **1986**,24,1401.

2. Koberstein,J.T.; Russell,T.P. *Macromolecules* **1986**, 19, 714.

3. Fu,B.; Feger,C.; MacKnight,W.J. *Polymer* **1985**, 26, 889.

4. Schneider,N.S.; Sung,C.S.P.; Matton,R.W.; Illinger,J.L. *Macromolecules* **1975**, 8, 62.

5. Pigott,K.A.; Frye,B.F.; Allen,K.R.; Steigiser,S.; Darr,W.C.; Saunders,J.H.; Hardy,E.E. *J.Chem.Eng.data* **1960**, 5, 391.

6. Bayer,O.; Mueller,E.; Petersen,S.; Piepenbrink,H.F.; Windemuth,E. *Rubber Chem.Tech.* **1950**, 23, 812 and *Angew.Chem.* **1950**, 62, 57.

7. Nakayama,K.; Ino,T.; Matsubara,I. *J.Macromol.Sci.* **1969**, A3, 1005.

8. Bonart,R.; Morbitzer,L.; Hentze,G. *J.Macromol.Sci.-Phys.* **1969**,B3,337.

9. Hwang,K.K.S.; Lin,S.B.; Tsay,S.Y.; Cooper,S.L. *Polymer* **1984**, 25, 947.

10. Abouzahr,S.; Wilkes,G.L.; Ophir,Z. *Polymer* **1982**,23,1077.

11. Harrell,L.L. *Macromolecules* **1969**,2,607.

12. Ng,H.N.; Allegrezza,A.E.; Seymour,R.W.; Cooper,S.L. *Polymer* **1973**, 14, 255.

13. Miller,J.A.; Lin,S.B.; Hwang,K.K.S.; Wu,K.S.; Gibson,P.E.; Cooper,S.L. *Macromolecules* **1985**, 18, 32.

14. Abouzahr,S.;Wilkes,G.L. *J.Appl.Polym.Sci.* **1984**,29,2695.

15. Bengston,B.; Feger,C.; MacKnight,W.J.; Schneider,N.S. *Polymer* **1985**, 26, 895.

16. Chen,C.H.Y.; Briber,R.M.; Thomas,E.L.; Xu,M.; MacKnight,W.J. *Polymer* **1983**, 24, 1333.

17. Fridman,I.D.; Thomas,E.L.; Lee,L.J.; Macosko,C.W. *Polymer* **1980**, 21, 393.

18. Camargo,R.E.; Macosko,C.W.; Tirrell,M.; Wellinghoff,S.T. *Polymer* **1985**, 26, 1145.

19. Cooper,S.L.; Tobolsky,A.V. *J.Appl.Polym.Sci.* **1966**, 10, 1837.

20. Bonart,R. *J.Macromol.Sci.* **1968**, B2, 115.

21. Blackwell,J.; Gardner,K.H. *Polymer* **1979**, 20, 13.

22. Born,L.; Crone,J.; Hespe,H.; Mueller,E.H.; Wolf,K.H. *J.Polym.Sci.-Phys.* **1984**, 22, 163.

23. Blackwell,J.; Nagarajan,M.R. *Polymer* **1981**, 22, 202.

24. Fridman,I.D.; Thomas,E.L. *Polymer* **1980**, 21, 388.

25. Koberstein,J.T.; Stein,R.S. *Polymer* **1984**, 25, 171.

26. Chau,K.W.; Geil,P.H. *Polym.Comm.* **1983**, 24, 50.

27. Allegrezza,A.E.Jr.; Seymour,R.W.; Ng,H.N.; Cooper,S.L. *Polymer* **1974**, 15, 433.

28. Yokoyama,T. "Adv. in Urethane Sci.Technol." **1975**, 6, 1; Frisch,K.C., Reegen,S.L. Eds., Technomic Pub., USA.

29. Tanaka,T.; Yokoyama,T.; Yamaguchi,Y. *J.Polym.Sci.* **1968**, A6, 2137.

30. Pimentel,G.C.; McClellan,A.L. "The Hydrogen Bond" W.H.Freeman, San Francisco, **1960**.

31. Tsubomura,H. *J.Chem.Phys.* **1956**, 24, 927.

32. Sung,C.S.P.; Schneider,N.S. *Macromolecules* **1975**, 8, 68.

33. Coleman,M.M.; Lee,K.H.; Skrovanek,D.J.; Painter,P.C. *Macromolecules* **1986**, 19, 2149.

34. Seymour,R.W.; Estes,G.M.; Cooper,S.L. *Macromolecules* **1970**, 3, 579.

35. Chee,K.K.; Farris,R.J. *J.Appl.Polym.Sci.* **1984**, 29, 2529.

36. Wilkes,G.L.; Wildnauer,R. *J.Appl.Phys.* **1975**, 46, 4148.

37. Estes,G.M.; Seymour,R.W.; Cooper,S.L. *Macromolecules* **1971**, 4, 452.

CHAPTER II

SPECTROSCOPIC ANALYSIS OF PHASE SEPARATION BEHAVIOR

Introduction

It is generally accepted that the strength and high elasticity of polyurethanes are due to the hard domains stabilized by the hydrogen bonding between hard segments.[1] The perfection and degree of phase separation have been found to be important to the properties of polymers and are dependent on molar composition, synthesis procedure and thermal history.[2,3] Hydrogen bonding may form between the N-H and C=O groups in the hard domain. If a polyether is part of the polymer, then hydrogen bonding between the N-H group of the hard segment dispersed in the soft matrix and the C-O-C group of the soft segment has also been suggested.[4-7] Hydrogen bonding properties of urethane functional groups, therefore, have been extensively investigated, because of its importance. Spectroscopic techniques, mainly infrared, have complemented other characterization techniques to better understand the phase-separated structures of polyurethanes. Even though a considerable amount of information has been obtained, a direct interpretation of the spectroscopic data is difficult. Recently, these difficulties have been presented in literature.[8-11]

It is well known that polyurethane structures and properties change as a function of temperature and these changes have been followed by thermal analysis,[12-14] spectroscopy,[8,9,14-16] dynamic mechanical analysis,[1,18,19] wide angle x-ray diffraction[20,21] and small angle x-ray scattering.[22] Several processes have been suggested to occur concurrently as a function of temperature. These structural changes are: (1) weakening and disassociation of hydrogen bonding; (2) disordering of hard segment domains; (3) hard-soft segment mixing; and (4) thermal degradation, mainly occurring in urethane linkages.[23] Vibrational spectroscopy, specifically, the infrared technique, has demonstrated its particular usefulness in characterizing the hydrogen bonding characteristics in each domain. Some of the localized vibrations such as the N-H stretching vibration or the C=O stretching vibration are strongly perturbed by the formation of hydrogen bonds. Both the frequency shifts and intensity changes are characteristic of the specificity or magnitude of the hydrogen bonds formed. The intensity of each type of hydrogen bonded vibration, if properly assigned, can potentially yield the degree of phase separation in the polyurethanes being studied.

In this chapter, a direct correlation between changing hydrogen bonding characteristics in soft and hard domains and macroscopic phase transformation as a function of temperature will be presented. Schematic representations of phase separated morphology at three different temperatures are

given in Figure 2.1. Characteristic hydrogen bonded species are also included in each diagram. By increasing the temperature above the "melting" transition of the hard domain, a homogeneous structure (b) is obtained which is accompanied by the disassociation of most of the hard segment-hard segment hydrogen bonding. If it is rapidly cooled (quenched), the high temperature structure is "frozen" resulting in a significant number of interactions between the hard and soft segments as shown in Figure 2.1c. Quenching to a lower temperature is then a good way to retain the degree of phase mixing at the elevated temperature. If the quenched temperature is much lower than the glass transition temperature (T_g) of the soft segment, the slow rate of segmental separation at the low temperature (depending on the segmental diffusion rate at the temperature) will prevent reformation of hard segment-hard segment hydrogen bonding. This low temperature structure undergoes phase separation to become an ambient temperature structure when the temperature is raised. In this way, direct correlation between microscopic evidence for hydrogen bonding characteristics and macroscopic phase transformation in soft and hard domains can be obtained. The definition of a homogeneous phase at a high temperature is difficult to establish. The samples to be studied are quenched from a temperature 20°C above the first order transition temperature reported for the sample.[24] The quenched samples studied are optically clear. The

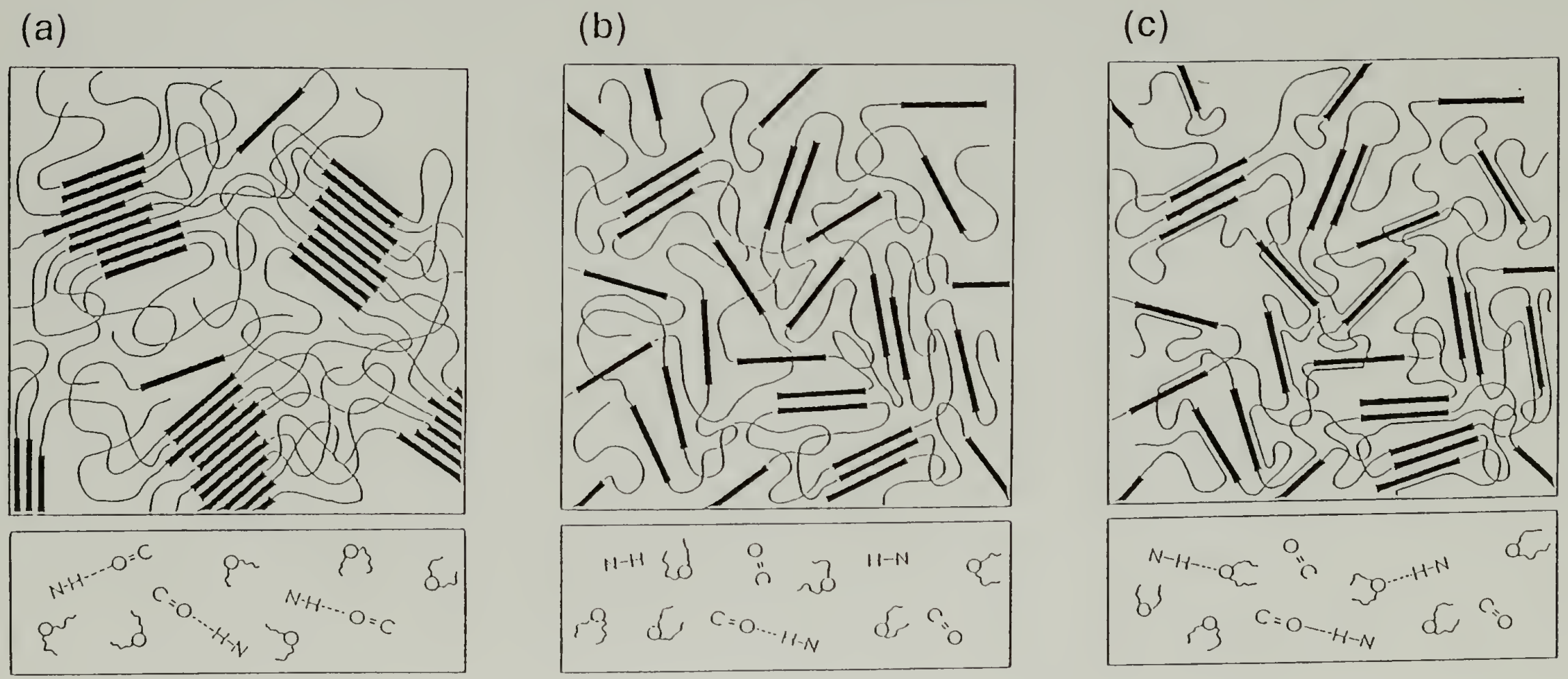

FIGURE 2.1 Schematic representations of polyurethane structures at various temperatures; (a) ambient temperature phase separated morphology; (b) most disassociated structures at high temperature; (c) dispersed phase "trapped" at extremely low temperature.

experimental results and the interpretation of phase separation in model polyurethane are reported here.

Experimental

The polyurethane samples used in this study have been described previously.[24] The distribution of the hard segment (methylene bis(phenyl isocyanate)(MDI) and butanediol (BD)) length is strictly monodisperse. The soft segment used is poly(propylene oxide) (PPO) (VORANOL™, molecular weight 2000). The preparation of the prepolymer and the monodisperse hard segments have also been described elsewhere.[24] In earlier studies, the polyurethane samples containing 3 or 5 MDI units (therefore 2 and 4 butanediol groups, respectively) have been designated as B2 or B4 polyurethanes and their chemical structures are shown schematically in Figure 2.2. The elemental analysis results for carbon, hydrogen, and nitrogen contents of the B2 and B4 materials are shown in Table 2.1. The close agreement between experimental and calculated values seems to support the well defined chemical structure of two materials. The results of the blend sample is also included for Chapter V.

The glass transition temperature for the soft segment is approximately -40°C. For the phase mixed system, the glass temperature depends on the degree of phase mixing and can be as high as 0°C. It is difficult to establish the glass transition temperature for the hard segment because of the

FIGURE 2.2 Schematic drawings of the model polyurethanes (n=2,4 corresponds to B2 and B4 polyurethanes respectively); (a) polymer; (b) hard-segment; (c) soft segment.

(A) 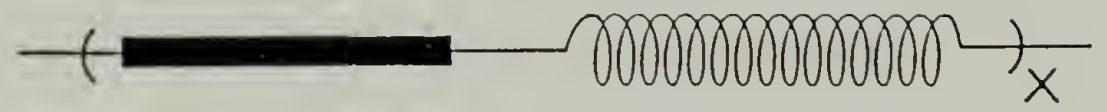

(B)  : —(MDI—BD)$_n$—MDI—

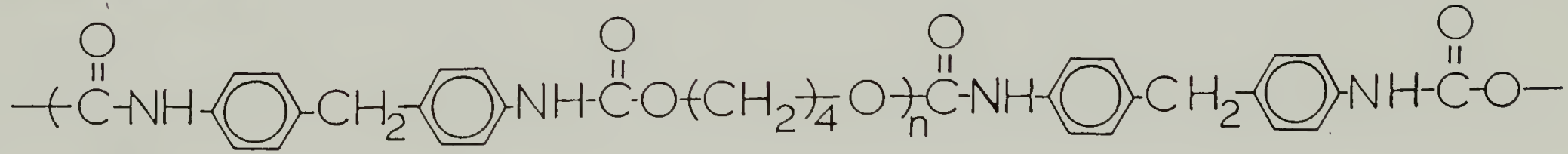

(C) 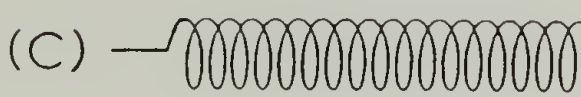 : —PPO—

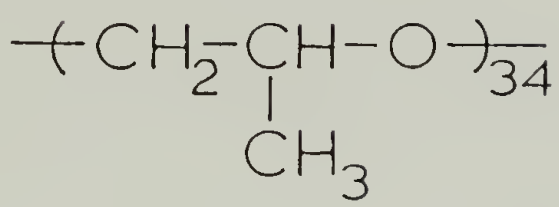

Table 2.1 Elemental Analysis Results

POLYMER	C	H	N	O
B2	63.10 (63.34)[a]	8.52 (8.74)	3.03 (2.83)	(25.09)
B4	63.90 (64.03)	8.18 (8.20)	3.95 (3.84)	(23.92)
B2+B4 (50/50 BLEND)	63.24 (63.69)	8.41 (8.47)	3.37 (3.34)	(24.51)

[a] : Calculated Values

small magnitude of heat capacity change. This value is in the range of 100°C.

This spectroscopic experiment was carried out on an IBM model 98 Fourier transform vacuum spectrometer. It was found that for this set of experiments involving a large temperature range, it was much easier to build a separate purge box in the sampling area to accommodate a specially designed infrared cell. The entire optical table is maintained under vacuum except for the sampling area. In this section, atmospheric absorptions were removed by dry nitrogen boiled off from liquid nitrogen. Since the major emphasis is to capture the temperature induced structural changes, a considerable effort was expended to design a sample cell with good temperature control which can be used over a large temperature range. This cell is shown schematically in Figure 2.3. With this cell, when connected to a proportional controller, a sample temperature from -100°C to 200°C can be comfortably reached. The temperature accuracy is within one degree of the set point.

For the quenching experiment, liquid nitrogen is blown directly from an opening on top of the cell, as well as, onto the sample held between two AgCl windows (Figure 2.3). The temperature of the sample is always measured with a copper-constantan thermocouple held between the windows in the infrared beam path. It took less than 20 seconds to cool the sample from 185°C to -70°C. The low temperature was maintained by blowing boiled off nitrogen gas from a separate

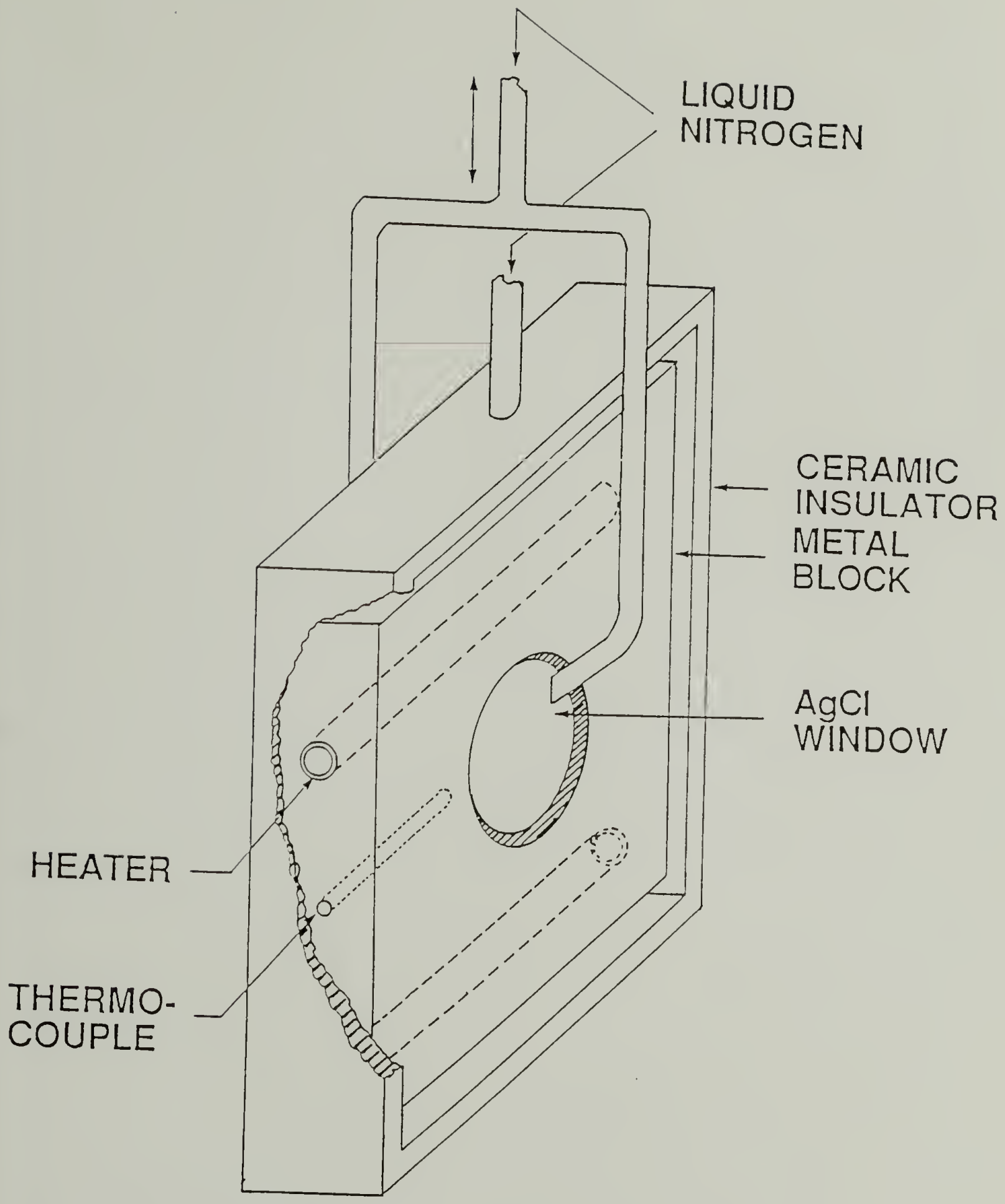

FIGURE 2.3 The variable temperature cell used for infrared experiments.

liquid nitrogen reservoir. No water condensation was observed at anytime during the experiment. The background spectra at each temperature was recorded and stored for later use. It was difficult to obtain a flat baseline at temperatures below -45°C. Since there was little or no change for the infrared spectra of polyurethanes below -45°C, this data was not used in our analysis. At each measurement temperature, the sample was equilibrated for 10 minutes before the spectra were obtained. The temperature cycle as a function of time is shown schematically in Figure 2.4. The infrared spectra obtained for the B2 model polyurethane at two temperatures are shown in Figures 2.5 and 2.6. The changes in the N-H stretching and C=O stretching vibrations as a function of temperature in the 3300 and 1700cm^{-1} regions are shown in Figures 2.7 and 2.8 respectively.

Results and Discussion

Spectroscopic Features Sensitive to Structural Changes

Infrared spectra of polyurethanes exhibit bands which are characteristic of localized chain conformation or packing. Most of the attention has been given to the characterization of the band intensity and shape of the localized vibrations associated with specific functional groups, i.e. N-H , -O- or C=O, which participate in specific hydrogen-bonding in and/or between the various domains. Most studies recognize this two phase system, i.e. hard domains

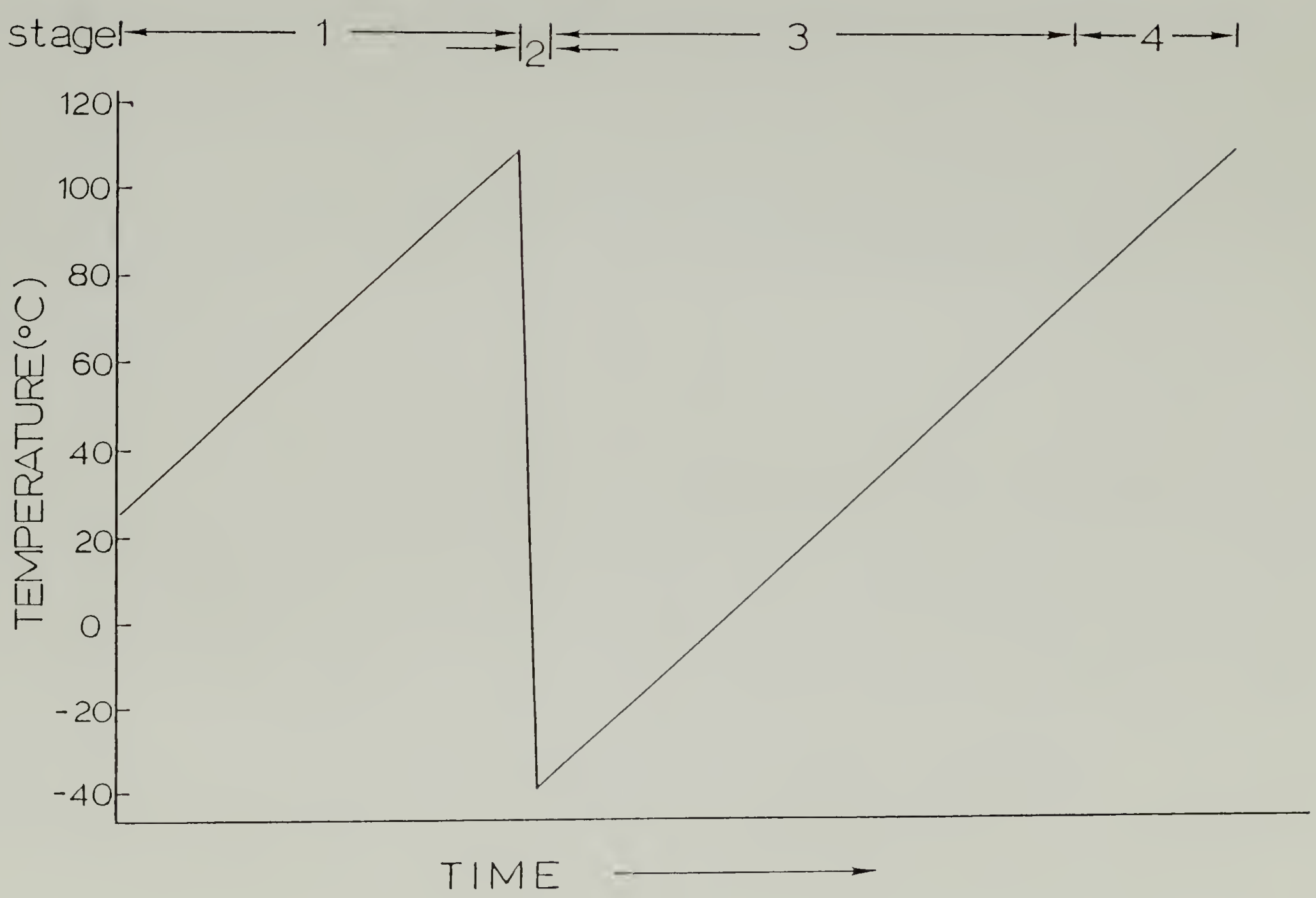

FIGURE 2.4 Temperature cycles during experiment.

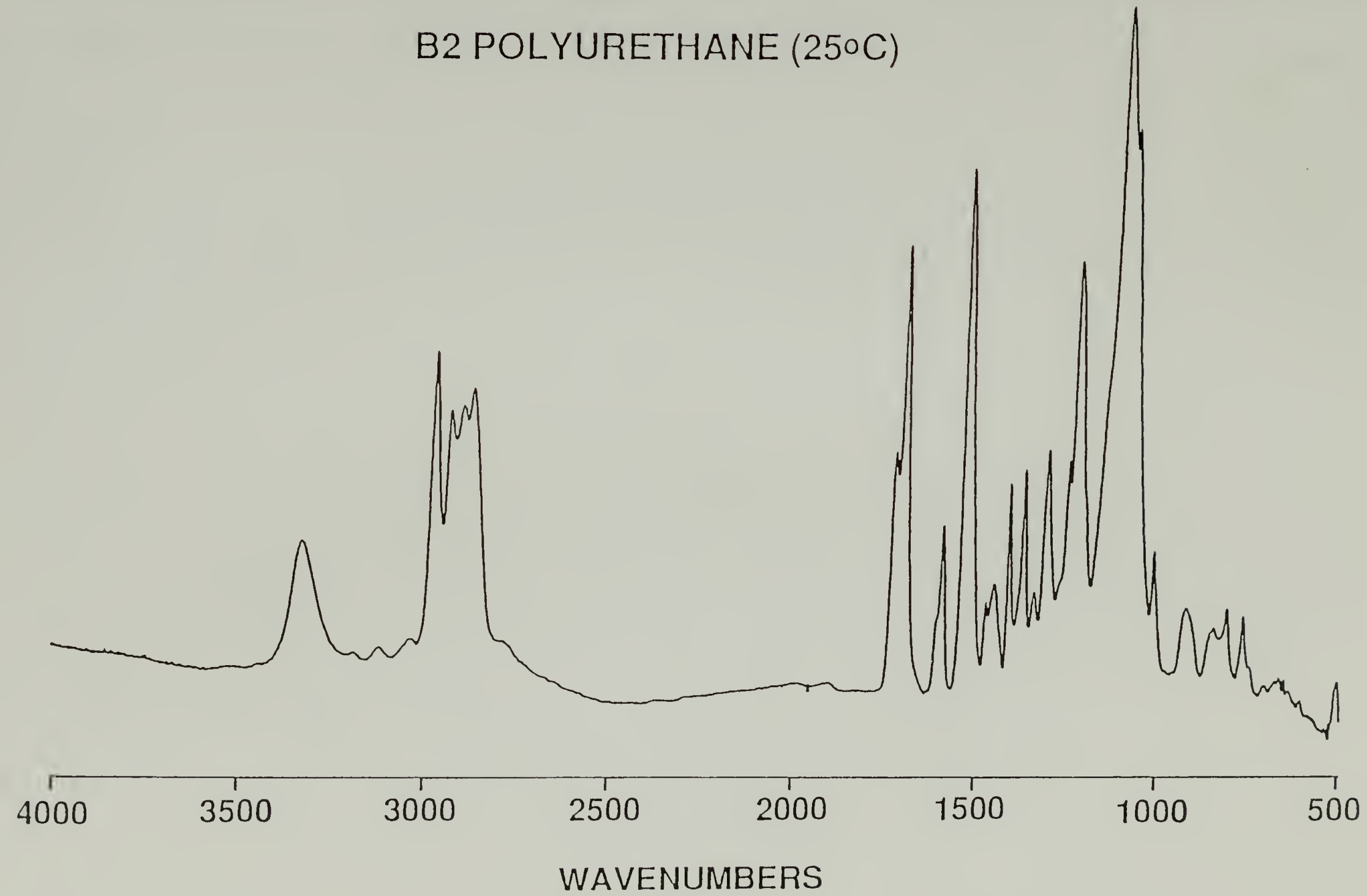

FIGURE 2.5 Infrared spectra obtained for the B2 polyurethane; 2cm^{-1} resolution; 200 scans; ambient temperature.

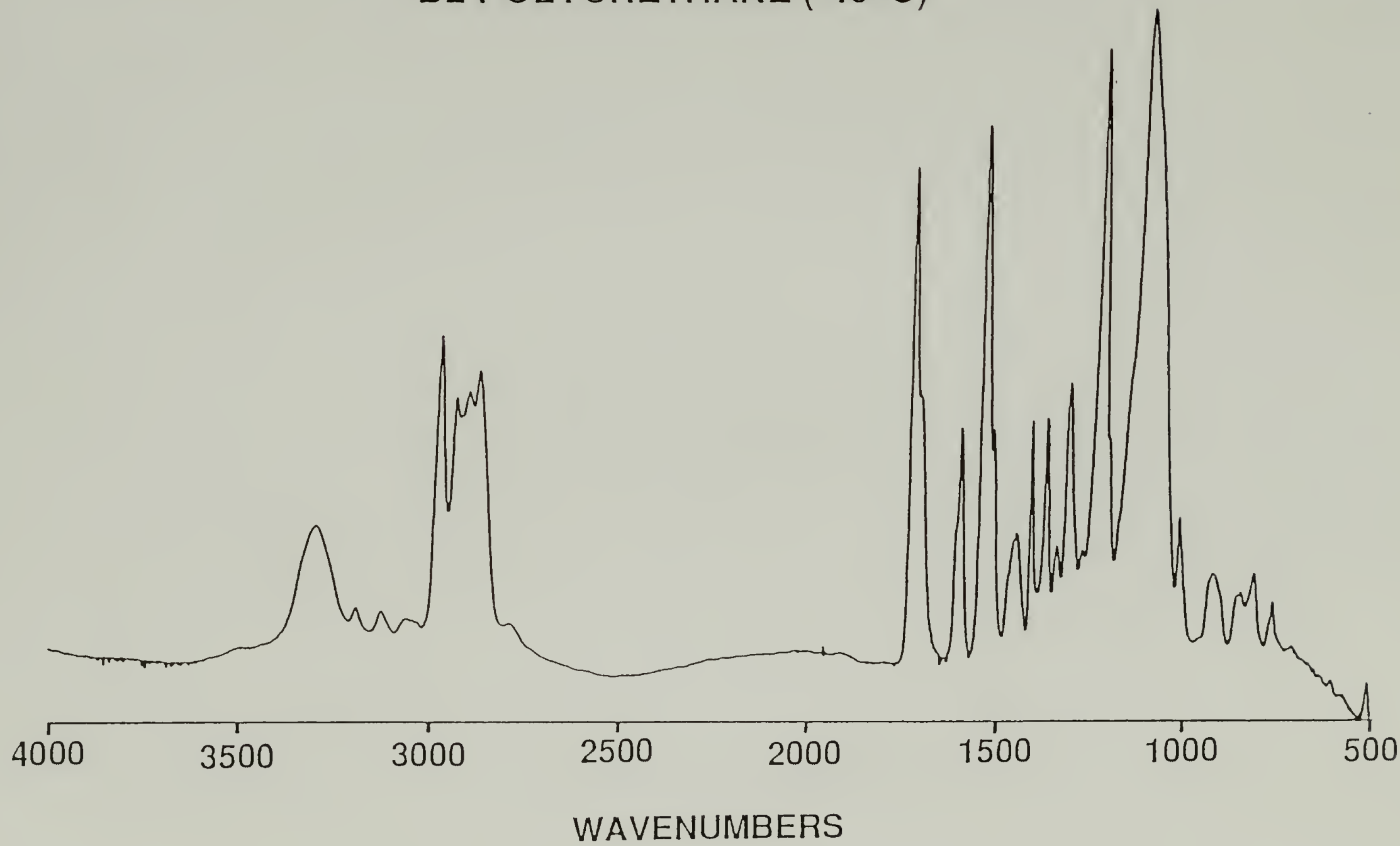

FIGURE 2.6 Infrared spectra obtained for B2 polyurethanes; 2cm^{-1} resolution; 200 scans; -40°C.

dispersed in soft segment matrix, which is too simplistic a picture. A morphological model incorporating highly ordered lamellar structure, amorphous regions (e.g. interphase), and regions of soft phase with a few hard segments dispersed within it should be considered.[22,25] It is well established that the position and intensity of these vibrations are extremely sensitive to the strength and specificity of the hydrogen bonds formed.[26] The phase separation in polyurethanes can be characterized by measuring the intensity and position of the hydrogen-bonded N-H stretching vibration.[8,9,14-16,24] If there is significant N-H ··· O=C hydrogen bonding, since both units are associated with the hard segments, it has usually been interpreted that extensive phase separation has occurred. It has also been suggested that N-H groups can form strong hydrogen bonds with the oxygen of the ether groups associated with the soft segments when available.[4-7] The observation of these hydrogen bonds suggests the existence of a dispersed phase consisting of hard segments mixed with soft segments. The converse of this statement, i.e. the existence of a dispersed phase does not necessarily mean there are well defined N-H ··· -O- hydrogen bonds. A significant number of studies have attempted to quantitatively assess the amount of hydrogen-bonded versus free species. Undoubtedly some of the difficulties in the interpretation of spectroscopic data are complicated by the two types of hydrogen bonds available and other second order spectroscopic effects involving the N-H stretching

fundamental and combinations of lower frequency Amide vibrations.[10,11]

The frequency shifts associated with both N-H and C=O vibrations when hydrogen bonds are formed can be understood intuitively. For the N-H stretching vibration, the formation of the hydrogen bonds alters the electronic distribution associated with the N-H bond.[27] For the C=O stretching vibration, there is the added contribution of transition dipole-dipole coupling.[28] Generally speaking, the N-H groups free from hydrogen-bonding have a stretching vibration at 3450cm-1. In contrast, the groups involved in hydrogen bonding have much lower frequencies, ranging from 3300 to as low as 3200cm-1. The exact position depends very much on the strength of the hydrogen bond formed.[29] This bond strength strongly depends on the local geometry,[30] such as the linearity of the bonds involved and the distance between the groups. The general approach is to treat the spectroscopic data as having two components, one free and one hydrogen-bonded, even though the frequency maxima for the hydrogen bonded component varies significantly as a function of composition or thermal history.[2]

Amide I vibration is usually referred to as a relatively localized normal vibration with the largest potential energy contribution from the C=O stretching internal coordinate. Similarly, since the C=O stretching vibration is sensitive to the specificity and magnitude of hydrogen bonding, it is plausible that the Amide I vibration actually consists of

several components associated with C=O groups in various environments. The Amide I as a function of temperature obtained for our samples is shown in Figure 2.8. Similar to the N-H stretching region, two clearly discernable components can also be found. The 1732cm^{-1} component is assignable to the carbonyls free of hydrogen bonding, and the lower frequency component, at approximately 1703cm^{-1}, is associated with hydrogen bonded carbonyls. The increase or decrease of the two components as a function of temperature reflects the changing hydrogen bonding properties in these phase separated polyurethanes. However, a number of studies have also found a third component.[8,31] Interpretation of this additional feature can be found elsewhere.[31]

One must accept that the hydrogen bonds formed are not uniform and a distribution must exist. The exact form of this distribution is dependent on various parameters such as chemical composition, sample preparation or temperature. Quantitative analysis of the amount of each is complicated by the fact that the absorptivity coefficient of the hydrogen bonded component is dependent on the strength of the hydrogen bonds formed.[9,29] However, the dipole moment change or band intensity need not be associated with the inductive effect, but rather dominated by the changing resonance structure.[27] Although the difference in the absorptivity coefficient for the Amide I band has not been observed to be significant,[8,27] the same cannot be said for the N-H stretching vibration. The ratio of the absorptivity coefficient, R, is described as

$$R = \frac{\varepsilon_b^{N-H}}{\varepsilon_f^{N-H}} \qquad (2.1)$$

where ε denotes the absorptivity coefficient, and b and f refer to the bonded and free components, respectively. The relative intensities of these two components can and have been used to determine the degree of phase separation in polyurethanes. However, recent studies have demonstrated that this simplistic analysis can be misleading.[8,9]

Spectral Observations

The room temperature spectra in the 3300 and 1700cm^{-1} regions of a B2 polymer are as expected. In each region dominant peaks are characteristic of hydrogen bonded components. The N-H groups free of hydrogen bonds cannot be seen easily. When the temperature is allowed to rise in stage 1 as shown in Figure 2.4, the hydrogen bonded component diminishes in intensity and shifts upward. This frequency shift reflects a change in hydrogen bond strength but does not imply that the hydrogen bonds have disassociated as Skrovanek et al. correctly pointed out.[9] At melting, the hydrogen bonded component diminished considerably in intensity as compared to the room temperature spectrum. In the carbonyl region the 1735cm^{-1} component is the dominant one. Because of the significant difference in the absorption coefficient, the N-H stretching at 3450cm^{-1} did not change as dramatically as the 3330cm^{-1} hydrogen bonded component.

Except for relatively minor band intensity and frequency changes, the infrared spectrum obtained by cooling the polyurethane sample directly from room temperature to low temperatures is quite similar to the spectrum obtained at room temperature. What is most interesting are the spectra obtained for the quenched B2 polyurethane. For simplicity, the N-H and C=O stretching regions will be described separately. For the quenched sample measured at low temperatures, in the N-H stretching region, the dominant peak is at 3295cm^{-1} with very weak shoulders at 3330cm^{-1} and 3260cm^{-1}. The N-H stretching vibration free from hydrogen bonding seems to be totally absent. When we slowly raised the temperature of the sample from -40°C to 50°C, the 3330cm^{-1} component changed continuously and gradually became dominant. When the sample was heated beyond 70°C in stage 4, this region changed as described in stage 1. The shifting of the N-H band for the quenched sample cannot be attributed to the different temperature dependence between N-H ··· O=C and N-H ··· -O- hydrogen bonding because the changing characteristics of the quenched sample are irreversible.

As can be seen in Figure 2.8, the carbonyl stretching region obtained for the quenched sample is totally unexpected. The dominant peak at the low temperature is the 1730cm^{-1}, representing free C=O stretching with the weaker component being the 1705cm^{-1} one. The relative intensity of the two components of this quenched sample again change significantly between -45°C to 50°C. The temperature induced

FIGURE 2.7 Variation of the N-H stretching region during temperature cycle shown in Figure 2.4.
(a) Stage 1
(b) Stage 2
(c) Stage 3
(d) Stage 4

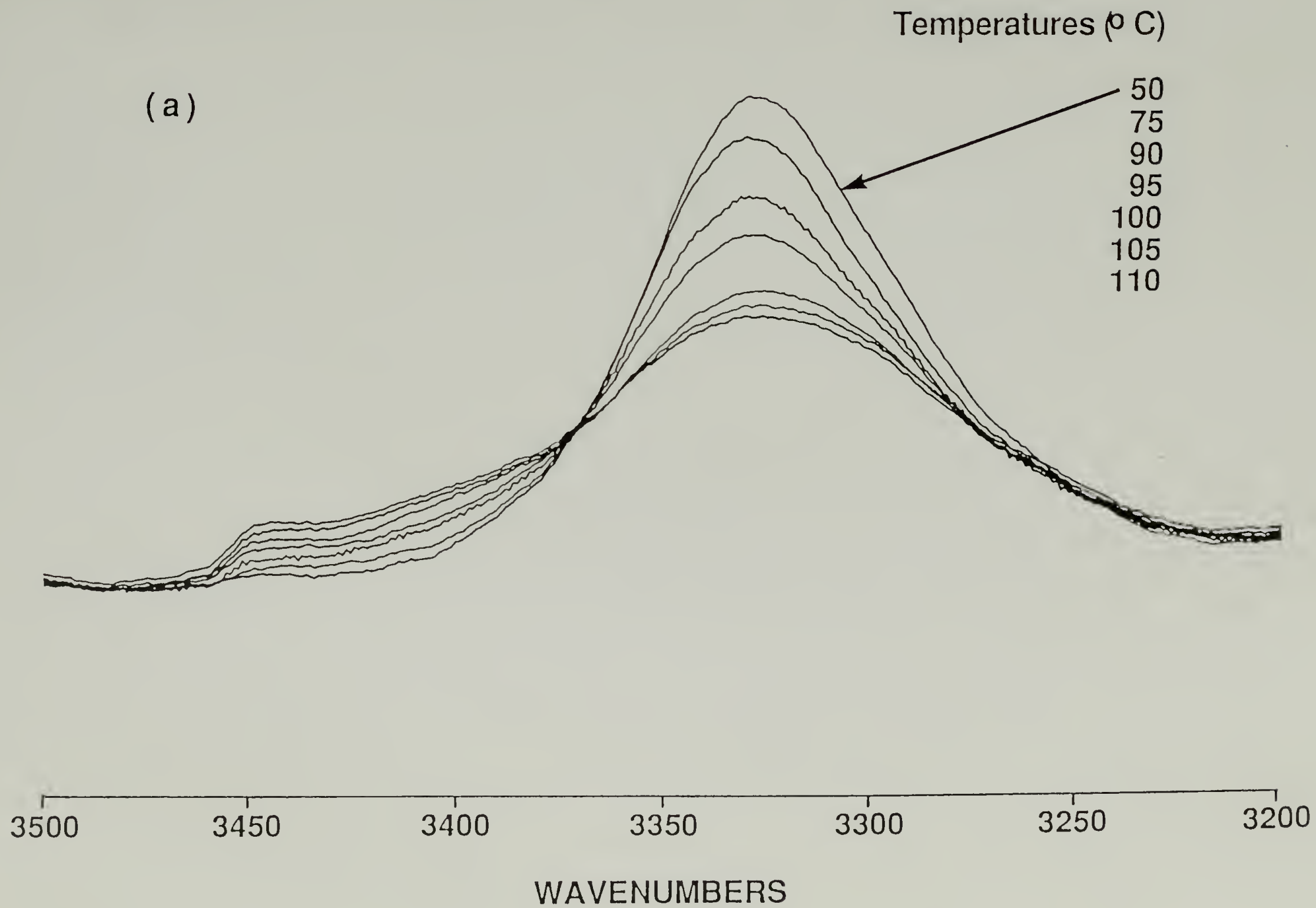
Temperatures (° C)
50
75
90
95
100
105
110
(a)
3500
3450
3400
3350
3300
3250
3200
WAVENUMBERS

(b)

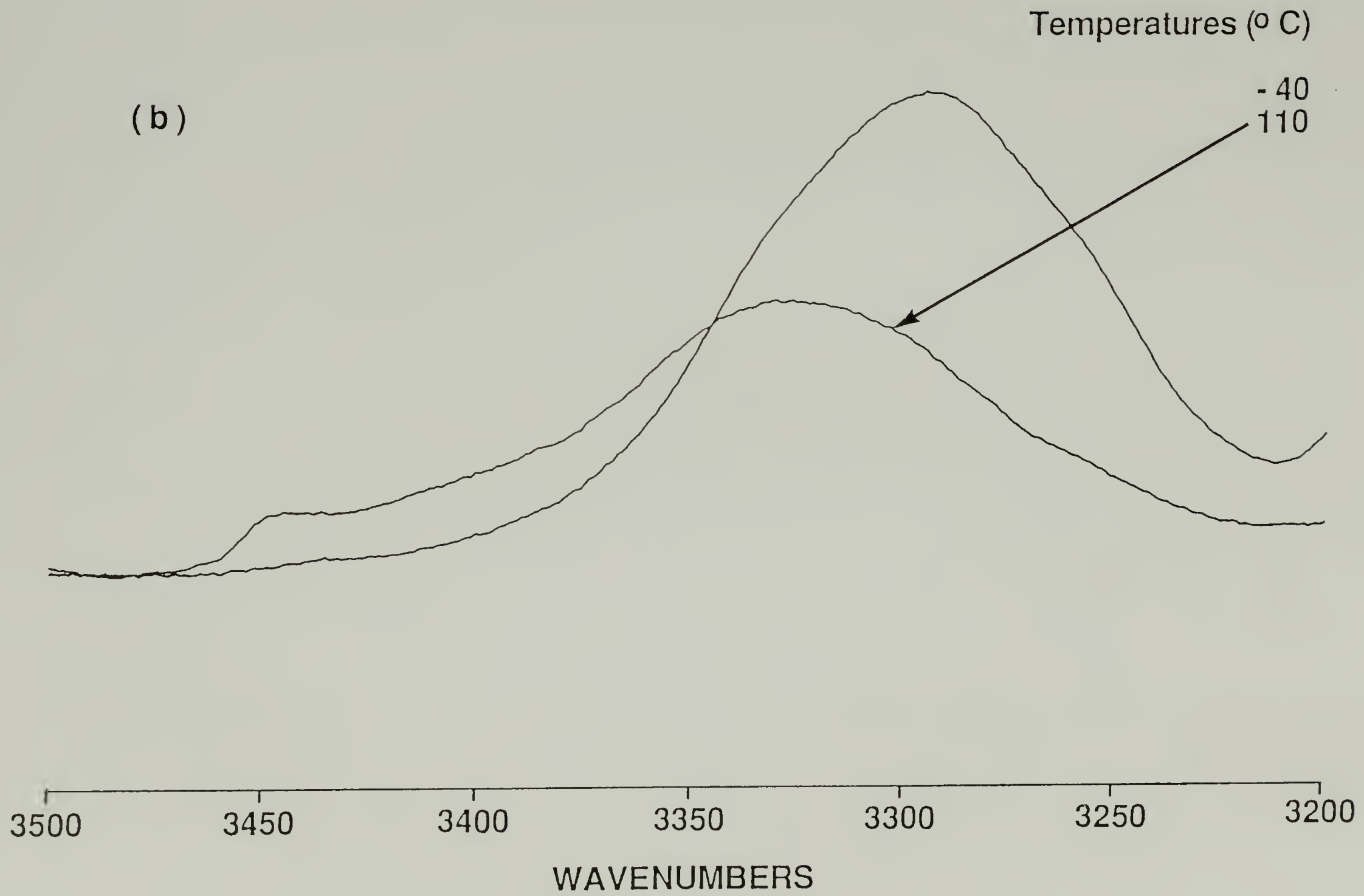
Temperatures (o C)
- 40
110
3500
3450
3400
3350
3300
3250
3200
WAVENUMBERS

(c)

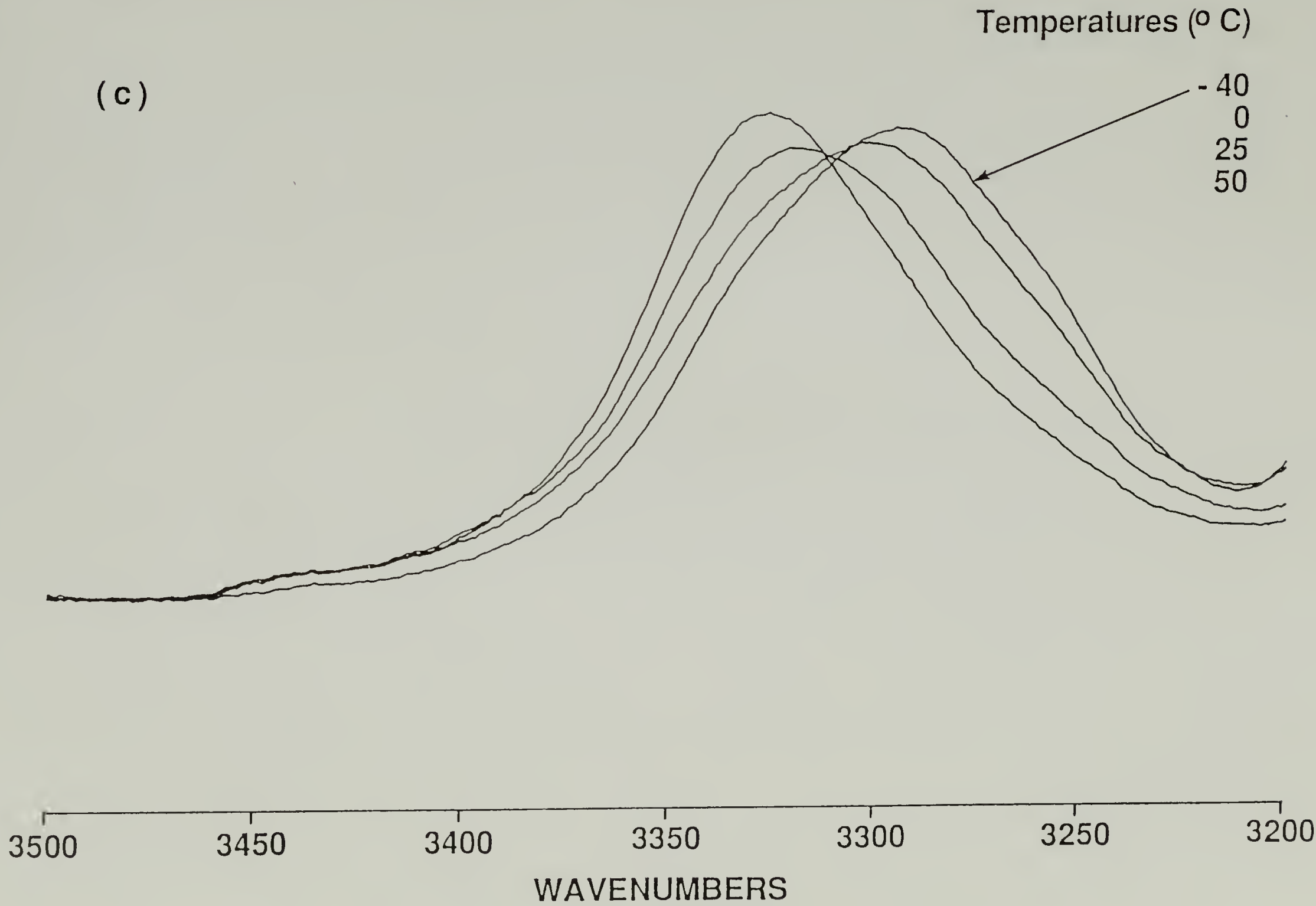
Temperatures (º C)
- 40
0
25
50
3500
3450
3400
3350
3300
3250
3200
WAVENUMBERS

(d)

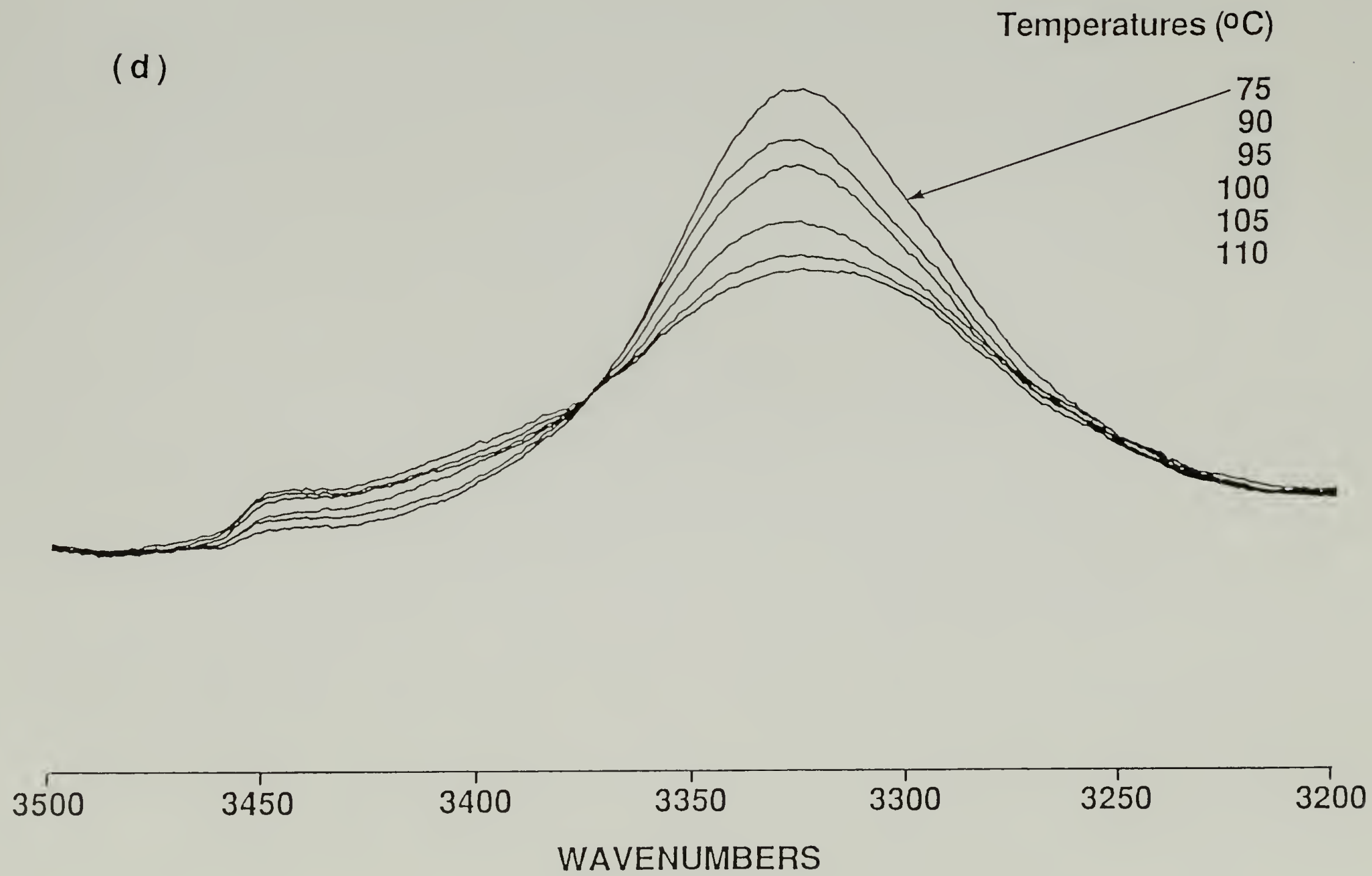
Temperatures (°C)
75
90
95
100
105
110
3500
3450
3400
3350
3300
3250
3200
WAVENUMBERS

FIGURE 2.8 Variation of the C=O stretching vibration during temperature cycle shown in Figure 2.4.
(a) Stage 1
(b) Stage 2
(c) Stage 3
(d) Stage 4

(a)

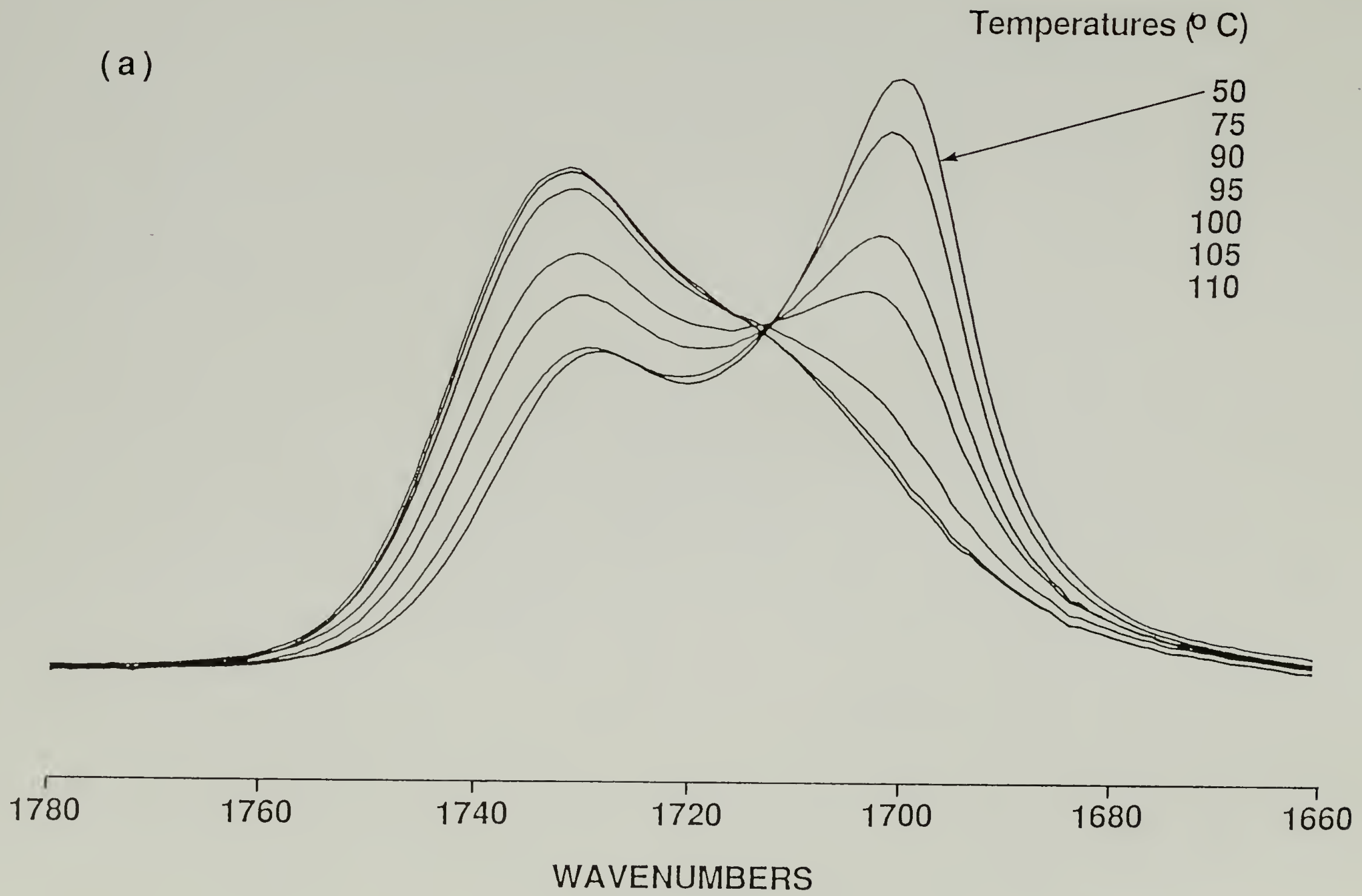
Temperatures (° C)
50
75
90
95
100
105
110
1780
1760
1740
1720
1700
1680
1660
WAVENUMBERS

(b)

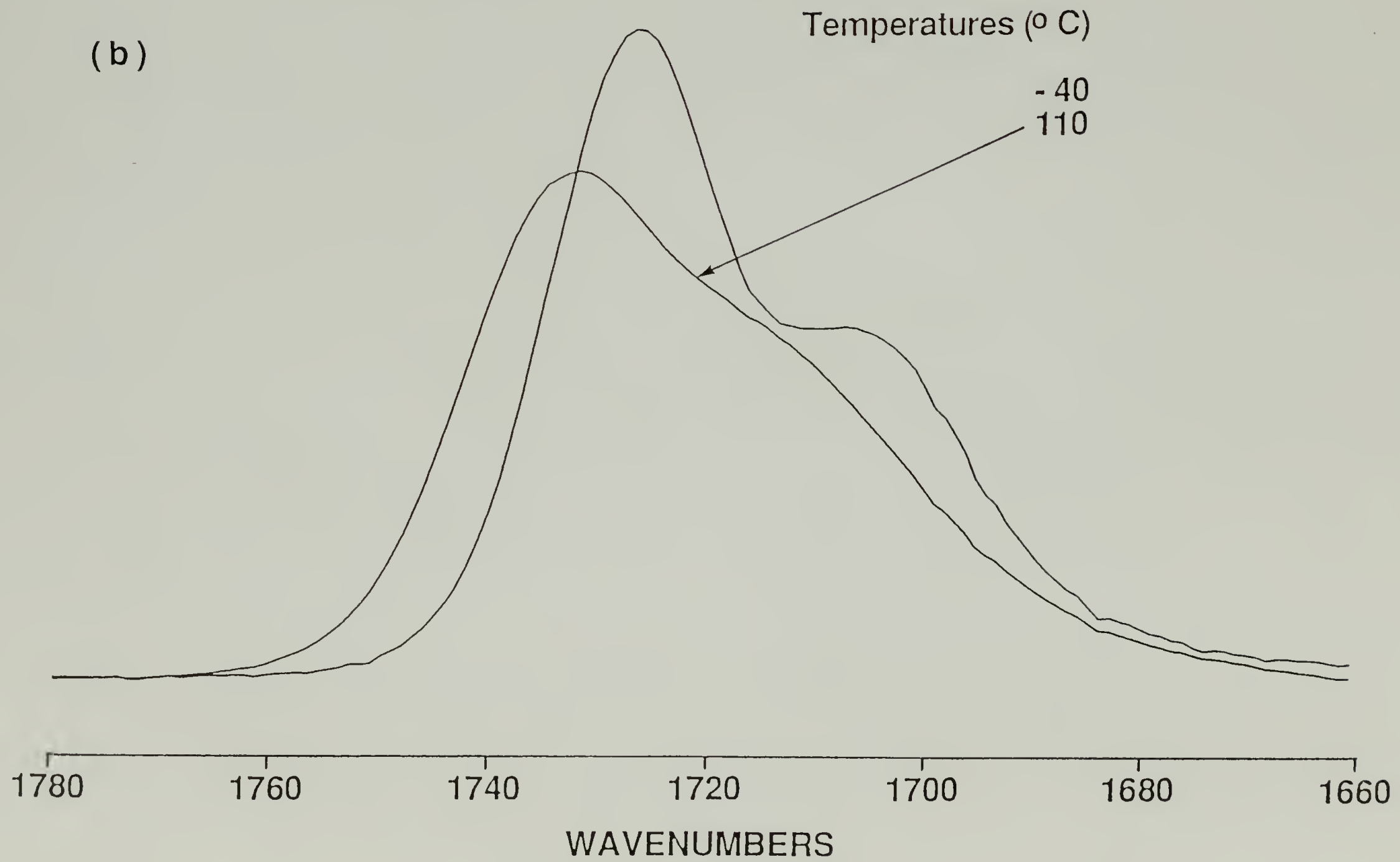
Temperatures (o C)
- 40
110
1780
1760
1740
1720
1700
1680
1660
WAVENUMBERS

(c)

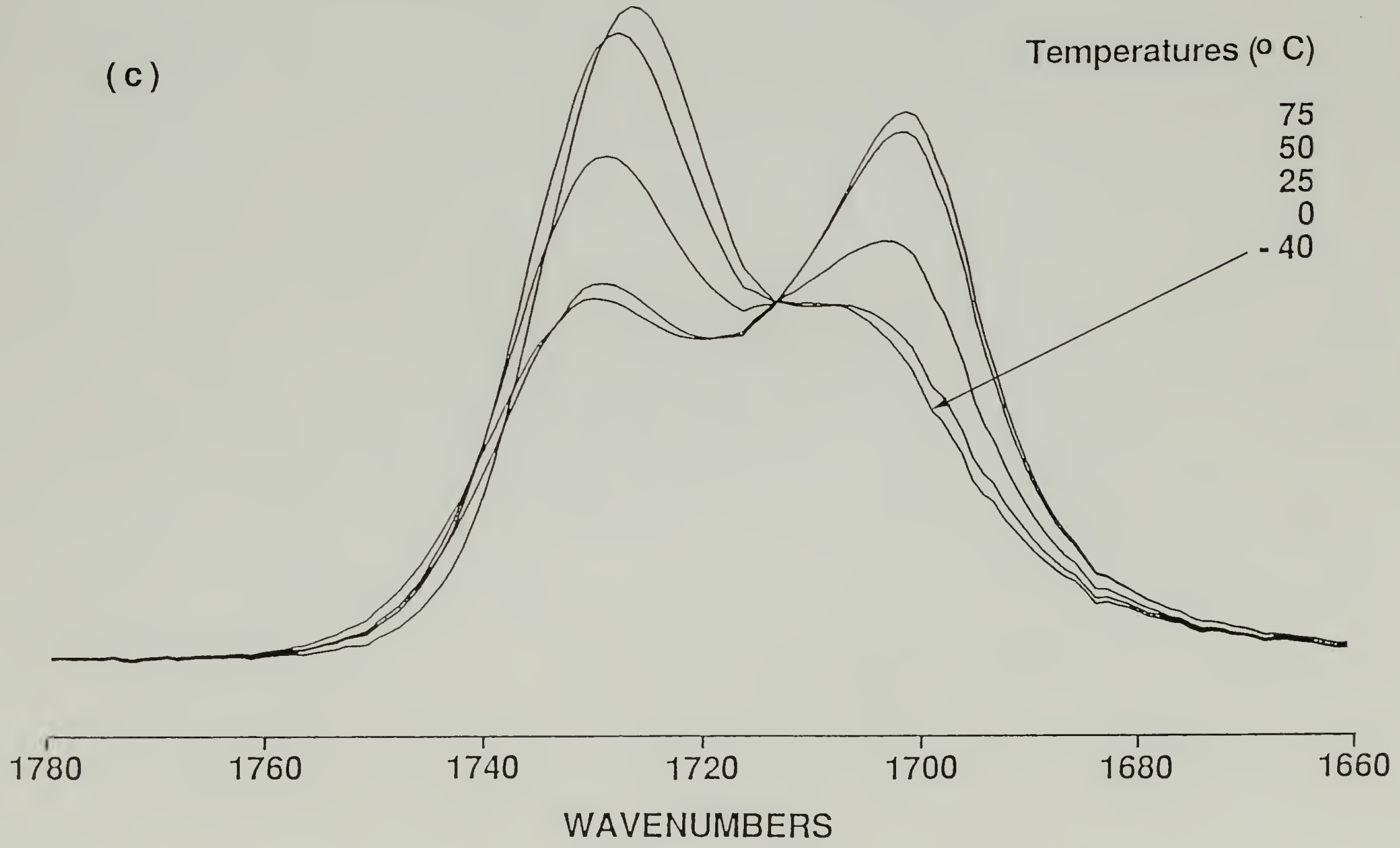
Temperatures (o C)
75
50
25
0
- 40
1780
1760
1740
1720
1700
1680
1660
WAVENUMBERS

(d)

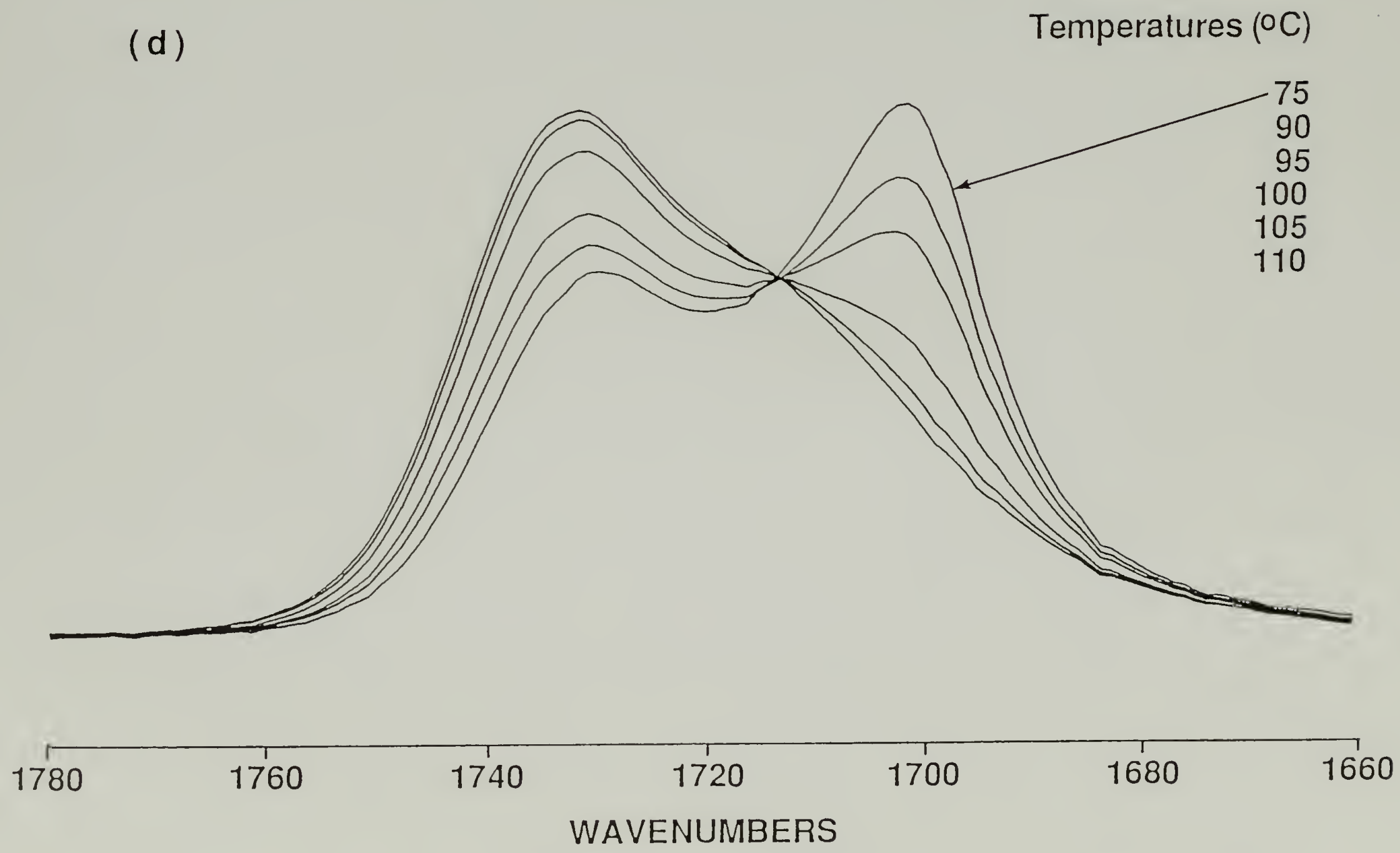
Temperatures (°C)
75
90
95
100
105
110
1780
1760
1740
1720
1700
1680
1660
WAVENUMBERS

changes in stage 4 are similar to what is observed in stage 1 for the N-H stretching vibration as well. As stated previously, the existence of a homogeneous phase is difficult to establish. The fact that the 1705cm^{-1} component is much weaker than the 1730cm^{-1} band also suggests that most C=O's are not bonded to N-H groups as expected for a dispersed phase.

Discussion

One of the most critical assignments in our analysis is the 3295cm^{-1} band. Our data suggests this component is to be associated with N-H bonded to the ether oxygen. The structure of the quenched sample reflects the phase mixed behavior of the melt and is preserved in the "frozen" state at -70°C, well below the glass transition temperature of the soft segments. We feel this "frozen" state is a well dispersed phase containing few isolated N-H groups. All the N-H groups participate in hydrogen-bonding either with the C=O or the -O- groups. This interpretation can be supported from basic concepts associated with the thermodynamics of these polyurethanes.

Previous studies have suggested that the glass transition temperatures of the soft and hard segments are approximately -40°C and 110°C respectively. In this experiment, the melt has been quenched with sufficient speed to trap the morphology of the melt state preventing phase separation to take place. There are approximately 34 ether

units per soft segment and 6 carbonyl units per hard segment. From stoichiometry, it is highly likely for ether oxygens to be around the N-H groups. The conformation around the soft segments allows a great deal of chain flexibility making it sterically favorable to form hydrogen bonding as well. The change in the rotational energy barrier is in the neighborhood of 1 Kcal/mole[32] and the gain for each hydrogen bond formed is approximately 5-10 Kcal/mole.[29] Thus, the disappearance of the free N-H band and the strong 3295cm^{-1} in the "frozen" sample can be explained. There are other explanations for the observed components in the 3200cm^{-1} region. The possibility that additional components arise from the Fermi resonance interaction between the N-H stretching fundamental and the combination of low frequency Amide vibrations does exist and some well defined vibrations have been observed in polypeptides.[10,11] However, these weak Fermi resonance components should not alter our interpretation. Christenson and his coworkers have argued for the assignment of an N-H ··· -O- band below the 3350cm^{-1} component and concluded the 3260cm^{-1} component is the appropriate one.[24] Their arguments based on steric considerations and model compound studies for the existence of such a component are rather persuasive. However, based on results in this chapter, the component at 3295cm^{-1} is more likely the correct assignment and the one at 3260cm^{-1} may be assignable to the second order effects associated with Fermi resonance interactions.[10,11] This assignment is consistent

with earlier analysis.[4] When the temperature is increased above -40°C, the soft segments gain sufficient mobility excluding hard segments for separation to occur disrupting the N-H ··· -O- hydrogen bonds. This process dominates in stage 3 in the schematic diagram shown in Figure 2.4.

The spectroscopic changes observed for the carbonyl stretching vibration are consistent with this interpretation. Initially as can be seen in Figure 2.8, the 1735cm^{-1} dominates in the quenched state, although the presence of the 1705cm^{-1} band can definitely be observed. There is an insufficient number of N-H groups for most of the C=O groups to be bonded to. When the temperature is raised, phase separation occurs and the hydrogen bonds between hard segments begin to form with other N-H groups. Finally beyond 70°C, these hydrogen bonds weaken but do not necessarily break, until the entire sample melts at 110°C. Therefore, transformation of N-H ··· -O- bonds in the phase mixed state into N-H ··· O=C bonds in the phase separated state is clearly supported by the spectroscopic changes observed in both the N-H or C=O stretching regions. It is to be noted that as the temperature increased, a clear indication of transformation of the phase-mixed state into the phase-separated state was observed.

In this analysis, one of the critical premises is that at temperature higher than hard domain dissociation temperature, phase mixing and/or incomplete domain structure of polyurethanes exists. This has been suggested by a number

of investigators. The DTA or DSC endotherm near 80°C has initially been interpreted to be the disassociation of hard segment-soft segment hydrogen bonds.[33] That transition has since been reinterpreted to be morphological in origin.[14] Wilkes noticed that the T_g of soft segments quenched to 20°C from a high temperature increased significantly.[34] Sung and her coworkers also measured the T_g of the soft segment as a function of the urethane hard segment concentration.[17] They found T_g values for the amorphous 2,4-TDI and polyester soft segment polyurethanes to be higher than expected.[17] In both cases, the increase in T_g values were explained as a result of increased hard segments dissolved in the soft segment matrix and result in hydrogen bonding of hard and soft segments, i.e., N-H ··· O=C when polyesters were used as soft segments.

Conclusion

Infrared spectroscopy has been widely used to study the micro-structure of polyurethanes. The changing distribution of hydrogen bonding properties in each domain can be assessed by this technique. In spite of its inherent selectivity for studying each functional group separately, there are some vague assumptions in the application of the spectroscopic data to better understand structural changes such as phase mixing or phase separation upon thermal treatment. This has

been mainly due to the lack of direct spectroscopic evidence, which is unique to each macroscopic phase structure.

In this study, new spectroscopic evidence identifying hard segment-hard segment hydrogen bonding (N-H ··· O=C) in hard domains and hard segment-soft segment hydrogen bonding (N-H ··· -O-) in phase-mixed states have been presented. These direct spectroscopic features have been sought but not found previously. If properly assigned, most of the spectroscopic data can then be correlated to the macroscopic structural transformation, mainly the degree of phase mixing or the separation kinetics. In this study, the qualitative structural pictures shown in Figure 2.1 are proven by the experimental evidence obtained.

It is now feasible to follow the phase-separation kinetics at the segmental level. The more detailed experimental work about the phase separation kinetics will be shown in the next chapter. If the thermodynamic arguments about equilibrium temperatures of hydrogen bonding between hard and soft segments given, are not grossly erroneous, then the results in this chapter suggest a new way of studying hydrogen bonding thermodynamics, i.e. establishing the equilibrium state at elevated temperatures followed by detailed characterization of the low temperature structures.

References

1. Cooper, S.L.; Tobolsky, A.V. *J.Appl.Polym.Sci.* **1966**, 10, 1837.

2. Lin, S.B.; Hwang, K.S.; Tsay, S.Y.; Cooper, S.L. *Colloid & Polymer Science* **1985**, 263, 128.

3. Abouzar, S.; Wilkes, G.L; *J.Appl.Polym.Sci.* **1984**, 29, 2695.

4. Yokoyama, T. "Adv. in Urethane Sci.Technol." **1975**, 6, 1; Frisch,K.C., Reegen,S.L. Eds., Technomic Pub., USA.

5. Tanaka, T.; Yokoyama, T., Yamaguchi, Y. *J.Polym.Sci.Part A* **1968**, 6, 2137.

6. Boyarchuk, Y.M.; Rappoport, L.Y.; Nikitin, V.N.; Apukhtina, N.P. *Polymer Sci. USSR* **1965**, 7, 859.

7. Paik Sung, C.S.; Schneider, N.S. *Macromolecules* **1975**, 8, 68.

8. Coleman, M.M.; Lee, K.H.; Skrovanek, D.J.; Painter, P.C. *Macromolecules* **1986**, 19, 2149.

9. Skrovanek, D.J.; Howe, S.E.; Painter, P.C.; Coleman, M.M. *Macromolelcules* **1985**, 18, 1676.

10. Moore, W.H.; Krimm, S. *Biopolymers* **1976**, 15, 2439.

11. Suzuki, S.; Iwashita, Y.; Shimanouchi, T.; Tsuboi, T. *Biopolymers* **1966**, 4, 337.

12. Leung, L.M.; Koberstein, J.T. *Macromolecules* **1986**, 19, 706.

13. Schneider, N.S.; Paik Sung, C.S.; Matton, R.W.; Illinger, J.L. *Macromolecules* **1975**, 8, 62.

14. Seymour, R.W.; Cooper, S.L. *Macromolecules* **1973**, 6, 48.

15. West, J.C.; Cooper, S.L. *J.Polym.Sci.-Polym. Symp.* **1977**, 60, 127.

16. MacKnight, W.J.; Yang, M. *J.Polym.Sci.Part C* **1973**, 42, 817.

17. Paik Sung, C.S.; Schneider, N.S. *Polymer Preprints* **1975**, 16, 589.

18. Camargo, R.E.; Macosko, C.W.; Tirrell, M.; Wellinghoff, S.T. *Polymer* **1985**, 26, 1145.

19. Brunette, C.M.; Hsu, S.L.; Rossman, M.; MacKnight, W.J.; Schneider, N.S. *Polym.Eng. & Sci.* **1981**, 21, 668.

20. Bonart, R.; Morbitzer, L; Hentze, G. *J.Macromol.Sci.-Phys.* **1969**, B3, 337.

21. Blackwell, J.; Lee, C.D.; "Adv. in Urethane Sci.Technol." Vol.9; Frisch,K.C., Klemper,D. Eds., **1984**, 25.

22. Koberstein, J.T.; Russell, T.P. *Macromolecules* **1986**, 19, 714.

23. Yang, W.P.; Macosko, C.W.; Wellinghoff, S.T. *Polymer* **1986**, 27, 1235.

24. Christenson, C.P.; Harthcock, M.A.; Meadows, M.D.; Spell, H.L.; Howard, W.L.; Creswick, M.W.; Guerra, R.E.; Turner, R.B. *J.Polym.Sci.-Phys.* **1986**, 24, 1401.

25. Koberstein, J.T.; Stein, R.S. *J.Polym.Sci-Phys.* **1983**, 21, 1439.

26. Pimentel, G.C.; McClellan, A.L. "The Hydrogen Bond" W.H.Freeman, San Francisco, **1960**.

27. Tsubomura, H. *J.Chem.Phys.* **1956**, 24, 927.

28. Krimm, S.; Abe, Y. *Proc.Nat.Acad.Sci.* **1972**, 69, 2788.

29. Pimentel, G.L.; Sederholm, C.H. *J.Chem.Phys.* **1956**, 24, 639.

30. Cheam, T.C.; Krimm, S. *J.Molecular Structure* **1986**, 146, 175.

31. Wang, Y.K.; Lee, H.S.; Hsu, S.L. Submitted to Macromolecules, and Harthcock, M.A. *Polymer* **1989**, in press.

32. Flory, P.J. "Statistical Mechanics of Chain Molecules" Interscience, New York, **1969**.

33. Clough, S.B.; Schneider, N.S. *J.Macromol.Sci.-Phys.* **1968**, 553.

34. Wilkes, G.L.; Bagrodia, S.; Humphries, W.; Wildnauer, R. *Polymer Preprints* **1975**, 16, 595.

CHAPTER III

PHASE SEPARATION KINETICS OF MODEL POLYURETHANES

Introduction

Segmented polyurethanes exist mainly as phase separated systems, because of their incompatible structural components. The degree of phase separation as reflected in the size and perfection of the domains is the most important criterion for the determination of overall sample mechanical properties.[1-3] Although phase separation kinetics of polymer mixtures have been active areas of study,[4-6] few investigations have been carried out to characterize the phase separation kinetics of polyurethane block copolymers.[2,7,8] Not only is the characterization of the phase separated structure present in segmented polyurethanes important from a practical standpoint, but also the mechanism associated with the phase separation is extremely interesting from a fundamental viewpoint as well. The connectivity between the components, the effects of chain stiffness, and the polydispersity of the hard or soft segments are all important parameters and need to be examined in greater detail in order to understand more fully the phase separation mechanism.

A few techniques have been applied to study the various aspects of phase separation kinetic behavior of

polyurethanes. For example, scattering technique, particularly small angle x-ray, can give the average size of the hard domains evolving from a homogeneous single phase.[2] By monitoring mechanical properties as a function of phase separation time, the phase separation kinetics can also be inferred.[9] It should be noted, however, that the direct relationship between the macroscopic mechanical properties and the degree of phase separation is generally hard to establish.

In the previous chapter, vibrational spectroscopy has been used as the principal technique to characterize the different hydrogen bonds formed and to infer phase separated structures in polyurethanes. Hydrogen bonding may form between the N-H and C=O groups of the hard segments. If a polyether is part of the polymer, then hydrogen bonding between the N-H group of the hard segment dispersed in the soft matrix and the C-O-C group of the soft segment is also possible.[10,11] Some of the localized vibrations such as the N-H stretching vibration or C=O stretching vibration are strongly perturbed by the formation of hydrogen bonds.[12] Both the frequency shifts and intensity changes are characteristics of the specificity or magnitude of the hydrogen bonds formed. The intensity of each type of hydrogen bonded vibration, if properly assigned, can potentially yield the degree of phase separation in the polyurethanes being studied, as reported in earlier studies.[13,14]

Thermal analysis, mainly DSC, with some degree of success, has been applied to characterize phase separation kinetics in polyurethanes or blends.[7,15] Since the glass transition temperature of the soft segments is affected by the presence of the hard segment in the soft domain, the purity of the soft domain, or the degree of phase separation, can be assessed by measuring the ΔT, defined as the temperature difference between T_g of the soft segment in the polyurethanes and T_g of the neat soft segment. More quantitative results were obtained by measuring the heat capacity change (ΔC_p) of the soft segment at the glass transition temperature.[8] The ratio of the ΔC_p of the polyurethane copolymer to the ΔC_p of the pure soft segments was correlated to the degree of phase separation. Therefore, the phase separation kinetics were studied by following the changes in this ratio as a function of time.

In this chapter, phase separation kinetics of model segmented polyurethanes have been studied by the Fourier transform infrared technique in conjunction with thermal analysis. Even though the infrared technique provides information regarding the microscopic environment around each segment (functional group) it is necessary to have macroscopic information to assess the overall structural changes such as the kinetics of the domain formation. Since the thermal method, which measures the heat flow during phase separation without affecting the kinetics, can be used to follow the phase separation process directly, such a study

has been carried out and the results will be correlated with the spectroscopic analysis.

The success in utilizing vibrational spectroscopy for the study of phase separation depends on the existence of bands sensitive to mixed and phase separated states, respectively. In a previous chapter, spectroscopic features, which are characteristic of urethane linkages dispersed in the soft segments as compared to interurethane hydrogen bonding confined to hard segment domains, have been observed and independent assignments have been made. With a specially designed sample cell, it was possible to trap a phase mixed structure at a temperature 60°C below the glass transition temperature of the soft segments. When this quenched sample was brought up to a higher temperature, the increase of one spectroscopic component and the corresponding decrease of the other, provided a direct measurement of phase separation kinetics.

Theory of Phase Separation Kinetics

Even though phase separation kinetics of polyurethanes have been studied by several workers, the complete phase diagram of the segmented block copolymer has not been obtained. Furthermore, it is not clear whether or not the conventional phase diagram can be applied to the phase behavior of the segmented polyurethane copolymers. Since the phase separation mechanism of the polyurethane is not known,

two possible mechanisms (nucleation and growth and spinodal decomposition mechanisms) have to be applied to determine the type of the phase separation mechanism.

Nucleation and Growth

According to the crystallization theory, the crystal growth rate, G, for a phase transformation in a condensed phase is given by

$$G = G_0 \exp\left(\frac{-\Delta F^{\ddagger}}{kT}\right) \exp\left(\frac{-\Delta \phi^{\ddagger}}{kT}\right) \tag{3.1}$$

where $\Delta\phi^{\ddagger}$ is the free energy required to build a nucleus of critical size, $\Delta F^{\ddagger}$ is the free energy barrier opposing transport of material across the interface and G_o is temperature independent coefficient.[16]

At a small degree of supercooling, the nucleation rate will increase very rapidly with decreasing temperature of crystallization. The transport term has an appreciable effect only at low temperatures where the local viscosity is shown to be inversely proportional to the temperature. Since the macroscopical viscosity and temperature have the relationship in Equation 3.2,

$$\eta = A \exp\left(\frac{E}{kT}\right) \tag{3.2}$$

where A is a constant and E is the activation energy, the transport term has a negative exponential relationship.[17]

By applying the WLF expression to the transport term and the classical nucleation theory to the second exponential term in Equation 3.1, the crystal growth is represented as

$$G = G_o \exp\left(\frac{-A}{R(T-T_o)}\right) \exp\left(-\frac{BTm}{T\Delta T}\right) \qquad (3.3)$$

where A is the activation energy associated with segmental motions, T_o a temperature below the glass transition temperature, $\Delta T = (T_m - T)$ the undercooling and B a constant defined as $4b_o\sigma\sigma_e/\Delta H_f$ in the case corresponding to a two dimensional crystal growth.[16] σ and σ_e refer, respectively, to the lateral and fold surface free energies of the polymer crystal and ΔH_f molar enthalpy of fusion. The qualitative functional dependence is calculated with T_g of 0°C and T_m of 97°C and its functional shape is shown in Figure 3.1. The maximum rate can be observed between the two extreme temperatures, i.e. T_g and T_m.

Overall crystallization kinetics have traditionally been treated in terms of the Avrami relationship.[18,19] The degree of phase transformation, X, is expressed as

$$X = 1 - \exp(-Zt^n) \qquad (3.4)$$

where Z is a rate constant related to the nucleation and growth rate. Equation 3.4 can be plotted by using standard conventions.

$$\ln[-\ln(1-X)] = \ln Z + n \ln t \qquad (3.5)$$

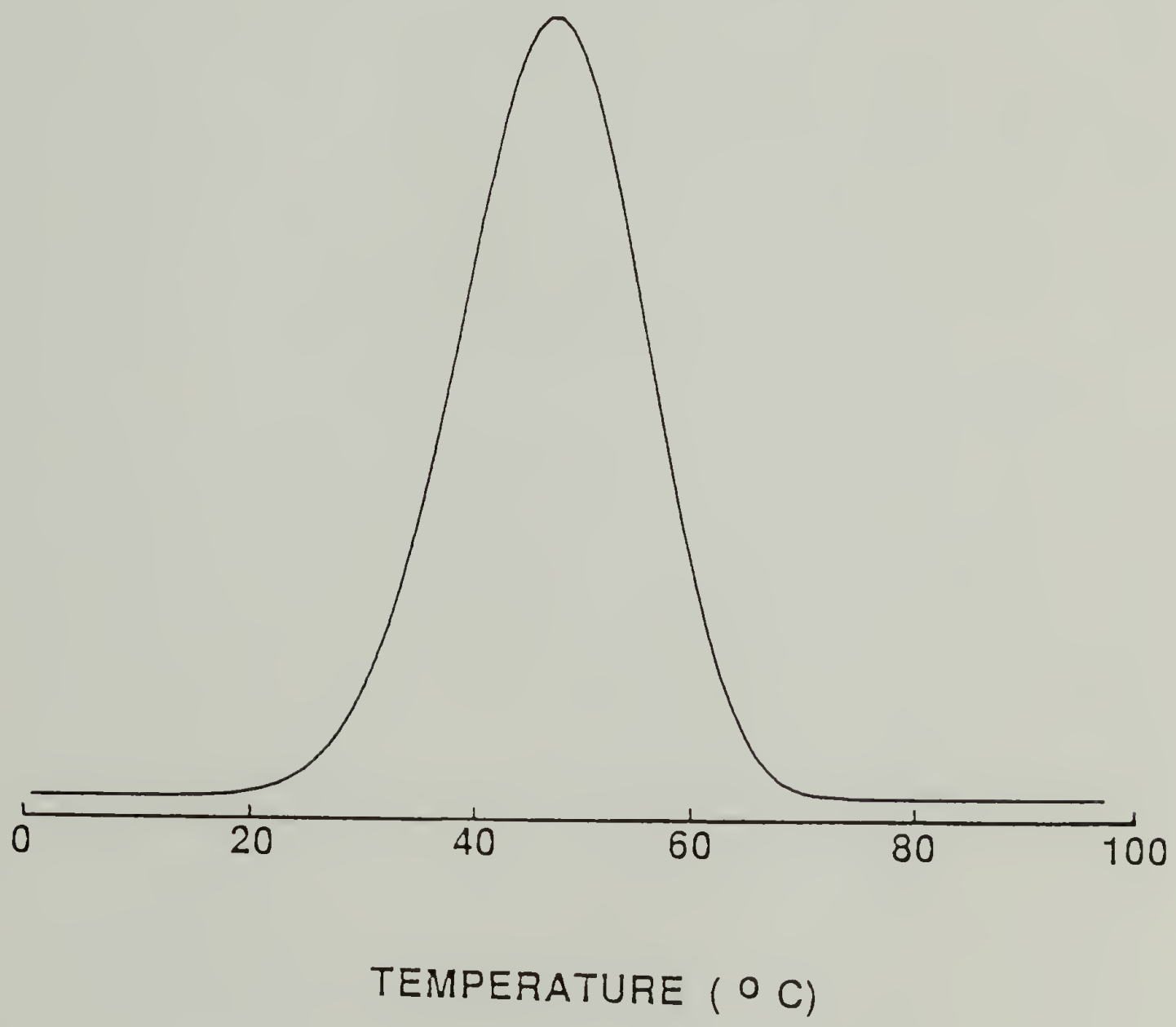

FIGURE 3.1 Temperature dependence of the crystal growth rate.

From the slope and intercept of the plot, ln[-ln(1-X)] vs ln t, the crystal morphology and the crystal growth rate constant can be calculated.

Spinodal Decomposition

The mathematical theory of spinodal decomposition consists of nothing more than deriving and solving a general diffusion equation. Diffusional flux, J, of two species is related to chemical potential difference ($\mu_A - \mu_B$) as in

$$- J = M \nabla(\mu_A - \mu_B) \tag{3.6}$$

where M is diffusion mobility. Chemical potential difference ($\mu_A - \mu_B$) is

$$\mu_A - \mu_B = \frac{\delta f}{\delta c_A} - 2K\nabla^2 c_A \tag{3.7}$$

where the first term is the free energy change due to concentration and the second term is due to the concentration gradient within the range of interaction of an atom and c_A is the concentration of the component A. The gradient energy coefficient, K, is the product of the interaction energy and square of the interaction distance. By substituting Equation 3.7 into Equation 3.6, it becomes

$$-J = M\frac{\delta^2 f}{\delta c^2} \nabla c - 2MK\nabla^3 c \tag{3.8}$$

From Fick's first law, taking divergence of Equation 3.8, the spinodal decomposition equation is obtained.[20]

$$\frac{\delta c}{\delta t} = M \frac{\delta^2 f}{\delta c^2} \nabla^2 c - 2MK\nabla^4 c + \text{nonlinear terms} \tag{3.9}$$

Equation 3.9 has a simple sine wave solution

$$c - c_0 = \exp[R(\beta)] \cos(\beta \cdot \mathbf{r}) \tag{3.10}$$

where the amplification factor $R(\beta)$ is given as

$$R(\beta) = -M\beta^2 \left(\frac{\delta^2 f}{\delta c^2} + 2K\beta^2 \right) \tag{3.11}$$

Equation 3.10 indicates that the scattering intensity of a certain wave vector β changes exponentially. From the $R(\beta)/\beta^2$ vs β^2 plot (refer to Equation 3.11), the diffusion coefficient D $\left(D = M\frac{\delta^2 f}{\delta c^2} \right)$ can be obtained from the intercept. A negative value of the diffusion constant is often used as definite evidence of the spinodal decomposition mechanism.[20]

Besides the definite scattering experimental data, characteristic morphological features are frequently used as an indication of the spinodal decomposition mechanism. Those important features are as follows;[5]

1. precipitated phases are interconnected with each other
2. the spacing observed in the scattering pattern is almost uniform
3. the phase domain grows at the later stage of phase separation.

Experimental

The model polyurethanes containing monodisperse hard and soft segments used in the previous chapter have been

characterized extensively. The sample used in this chapter contains three MDI units and two butanediol (B2) per hard segment. The chemical structure of the polymer is shown in Figure 2.2.

Infrared Spectroscopic Studies

One of the key points in this experiment is the ability to obtain a sampling temperature accurately and over a large range. A variable temperature cell used in this experiment was shown in Figure 2.3. The experimental set-up with both cold and hot nitrogen gas are shown in Figure 3.2. The cold N_2 gas was obtained by boiling the liquid nitrogen. The flow rate of the gas was controlled by the transformer connected to the heater and the flow meter as shown in the Figure 3.2. For the hot gas, the nitrogen gas was passed through the heating chamber that contains the heating wire inside. The final gas temperature can be controlled by changing the ratio of the flow rate of the hot to cold nitrogen gas.

The temperature profiles as a function of time used in this experiment are shown in Figure 3.3. For high temperature phase separation experiments (Figure 3.3a), a rapid lowering of the sample temperature after initial heating can be accomplished by blowing cold N_2 gas directly onto AgCl windows. When the isothermal phase-separation temperature was reached, a combination of cold and hot nitrogen gas was used to stabilize the sample temperature. For the quenching step during the low temperature phase

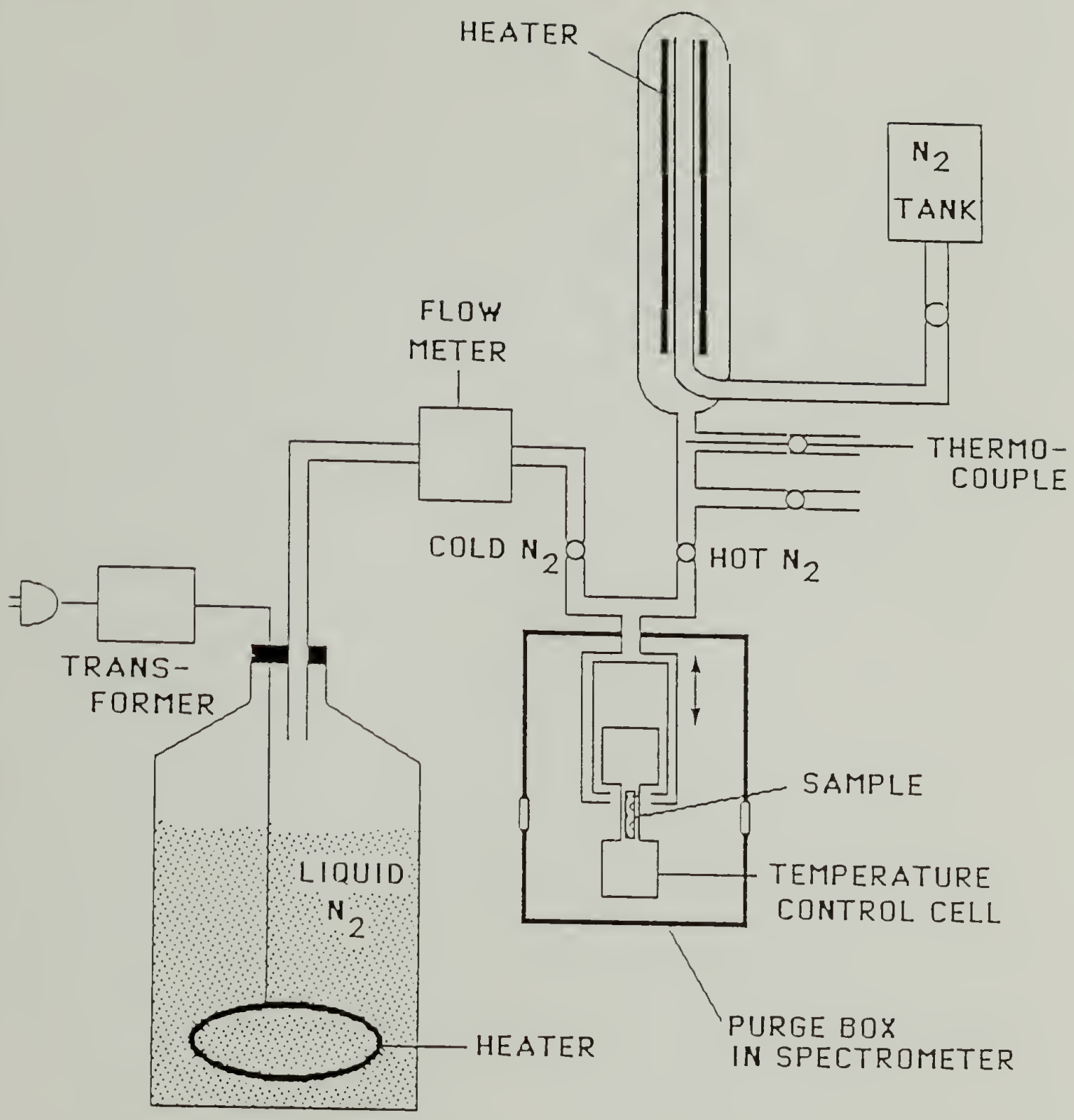

TEMPERATURE CONTROL SET-UP

FIGURE 3.2 Schematic drawing for the isothermal temperature set-up using both hot and cold nitrogen gas.

FIGURE 3.3 Temperature variations during (a) high temperature phase separation experiments (FTIR and DSC) (b) low temperature phase separation experiments (FTIR).

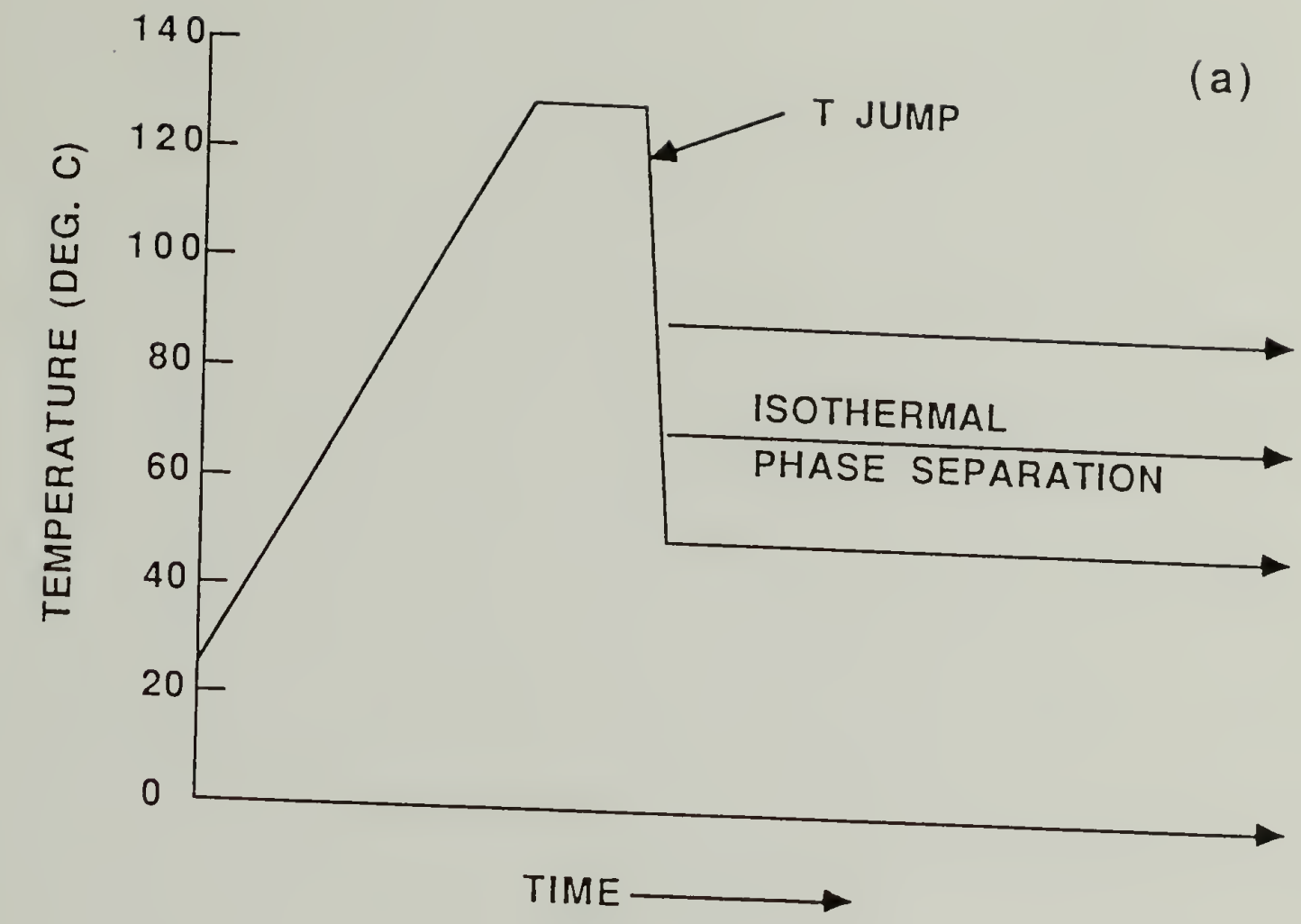
140
120
100
80
60
40
20
0
TEMPERATURE (DEG. C)
(a)
T JUMP
ISOTHERMAL
PHASE SEPARATION
TIME

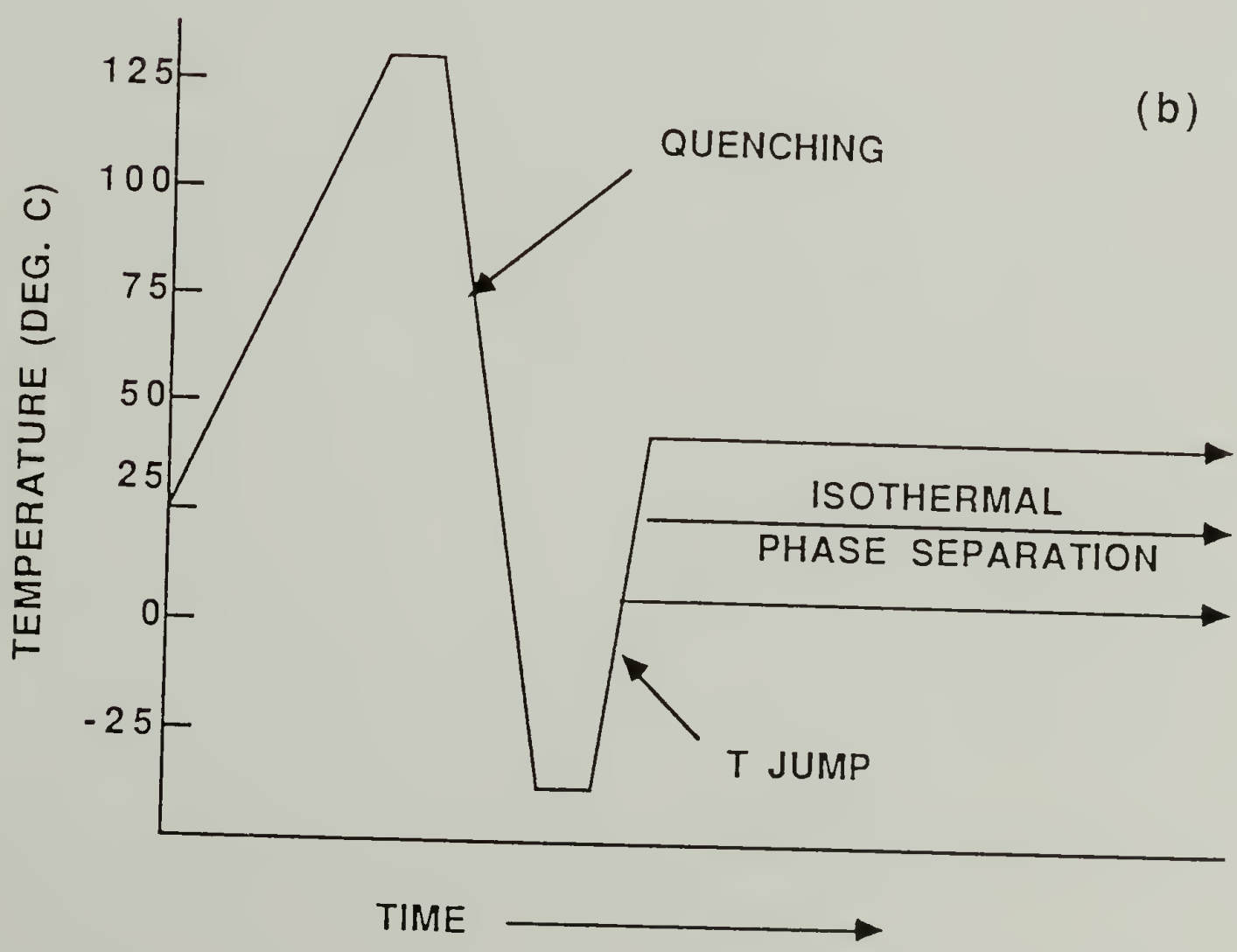
125
100
75
50
25
0
-25
TEMPERATURE (DEG. C)
(b)
QUENCHING
ISOTHERMAL
PHASE SEPARATION
T JUMP
TIME

separation experiment (Figure 3.3b), the liquid nitrogen is sprayed onto the windows directly while the heating cell block is cooled with the liquid nitrogen at the same time. Extremely fast quenching can be accomplished with this setup. During the quenching step shown schematically in Figure 3.3b, samples can be cooled from 130 to -80°C in less than 30 seconds. The sample temperature was measured directly with a copper-constantan thermocouple held between the two windows. Films suitable for spectroscopic studies were obtained by casting 2%(w/v) solution in THF directly on the AgCl salt plate. It was slowly dried for 24 hours in the atmosphere until most of the solvent evaporated, then vacuum dried at 70°C for a few days.

All the infrared spectra were obtained with an IBM model 98 vacuum Fourier transform infrared spectrometer. Spectral resolution is maintained at $2cm^{-1}$. In two experiments, at 45 and 55°C, when high time resolution was required to follow the high rate of phase separation, we reduced the spectral resolution to $4cm^{-1}$. Although there are multiple bands of interest in the carbonyl stretching region, we have not carried out band deconvolution because of uncertain band width, differences in the inherent extinction coefficients and the number of components present.[21] Since the peak position of the carbonyl band at approximately $1730cm^{-1}$ shows little shift during isothermal phase separation, it is assumed that band height measurements can be used to represent the changing band intensity as a function of time

without significant error. When more reliable band assignments become available, deconvolution procedures can be applied. Infrared spectrum of the B2 model polyurethane at ambient temperature is shown in Figure 2.5.

Thermal Analysis

Since it was difficult to change the temperature quickly without significant overshooting, only high temperature phase separation kinetic studies were reliably carried out with DSC. The same samples as used in infrared measurements were studied. A Perkin-Elmer DSC-7 calorimeter controlled by a Perkin-Elmer 7500 computer was used with the indium standard. Phase-mixing was initially obtained by heating the sample to ~130°C, which is above the hard-domain dissociation temperature (T_d). Since the phase separation rate above 100°C was very slow, the temperature was lowered from 130°C to 100°C slowly and equilibrated for 10 minutes, before being quenched to the isothermal phase separation temperature. This was done to minimize the transient state during the temperature change. After lowering to the isothermal phase separation temperature, heat flow was monitored isothermally as a function of time.

Results and Discussion

Spectroscopic Study of Phase Separation Kinetics

The utility of using a spectroscopic technique to measure phase separation kinetics depends very much on the ability to identify bands which are characteristic of the homogeneous state versus the phase separated state. It is generally accepted that the N-H stretching vibration in the 3300cm^{-1} region is the one most sensitive to the hydrogen bonding distribution in polyurethanes.[22,23] However, in most observations, the usually complex broad features of this band cannot be easily analyzed.

The stable hard segments rich domains in polyurethanes are characterized by interurethane C=O ··· H-N hydrogen bonds. The typical infrared spectrum obtained for our samples in the carbonyl stretching region shows two distinct peaks. The peak at 1730cm^{-1} is assigned to the free carbonyl peak and the clearly distinguishable one at 1700cm^{-1} is assigned to carbonyl groups hydrogen bonded to N-H group. The generally higher absorbance observed for the 1700cm^{-1} peak relative to the 1730cm^{-1} component is characteristic of a typical phase separated structure of polyurethanes.

If the model B2 polyurethane is heated above the hard domain dissociation temperature (~100^{o}C),[24] the relative intensity of the two carbonyl peaks changes significantly as the heterogeneous structure transforms to a homogeneous one.

Since most of the hard segments in the homogeneous state are surrounded by the soft segments, the carbonyl groups are free of hydrogen bonding as characterized by the high absorbance of the 1730cm^{-1} peak. As demonstrated in the previous chapter, this phase mixed state can be preserved at extremely low temperatures by rapidly quenching the sample to below the glass transition temperature of the soft segments.[13,14]

Isothermal phase separation kinetics can then be studied by raising the sample temperature quickly to the phase separation temperature and measure the changes in the infrared spectrum as a function of time. When a homogeneous structure phase separates, the carbonyl group is transformed from a free state to a state hydrogen bonded to a N-H group. Changes in the carbonyl region during isothermal phase separation is shown in Figures 3.4a and b as a function of time. The time equals zero spectrum is first spectrum collected after the quenching. Since the 1730cm^{-1} peak is assigned to be the free carbonyl peak, the high absorbance value of that component indicates a high degree of phase mixing at time zero. As isothermal phase separation proceeds, the 1700cm^{-1} component, assigned to carbonyl groups hydrogen bonded to N-H, increases, while the 1730cm^{-1} component decreases in intensity. Our data clearly indicate that the phase separation process involves a gradual migration of the hard segments dissolved in the soft matrix into the hard domain.

FIGURE 3.4 Changes observed as a function of low temperature isothermal phase separation time for the C=O stretching region of B2 polyurethane; Spectrum obtained at t=0 has low absorbance at 1700cm^{-1} and high absorbance at 1730cm^{-1}.
(a) 10°C
(b) 20°C

(a) 10° C

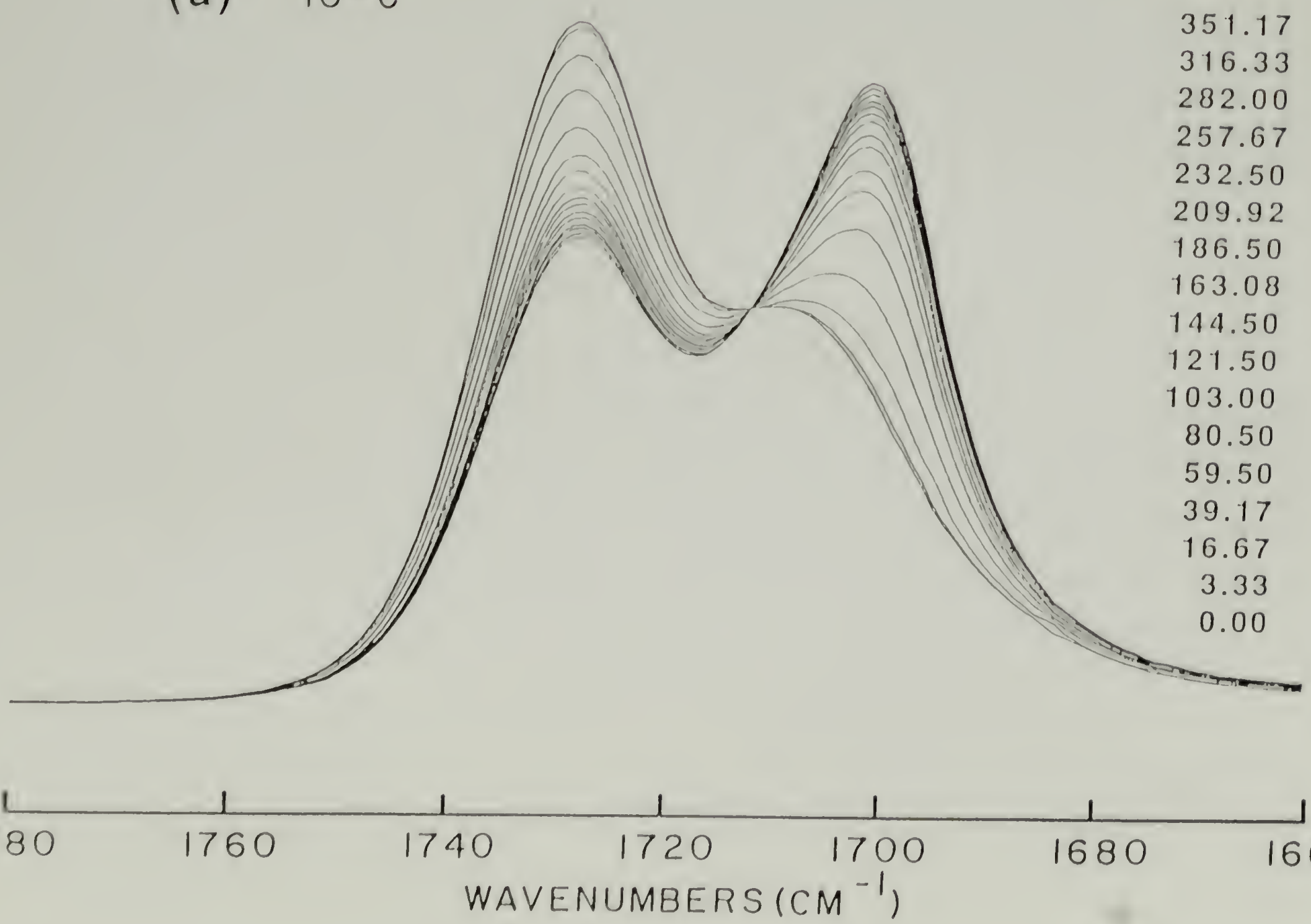
Time (min)
351.17
316.33
282.00
257.67
232.50
209.92
186.50
163.08
144.50
121.50
103.00
80.50
59.50
39.17
16.67
3.33
0.00
1780
1760
1740
1720
1700
1680
1660
WAVENUMBERS (CM⁻¹)

(b) 20°C

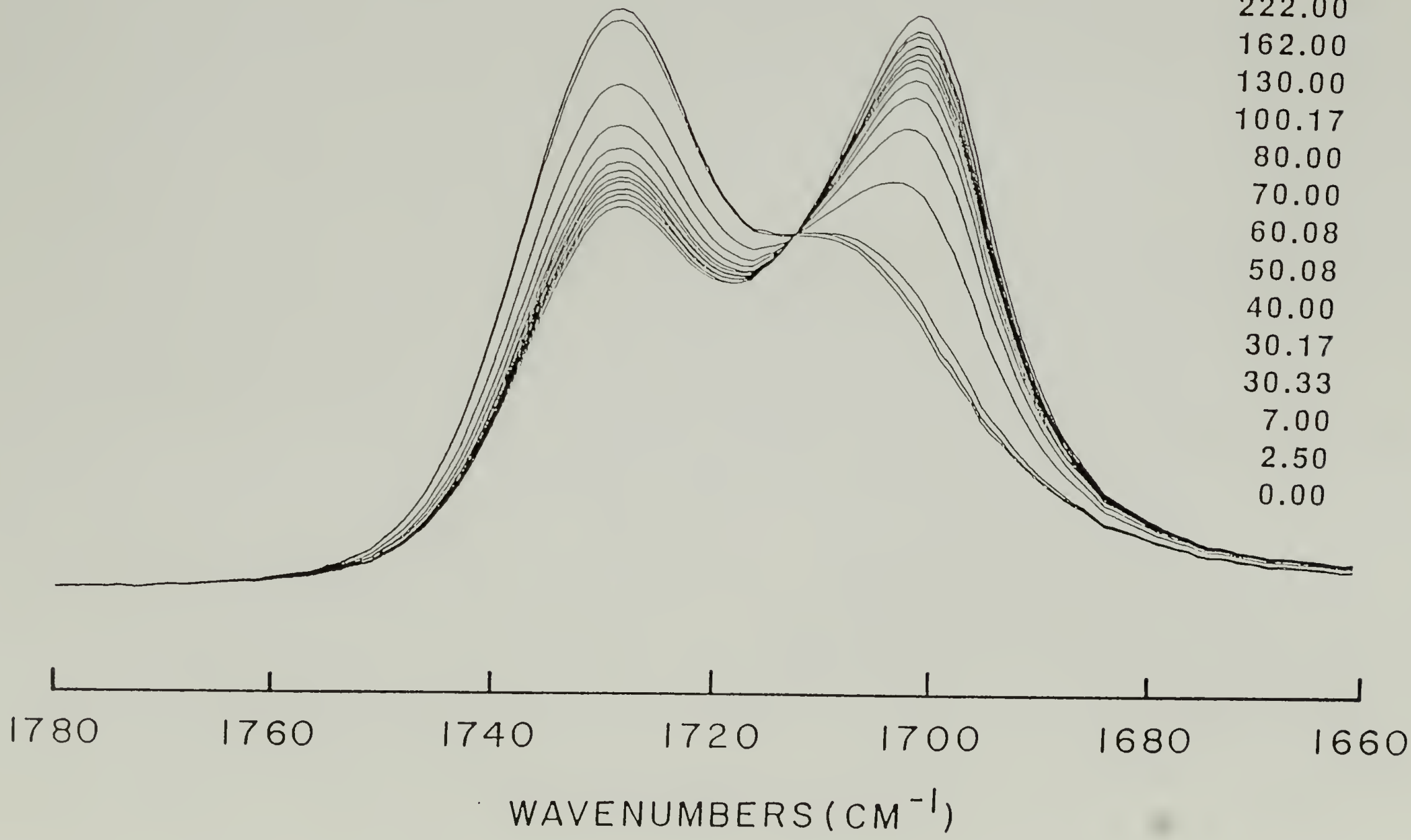
TIME(MIN)
222.00
162.00
130.00
100.17
80.00
70.00
60.08
50.08
40.00
30.17
30.33
7.00
2.50
0.00
1780
1760
1740
1720
1700
1680
1660
WAVENUMBERS(CM-1)

For high temperature phase separation kinetics, the temperature of the melt was quickly cooled down to the phase separation temperature. After the temperature was stabilized by the cold and hot gases, the spectra were collected with time. The time for the temperature jump was approximately seconds. The C=O stretching spectra obtained during phase separation at 65°C are shown in Figure 3.5. General features shown in Figure 3.5 are very similar to those shown in Figure 3.4.

Previous studies have shown that frequency and intensity differences at different temperatures for both the hydrogen bonded and free C=O vibrations can be significant and difficult to define.[25,26] Measuring the relative intensity of the two components at a constant temperature removes this difficulty. The overall integral intensity of the two components is independent of the phase separation time at a given temperature, as shown in Figure 3.6. The interconversion between the two principal components is considerable. Since its inherent extinction coefficient remains relatively constant, the C=O stretching vibration is a suitable band for estimating the amount of hydrogen bonding present at a given time and for following the phase separation kinetics. It should be emphasized that our measurements are taken at a constant temperature, thus eliminating many of the temperature induced spectroscopic effects. The changes we observe, therefore, are strictly related to the structural change during phase separation.

FIGURE 3.5 Changes observed as a function of high temperature (65°C) isothermal phase separation time for the C=O stretching region of B2 polyurethane; Spectrum obtained at t=0 has low absorbance at 1700cm^{-1} and high absorbance at 1730cm^{-1}.

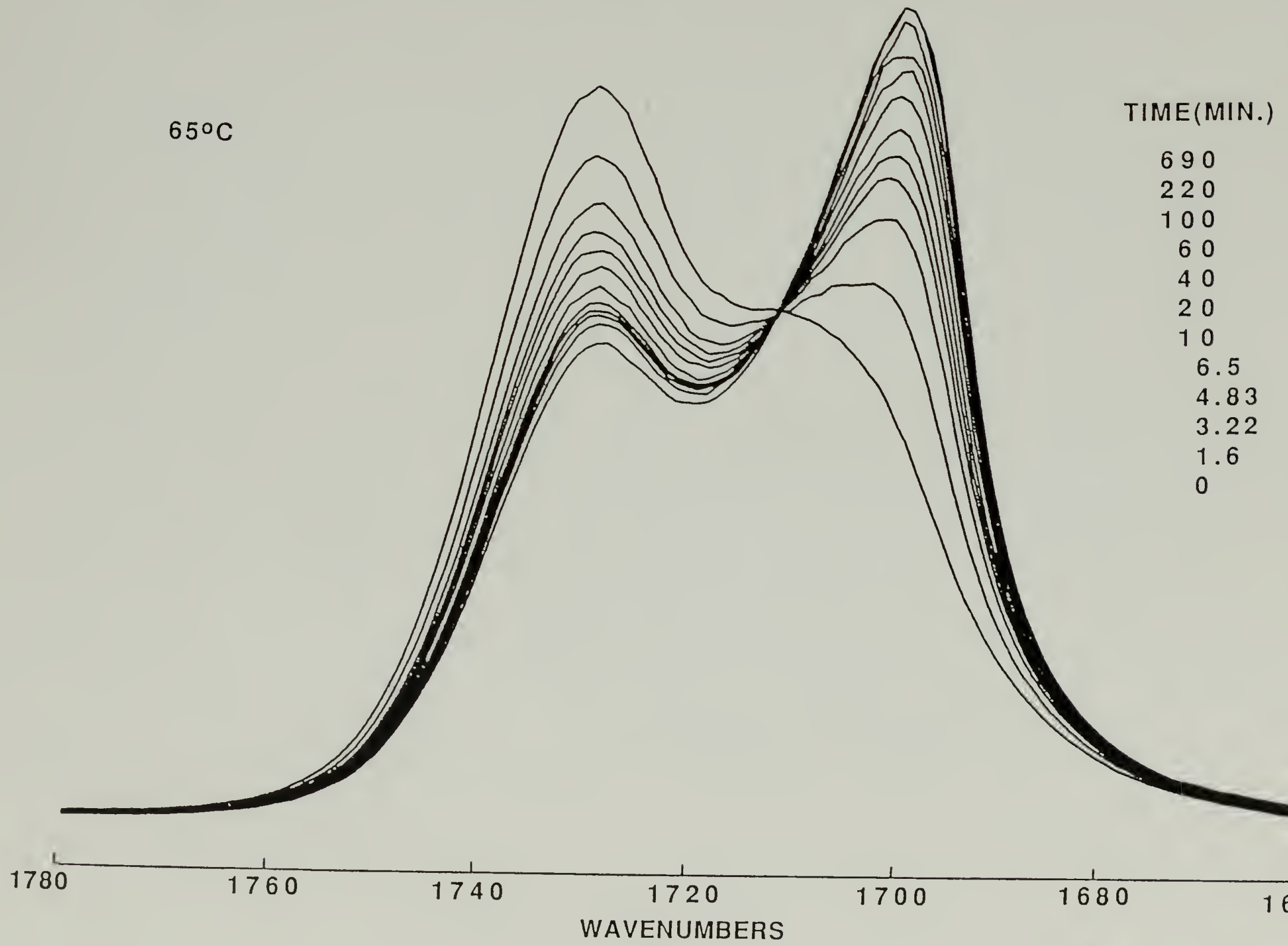
65°C
TIME(MIN.)
690
220
100
60
40
20
10
6.5
4.83
3.22
1.6
0
1780
1760
1740
1720
1700
1680
1660
WAVENUMBERS

FIGURE 3.6 The total integrated intensity of the C=O stretching bands around the 1700cm^{-1} region as a function of time during isothermal phase separation at 10^{o}C (top) and 20^{o}C (bottom).

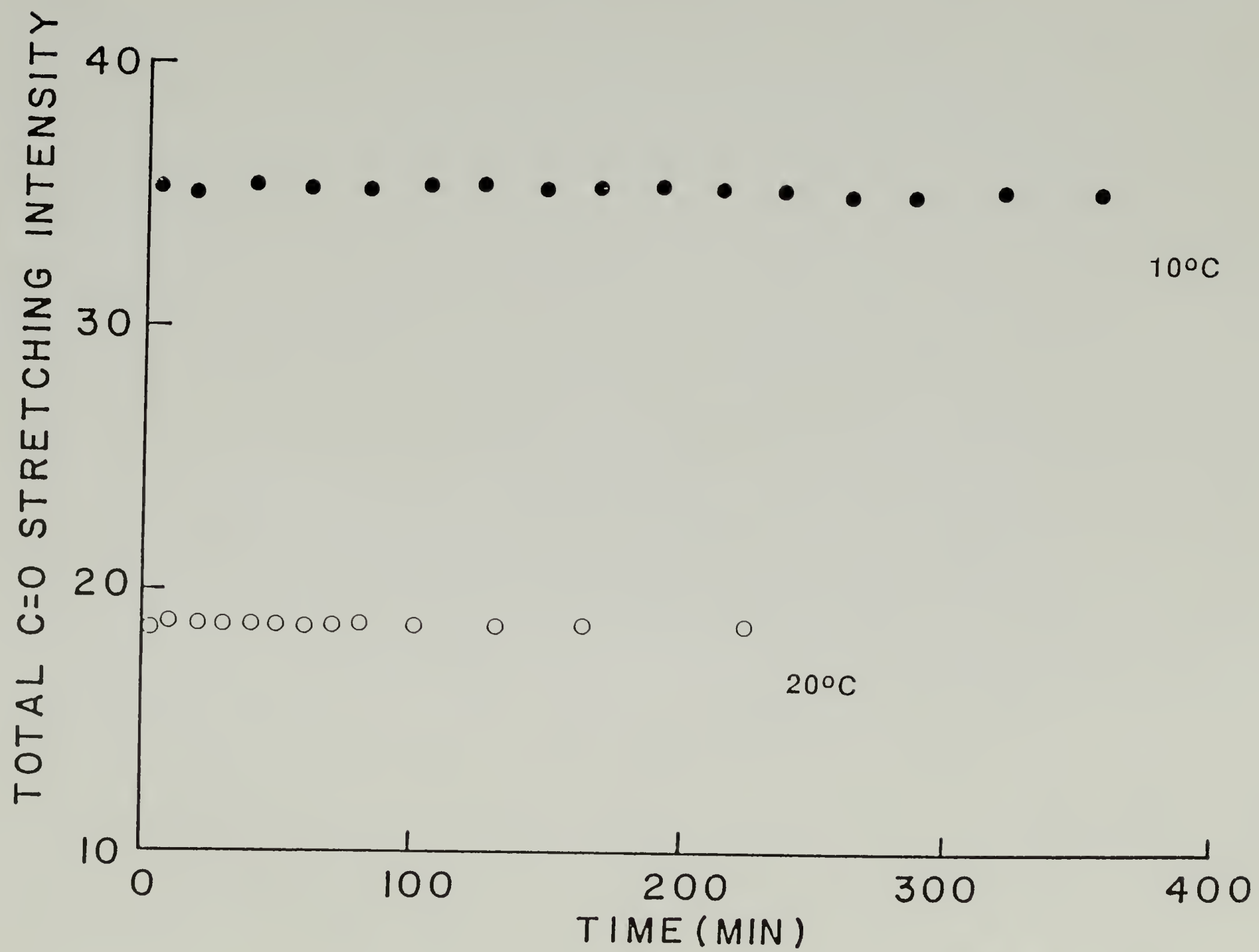
TOTAL C=O STRETCHING INTENSITY
40
30
20
10
0
100
200
300
400
TIME (MIN)
10°C
20°C

In our analysis, the peak intensity of the 1730cm^{-1} component is used to obtain a fractional degree of phase separation as shown in Figure 3.7. Typically, after a short slow initiation period, phase separation increases rapidly above an approximately 70% degree of phase separation and then decreases before reaching the maximum degree of phase separation asymptotically. The data plotted in Figure 3.7 resemble a crystallization isotherm, even though they deviate slightly from the usual sigmoidal shape for data obtained at later stages of phase separation. It is also apparent that fractional phase separation is very sensitive to the temperature.

In theory, the N-H stretching vibration should also yield complementary structural information to the C=O stretching vibration. N-H groups can form hydrogen bonding with the C=O group of the hard segments as well as the ether group of the soft segment.[10,11] This vibration, however, is complicated not only by the two types of hydrogen bonding observed, but also other second-order spectroscopic effects involving the N-H stretching fundamental and combinations of lower frequency amide vibrations.[27] Changes in the N-H stretching regions during two different isothermal phase separation processes are shown in Figures 3.8a and b. Even though spectral complications do not allow a simple quantitative analysis, changes occurring during isothermal phase separation, as shown in Figure 3.8, can be understood qualitatively because the temperature effect is removed.

FIGURE 3.7 Decrease of the $1730cm^{-1}$ (increase of $1700cm^{-1}$) component as a function of time; $\phi(t)$ denotes the fractional degree of phase separation and is

calculated as $\frac{I(t)-I(0)}{I(\infty)-I(0)}$ where $I(0), I(t), I(\infty)$ being intensity of $1730cm^{-1}$ component at phase separation time zero (just after quenching), t, infinity (extrapolated), respectively.

(a) 10, 20°C

(b) 5, 15, 25, 38°C

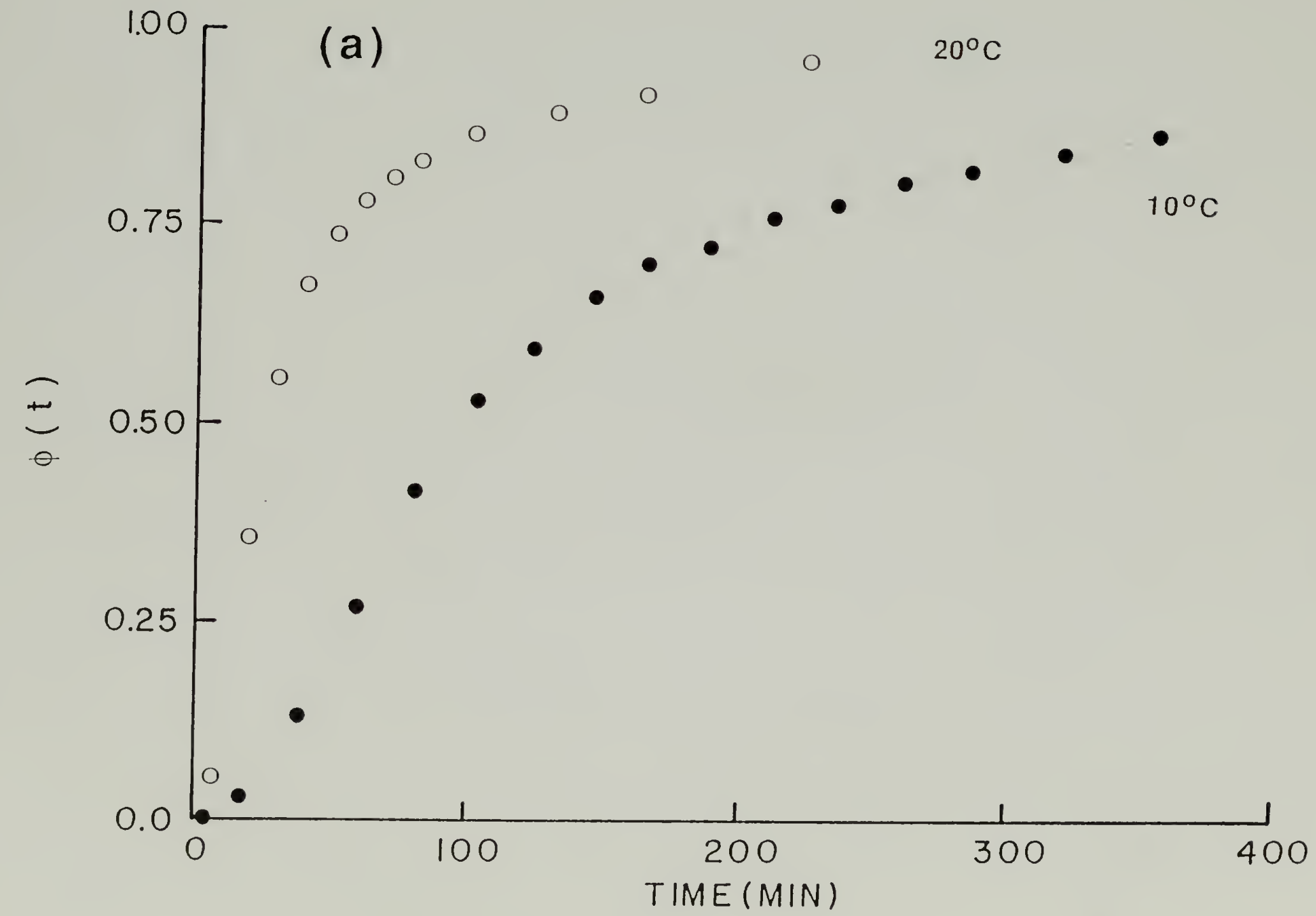
(a)
20°C
10°C
1.00
0.75
0.50
0.25
0.0
θ(t)
0
100
200
300
400
TIME (MIN)

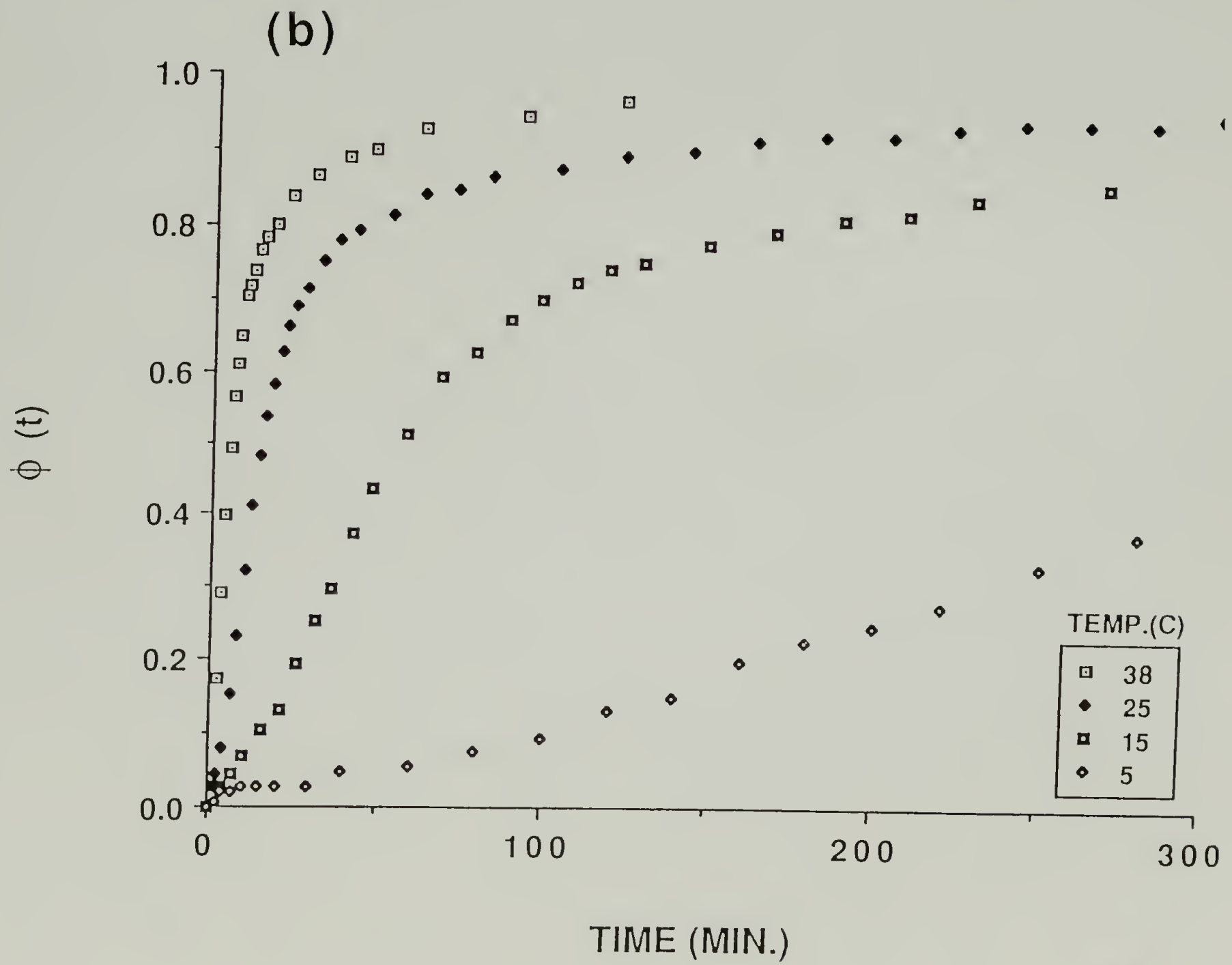
(b)
1.0
0.8
0.6
0.4
0.2
0.0
θ (t)
0
100
200
300
TIME (MIN.)
TEMP.(C)
38
25
15
5

FIGURE 3.8 Changes observed in the N-H stretching region of B2 polyurethanes as a function of isothermal phase separation time at low and high temperature; Spectrum obtained at t=0 has low absorbance at $3330cm^{-1}$.
(a) 15°C
(b) 65°C

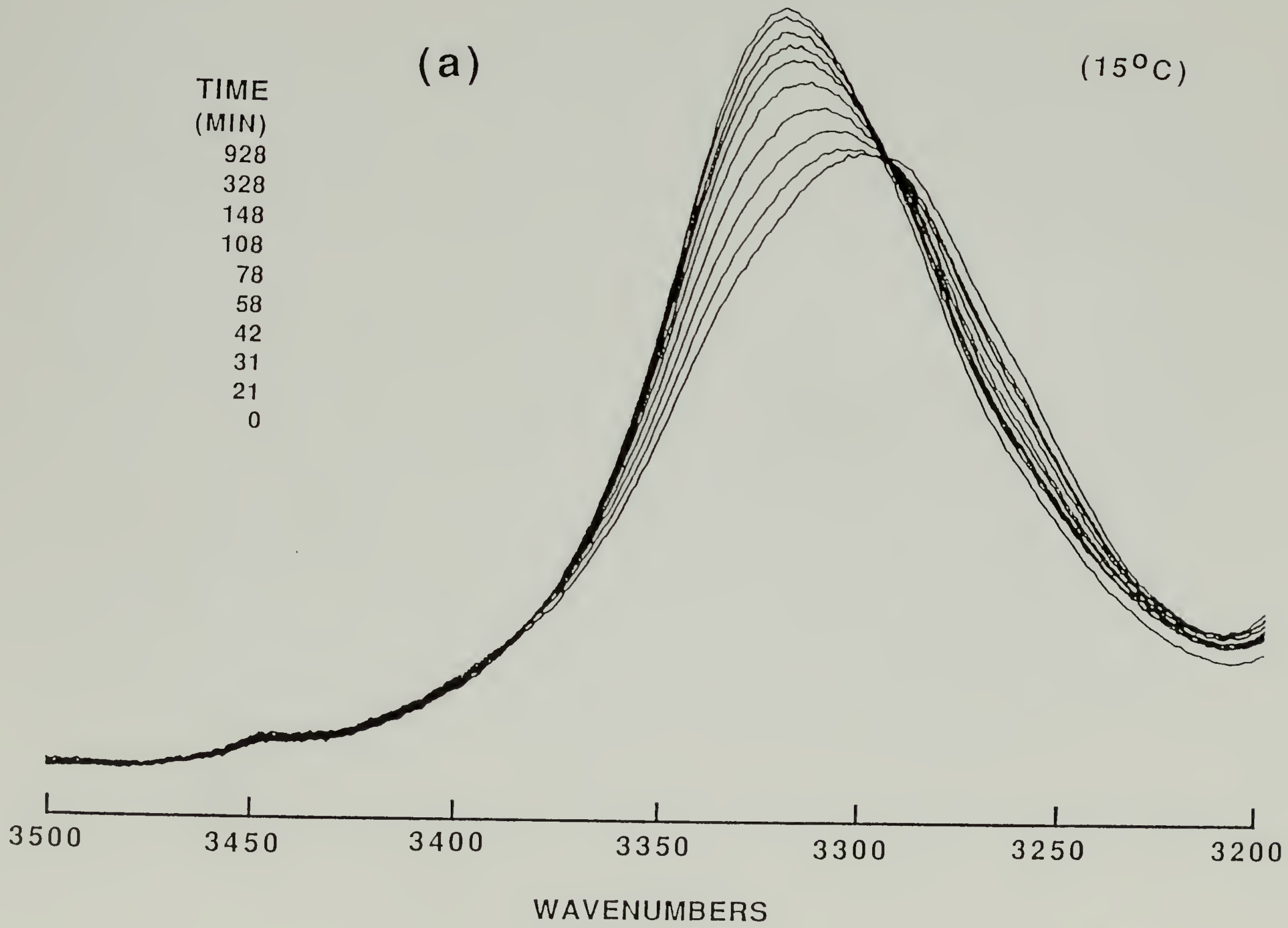
(a)
(15°C)
TIME
(MIN)
928
328
148
108
78
58
42
31
21
0
3500
3450
3400
3350
3300
3250
3200
WAVENUMBERS

(b)

65°C

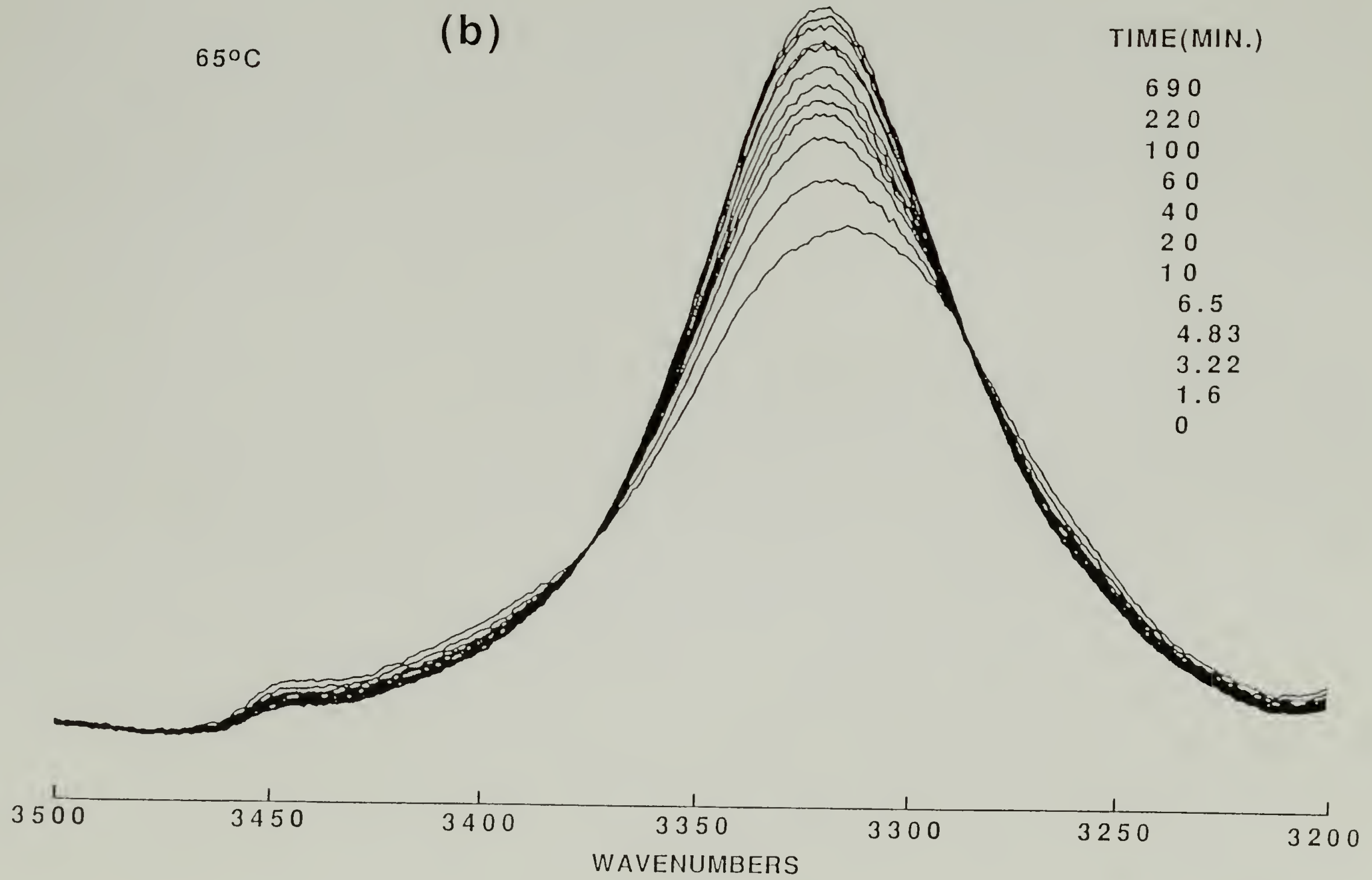
TIME(MIN.)
690
220
100
60
40
20
10
6.5
4.83
3.22
1.6
0
3500
3450
3400
3350
3300
3250
3200
WAVENUMBERS

Generally speaking, the frequency of N-H groups free from hydrogen bonding is at 3450cm^{-1}. The extremely weak 3450cm^{-1} peak in Figure 3.8 indicates that most of the N-H groups are hydrogen bonded either with the hard segment or the soft segment. The peaks at 3330 and 3295cm^{-1} have been assigned to N-H groups hydrogen bonded to C=O groups and the ether oxygens, respectively.[13] The number of N-H···C-O-C(ether) hydrogen bonds should diminish, with a corresponding increase in the number of N-H···C=O bonds during isothermal phase separation. It is, therefore, expected that the 3330cm^{-1} component is to increase and the 3295cm^{-1} component to decrease in intensity as a function of time. In most cases these two components are difficult to separate cleanly. The decrease of the 3295cm^{-1} component is only seen as a decreasing shoulder due to the broad nature of the peak (refer to time zero spectrum of Figure 3.8). The increase of the 3330cm^{-1} peak, however, is quite obvious. As phase separation proceeds, it grows from a weak shoulder into the dominant peak clearly indicating the formation of hydrogen bonds between the hard segments, i.e. hydrogen bonding between the N-H and C=O groups.

In the case of the polyether based polyurethanes, the carbonyl stretching region gives information purely pertaining to the hard segments. When a polyester compound is used as a soft segment in the polyurethanes, it becomes difficult to use the carbonyl stretching peak to assess the fractional degree of phase separation or phase separation

kinetics. Figure 3.9 shows that the total absorbance of the N-H stretching peak can be used to characterize the kinetics. The degree of phase separation data obtained from the C=O peak is also included to demonstrate the good correlation between two different spectral regions.

The phase separation rate can be obtained generally from the time required to achieve 50% phase separation, $t_{1/2}$. The rates for each temperature can be obtained from the data presented in Figure 3.7 and are summarized in Figure 3.10. The temperature range selected for the rate measurement was from $0^{o}C$ to $100^{o}C$. The selection of the this range was determined by the glass transition temperature of the soft segments and the dissociation temperature of the hard domain. The phase separation rate data of the segmented polyurethane over this temperature range have not been previously reported. The plotted data shown in Figure 3.10 resembles the temperature dependence of the crystallization rate as shown in Figure 3.1.

There is a close analogy between the formation of the hard domain from the "homogeneous" mixed phase during phase separation and the formation of a crystalline phase from the homogeneous melt during crystallization. Therefore, Figure 3.10 can be understood qualitatively in terms of Equation 3.3 which explains the slow rates at low and high temperatures and relatively faster rates at intermediate temperatures.

It should be noted that the fully phase separated B2 polyurethane does not show any birefringence through a cross

FIGURE 3.9 Changes of the integrated N-H stretching band during isothermal phase separation at 25°C; The intensity change of the free C=O peak is included for comparison.

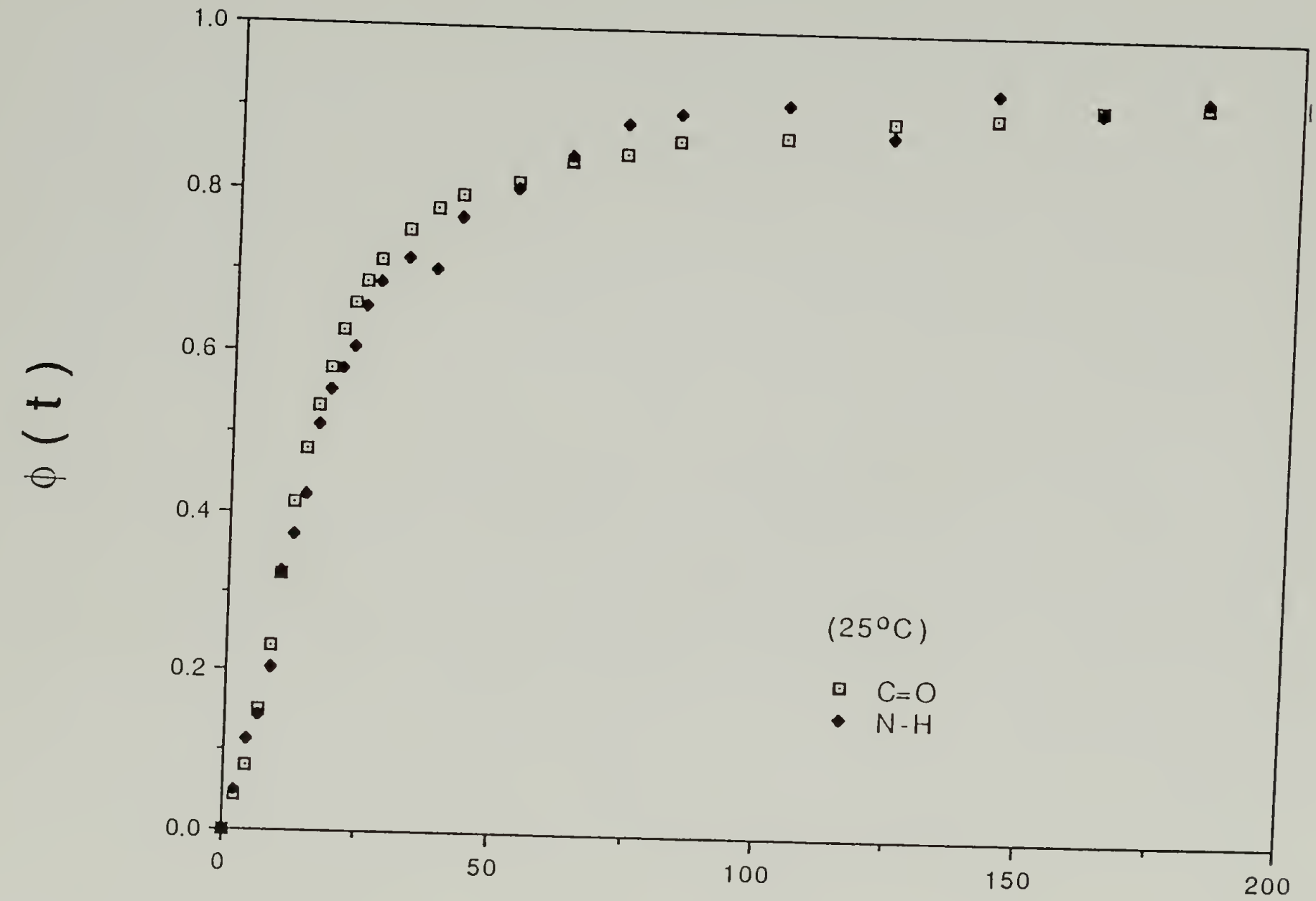
1.0
0.8
0.6
0.4
0.2
0.0
0
50
100
150
200
ϕ (t)
(25°C)
C=O
N-H
TIME (MIN.)

FIGURE 3.10 Phase separation rate of B2 polyurethane as a function of temperature; $t_{1/2}$ is the time for 50% phase separation.

PHASE SEPARATION RATE

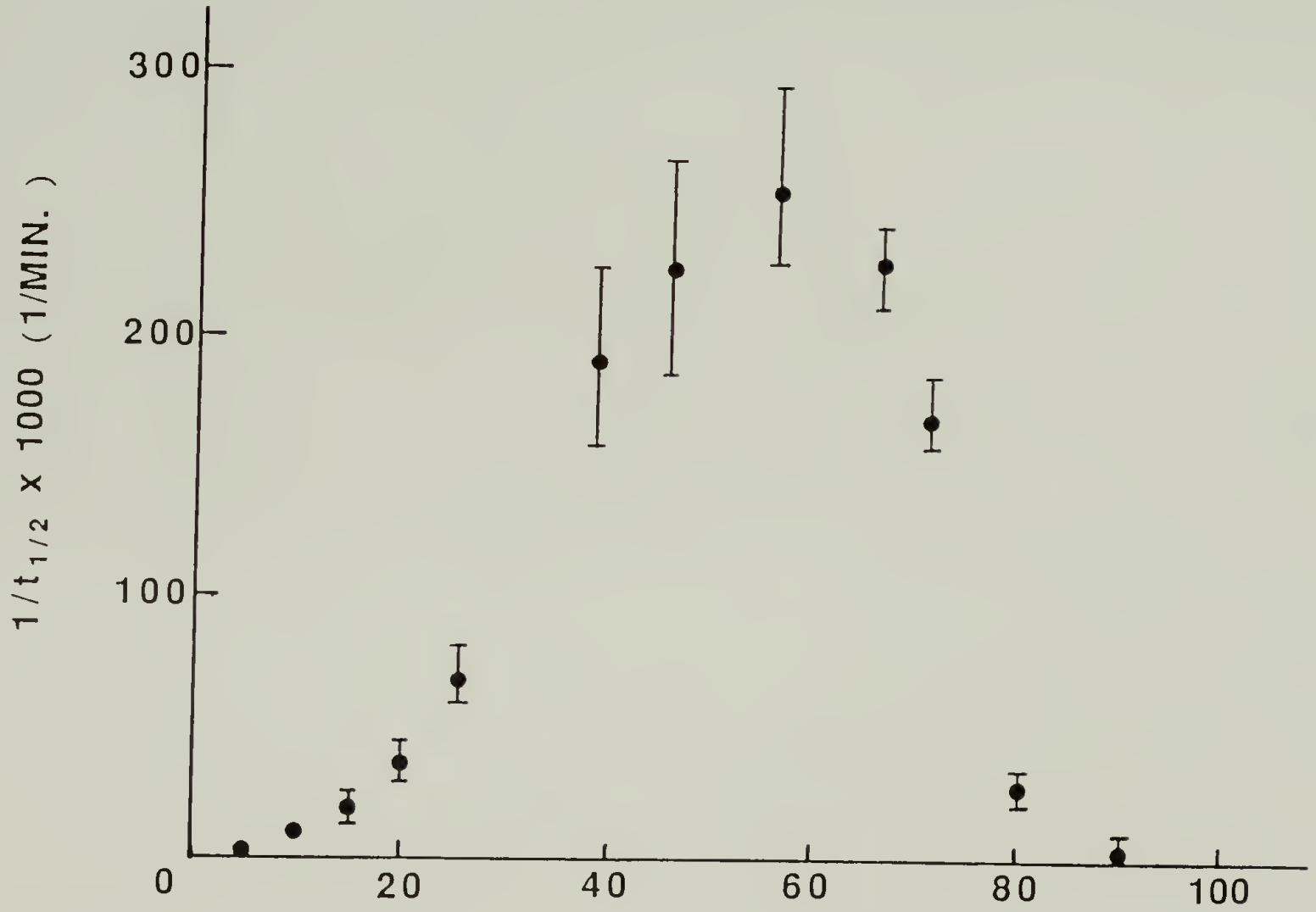

polarizing optical microscope. Furthermore, wide angle x-ray diffraction patterns of B2 model polyurethanes also do not show any crystalline peak, even when the sample is well annealed above the glass transition temperature of the soft segment.[24] Therefore, the spectral changes with time in Figures 3.4 and 3.8 are due to the phase separation process not to crystallization.

The slowing of the phase separation rate at high temperatures then needs to be explained further. One possibility is the fact that hard segment movements may meet resistance from the contractile force of the soft segments. The stress, σ, for N_C network chains as a function of strain, α, for uniaxial stretching at constant volume, can be expressed as Equation 3.12.

$$\sigma = kT\ (N_C/V)\ (\alpha^2 - 1/\alpha) \qquad (3.12)$$

The contractile force at the constant extension ratio is proportional to the temperature. Since the flexible soft segment is shown to exist in an extended state for the phase separated structure,[28-30] the force against phase separation at a high temperature is expected to be higher, thus slowing phase separation. The slow phase separation rate on the high temperature side of the curve in Figure 3.10 is, therefore, thought to be affected by the loss of conformational entropy of the soft segment when phase separated.

Phase Separation Mechanism

There are no established mechanisms which can be used to explain the phase separation of copolymers. One of the possibilities is the concept of spinodal decomposition which occurs in the case of the thermodynamically unstable polymer blends.[20,31,32]

If the non-linear terms in Equation 3.9 are neglected, the linear combination of Equation 3.10 can also be the solution of Equation 3.9.

$$C - C_o = \sum_{\text{all}\,\beta} A(\beta) \exp\{R(\beta)t\} \cos(\beta \cdot \mathbf{r}) \tag{3.13}$$

$A(\beta)$ is the amplitude of each component. When $R(\beta)$ is negative, the composition modulation function of that frequency will decrease exponentially. For positive $R(\beta)$, the modulation function will increase rapidly and eventually the component with maximum $R(\beta)$ will dominate the spinodal decomposition. Equation 3.13 can be, therefore, approximated as in

$$C - C_o \cong A(\beta_m) \exp\{R(\beta_m)t\} \cos(\beta_m \cdot \mathbf{r}) \tag{3.14}$$

where subscript m stands for the wavenumber for maximum amplification factor.

One dimensional spatial concentration variation of the hard segment at two different times during spinodal decomposition is shown schematically in Figure 3.11. At time zero, the concentration is uniform because of the homogeneous

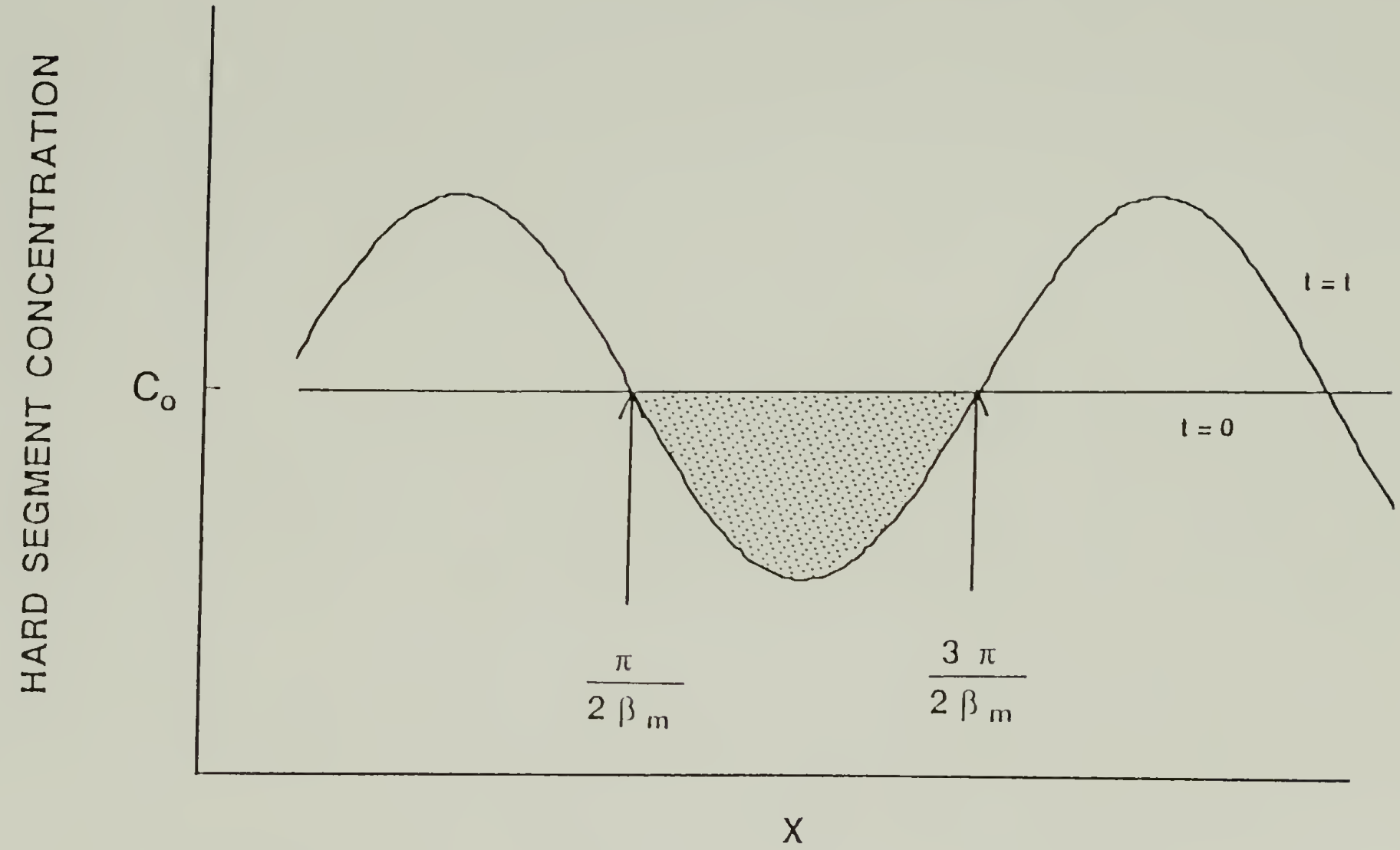

FIGURE 3.11 Concentration modulation at time t due to the β_m component during spinodal decomposition.

structure of the phase mixed state. As phase separation proceeds, the sinusoidal concentration modulation is developed according to Equation 3.14. The concentration fluctuation at time t is also included in Figure 3.11.

The total reduction, Q, of the hard segments in the soft matrix, which is shown as the shaded area in Figure 3.11 can be obtained as[5]

$$Q = \left[\left| \int_{\frac{\pi}{2\beta_m}}^{\frac{3\pi}{2\beta_m}} (C - C_o)\, dx \right| \right]^3 = \left[\frac{2}{\beta_m} A(\beta_m) \right]^3 \exp\{3R(\beta_m)t\} \tag{3.15}$$

so that

$$\ln Q = 3 \ln\left[\frac{2}{\beta_m} A(\beta_m) \right] + 3R(\beta_m)t \tag{3.16}$$

According to Equation 3.16, lnQ has a linear relationship with the time t. It is well known that the wavenumber for maximum concentration modulation, β_m, does not change during the early stage of the spinodal decomposition.[20] Since $R(\beta_m)$ is a function of β_m and the diffusion coefficient D, which is independent of the concentration and thus time as shown in Equation 3.11, the plot of lnQ vs t should give a straight line with slope $3R(\beta_m)$.

In Figure 3.12, logQ is plotted against the phase separation time. It is obvious that the data does not support the spinodal decomposition mechanism over any significant range of time. More extensive experimental data are, of course, to be examined to draw the exact conclusion about the spinodal phase separation mechanism. The validity

FIGURE 3.12 Integrated hard segment depletion (log Q) vs time t during spinodal decomposition.

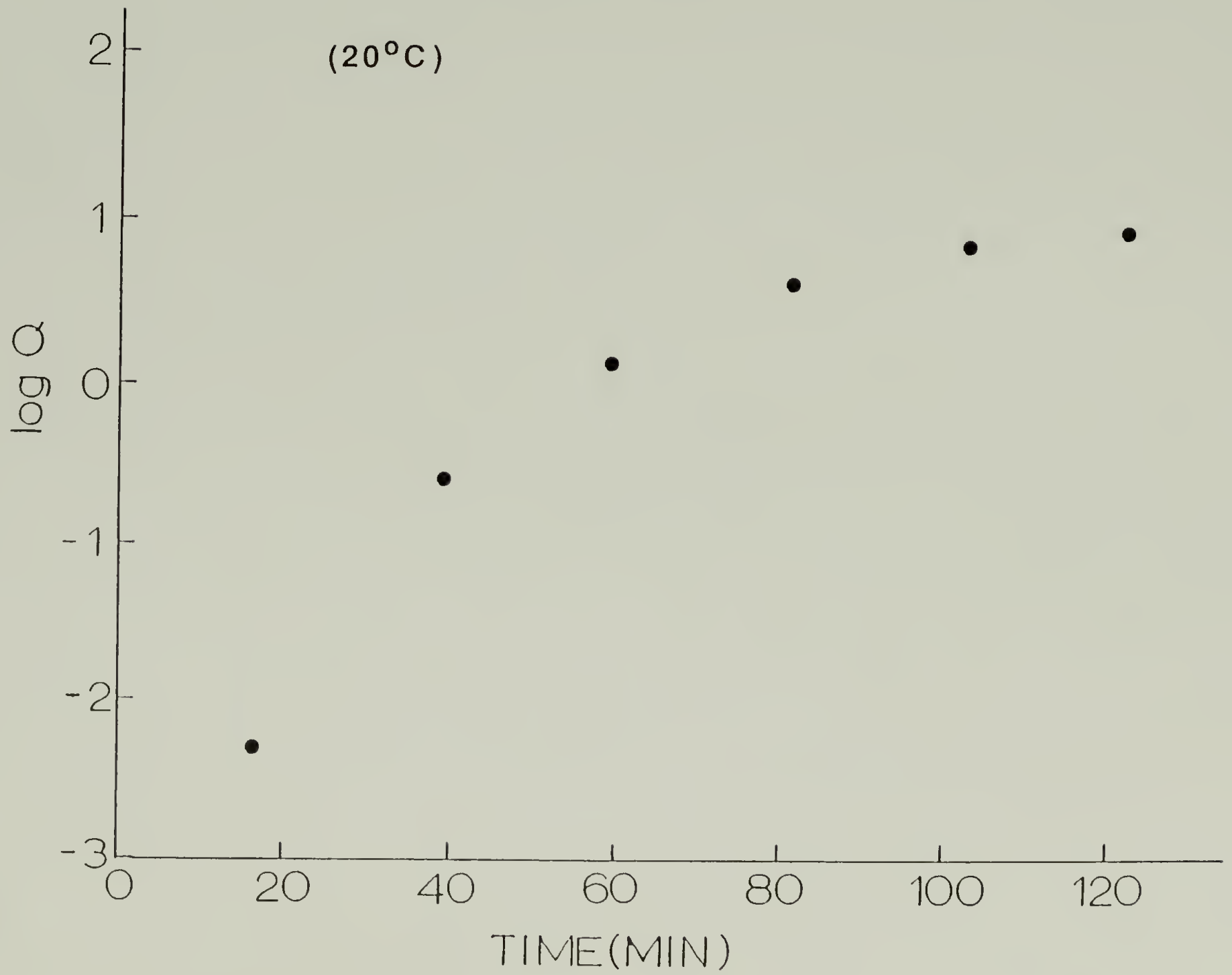
(20°C)
log Q
2
1
0
-1
-2
-3
0
20
40
60
80
100
120
TIME(MIN)

of the series of approximations used to derive the Equation 3.16 should also be examined further.

The phase separation kinetics of the segmented polyurethanes have not been thoroughly studied by the more conventional techniques. It is mainly due to the small domain size. For example, since the wavelength of the visible light is too long compared to the hard domain size, light scattering shows no appreciable hallow pattern indicating phase separation. Also, observation through the cross-polar optical microscope does not reveal any anisotropy over the entire field of view. Since the infrared method is extremely sensitive to the local environment, it is not surprising to detect the phase separation behavior only through the time variation of the infrared bands.

As an alternative, we can model this phase separation process as one of nucleation and growth. However, the meaning of nucleus may not correspond to the crystallites in the usual sense. There is virtually no information regarding the crystalline structure of B2 polyurethanes. In this case, the nucleus may simply be aggregates of hard segments in the homogeneous molten phase. With Equation 3.4, the decrease of the hard segments dispersed in the soft domains can be expressed as

$$\frac{M_t}{M_o} = 1 - \lambda \left(1 - \exp\left(-zt^n\right) \right) \qquad (3.17)$$

where M_t and M_o are the hard segment concentrations in the soft domains at time t and t=0, respectively, and λ is the equilibrium weight fraction of the hard segment in the hard segment domains. Since the spectroscopic intensity measurements are associated with the volume fraction, Equation 3.18 is more appropriate for analyzing the data

$$\frac{M_t - M_\infty}{M_o - M_\infty} = \frac{I(t) - I(\infty)}{I(o) - I(\infty)} = \exp\ (-zt^n) \qquad (3.18)$$

where I(t), I(O) and I(∞) are the intensities associated with the free carbonyl component at time t, at t=O, and after equilibrium has been achieved. In Figure 3.13, the Equation 3.18 is plotted using standard conventions as shown in Equation 3.5.

From Figure 3.13 it is clear that the phase separation mechanism is changing as a function of time. The lines in Figure 3.13 have been obtained by a linear regression fit to the data. It is possible to interpret the "dimensionality" of the growth process as 2 in the early stage. In the infrared spectrum obtained for the quenched sample the $1705cm^{-1}$ band can be observed next to the $1735cm^{-1}$ band. The $1705cm^{-1}$ band appears to be due to the hydrogen bonding between the hard segments in the residual nuclei or aggregates even in the molten state. Because of hydrogen bonding, there is strong anisotropic interaction between the hard segments. Therefore, the coefficient n=2 can be explained by heterogeneous nucleation and two dimensional

FIGURE 3.13 Avrami plot of the intensity observed for the decrease of the 1735cm^{-1} component as a function of time and temperature. The lines drawn are fitted to the data shown.

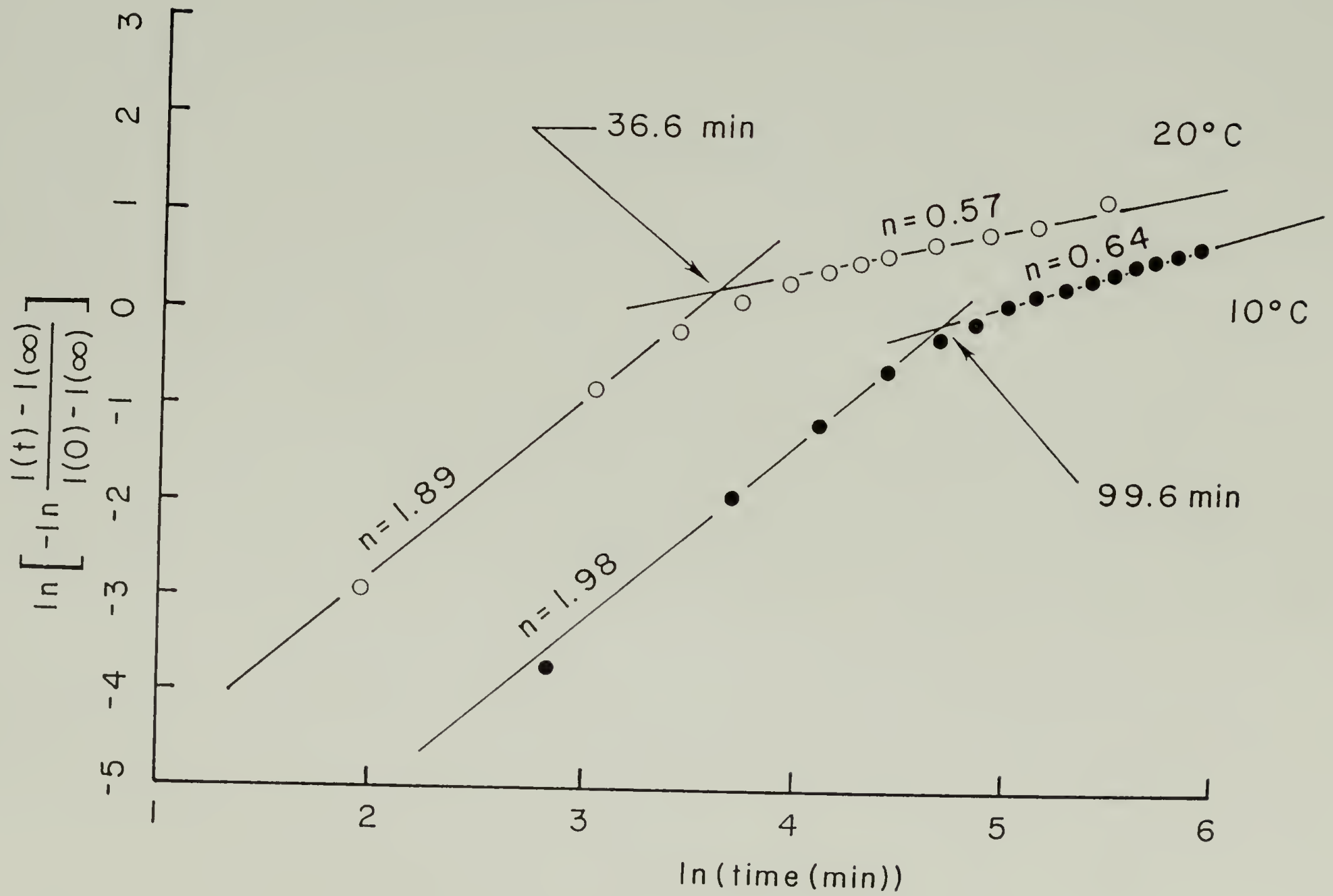
36.6 min
20°C
n=0.57
n=0.64
10°C
99.6 min
n=1.89
n=1.98
$\ln\left[-\ln\frac{I(t)-I(\infty)}{I(0)-I(\infty)}\right]$
ln (time (min))

growth in a cylindrical fashion as shown schematically in Figure 3.14. The hard segment domains are in the order of several hundred angstroms, fairly small in comparison to the overall sample thickness. Therefore, the "Avrami" coefficient is not strongly affected by the experimental geometry associated with the infrared technique. Even for these well-defined model polyurethanes, there may still be a very small amount of unreached model hard segments. The unreached hard segments are not expected to affect the overall phase separation behavior.

The changing time dependence of phase separation is extremely interesting. The overall volume fraction of the hard segments in the polyurethane is approximately 30%. When phase separation starts to occur, the regions around the nuclei become depleted in the hard segment content, which makes it difficult for additional hard segments to reach the surface of the nuclei. On this basis, the change in dimensionality from 2 to 0.6 can be assigned to a diffusion dominated mechanism operative at the later stages of phase separation.

Thermal Analysis of Phase Separation Kinetics

DSC traces during isothermal phase separation for two different samples are shown in Figure 3.15. A clear endothermic peak during the heating process was observed for the B2 model polyurethane. The presence of an exothermic peak during the isothermal phase separation of the B2 sample

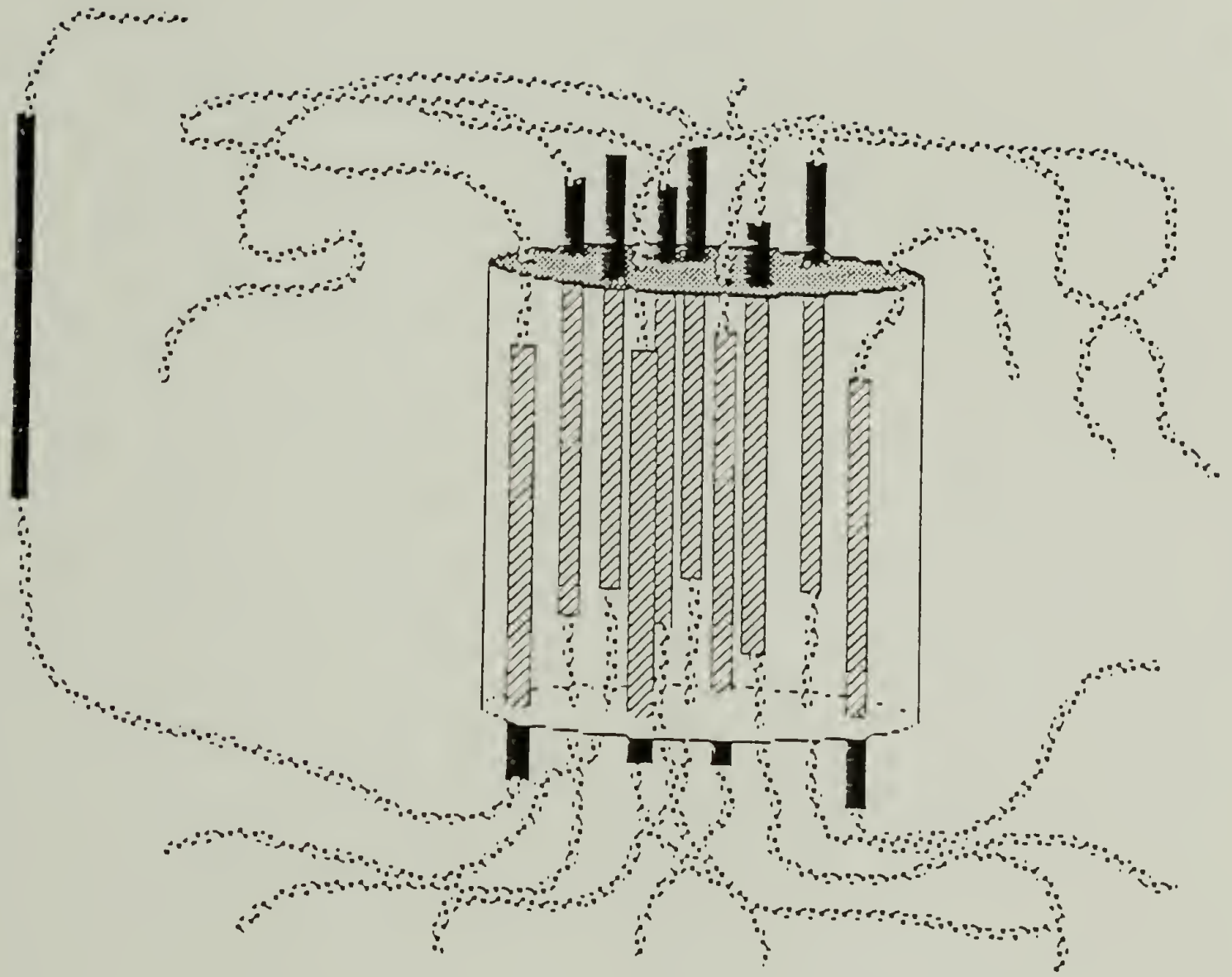

FIGURE 3.14 Schematic drawing of the growing hard segment domain associated with a nucleation and growth mechanism.

FIGURE 3.15 DSC traces for two (B2 and B4) polyurethanes during isothermal (55°C) phase separation; t=0 corresponds to time just after quenching to phase separation temperature; Transient state after quenching is observed for both samples.

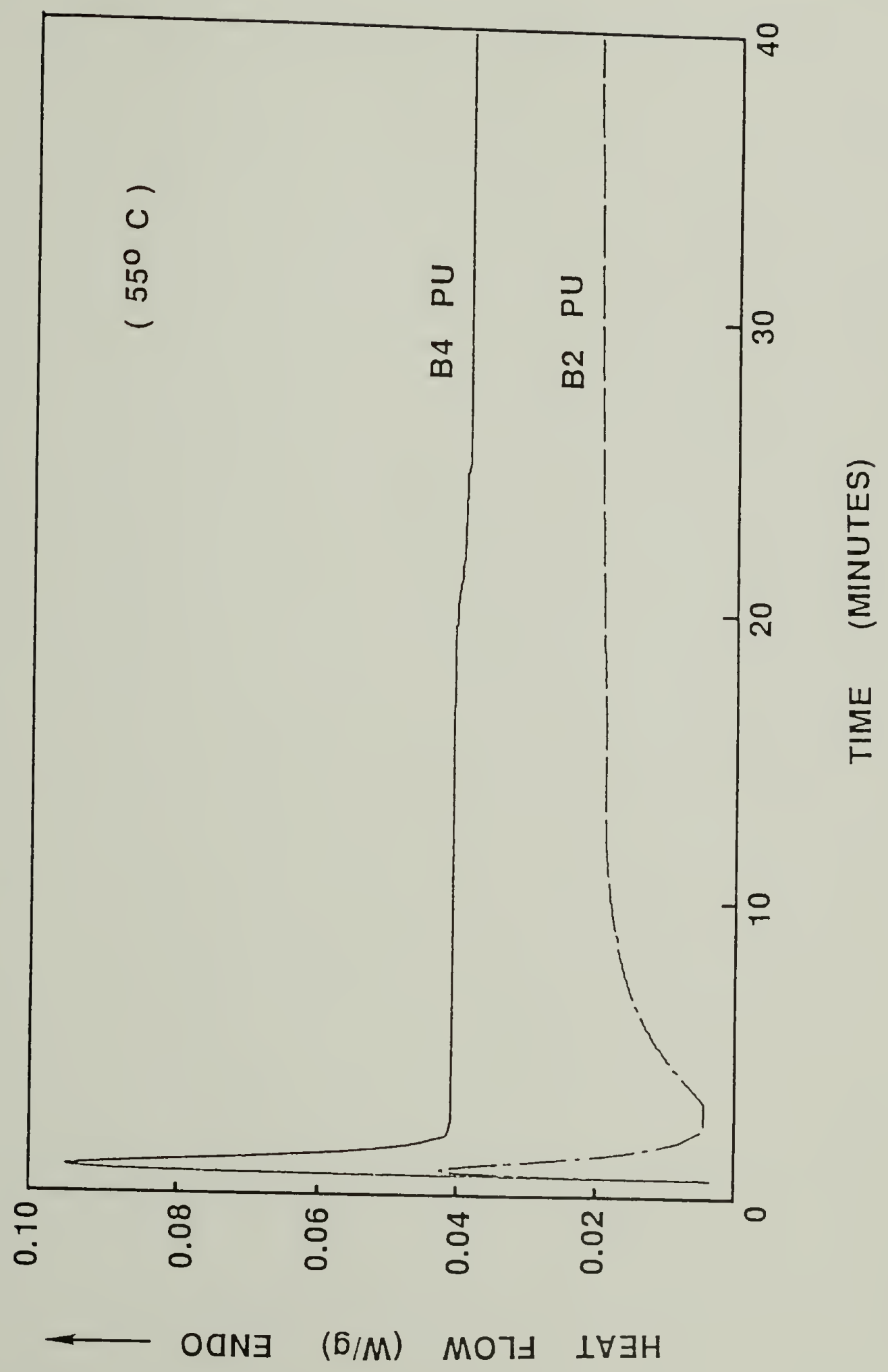
(55° C)
B4 PU
B2 PU
0.10
0.08
0.06
0.04
0.02
0
10
20
30
40
HEAT FLOW (W/g) ENDO
TIME (MINUTES)

demonstrates that heat flow during isothermal phase separation can be detected with the DSC technique. The B4 model polyurethane is partially crystalline and undergoes a transition from a heterogeneous to a homogeneous phase around 170°C.[24] Since both samples were heated only to 130°C, the exothermic peak was not observed for the B4 sample. Accordingly, the difference in DSC traces between B2 and B4 is purely due to the phase separation process of the B2 sample (refer to Figure 3.15). The dissociation energy of the hydrogen bond is known to be in the range of 5-8 kcal/mol.[33] Since the C=O···H-N hydrogen bonds are formed during isothermal phase separation, it is not surprising that the exothermic peak has been detected. As suggested in the previous chapter, the interurethane hydrogen bonds are replacing some of the N-H···-O- hydrogen bonds.[13,14] Therefore, the disruption of the latter must be considered as well. The frequency of the N-H···-O- band seems to suggest that this hydrogen bond is in fact stronger than C=O···H-N at room temperature or below. It has also been noted that the hydrogen bonding between the hard segment and the soft segment becomes less stable at the high temperatures used during DSC experiments.[13] It can be observed by comparing the two sets of spectra in Figures 3.8a and b. For the spectra obtained at the higher temperature, i.e. 65°C, the contribution of the 3295cm^{-1} peak is appreciably decreased as evident from the low shoulder. This indicates that the hydrogen bonding between C=O and -O- becomes unstable at this

temperature. Since the C=O···H-N bond is formed at the expense of the less stable N-H···-O- (ether) bond during phase separation at a high temperature, an exothermic peak, not an endothermic, is then expected. The free energy difference before and after phase separation and non-bonded interactions due to other secondary forces are also believed to contribute to the overall heat flow during isothermal phase separation even though they are not considered to be major factors.

Exothermic peaks during isothermal phase separation for the B2 polyurethane at several different temperatures are shown in Figure 3.16. Spectroscopic data shown in Figure 3.10, indicate that the phase separation rate is at a maximum around 55^{o}C and then decreases as temperature increases. The DSC data in Figure 3.16 shows the same trend. The exothermic peak becomes wider and shallower as the temperature increases from 55^{o}C to 80^{o}C, indicating that the phase separation rate progressively becomes slower as the temperature increases above 55^{o}C.

Fractional degrees of phase separation obtained at 70^{o}C with two different techniques, i.e, infrared and DSC, are shown in Figure 3.17. Even though the infrared and DSC technique measure very different structural features, Figure 3.17 indicates that there is a strong correlation between segmental interaction, mainly hydrogen bonding, and macroscopic thermal characteristics. Since the infrared technique detects the formation of hydrogen bonding between

FIGURE 3.16 DSC traces for B2 polyurethanes during isothermal phase separation at different temperatures.

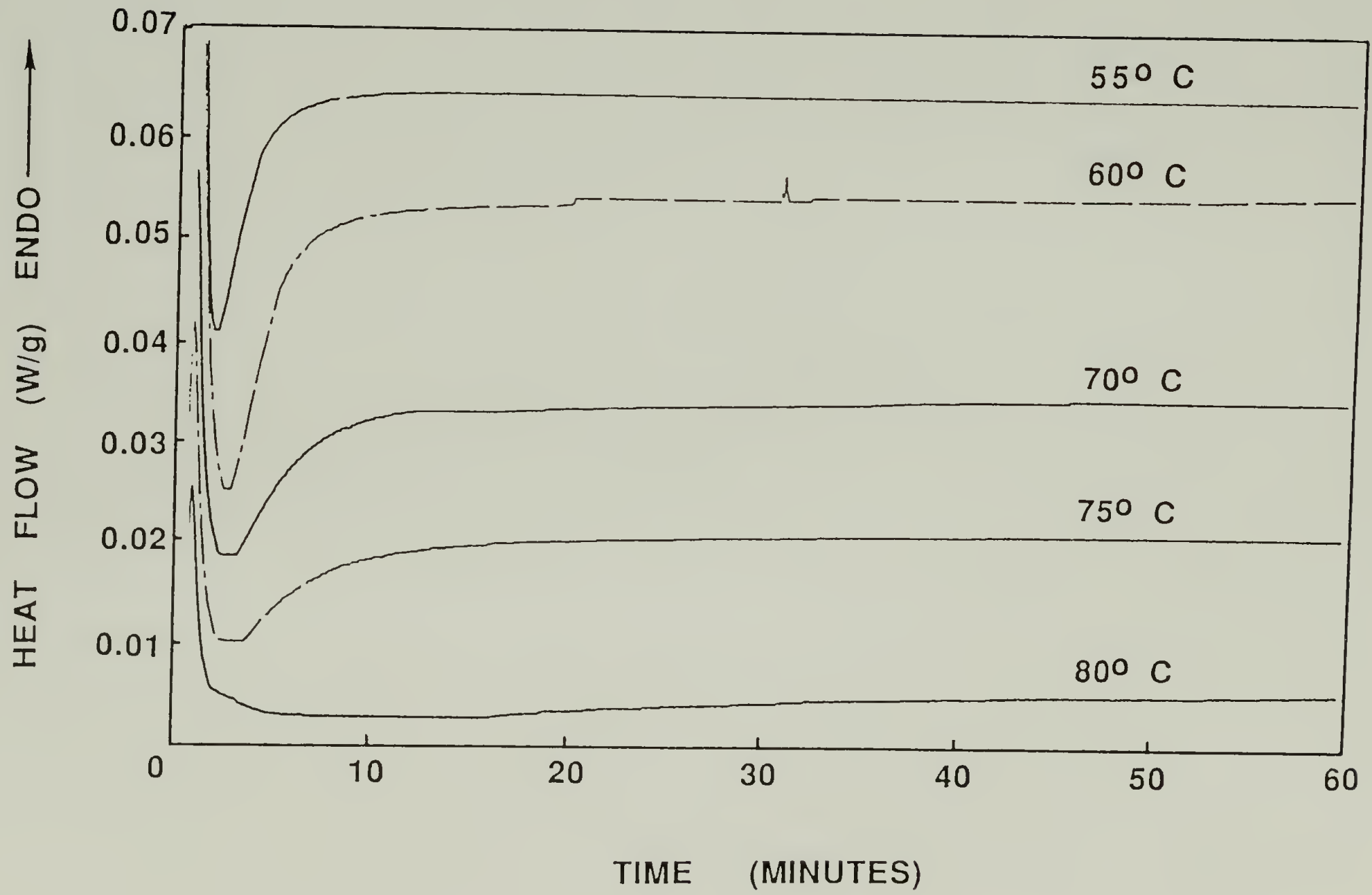
0.07
0.06
0.05
0.04
0.03
0.02
0.01
0
HEAT FLOW (W/g) ENDO
55° C
60° C
70° C
75° C
80° C
10
20
30
40
50
60
TIME (MINUTES)

FIGURE 3.17 Fractional phase separation, $\phi(t)$, as a function of isothermal (70°C) phase separation time; $\phi(t)$ is obtained as $\frac{I(t)-I(0)}{I(\infty)-I(0)}$ where $I(t)$ is the absorbance of 1730 cm^{-1} component for the FTIR data and exothermic energy evolved up to time t for the DSC data.

PHASE SEPARATION KINETICS AT 70 DEG. C

= COMPARISON BETWEEN IR AND DSC =

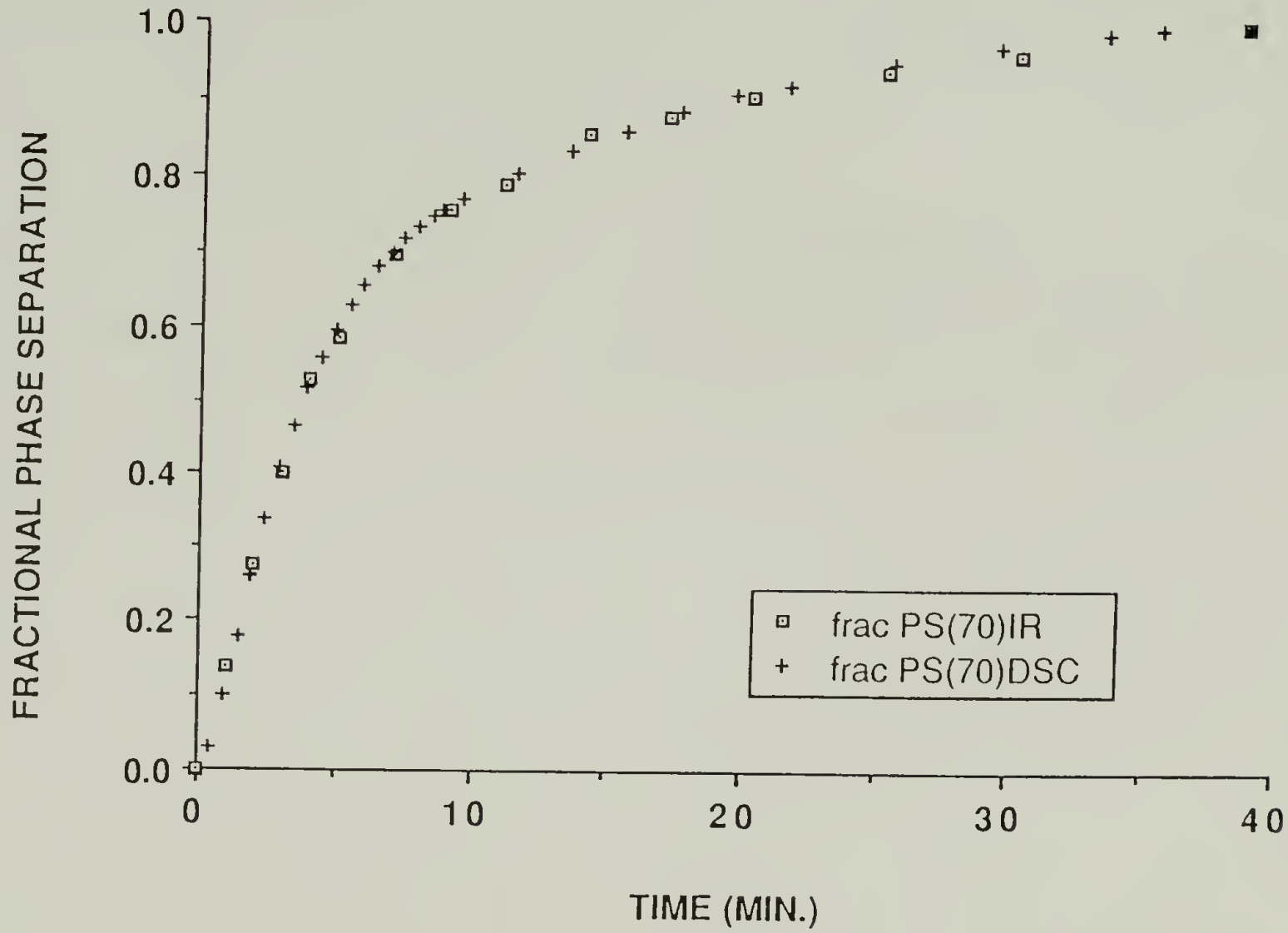

the hard segments and the DSC technique measures the energy generated by the formation of hydrogen bonding, it is not unexpected to have consistent results between the two techniques.

Conclusion

The phase separation kinetic data shown in Figure 3.10 is one of the first complete sets of experimental work for the segmented polyurethanes. Furthermore, the infrared phase separation kinetic data are supported with DSC data. Even though the wide angle x-ray scattering (WAXS) pattern shows no crystallinity in the B2 polyurethane, the exothermic peak observed during isothermal phase separation indicates that the formation of new segmental interactions, mainly hydrogen bonding, can be detected. Care must be exercised in carrying out the phase separation kinetic experiment since the exothermic peak is very small. In the case of the phase separation without formation of strong secondary bonds, the signal is expected to be even smaller. This makes the thermal analysis for direct observation of the phase separation process extremely difficult.

From the N-H stretching regions (Figure 3.8), it was clearly demonstrated that the interaction between hard segment and soft segment is gradually replaced by the interaction between hard segments during phase separation. It indicates a strong correlation between the macroscopic

phase transformation and the microscopic, molecular interaction in the case of polyurethanes.

The phase separation mechanism has also been discussed.[29] Our spectroscopic data do not seem to satisfy the linearized Cahn-Hilliard spinodal decomposition equation (Equation 3.9). It is well known that a spontaneous phase separation may not be possible, even for the unstable region in the temperature-composition phase diagram, if high interfacial energy is required.[34] In the case of segmented polyurethanes, high coherent interfacial energy is required due to the connectivity of the chains which run through the multiple soft and hard domains. The lack of a spinodal mechanism over a wide range of temperature in this case, therefore, may be due to the high interfacial energy. To reach a concrete conclusion, we need additional experimental data as well as theoretical development which shows the effect of high interfacial energy on the spinodal decomposition mechanism for segmented block copolymers.

The phase separation kinetic data have been analyzed in terms of the nucleation and growth mechanism. The overall data appear to show good linear relationship as predicted by the conventional Avrami type equation. The model for the domain morphology has been suggested as a growing two dimensional lamellar.

The nucleation and growth mechanism was found to change during the phase separation. The separation rate is significantly retarded at the later stage (second half) of

the phase separation. The diffusion controlled mechanism is believed to become the dominant factor in controlling the phase separation rate at the later stage resulting in the significant reduction of the phase separation rate.

References

1. Brunette, C.M.; Hsu, S.L.; Rossman, M.; MacKnight, W.J.; Schneider, N.S. *Polym.Engr.Sci.* **1981**, 21, 668.

2. Wilkes, G.L.; Emerson, J.A. *J.Appl.Phys.* **1976**, 47, 4261.

3. Miller, J.A.; Lin, S.B.; Hwang, K.K.S.; Wu, K.S.; Gibson, P.E.; Cooper, S.L. *Macromolecules* **1985**, 18, 32.

4. Hashimoto, T.; Sasaki, K.; Kawai, H. *Macromolecules* **1984**, 17, 2812.

5. Nishi, T.; Wang, T.T.; Kwei, T.K. *Macromolecules* **1975**, 8, 227.

6. Snyder, H.L.; Meakin, P.; Reich, S. *Macromolecules* **1983**, 16, 757.

7. Kwei, T.K. *J.Appl.Polym.Sci.* **1982**, 27, 2891.

8. Camberlin, Y.; Pascault, J.P. *J.Polym.Sci.-Phys.* **1984**, 22, 1835.

9. Wilkes, G.L.; Wildnauer, R. *J.Appl.Phys.* **1975**, 46, 4148.

10. Boyarchuk, Y.M.; Rappoport, L.Y.; Nikitin, V.N.; Apukhtina, N.P. *Polym.Sci. USSR* (English Transl.) **1965**, 7, 859.

11. Yokoyama, T. "Adv. in Urethane Sci.Technol." **1975**, 6, 1; Frisch, K.C., Reegen, S.L. Eds., Technomic Pub., USA.

12. Coleman, M.M.; Lee, K.H.; Skrovanek, D.J.; Painter, P.C. *Macromolecules* **1986**, 19, 2149.

13. Lee, H.S.; Wang, Y.K.; Hsu, S.L. *Macromolecules* **1987**, 20, 2089.

14. Lee, H.S.; Wang, Y.K.; MacKnight, W.J.; Hsu, S.L. *Macromolecules* **1988**, 21, 270.

15. Chee, K.K.; Farris, R.J. *J.Appl.Polym.Sci.* **1984**, 29, 2529.

16. Hoffman, J.D.; Weeks, J.J. *J.Chem.Phys.* **1962**, 37, 1723.

17. Sanchez, I. *J.Macromol.Sci.-Revs.* **1974**, C10, 113.

18. Avrami, M *J.Chem.Phys.* **1939**, 7, 1103.

19. Avrami, M *J.Chem.Phys.* **1940**, 8, 212.

20. Cahn, J.W. *Trans.TMS-AIME* **1968**, 242, 166.

21. Skrovanek, D.J.; Howe, S.E.; Painter, P.C.; Coleman, M.M. *Macromolecules* **1985**, 18, 1676.

22. Tsubomura, H. *J.Chem.Phys.* **1956**, 24, 927.

23. Skrovanek, D.J.; Howe, S.E.; Painter, P.C.; Coleman, M.M. *Macromolecules* **1985**, 18, 1676.

24. Christenson, C.P.; Harthcock, M.A.; Meadow, M.D.; Spell, H.L.; Howard, W.L.; Creswick, M.W.; Guerra, R.E.; Turner, R.B. *J.Polym.Sci.-Phys.* **1986**, 24, 1401.

25. Koberstein, J.T.; Gancarz, I. *J.Polym.Sci.-Phys.* **1986**, 24, 2487.

26. Skrovanek, D.J.; Painter, P.C.; Coleman, M.M. *Macromolecules* **1986**, 19, 699.

27. Suzuki, S.; Iwashita, Y.; Shimanouchi, T.; Tsuboi, T. *Biopolymers* **1966**, 4, 337.

28. Hashimoto, T.; Shibayama, M.; Kawai, H. *Macromolecules* **1983**, 16, 1093.

29. Miller, J.A.; Pruckmayr, G.; Epperson, E.; Cooper, S.L. *Polymer* **1985**, 26, 1915.

30. Miller, J.A.; Cooper, S.L.; Han, C.C.; Pruckmayr, G. *Macromolecules* **1984**, 17, 1063.

31. Cahn, J.W. *J.Chem.Phys.* **1965**, 42, 93.

32. Hilliard, J.E. "Phase Transformations" ASM, Ohio, **1970**.

33. Pimentel, G.C.; McClellan, A.L. "The Hydrogen Bond" W.H.Freeman, San Francisco, **1960**.

34. Hilliard, J.E. "Phase Transformations" Chap.12 M.Cohen Ed. ASM, **1968**.

CHAPTER IV

A SPECTROSCOPIC STUDY ON THE DOMAIN MISCIBILITY OF THE VARIOUS POLYURETHANES

Introduction

There has been aN extensive study on the phase separation of multicomponent polymer systems including any combination of homopolymers,[1-3] random or alternating block copolymers[4-6] and even segmented block copolymers.[7-10] Since phase diagrams of some of the systems are well characterized, structure of individual phase after phase separation is well documented. In a homopolymer blend, information such as the composition of each phase and amount of each component can be calculated from the phase diagram.[11] For the copolymers, main emphasis has been the characterization of the domain structure and the phase diagram is often constructed to show the domain structure as a function of temperature and composition.[12,13] Each phase is usually assumed to be almost pure because of the highly incompatible components. Furthermore, the high interfacial energy and significant difference in solubility parameter yields a high positive interaction parameter between the components of the copolymer making incomplete phase separation extremely difficult to achieve.

In the case of polyurethanes, which contain various chemical species for hard segments as well as soft segments, the degree of interaction between components can be varied over a broad spectrum range. The interaction between hard segments and soft segments for polyether based polyurethane is, for example, expected to be fairly different from that for butadiene based polyurethanes. Therefore, not only the structure of each phase but also the degree of phase mixing have to be characterized in the case of the polyurethane system having a strong interaction between the two components.

Infrared spectroscopy is a extremely useful technique to characterize the functional group of each component. The information obtained is related only to the local environment of the segments. By observing the spectroscopic change of each phase or each segment as a function of structural transformation, information of each phase can be obtained.

It is generally accepted that the heterogeneous domain structure of polyurethanes is stabilized by the formation of hydrogen bonding between hard segments. If polyethers or polyesters is used as soft segments, hydrogen bonding between hard and soft segments is also possible.[14,15] Since the relative amount of hydrogen bonding between hard segments to that between hard and soft segments is directly related to the degree of phase separation, information regarding the degree of phase separation can be obtained from the infrared spectrum.

In this chapter, unique spectroscopic observations, which can be used to assess the phase homogeneity at different temperatures, are presented and the results are discussed for three different polyurethane samples.

Experimental

There has been extensive characterization for the samples used here.[16-18] B2 (B4) polyurethane contains three (five) MDI (methylene bis(phenyl isocyanate) and two (four) butanediol (BDO) units per each hard segment. As a soft segment, polypropylene oxide is used. The chemical structure of the B2 and B4 polyurethanes are shown in Figure 2.2.

For the hard segment of the butadiene based polyurethane, TDI (toluene diisocyanate), (which is a mixture of the 2,4 and 2,6 isomers having a 80:20 mole ratio) was used with butanediol chain extender. The polymerization was done in solution to ensure the homogeneous mixing of the components. The mole ratio of TDI: BDO: polybutadiene is 3.3: 2.3: 1. The polybutadiene prepolymer has a molecular weight of 2200 and a polydispersity of 1.2. The polybutadiene has about 65% 1,2 vinyl and 35% 1,4 addition configuration. The chemical structure of the butadiene based polyurethane is shown in Figure 4.1. Detailed synthetic procedure can be found elsewhere.[19]

The polymers were dissolved in THF solvent (2% w/v) before they were cast onto AgCl windows. The cast film was

HARD SEGMENT

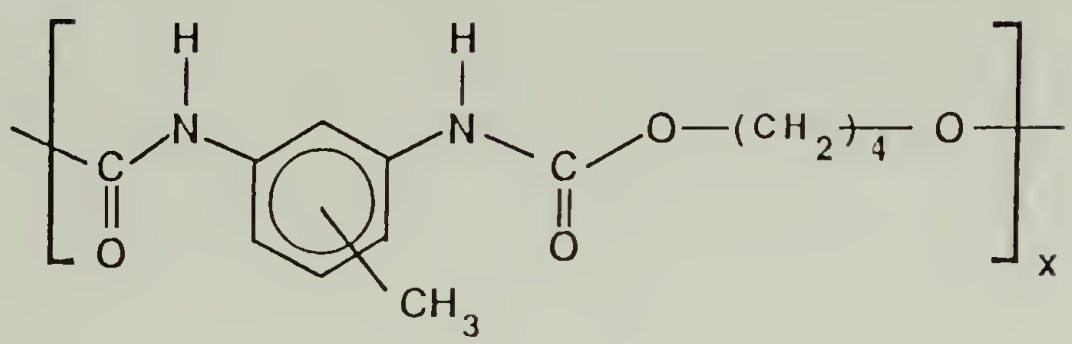

SOFT SEGMENT

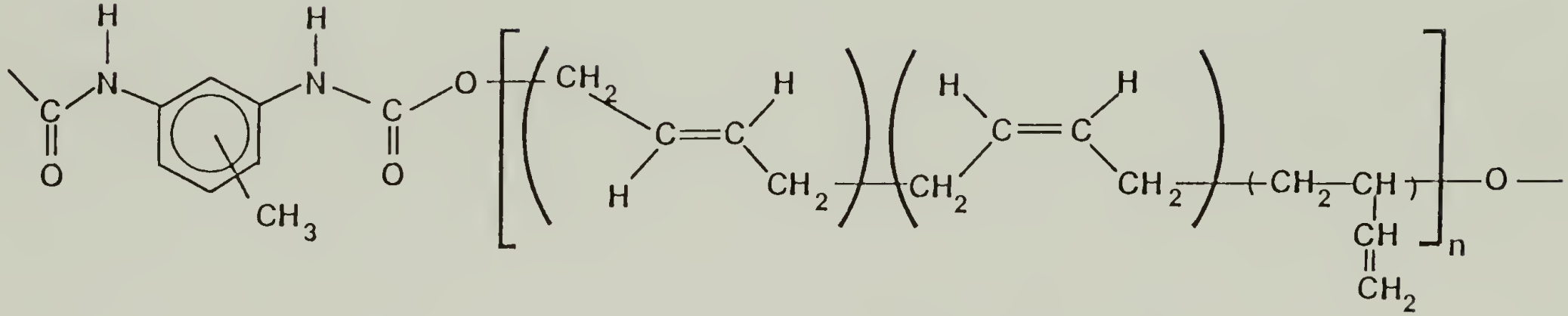

FIGURE 4.1 Schematic drawings of the hard and soft segments of the butadiene based polyurethanes.

dried at the atmospheric condition for several hours followed by vacuum drying for several days at room temperature. All the infrared spectra were obtained with IBM model 98 vacuum infrared spectrometer. A special cell is designed for heating and quenching the sample inside the spectrometer. Temperature control cell diagram and the temperature history for heating and quenching are shown in Figures 2.3 and 2.4, respectively.

Results and Discussion

The free energy change, ΔG_s, upon phase separation of segmented polyurethanes can be expressed as

$$\Delta G_s = \Delta H_s - T\Delta S_s \qquad (4.1)$$

where ΔH_s and ΔS_s are ethalic and entroic contribution associated with the phase separation, respectively. Phase separated structure of polyurethanes are mainly due to the incompatibility between the two components, i.e. hard and soft segments.[20,21] Furthermore, the heterogeneous structure of polyurethanes is stabilized by favorable interactions such as hydrogen bonding between hard segments. At room temperature, the enthalpic contribution of the hard segment interaction to the free energy is enough to compensate for the entropic loss resulting from the phase separation. Since the entropic contribution to the free energy increases with temperature, the heterogeneous structure becomes thermodynamically unstable at high temperatures.

It has been found that the radius of gyration scales with the molecular weight by 2/3 power in the case of polystyrene and polyisoprene diblock copolymer.[22] It indicates that the chain in diblock copolymer has a somewhat extended conformation. In the case of soft segment of which two hard segments at both ends are incorporated in the rigid hard domain, the conformation of the soft chains is more extended than the diblock copolymer.[23] This extended conformation of the soft segment will exert increased entropic retractice force on the hard segments, especially at the elevated temperature. The phase mixing of polyurethane at the increased temperature is, therefore, facilitated by that entropic driving force.

The two types of polyurethanes being used in this study have a distinctively different chemical structure. In the instance of the butadiene based polyurethane, there is no strong interaction between hard and soft segments. However, for the polypropylene oxide based B2 and B4 polymers, the hydrogen bonding between hard segment and soft segment is possible through the ether functional group of the soft segment and N-H of the urethane functional group. Therefore, the phase mixing behavior of the polypropylene oxide based polyurethane at elevated temperatures is expected to be very different from that of the polybutadiene based polyurethanes.

In Figure 4.2, the N-H stretching regions of the infrared spectrum of four different samples are shown. The dotted spectra are obtained at room temperature and are used

FIGURE 4.2 N-H stretching regions of four different samples at high and quenched states; (a) B2 (b) B4 quenched from 185°C (c) B4 quenched from 210°C (d) Polybutadiene and TDI based polyurethane; Dotted spectra are obtained at room temperature and used as reference.

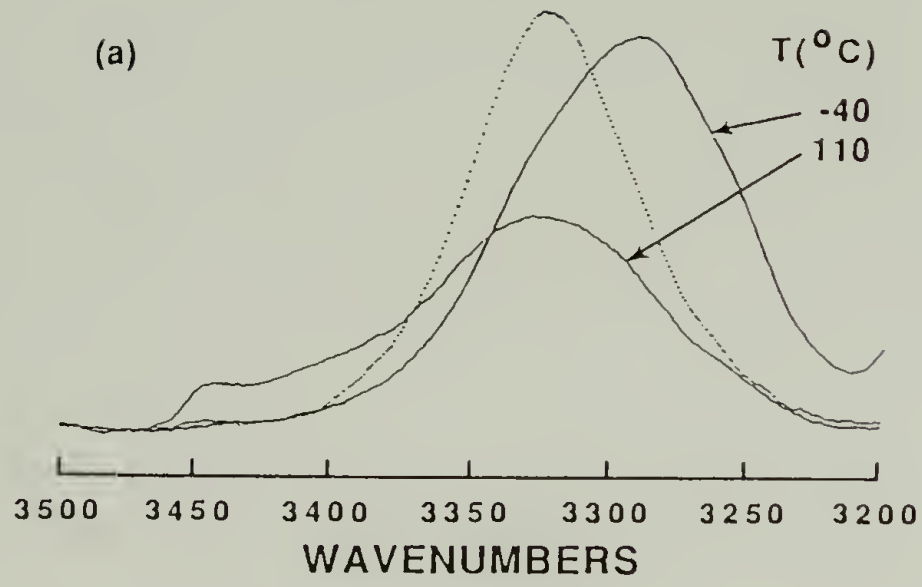
(a)
T(°C)
-40
110
3500 3450 3400 3350 3300 3250 3200
WAVENUMBERS

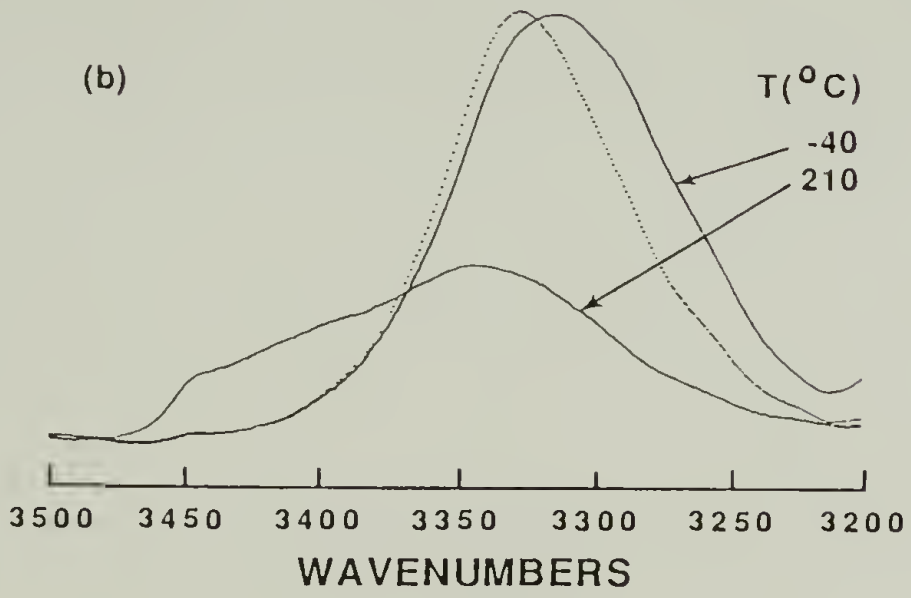
(b)
T(°C)
-40
210
3500 3450 3400 3350 3300 3250 3200
WAVENUMBERS

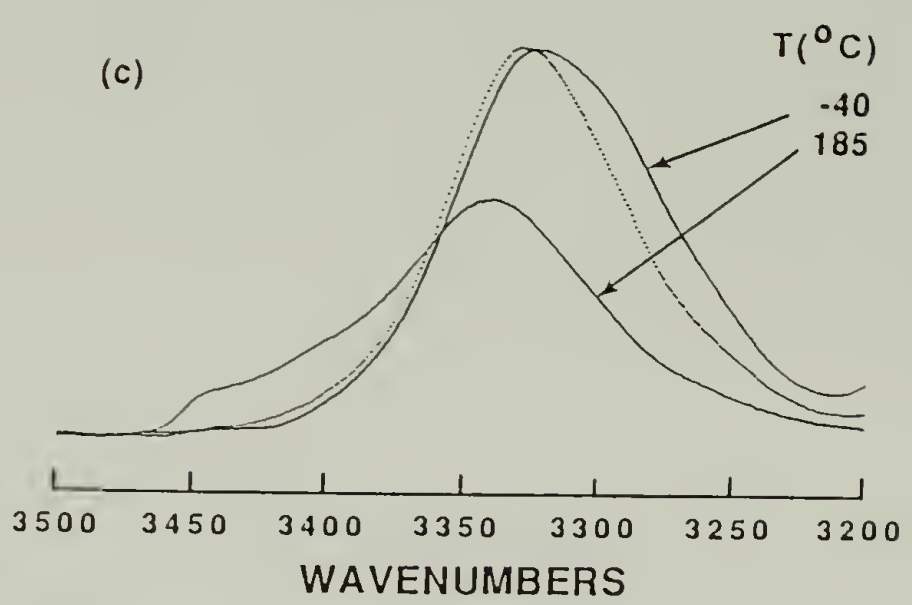
(c)
T(°C)
-40
185
3500 3450 3400 3350 3300 3250 3200
WAVENUMBERS

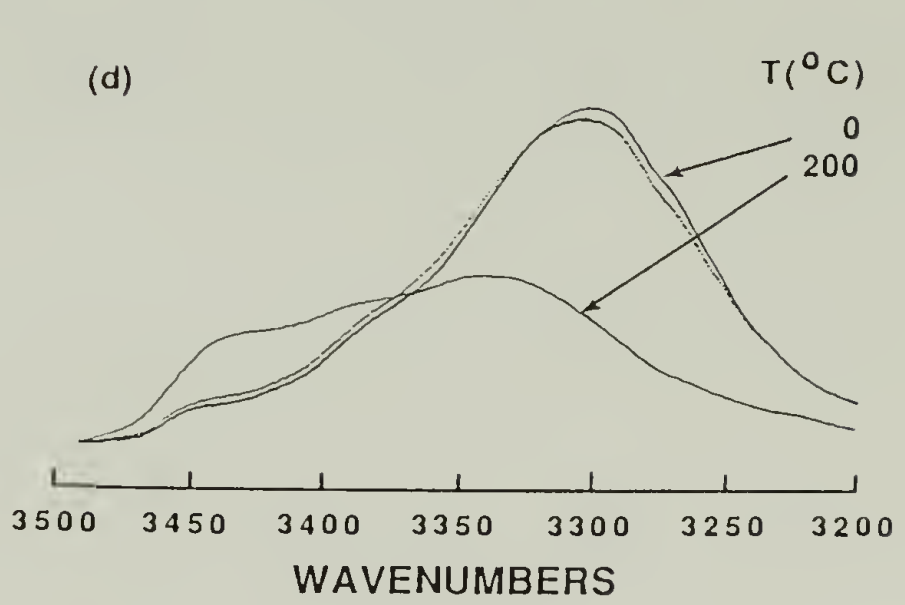
(d)
T(°C)
0
200
3500 3450 3400 3350 3300 3250 3200
WAVENUMBERS

as the reference spectrum. The temperature is initially increased above the hard domain dissociation temperature to break most of the hydrogen bonding between hard segments. The high temperature spectrum is also shown. The sample is then rapidly quenched below the glass transition temperature of the soft segment to preserve the high temperature structure. The low temperature spectra are also displayed in the figures.

The changes observed in the N-H stretching region at elevated temperatures are very similar for all samples and discussions regarding the first sample (B2 polyurethane) can be found in Chapter II. Upon heating, the peak around 3330cm^{-1}, which is assigned to be the N-H group hydrogen bonded to the carbonyl group, loses most of its intensity while the peak at 3450cm^{-1} which is due to the free N-H group increases in intensity. The intensity change is adequately explained by the breaking or weakening of hydrogen bond at elevated temperatures. The unbalance of the intensity redistribution is also easily understood by the significantly different extinction coefficient between the two groups, i.e., free and hydrogen bonded N-H groups.[24,25] The extinction coefficient of the hydrogen bonded N-H group is extremely sensitive not only to the distance between the hydrogen donor and acceptor but also to the geometry of the hydrogen bond.[26,27]

The spectra obtained by quenching the high temperature structure show characteristic features of each sample.

First, the N-H region of the B2 sample at low temperature (refer to Figure 4.2a) shows high absorbance at 3295cm^{-1}; which is due to the N-H group hydrogen bonded to the ether oxygen of the soft segments.[17] The complete disappearance, upon quenching, of free N-H component at 3450cm^{-1}, which is due to the formation of the hydrogen bonding between N-H group in the soft matrix and the ether group of the soft segments, strongly supports the phase mixed state at high temperature. A more careful discussion about the B2 sample can be found in Chapter II.

The low temperature behavior of the butadiene based polyurethane (Figure 4.2d) is totally different from that of the polyether based polyurethanes. Upon quenching, the spectrum returns back to the room temperature spectrum indicating that butadiene based polyurethane has the similar phase status at high temperature as at room temperature. In other words, the polybutadiene based polyurethane seems to exist as a phase separated state even above the hard domain dissociation temperature. More supporting evidence will be shown later in the carbonyl stretching region. Even though the spectrum of this sample at -80°C is slightly distorted by ice condensation, it is essentially the same as the spectrum at 0°C in Figure 4.2d. The zero degree spectrum is, therefore, believed to be characteristic of the very low temperature spectrum.

The N-H regions of the B4 samples quenched from two different temperatures are shown in Figures 4.2b and 4.2c.

The contribution of the 3295cm^{-1} peak at the low temperature seems to be higher for the sample quenched from the higher temperature, i.e. 210°C. That is indicative of a more phase mixed state at an even higher temperature. Since the melting transition of the B4 sample is known to be 175°C,[16] the results indicate that this polyurethane does not exist as a grossly phase mixed state even above the melting transition. The degree of phase mixing, however, seems to increase as the temperature increases well above the melting transition temperature.

The carbonyl stretching region in Figure 4.3 strongly supports the results obtained from the N-H stretching region. Upon quenching the B2 sample (Figure 4.3a), the peak at 1730cm^{-1}, which is assigned to carbonyl group free of hydrogen bonding, remains as a dominant peak. Since the peak intensity at 1730cm^{-1} is directly related to the amount of the carbonyl group in the soft matrix, this again indicates a highly phase mixed state at a high temperature.

The carbonyl spectrum of the polybutadiene based polyurethane at low temperature (Figure 4.3d) is completely opposite to the B2 sample. The dominant peak upon quenching is observed at 1700cm^{-1} which is assigned to carbonyl group hydrogen bonded to the N-H group. The close similarity between the room temperature spectrum and quenched spectrum once again indicates the phase separated state of this sample above the first order transition temperature.

FIGURE 4.3 C=O stretching regions of Figure 4.2; Dotted spectra are obtained at room temperature and used as reference.

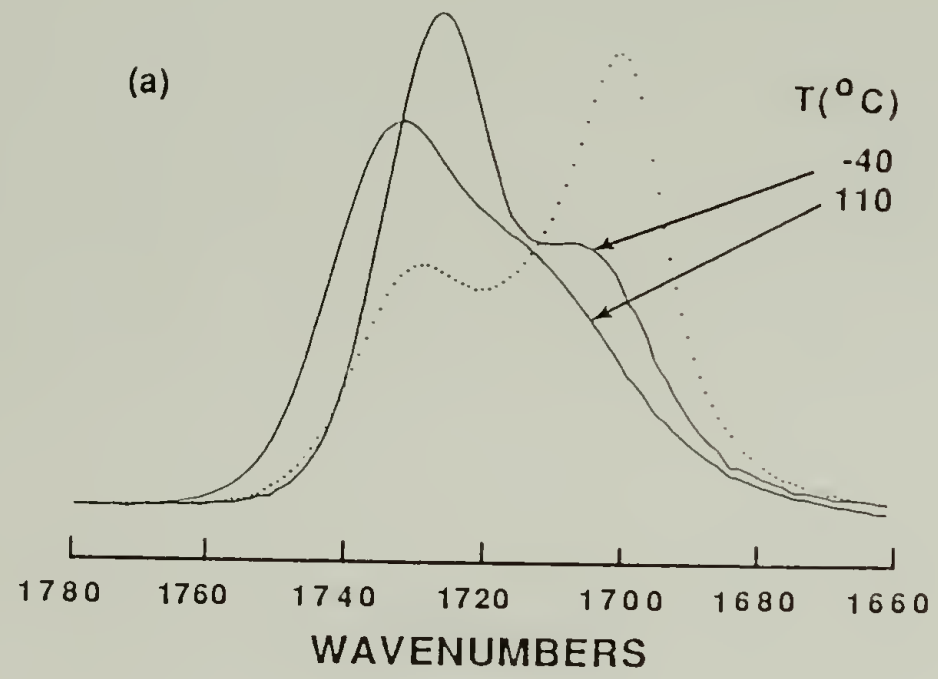
(a)
T(°C)
-40
110
1780
1760
1740
1720
1700
1680
1660
WAVENUMBERS

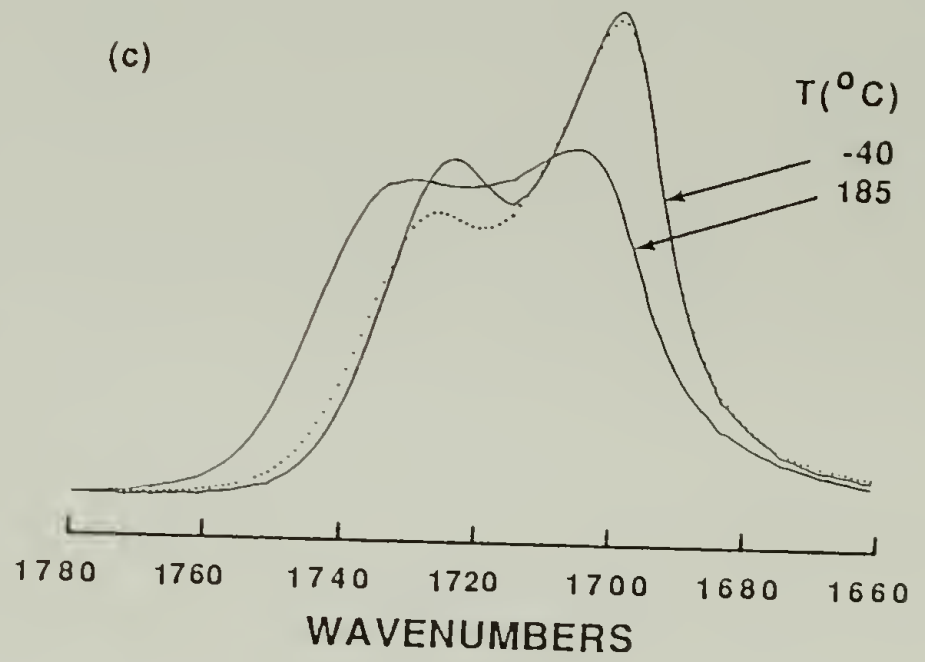
(c)
T(°C)
-40
185
1780
1760
1740
1720
1700
1680
1660
WAVENUMBERS

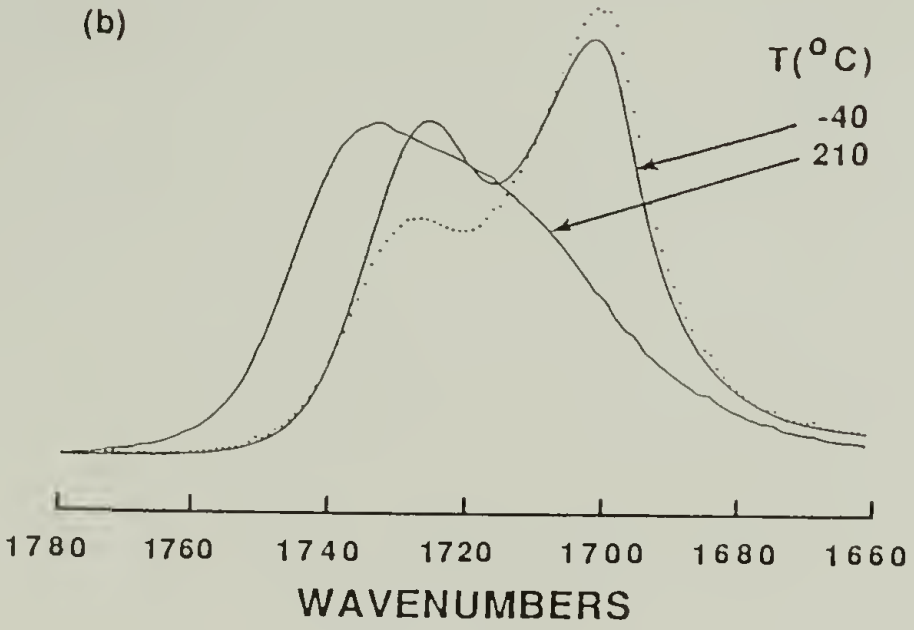
(b)
T(°C)
-40
210
1780
1760
1740
1720
1700
1680
1660
WAVENUMBERS

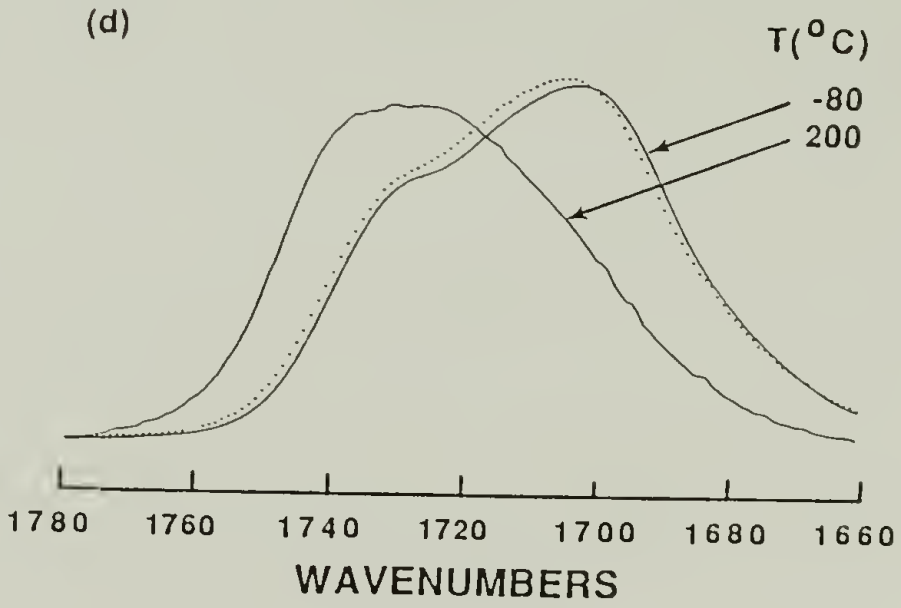
(d)
T(°C)
-80
200
1780
1760
1740
1720
1700
1680
1660
WAVENUMBERS

The carbonyl regions of the B4 samples are shown in Figures 4.3b and 4.3c. The relative intensity of the free carbonyl peak to the hydrogen bonded peak is larger for the B4 sample quenched from the higher temperature. This again confirms the increased phase mixed state at the higher temperature (210°C), even though both temperatures are above the melting transition.

In Figures 4.2 and 4.3, the degree of phase mixing decreases from a to d. Above the first order transition temperature, the B2 sample shows a highly phase mixed state whereas polybutadiene based polyurethane exists as a phase separated state. The B4 samples show intermediate properties depending on the highest temperature to which they have been subjected during the heating process.

By increasing the temperature of the samples which are quenched from a high temperature, it is shown in Figure 4.4 that the phase separation process is taking place. The N-H stretching regions are shown in Figure 4.4, where phase separation is taking place as an increasing function of temperature. It was demonstrated in Chapter II that a N-H···ether component is transformed into a N-H···O=C component during phase separation. The N-H···ether component at 3295cm^{-1} is decreasing while the N-H···O=C component at 3330cm^{-1} is increasing during phase separation for the B2 & B4 samples. Such phenomenon is most obvious for the B2 sample (Figure 4.4a) because it has the most complete phase mixing in a quenched state. B4 polymers (Figures 4.4b and

FIGURE 4.4 N-H stretching regions during phase separation as a increasing function of temperature from a quenched state; Samples are same as Figure 4.2; Dotted spectra are obtained at room temperature and used as reference.

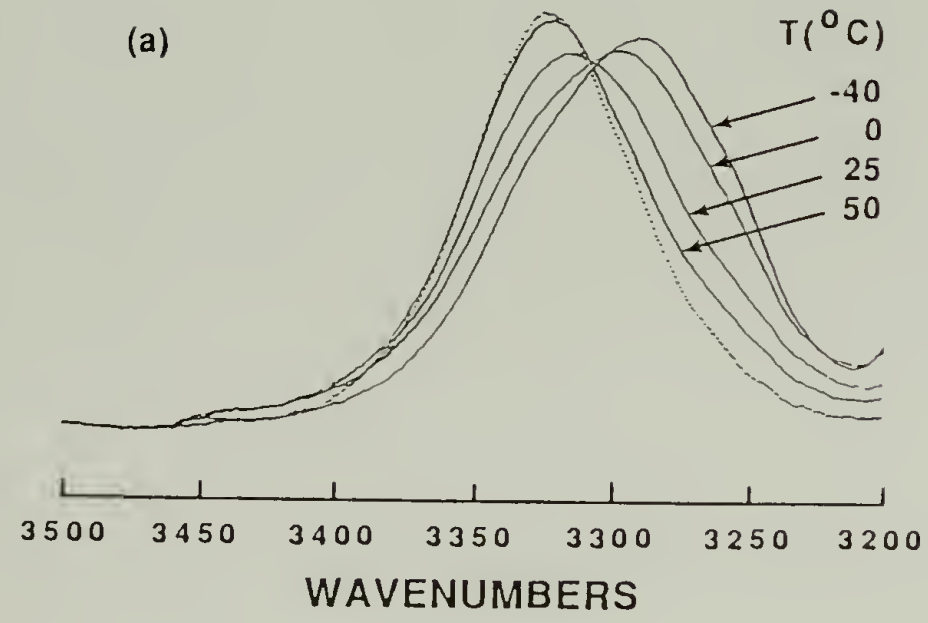
(a)
T(°C)
-40
0
25
50
3500 3450 3400 3350 3300 3250 3200
WAVENUMBERS

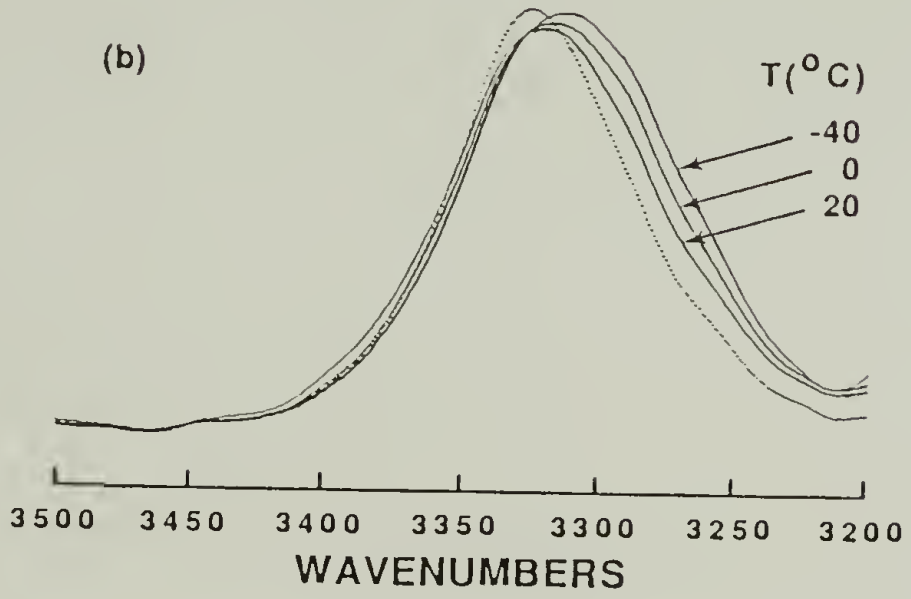
(b)
T(°C)
-40
0
20
3500 3450 3400 3350 3300 3250 3200
WAVENUMBERS

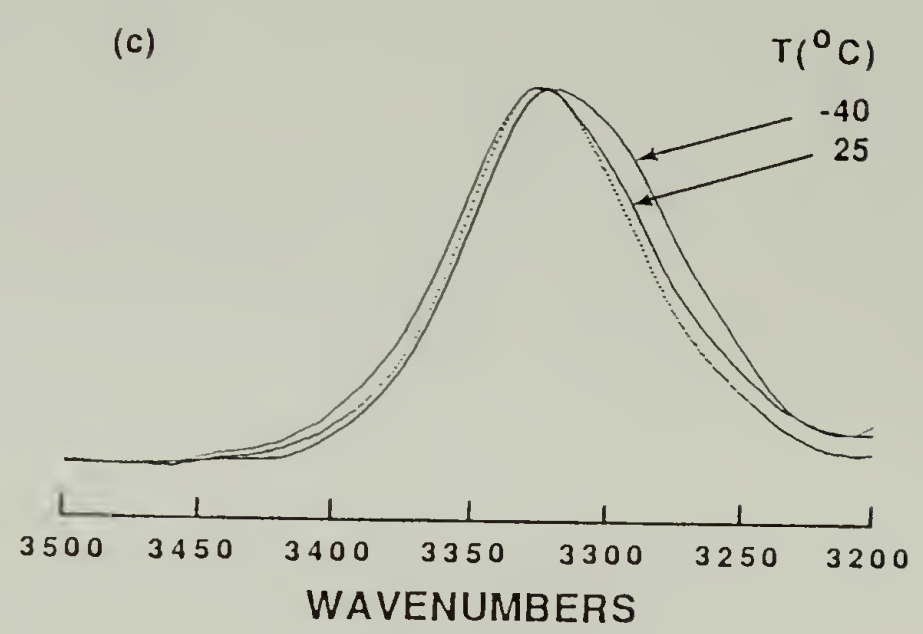
(c)
T(°C)
-40
25
3500 3450 3400 3350 3300 3250 3200
WAVENUMBERS

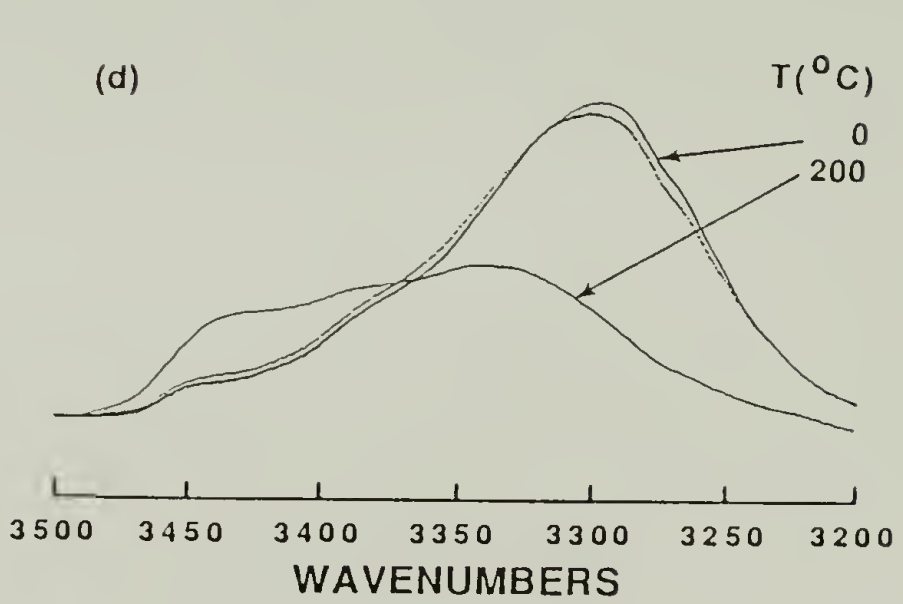
(d)
T(°C)
0
200
3500 3450 3400 3350 3300 3250 3200
WAVENUMBERS

4.4c) show a similar tendency even though their magnitude is smaller than B2 polymer. The decrease of the 3295cm^{-1} component for the B4 sample is only observed as a decreasing shoulder at that frequency. For the polybutadiene based sample, the N-H spectrum shows little change during that heating cycle up to ambient temperature.

In Figures 4.5a,b,c, the frequency change of the N-H stretching band during phase separation of the quenched sample is shown with the reference state of which frequency is obtained by slowly cooling without phase mixing. Since the increased phase mixing for polyether based polyurethanes gives a high absorbance at 3295cm^{-1}, it tends to decrease the maximum frequency of the N-H stretching peak. The deviation from the linear line in Figure 4.5, therefore, should be related to the degree of phase mixing.

For the B2 sample in Figure 4.5a, the quenched sample shows a highly phase mixed state at ~-40^{o}C. The phase separation takes place as the temperature increases up to 50^{o}C where almost complete phase separation is obtained. Figure 4.5a also shows that the B2 sample starts to phase-mix at around 95^{o}C at which time the frequency tends to deviate from the linear line. This result is again consistent with the thermal analysis data which shows the hard domain dissociation temperature at 98^{o}C.[16]

For the B4 material quenched from two different temperatures, the different degree of phase mixing is quite obvious from Figure 4.5b. The B4 polymer quenched from 185^{o}C

FIGURE 4.5 N-H stretching frequency change during phase separation from the quenched state; Linear data points are obtained by slowly cooling the sample from the room temperature.
(a) B2
(b) B4
(c) Polybutadiene based polyurethane

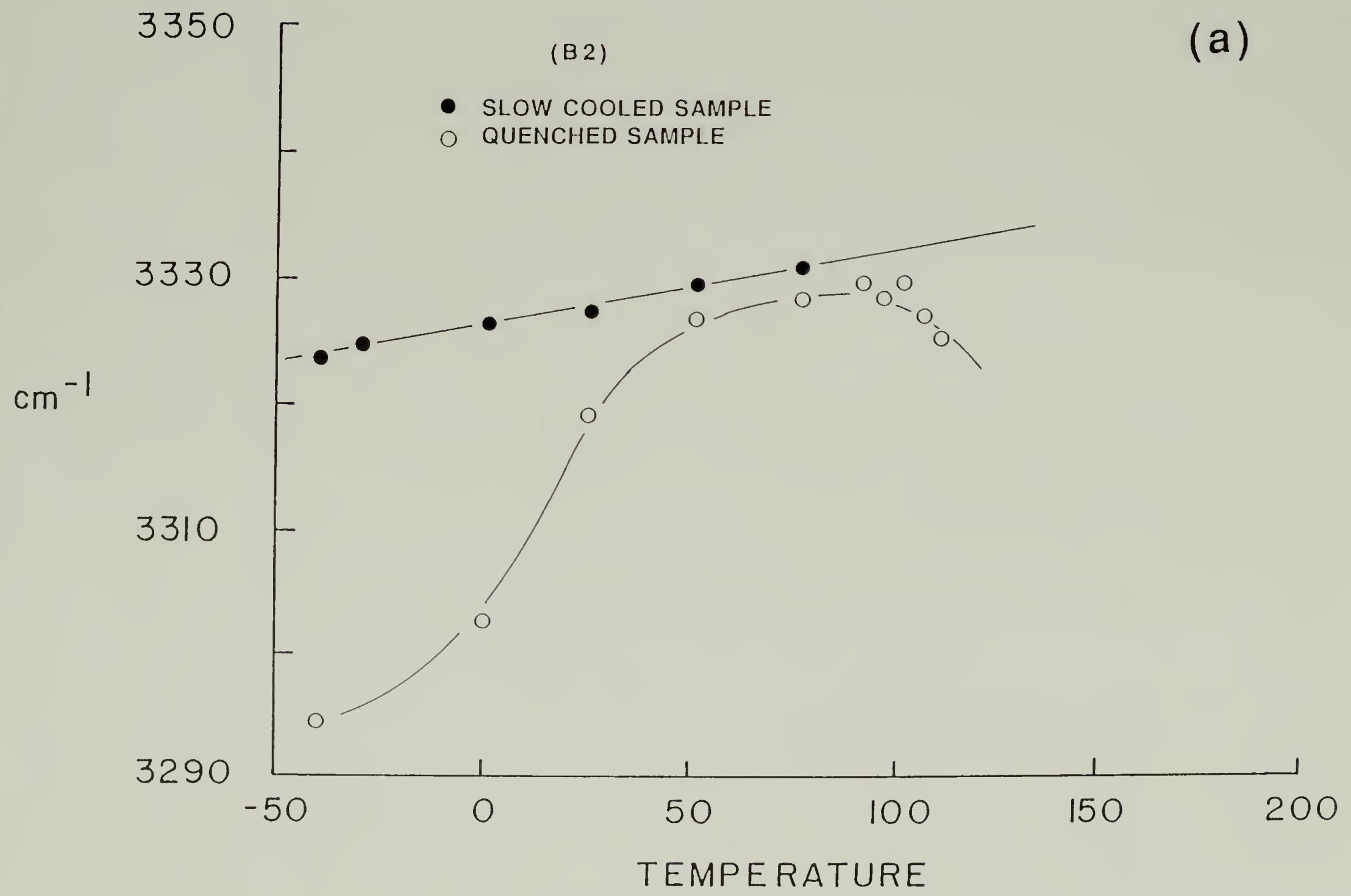
(a)
(B2)
SLOW COOLED SAMPLE
QUENCHED SAMPLE
3350
3330
3310
3290
cm⁻¹
-50
0
50
100
150
200
TEMPERATURE

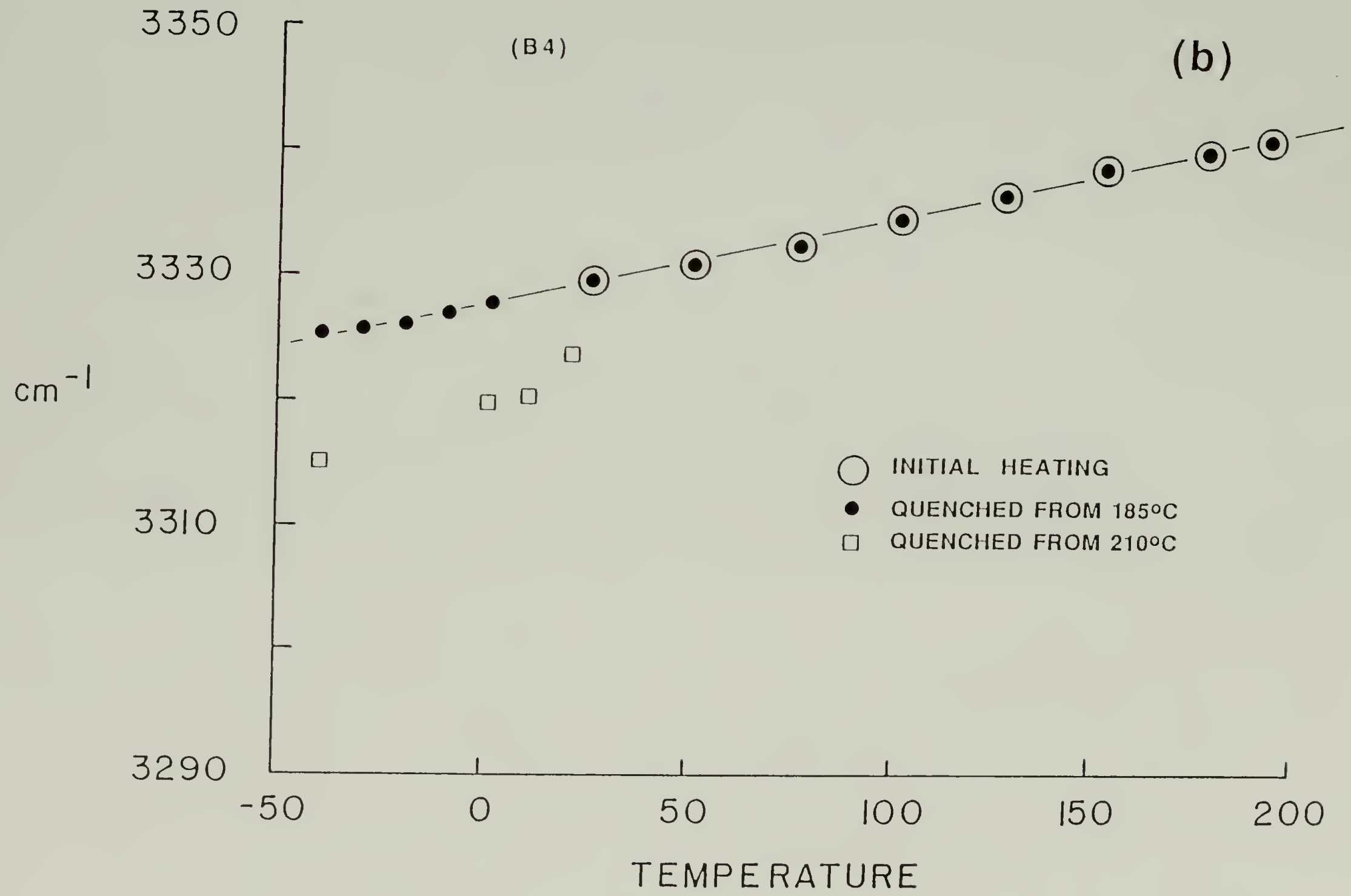
(B4)
(b)
3350
3330
3310
3290
cm⁻¹
-50
0
50
100
150
200
TEMPERATURE
INITIAL HEATING
QUENCHED FROM 185°C
QUENCHED FROM 210°C

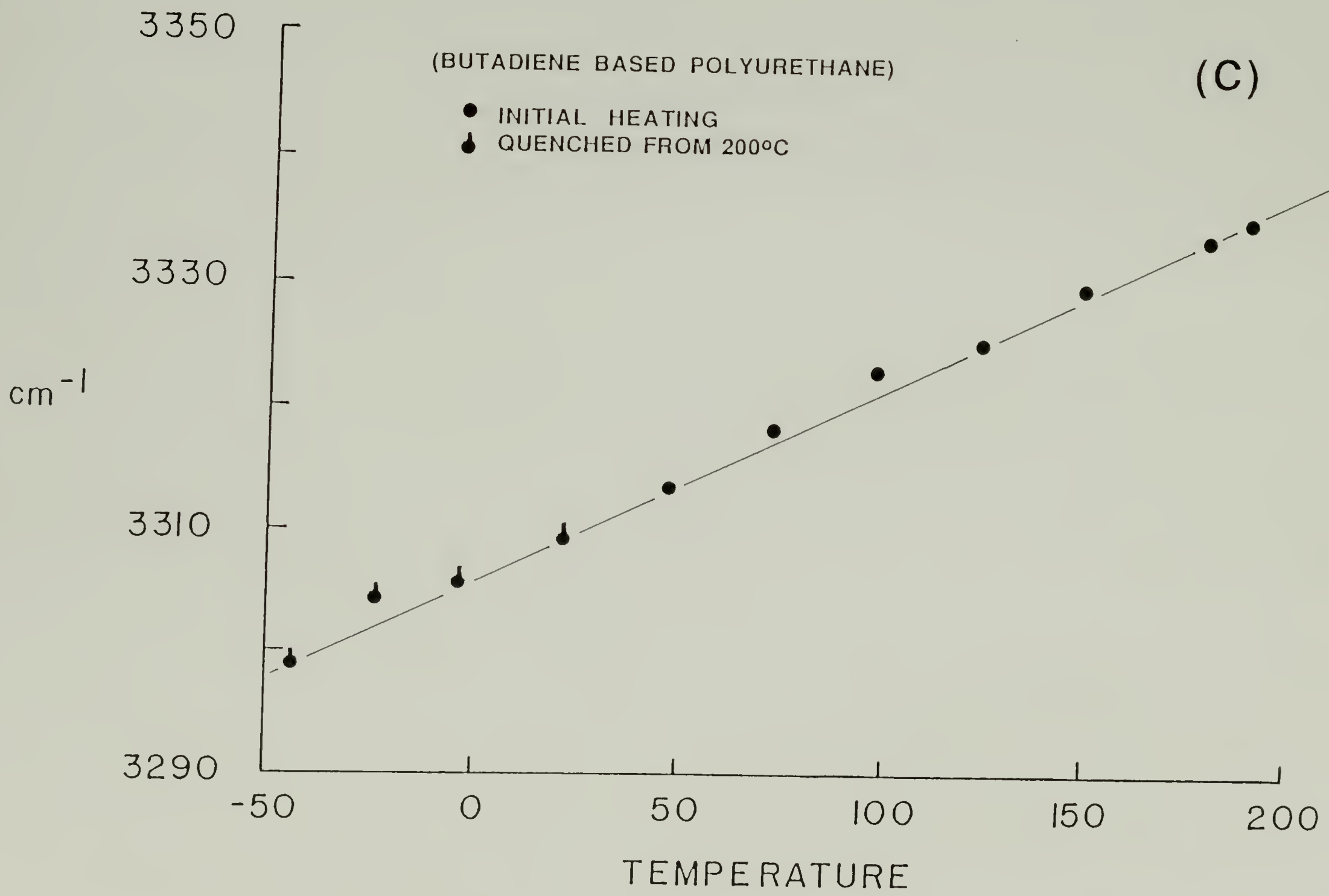
(BUTADIENE BASED POLYURETHANE)
(C)
INITIAL HEATING
QUENCHED FROM 200°C
3350
3330
3310
3290
cm⁻¹
-50
0
50
100
150
200
TEMPERATURE

shows negligible amounts of frequency shift, whereas, the same sample quenched from 210°C shows an appreciable degree of a phase mixed state. It is to be noted that the initial heating cycle does not show any deviation from the linear relationship even though the temperature is above the melting temperature around 170°C. This is due to the unstable hydrogen bonding at that temperature. Since the polyether chain is extremely flexible due to the low rotational energy barrier, the hydrogen bonding between N-H groups and the flexible polyether chain becomes unstable at that high temperature. The frequency shift is, therefore, not observed at a high temperature (above 170°C) even though the degree of phase mixing is increased.

For butadiene based polyurethane (Figure 4.5c), all data stays on the same linear line regardless of whether it is quenched or slowly cooled. Results in Figure 4.5 are consistent with the explanation given previously about the degree of phase mixing at a high temperature.

Conclusion

In the case of the butadiene based polyurethane, no significant interactions between hard and soft segments are expected. Since the solubility parameter difference between hard segment (TDI and BD) and soft segment (butadiene) has been reported to be appreciable,[28] the existence of the phase

separated state even above the domain dissociation temperature is not unexpected.

Butadiene based polyurethanes have been carefully characterized by several investigators.[29-31] According to the DSC results, the glass transition temperature of the soft segment is only 8 degrees above the glass transition temperature of the homopolymer, indicating a completely phase separated state at room temperature.[29] The small difference can be explained by the hindered chain mobility due to copolymerization, not by the small amount of hard segments dissolved in the soft matrix. In some cases, the observation of two glass transitions corresponding to each phase is also a convincing evidence that a heterogeneous structure of the polybutadiene based polyurethanes exist. The results obtained support the phase separated structure not only at the room temperature observed previously, but also above the hard domain dissociation temperature.

The results for the B4 material indicate how sensitive the phase separation can be depending on the hard segment length. By nearly doubling the hard segment length from the B2 to B4 sample, the polyurethanes strongly resist to phase mixing even above the melting transition.

This study also shows the relationship between the phase separation and the interaction among the hard segments as well as among the hard and soft segments. Increasing cross interaction (interaction between hard segments and soft segments) by either decreasing hard segment length or using a

polyether soft segment as in the B2 sample, the phase mixing can be accomplished at a lower temperature. If the hard segments length is increased as in the B4 sample, more severe conditions have to be applied to achieve the phase mixing. When there is little cross interaction as in polybutadiene based polyurethanes, the phase mixing can be hardly obtained even above the hard domain dissociation temperature.

High temperature infrared spectra do not give enough information about the degree of phase mixing. Increased free carbonyl component at a high temperature is not a necessary condition for the phase mixing because the hydrogen bonding can become unstable at high temperatures without significant phase mixing. It is, therefore, necessary to preserve the high temperature structure by rapid quenching and to study the structure at a low temperature where all the possible hydrogen bonding becomes stable. The results obtained in this chapter once again demonstrate that Fourier transform infrared spectroscopy can be utilized to obtain the information about the domain homogeneity if the temperature quenching is fast enough to capture the high temperature structure.

References

1. Nishi,T.; Wang,T.T.; Kwei,T.K. *Macromolecules* **1975**, 8, 227.

2. Hashimoto,T.; Sasaki,K.; Kawai,H. *Macromolecules* **1984**, *17*, 2812.

3. Snyder,H.L.; Meakin,P.; Reich,S. *Macromolecules* **1983**, *16*, 757.

4. Leibler,L. *Makromol.Chem. Rapid Comm.* **1981**, 2, 393.

5. Cruz,M.O.; Sanchez,I.C. *Macromolecules* **1987**, 20, 440.

6. Jiang,M.; Cao,X.; Yu,T. *Polymer* **1986**, 27, 1917 and others 1923 and 1928.

7. Wilkes,G.L.; Emerson,J.A. *J.Appl.Phys.* **1976**, 47, 4261.

8. Wilkes,G.L.; Wildnauer,R. *J.Appl.Phys.* **1975**, 46, 4148.

9. Chee,K.K.; Farris,R.J. *J.Appl.Polym.Sci.* **1984**, 29, 2529.

10. Kwei,T.K. *J.Appl.Polym.Sci.* **1982**, 27, 2891.

11. Paul,D.R.; Newman,S. "Polymer Blends" Vol.1, Academic Press, New York **1978**.

12. Matsuo,M.; Sagaye,S. "Colloidal and Morphological Behavior of Block and Graft Copolymers" G.E. Molau Ed., Plenum, New York **1971**.

13. Leibler,L. *Macromolecules* **1980**, 13, 1602.

14. Yokoyama,T. "Adv. in Urethane Sci.Technol." **1975**, 6, 1; Frisch,K.C., Reegen,S.L. Eds., Technomic Pub., USA.

15. Tanaka,T.; Yokoyama,T.; Yukio,Y. *J.Polym.Sci.-A1* **1968**, 6, 2137.

16. Christenson,C.P.; Harthcock,M.A.; Meadows,M.D.; Spell,H.L.; Howard,W.L.; Creswick,M.W.; Guerra,R.E.; Turner,R.B. *J.Polym.Sci.-Phys.* **1986**, 24, 1401.

17. Lee,H.S.; Wang,Y.K.; Hsu,S.L. *Macromolecules* **1987**, 20, 2089.

18. Lee,H.S.; Wang,Y.K.; MacKnight,W.J.; Hsu,S.L. *Macromolecules* **1988**, 21, 270.

19. Bengston,B.; Feger,C.; MacKnight,W.J.; Schneider,N.S. *Polymer* **1985**, 26, 895.

20. Cooper,S.L.; Tobolsky,A.V. *J.Appl.Polym.Sci.* **1966**, 10, 1837.

21. Cooper,S.L.; West,J.C.; Seymour,R.W. "Encyclopedia of Polymer Science and Technology" Suppl.Vol.1, N.M.Bikales, M.Bickford Eds., Interscience Pub., New York, **1976**.

22. Hashimoto,T.; Shibayama,M.; Kawai,H. *Macromolecules* **1983**, 16, 1093.

23. Miller,J.A.; Cooper,S.L.; Han,C.C.; Pruckmayr,G. *Macromolecules* **1984**, 17, 1063.

24. Tsubomura,H. *J.Chem.Phys.* **1956**, 24, 927.

25. Skrovanek,D.J.; Howe,S.E.; Painter,P.C.; Coleman,M.M. *Macromolelcules* **1985**, 18, 1676.

26. Pimentel,G.C.; Sederholm,C.H. *J.Chem.Phys.* **1956**, 24, 639.

27. Cheam,T.C.; Krimm,S. *J.Molecular Structure* **1986**, 146, 175.

28. Camberlin,Y.; Pascault,J.P. *J.Polym.Sci.-Phys.* **1983**, 21, 415 and **1984**, 22, 1835.

29. Brunette,C.M.; Hsu,S.L.; Rossman,M.; MacKnight,W.J.; Schneider,N.S. *Polym.Eng.Sci.* **1981**, 21, 668.

30. Schneider,N.S.; Matton,R.W. *Polym.Eng.Sci.* **1979**, 19, 1122.

31. Brunette,C.M.; Hsu,S.L.; MacKnight,W.J.; Schneider,N.S. *Polym.Eng.Sci.* **1981**, 21, 163.

CHAPTER V

MISCIBILITY BEHAVIOR OF MODEL POLYURETHANES INCORPORATING DIFFERENT LENGTH OF HARD SEGMENTS

Introduction

A close correlation can be established between the overall sample mechanical properties and the microstructure of polyurethanes. The thermoplastic elastomeric properties of polyurethanes are directly related to the existence of the heterogeneous domain structure.[1] Even though this phase separated structure strongly affects the overall mechanical properties, the role of various parameters affecting the phase separation process has not been completely determined. The effects of having a broad segmental molecular weight distribution on material structures and properties is difficult to define.[2] However, this problem is minimized by using model polyurethanes composed of monodisperse hard and soft segments in order to achieve well defined micro and macrostructures.

Few model polyurethanes having monodisperse hard and soft segments have been synthesized.[3-5] Harrell et al. first reported a series of polyurethanes with a monodisperse hard segment based on piperazine and glycol bischloroformate.[6] Polyurethanes better representing the chemical structure of the commercial systems have also been investigated.[4,5] These

candidates, which generally possess good mechanical properties even at elevated temperature, have hard segments based on methylene bis(phenyl isocyanate) and butanediol and soft segments based on poly(tetramethylene oxide) or poly(propylene oxide).[4]

The miscibility behavior of hard segments of different length has not been carefully studied. It is generally assumed that the hard segments form the single hard domain even though there is a broad segmental length distribution. Since the preparation of the polyurethanes with the monodisperse hard segment needs rather elaborate synthesis, only the miscibility of the model hard segments with different hard segments or soft segments has been investigated by several studies.[7-9]

As expected, the physical blend of the hard and soft segment showed limited solubility. In the case of the binary mixture of short hard segments (ethanol terminated MDI) and soft segments such as poly(tetramethylene oxide) or poly(ethylene oxide), a eutectic point has been observed.[8] When poly(propylene oxide) is used as a soft segment in the blend, strong segregation has been observed. In the instance of even longer hard segments containing three MDI units, the hard segment melting temperature is hardly affected by the poly(propylene oxide) soft segment indicating that the PPO soft segment has little interaction with the hard segment.[9]

Although the existence of hard domains in polyurethanes is well accepted, details of the domain structure in

polyurethanes with different hard segment length distribution has not been analyzed extensively.[7] In the initial study,[7] the eutectic-type phase diagram with the eutectic point close to the shorter hard segment indicated that the long hard segments have limited solubility in the small hard segments. It has also been claimed that the solid solution below the eutectic temperature is not likely to be mixed crystals.[7]

The general requirement for the formation of the solid solution crystals is similarity in component size and shape.[10] If this condition is satisfied, the incorporation of the diluent molecule in the lattice of the matrix will not change the crystal lattice parameters or symmetry. The crystal structure of the two components, furthermore, should have the same symmetry and molecular packing to have a continuous series of solid solution.[10] These requirements are expected to be generally valid in the case of the crystal solid solution formation of polyurethane hard segments, even though the requirements may not be so strict due to relatively low crystallinity of the hard segment. For polyurethanes, the hard segments and soft segments are chemically connected to form an alternating block copolymer. The miscibility between the two hard segments of different segmental length is expected to be enhanced by the identical soft segment.

As far as hard segment conformation is concerned, two models, extended[11-13] and folded chain models,[14-16] have been suggested to explain the various experimental observations. The extended chain model is mostly based on the WAXS

results.[11-13] In order to accommodate the regularly packed hydrogen bonds, hard segments, which have mostly extended conformation, are assumed to pack regularly in three dimensional space. Most of the WAXS studies, however, have been carried out on the annealed and oriented materials,[12,13] making those results to be little use to understand the general domain structure of polyurethanes.

The folded hard segment conformation model has been suggested based on the extensive SAXS studies.[14-16] The calculated broad interphase boundary thickness, assuming the extended conformation, due to the broad distribution of hard segment length does not appear to conform to the experimental results. The folded chain model, therefore, seems to be persuasive considering the domain and interphase boundary thicknesses obtained experimentally as well as theoretically. It has been suggested that the main driving force for the folded chain conformation of the hard segment is the broad distribution of the hard segment length.[15] The hard domain thickness appears to be determined by the short hard segment. The longer hard segment has to fold back into the same domain to reduce the interfacial free energy.

In this study, two polyurethanes, each having monodisperse hard segments of different length (3 and 5 MDI units), are blended and the miscibility behavior and resultant structures are studied by infrared and DSC. The effect of one type of hard segment on the melting temperature of the other hard segment is also analyzed by the melting

temperature depression relation derived from the free energy of mixing equation given by Flory[17] and further extended by Scott[18] for polymer blends.

The two models concerning the hard segment conformation are also examined with the SAXS results. Since the polyurethanes used in this study contains monodisperse distribution of the hard segment length, the effect of the segment length distribution on the hard segment conformation is also studied.

Experimental

The polyurethanes, B2 and B4, used in this chapter are well explained in the previous chapters. Synthesis procedure and structural characterization for these polyurethanes has also been published.[3] Chemical structures of the B2 and B4 polymers, having two and four BD units per hard segment respectively, are shown in Figure 2.2. The schematic drawing in Figure 5.1 shows the difference in the hard segment length of the B2 and B4 polymers.

Each polyurethane was initially dissolved in DMF to form ~2%(w/v) solution. The two polymer solutions were then mixed to obtain the desired blend composition. Because of its low vapor pressure at room temperature, DMF was used to minimize the concentration change during solution manipulation. The blend composition ratio is the weight ratio throughout this chapter unless otherwise stated.

B2 :

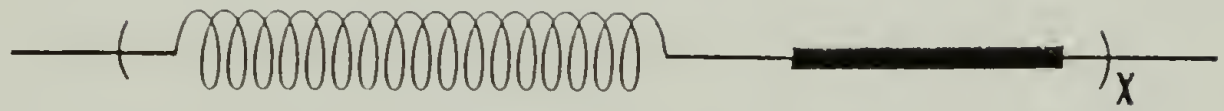

B4 :

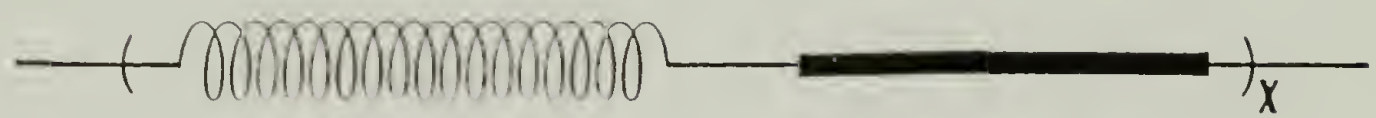

FIGURE 5.1 Schematic drawing of the B2 and B4 polyurethanes denoting the hard segment length difference.

For the infrared and SAXS experiments, the resulting mixed solutions were cast onto a KBr disk and Teflon mold, respectively. The solvent was evaporated initially under atmospheric pressure to remove most of the solvent before it was further dried in vacuo at 70°C for several days. For SAXS experiment, the film thickness after complete drying was approximately 300μm. All infrared spectra were obtained with the Bruker model IFS 113v vacuum Fourier transform infrared spectrometer. The heating experiment was done by the temperature control cell shown in Figure 2.3.[19] For infrared experiment, the materials were sandwiched between two KBr windows to prevent sample flow during the high temperature experiments.

For the DSC experiments, the mixed solution was directly cast onto DSC aluminum pans. This procedure needed to be repeated several times in order to have a ~5mg sample. These samples were dried under vacuo at 60°C or 85°C. To approach the equilibrium state as closely as possible, the vacuum was applied slowly and each sample was annealed at 60°C or 85°C for several days. A Perkin-Elmer DSC 2 was used with indium (mp 156.3°C) and naphthalene (mp 80.3°C) calibration. The heating rate was 20°C per minute. The transition temperatures were defined by the peak position of the endotherms due to the broad nature of the peaks. Samples prepared from THF solution showed an identical behavior indicating that the transitions observed are unaffected by the nature of the solvent.

SAXS experiment was performed on a Kratky SAXS apparatus alligned for infinite slit geometry. The sample was placed at 53cm away from the one-dimensional position sensitive detector and the scattering data have been corrected for parasitic scattering and wire sensitivity. X-ray generated at 35kV and 25mA was filtered with Ni crystal to obtain Cu Kα radiation. The smeared scattering profiles of B2 and B4 samples are shown in Figures 5.2 and 5.3. Profile of the blend sample (50/50 weight ratio) is also included. The domain spacings calculated with the Bragg relationship can be found in Table 5.1.

Infrared spectra of B2 and B4 polymers obtained at room temperature are shown in Figure 5.4. Most of the peaks are well assigned in the literature.[3] Since the chemical structure of the two polymers is similar, the infrared spectra of two polymers are difficult to distinguish. However, two spectra can be differentiated from the relative intensity of the hard segment to the soft segment (for example, N-H stretching peak at 3330cm^{-1} to C-H stretching peak at around 2900cm^{-1}) since the hard segment content of the B4 polymer (45%) is greater than that of B2 polymer (33%).

Results and Discussion

SAXS Studies

SAXS theory has been well established and its application polyurethanes has been discussed extensively.[15,20]

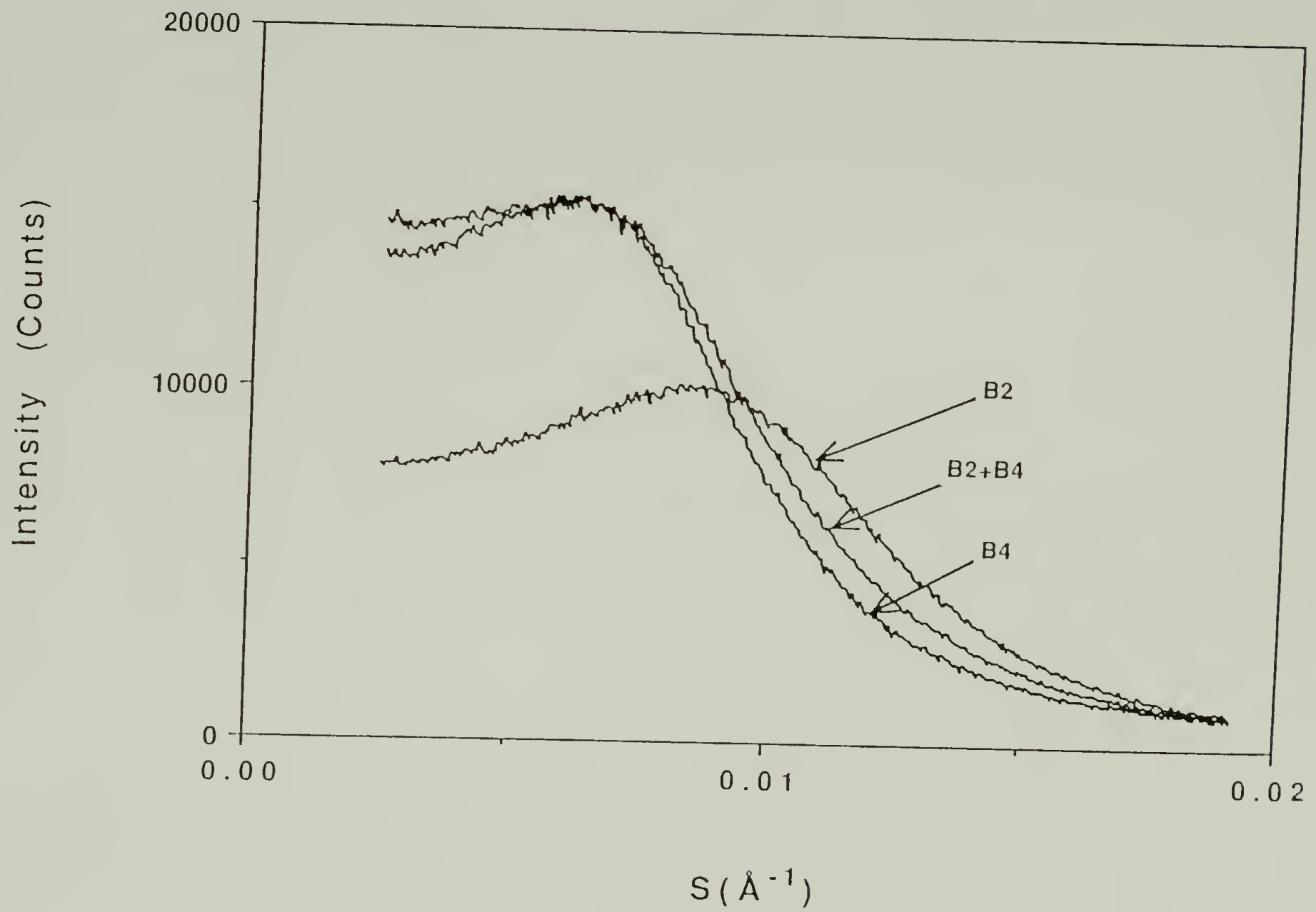

FIGURE 5.2 Small angle x-ray scattering profiles for B2, B4, and 50/50 blend sample.

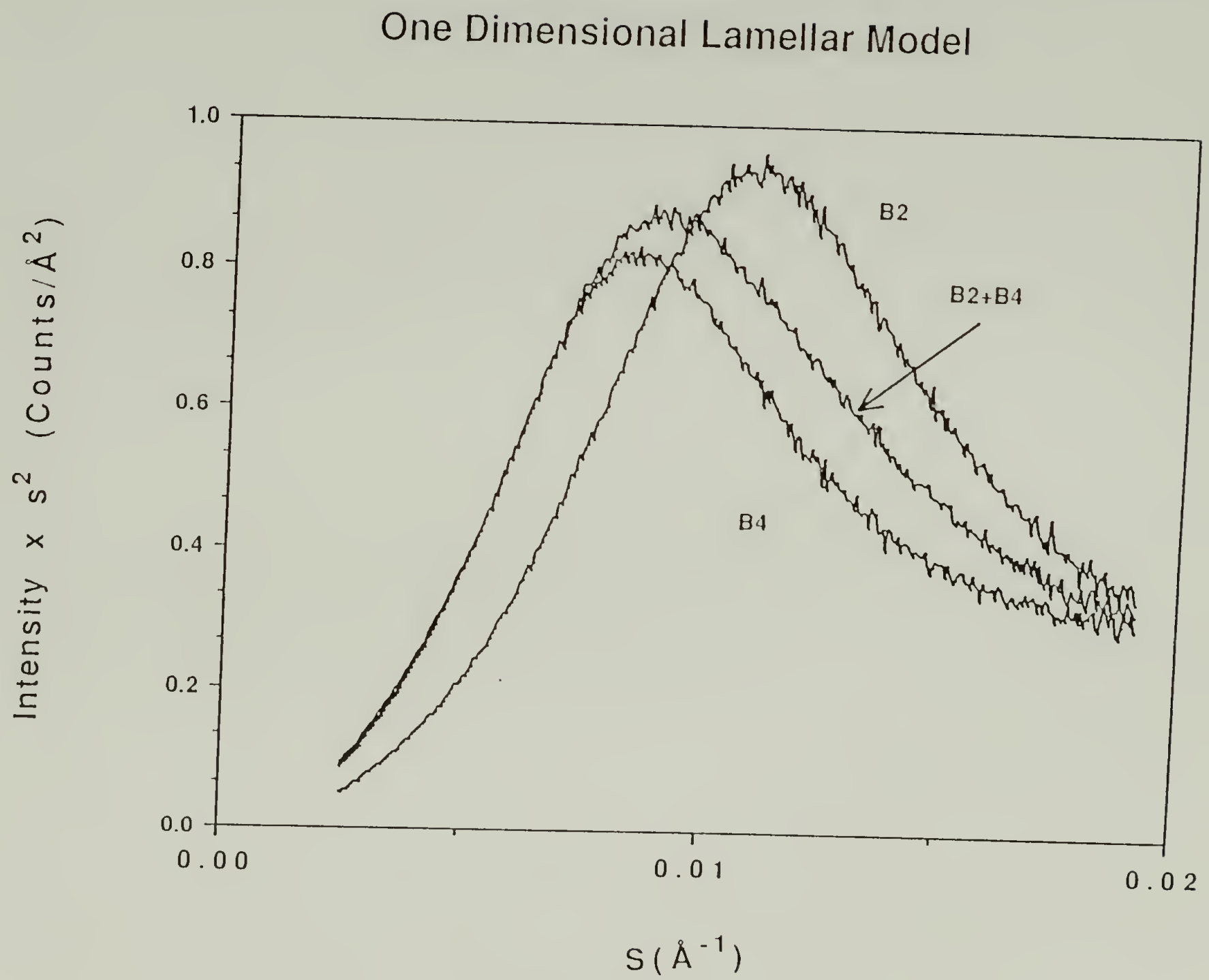

FIGURE 5.3 Small angle x-ray scattering profiles corrected for lamellar geometry.

FIGURE 5.4 Infrared spectra of the polyurethanes obtained with $2cm^{-1}$ resolution, 200 scan, at room temperature.
(a) B2 polymer
(b) B4 polymer

(a) B2 POLYURETHANE (25°C)

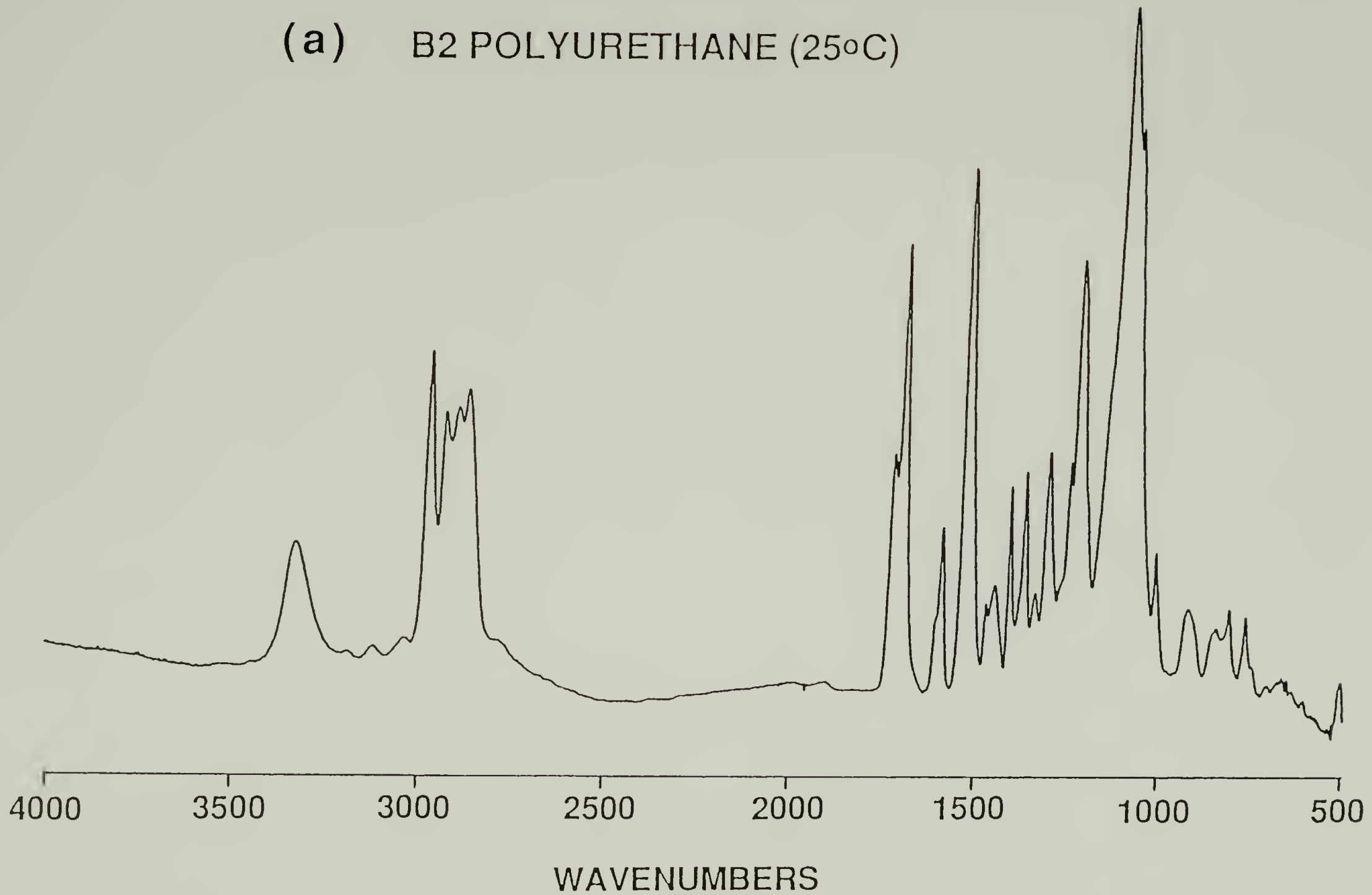

(b) B4 POLYURETHANE (25°C)

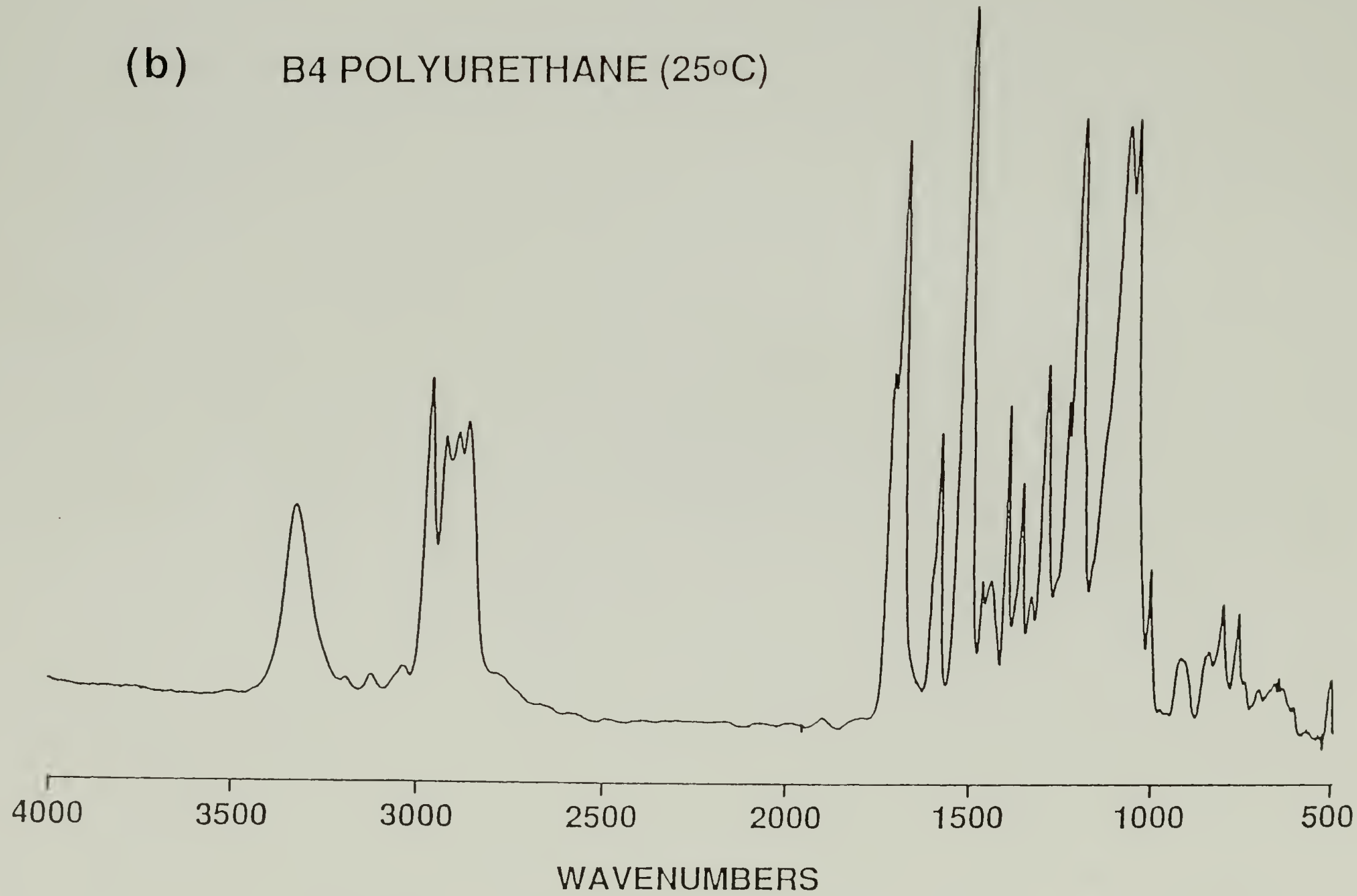

Interdomain spacing d can be obtained from the position of the maximum in the scattering profile with the Bragg's relationship by

$$|\mathbf{s}| = \frac{2\sin\theta_m}{\lambda} = \frac{n}{d} \tag{5.1}$$

where λ is the wavelength, n is the order of reflection, $2\theta_m$ is the angular position of the maximum in the scattering profile, and **s** is the reciprocal lattice vector. The scattering vector **h** is related to **s** by the relation

$$|\mathbf{h}| = \frac{4\pi \sin\theta}{\lambda} = 2\pi|\mathbf{s}| \tag{5.2}$$

where 2θ is the scattering angle. The Raleigh factor R(h) of scattered radiation from the spherically symmetric systems is[20]

$$R(h) = i_e \langle \Delta\rho^2 \rangle \int_0^\infty \gamma_{3D}(r) \frac{\sin(hr)}{hr} 4\pi r^2 \, dr \tag{5.3}$$

where i_e is the Thomson scattering factor for a single electron. Raleigh factor, R(h), is defined as

$$R(h) = \frac{I(h)\, p^2}{I_o V} \tag{5.4}$$

where I(h) is intensity of scattered radiation corresponding to a scattering vector **h**, p is the sample to detector distance, I_o is the incident beam intensity, and V is the illuminated sample volume. The three-dimensional correlation function $\gamma_{3D}(r)$ indicates the spatial correlations between local fluctuations in electron density, and is defined as

$$\gamma_{3D}(r) = \frac{\langle \Delta\rho_j \Delta\rho_k \rangle_r}{\langle \Delta\rho^2 \rangle} \tag{5.5}$$

In the case of scattering from the lamellar morphology, the intensity of the scattered radiation has to be modified as

$$i(h) = 2V\langle \Delta\rho^2 \rangle \int_0^\infty \gamma_{1D}(r) \cos(hr)\, dr \tag{5.6}$$

where one-dimensional correlation function $\gamma_{1D}(r)$ is defined as

$$\gamma_{1D}(r) = \int_0^\infty \frac{\Delta\rho(x+r)\Delta\rho(x)}{\langle \Delta\rho^2 \rangle} dx \tag{5.7}$$

In Equation 5.7, the integration is along the direction x which is the direction perpendicular to the lamellar face. Since each lamellar bundles inside the real sample orient randomly resulting in the macroscopically isotropic material, the experimental intensity I(h) is to be modified as

$$I(h) = \frac{i(h)}{4\pi |\mathbf{s}|^2} \tag{5.8}$$

to obtain the domain spacing only along the lamellar thickness direction. Therefore, the domain spacing of the lamellar morphology has to be obtained from the inverse of the $|\mathbf{s}|$ corresponding to the maximum $s^2R(h)$ value rather than R(h).

Scattering peaks in Figure 5.2 are rather broad. The strongly scattered intensity of B4 polyurethane especially at low angle can be explained in terms of the high sample

crystallinity. The scattering of the blend sample appears to resemble the B4 more than the B2 polyurethane especially at low angle. The scattering data of three samples shown in Figure 5.2 are replotted in Figure 5.3 as $s^2R(h)$ vs $|\mathbf{s}|$ and the domain spacings from the modified plot are also included in Table 5.1. Two samples, B2 and B4, show scattering maximum at distinctively different $|\mathbf{s}|$ value. The differences, i.e. [d(B4)-d(B2)], are 47 and 27Å for three and one dimensional models, respectively. The differences in the domain spacing are likely due to the hard segments because the main difference between two polyurethanes is the length of the hard segment.

According to the crystal structures of the MDI and BD based polyurethanes, the unit cell dimension c, which contains two MDI and BD, is approximately 35Å.[21-23] Since the hard segment chain has about 30 degree with the lamellar thickness direction,[21,24] the contribution of 35Å to the lamellar thickness will be approximately 30Å. A good agreement between the experimental value of 27Å with the calculated value of 30Å indicates that the hard segments in the hard domain are mostly extended.

Even though the extended chain model suggested for this materials seems to contradict previous studies,[14-16] the differences are probably due to the different distribution of the hard segment length. As explained previously, the materials used in this chapter has monodisperse hard segment length distribution. The broad distribution of hard segment,

which was claimed as a main driving force for the folded chain model, can not play a significant role in determining the chain conformation for this material. Furthermore, chain folding of the hard segments with monodisperse length distribution could not decrease the interfacial free energy unless all the hard segments fold exactly same manner which is statistically unlikely.

Table 5.1 Interdomain Spacings(Å)[a]

Sample	Three-Dimensional(I)	One-dimensional(Is^2)
B2	113	92
B4	160	119
Δd	47	27

[a] : From smeared intensity

The previous result does not necessarily imply the long range crystalline order of the hard segments. The hard segment may contain a certain amount of conformation disorder. It is rather to indicate that there is an extensive orientational correlation between the hard segments resulting in significant amount of laterally interaction,

which has been observed as a hydrogen bonding. The dominant structure of the hard segments implied by the above result is that each hard segment traverses the single hard domain lamella and both ends of the hard segment appears to be in the opposite face of the same lamella.

The scattering profile of the blend sample shown in Figure 5.3 does not provide any conclusive evidence concerning the miscibility of the two hard segment, i.e. B2 and B4 hard segment. However, the scattering at low angle of the blend sample appears to resemble that of B4 polyurethane and scattering at high angle seems to have additional contribution from the B2 polyurethane. In other word, long range periodicity shown at low angle is more affected by the B4 material. Scattering from B2 may be seen at higher angles.

Infrared Spectroscopic Studies

Infrared spectroscopy has been extensively used to understand the role of the hydrogen bonding on the phase separation behavior of polyurethanes and its effect on the physical properties.[25-27] The direct relationship between hydrogen bonding and the phase state enables the convenient assessment of the degree of phase separation.

Infrared spectra between 1400 and 1850cm^{-1} of the B4 polymer obtained at several temperatures are shown in Figure 5.5a with the band assignments given in Table 5.2. The spectra of the 50/50 (B2/B4) blend are also shown in Figure

5.5b. Even though all four major peaks are due to the hard segments, only two peaks, i.e. C=O stretching peaks around 1700-1730cm^{-1} and amide II peak at 1534cm^{-1}, are shown to be sensitive to the temperature. Both the shift of the amide II peak to low frequency and the relative intensity change of the 1700cm^{-1} peak to the 1730cm^{-1} peak as an increasing function of temperature have all been well explained by the weakening and dissociation of the hydrogen bond at high temperatures.[28] The remaining two peaks at 1600 and 1415cm^{-1} show little temperature dependence.

Table 5.2 Assignments for the Bands shown in Figure 5.3.

Frequency (cm^{-1})	Assignment[a]
1730	ν(C=O) free
1702	ν(C=O) Hydrogen-bonded
1598	ν(C=C) Phenyl ring of the MDI unit
1534	σ(N-H) + ν(C-N) ; Amide II
1414	ν(C=C) Phenyl ring of the MDI unit

[a] : ν = stretching
σ = in plane bending

Upon dissociation of the hard domain, the hard segment, which was previously confined inside the hard domain, becomes

FIGURE 5.5 Infrared spectra between 1850 and 1400cm^{-1} at temperatures shown in the spectra.
(a) B4 polymer
(b) 50/50 (B2/B4) blend.

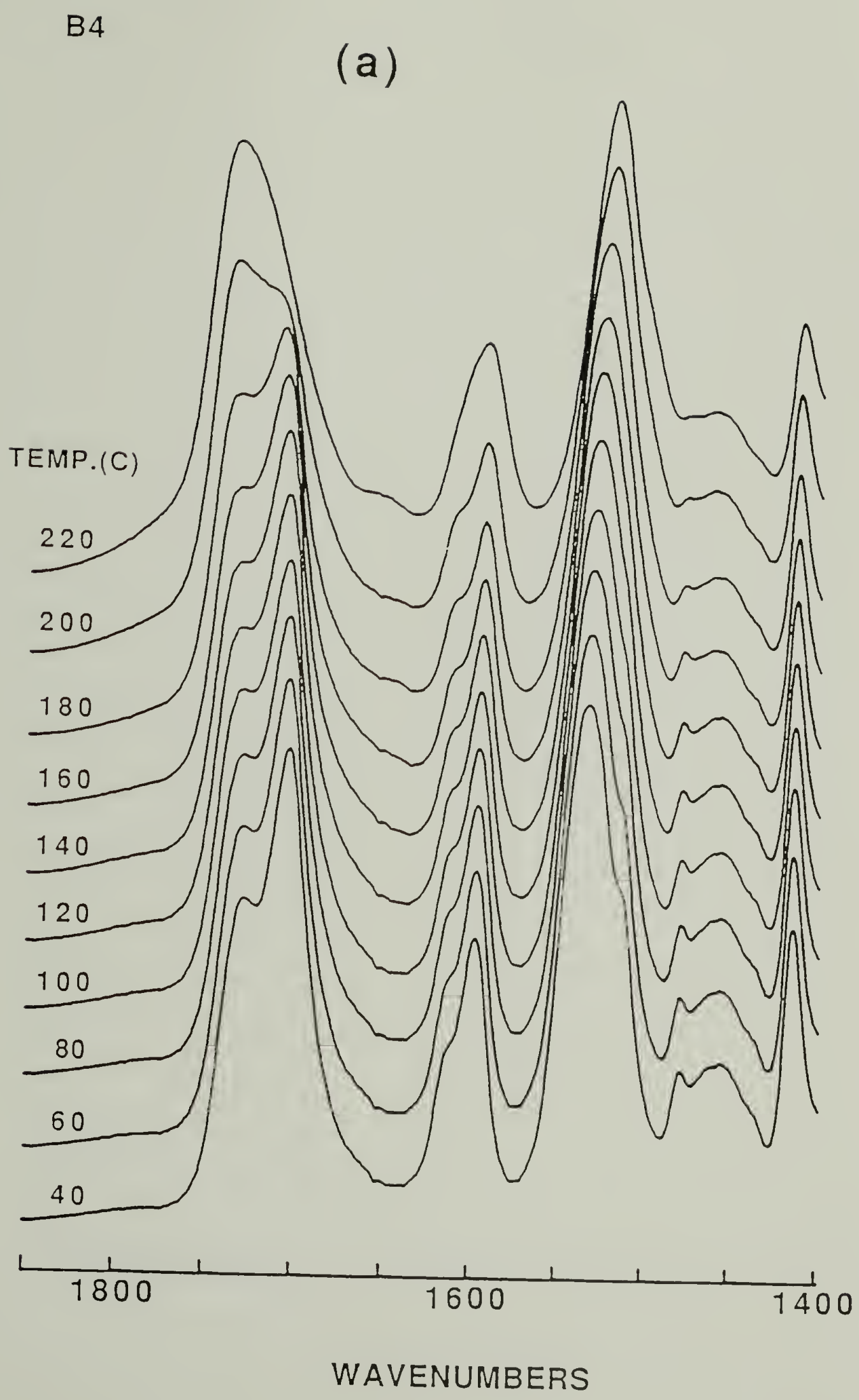
B4
(a)
TEMP.(C)
220
200
180
160
140
120
100
80
60
40
1800
1600
1400
WAVENUMBERS

(b) 50 : 50 (B2 : B4) BLEND

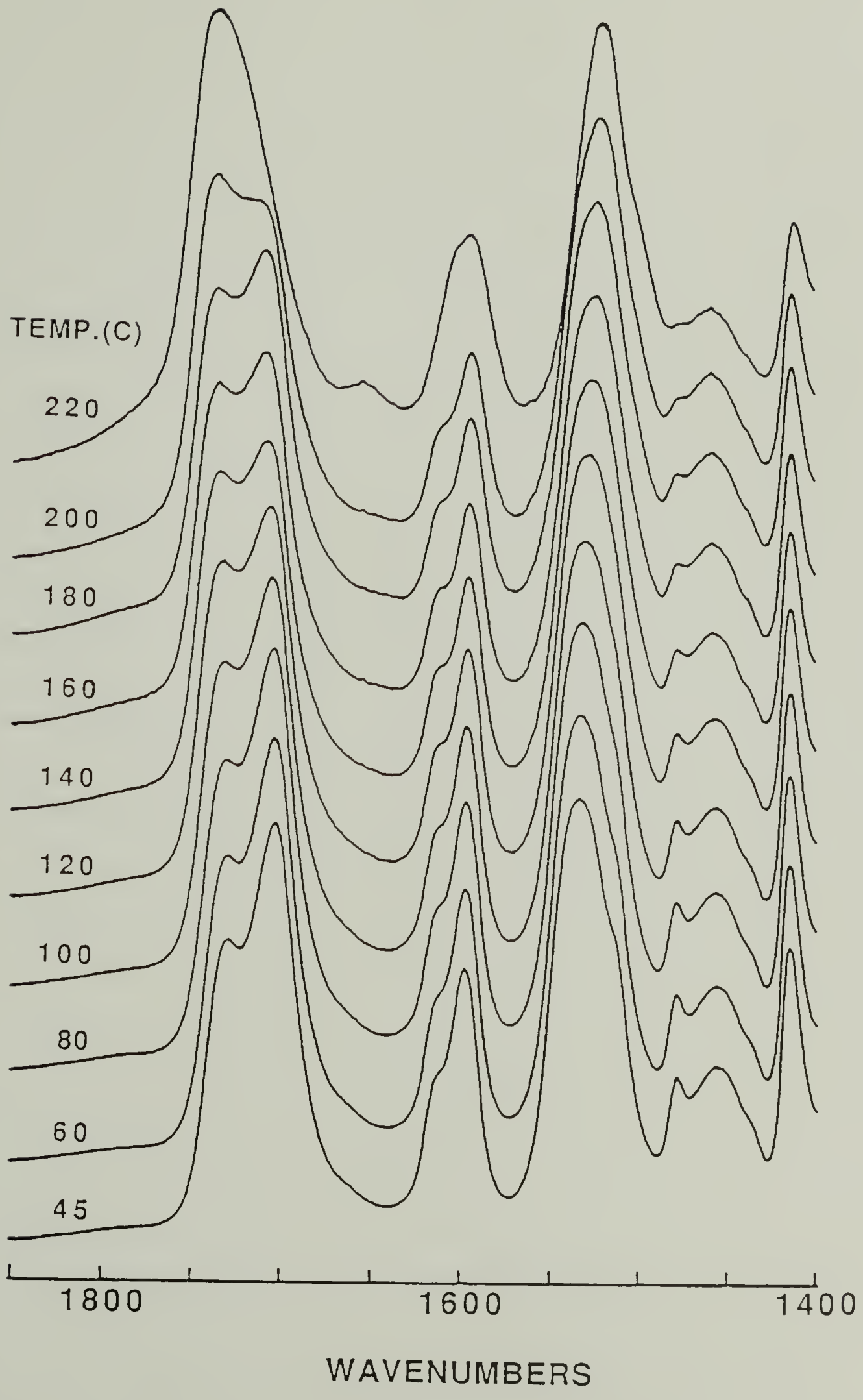

surrounded by the soft segment. Most of the carbonyl functional groups are, therefore, transformed from the hydrogen bonded state (bonded state) to the state free of hydrogen bonding (free state) since the soft segment contains no proton donor to form hydrogen bonds with the carbonyl group.[19,26,27] Therefore,the intensity ratio, i.e. $A(1700cm^{-1})/A(1730cm^{-1})$ will undergo an abrupt change at melting. The intensity variations as a function of the temperature for the three samples with different blend compositions are plotted in Figure 5.6.

The melting transition of the B4 sample is clearly observed around 175°C. For the 99/1(B2/B4) sample, the intensity ratio changes abruptly at approximately 100°C. The two temperatures at which greatest spectroscopic changes occur are close to the previously reported transition temperatures for the B2(98°C) and B4(171°C) measured by calorimetric method.[3] For the 50/50 blend, two distinct transitions were clearly observed at approximately the temperatures expected for the two "neat" components.

The N-H stretching vibration of the 50/50 mixture as a function of temperature is shown in Figure 5.7. The small shoulder at $3450cm^{-1}$ is assigned to free N-H stretching and the broad peak around $3340cm^{-1}$ is assigned to the hydrogen bonded component.[29] As with the C=O peak, the hydrogen bonded N-H component is transformed into the free component as temperature increases. Since the extinction coefficient of the N-H stretching peak is a strong function of the hydrogen

FIGURE 5.6 Absorbance ratio of the two C=O stretching peaks, i.e. A(1702cm^{-1})/A(1730cm^{-1}) of three samples as a function of temperature; Blend compositions are indicated in Figure; The top two samples are shifted vertically for clarity; The ratio values at ambient temperatures before shifting were approximately 1.55 for all three samples.

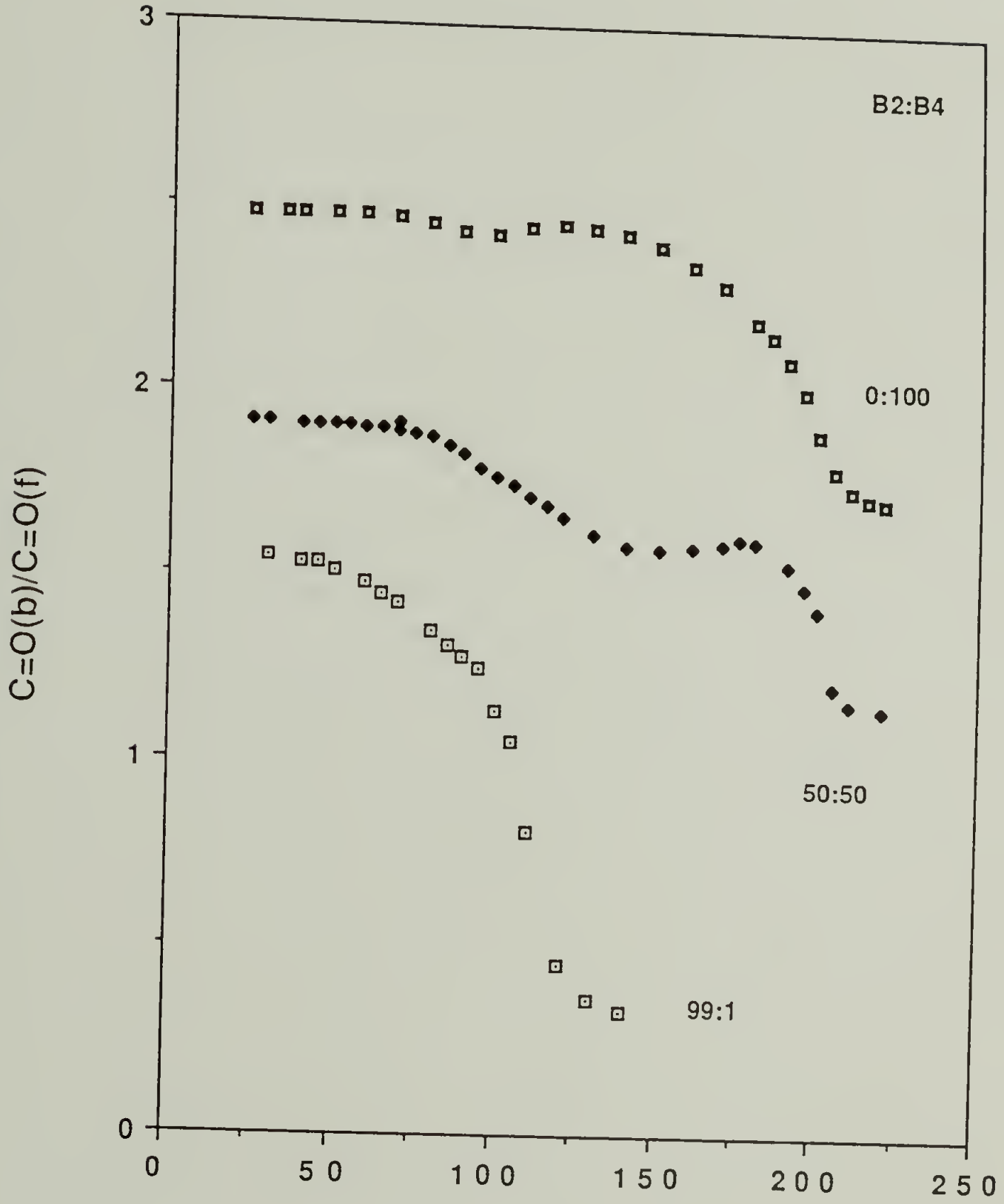
3
2
1
0
0
50
100
150
200
250
B2:B4
0:100
50:50
99:1
C=O(b)/C=O(f)
TEMPERATURE (C)

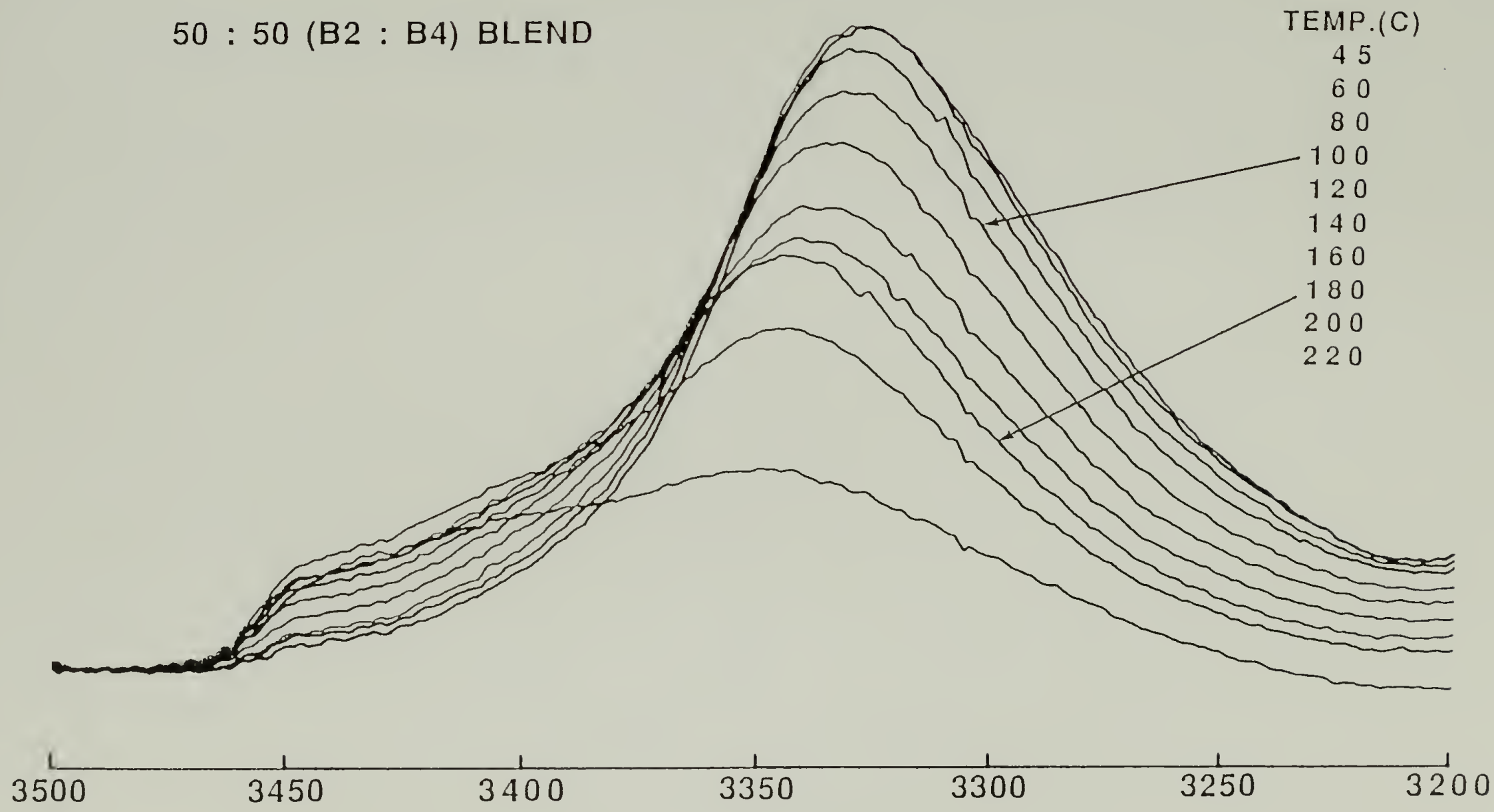

FIGURE 5.7 N-H stretching regions of the 50/50 (B2/B4) blend sample as a function of temperature.

bond strength,[30,31] the overall intensity of the N-H stretching peak is also sensitive to the hydrogen bonded state of the urethane functional groups. The two abrupt changes of the intensity near 100°C and 180°C can be observed from Figure 5.7 supporting the results obtained from the C=O stretching region. The overall intensity of the N-H stretching peak of the sample with 99/1 (B2/B4) blend composition ratio is plotted in Figure 5.8. The corresponding absorbance intensity for the 1702cm^{-1} C=O stretching band is also included for comparison. The overall intensity of the N-H stretching region also clearly shows the transition behavior. The close correlation between the two different spectral regions confirms that the transition behavior can be studied spectroscopically when the microscopic phenomenon such as the formation of the hydrogen bonding is related to the phase changes.

Even though the immiscibility of the two polyurethanes with different hard segment length is clearly shown for the 50/50 blend, spectroscopic change for blends with more asymmetric compositions becomes difficult to observe. More systematic studies with a wide range of composition can only be carried out with the thermal method.

Differential Scanning Calorimetric Studies

A series of samples with different blend compositions have been prepared as shown in Table 5.3. The weight fractions of the soft segment and each hard segment are also

FIGURE 5.8 Intensity changes of two spectral regions of 99/1 (B2/B4) sample as a function of temperature (a) 1702cm^{-1} peak height (b) integrated area of N-H stretching peak.

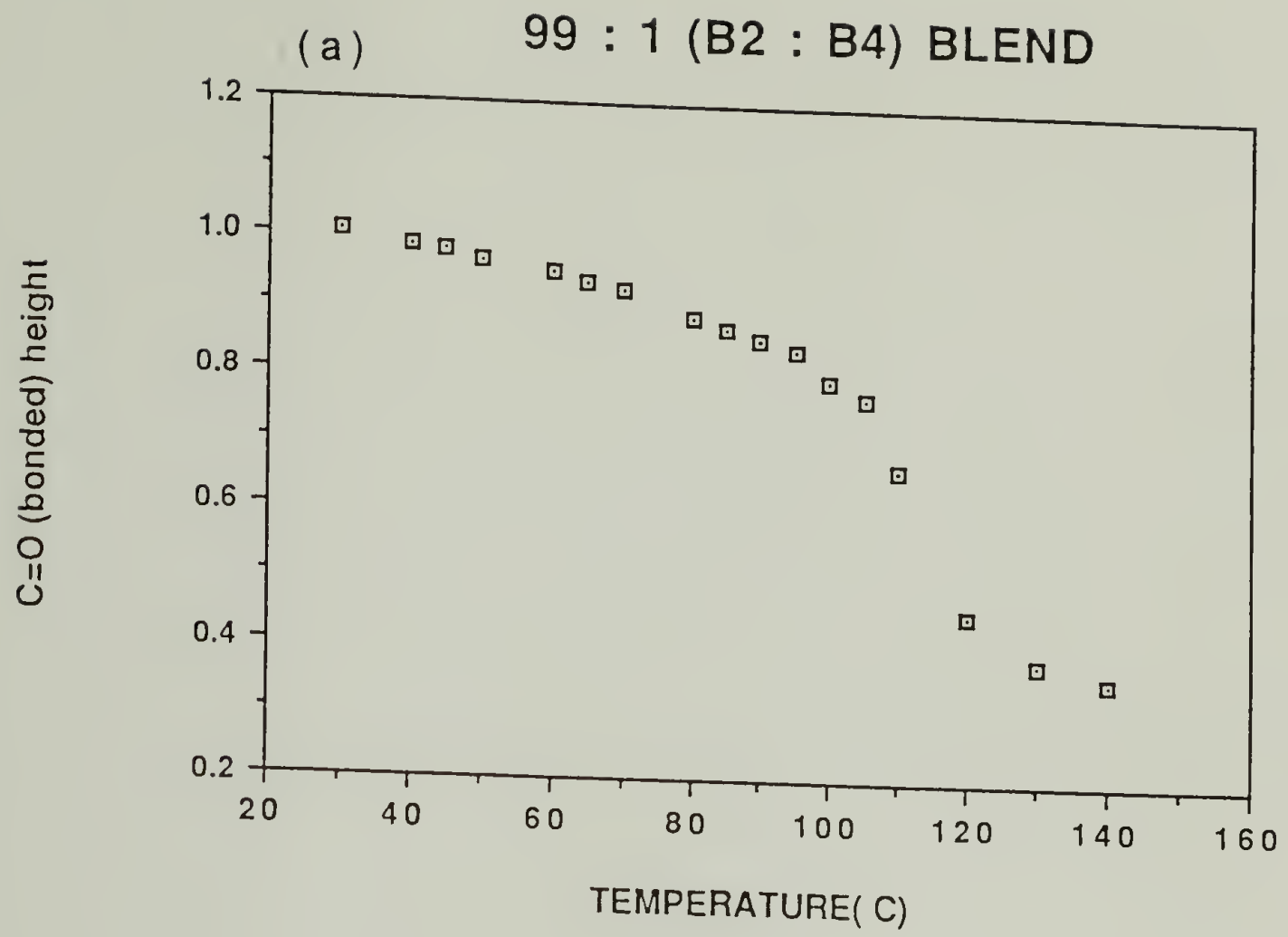
(a)
99 : 1 (B2 : B4) BLEND
C=O (bonded) height
1.2
1.0
0.8
0.6
0.4
0.2
20
40
60
80
100
120
140
160
TEMPERATURE(C)

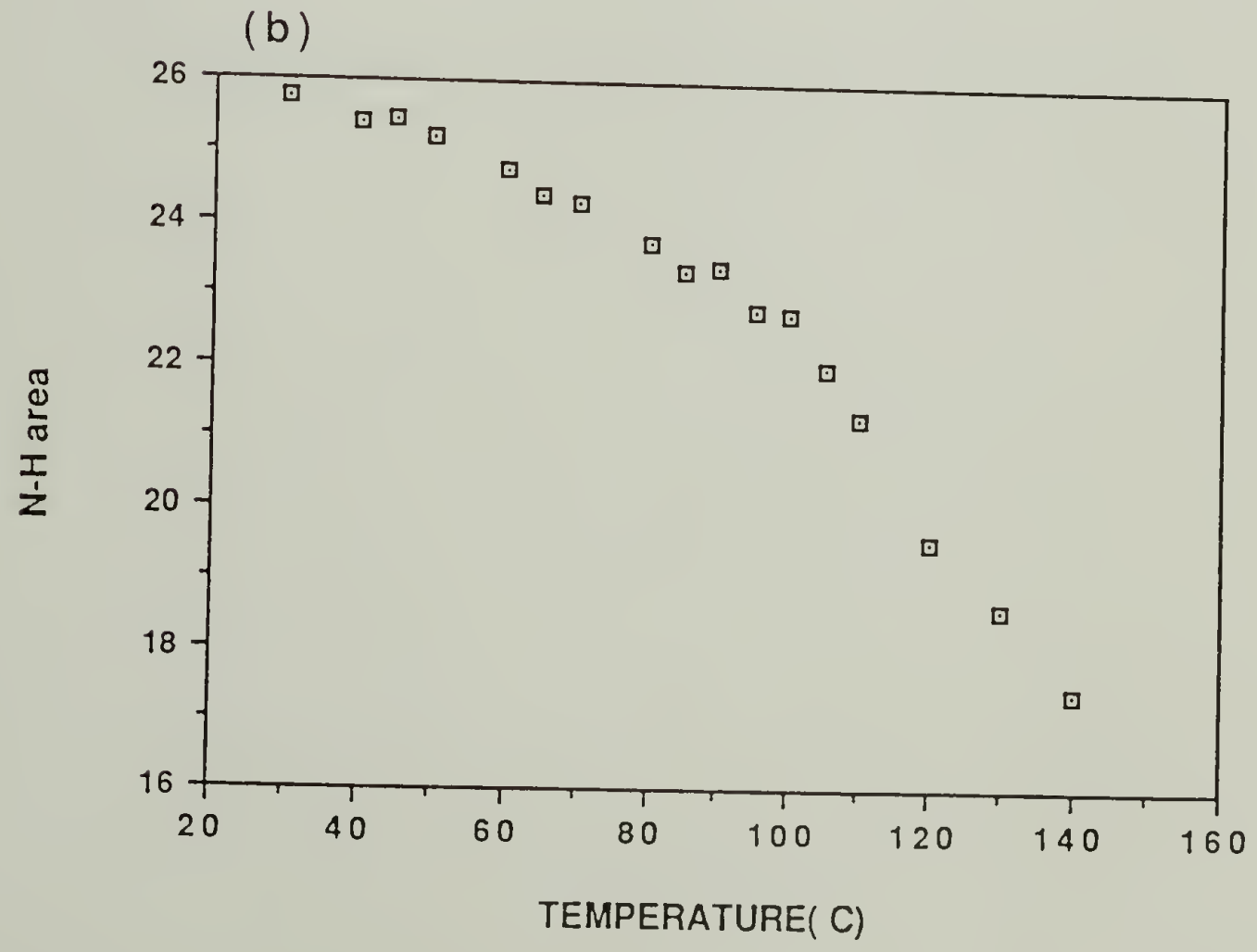
(b)
N-H area
26
24
22
20
18
16
20
40
60
80
100
120
140
160
TEMPERATURE(C)

Table 5.3 Weight Fraction of Soft Segment and Hard (B2 and B4) Segments[a].

B2/B4[b] BLEND	SOFT SEGMENT	B2 HARD SEGMENT	B4 HARD SEGMENT
100/0	67.5	32.5	0.0
99/1	67.4	32.2	0.5
95/5	66.9	30.9	2.3
90/10	66.2	29.3	4.5
70/30	63.7	22.8	13.5
50/50	61.2	16.3	22.6
30/70	58.7	9.8	31.6
10/90	56.2	3.3	40.6
5/95	55.5	1.6	42.8
1/99	55.0	0.3	44.6
0/100	54.9	0.0	45.1

a: Hard segment includes butanediol as well as MDI
b: Polymer Weight Fraction

included. As blend composition varies from pure B2 polymer to pure B4 polymer, the weight fraction of the soft segment changes only from 67.5% to 54.9% due to the nature of the segmented copolymer. However, the weight fractions of the two hard segments change appreciably as seen from the third and fourth column of Table 5.3.

DSC thermograms of the selected samples annealed at 60°C are shown in Figure 5.9. For the samples with intermediate blend compositions such as 30/70 through 70/30 (B2/B4), two endothermic transitions have been clearly observed at ~93°C and 160-200°C. Samples with extremely asymmetric compositions show only a single transition. These DSC results are consistent with the results obtained from the infrared spectroscopic method, i.e. the samples with intermediate blend composition show only limited miscibility between the two hard segments with different segment lengths. Although the chemical structure of the two hard segments is identical, and both polymers have identical soft segments, separate hard domains still exist.

The SAXS long spacings observed for the B2 and B4 polymers for lamellar model are 92 and 119Å respectively as shown in Table 5.1. These values include, of course, the soft segment layer. The hard domain thickness of the model hard segment obtained with MDI and butanediol has been studied previously.[7] Three and five MDI units extended with the butanediol have an average thickness of 53Å and 88Å

FIGURE 5.9 DSC thermograms of the samples with various blend compositions; Samples were annealed at
(a) 60°C
(b) 85°C

ANNEALED AT 60°C

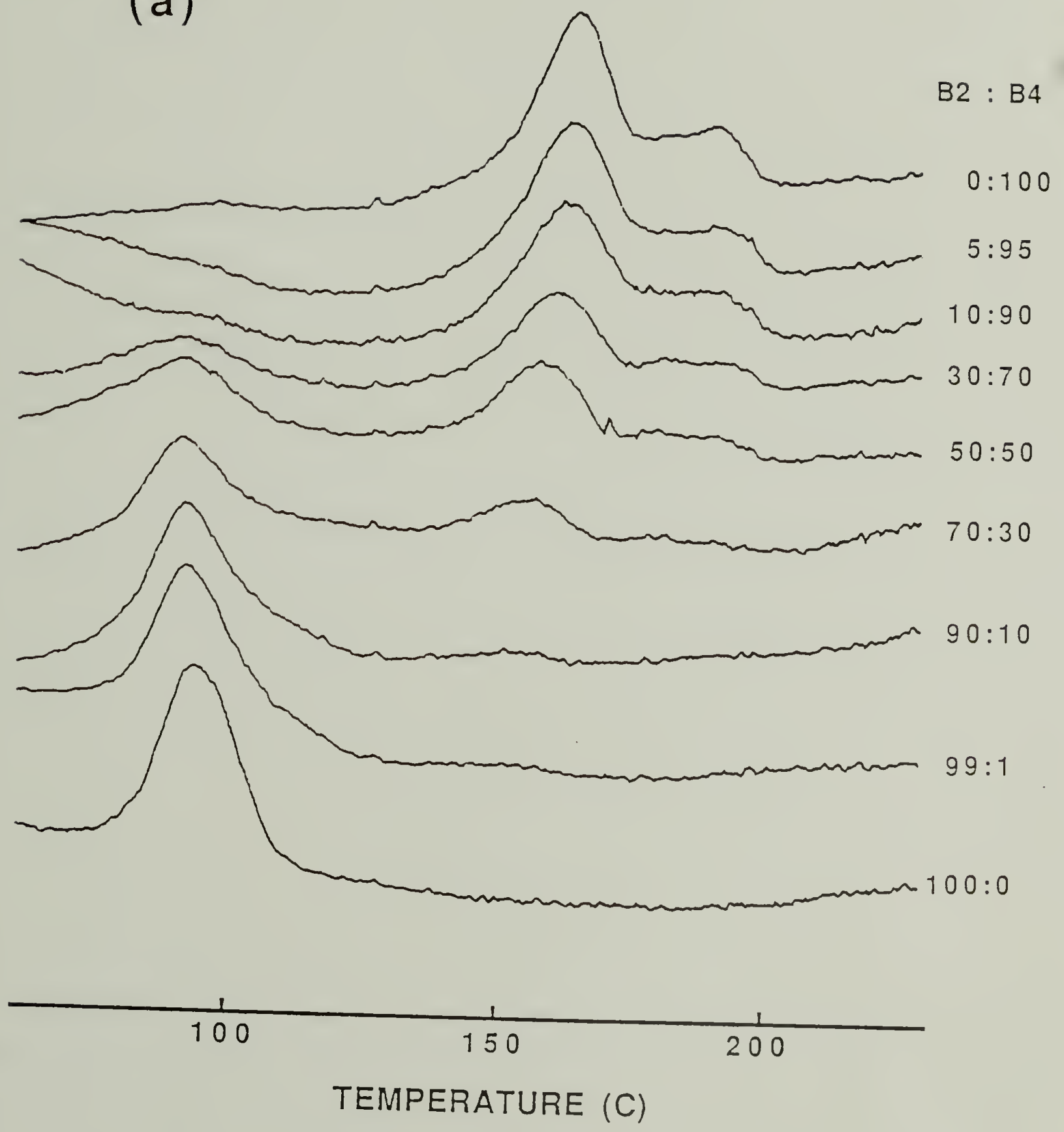

ANNEALED AT 85°C

(b)

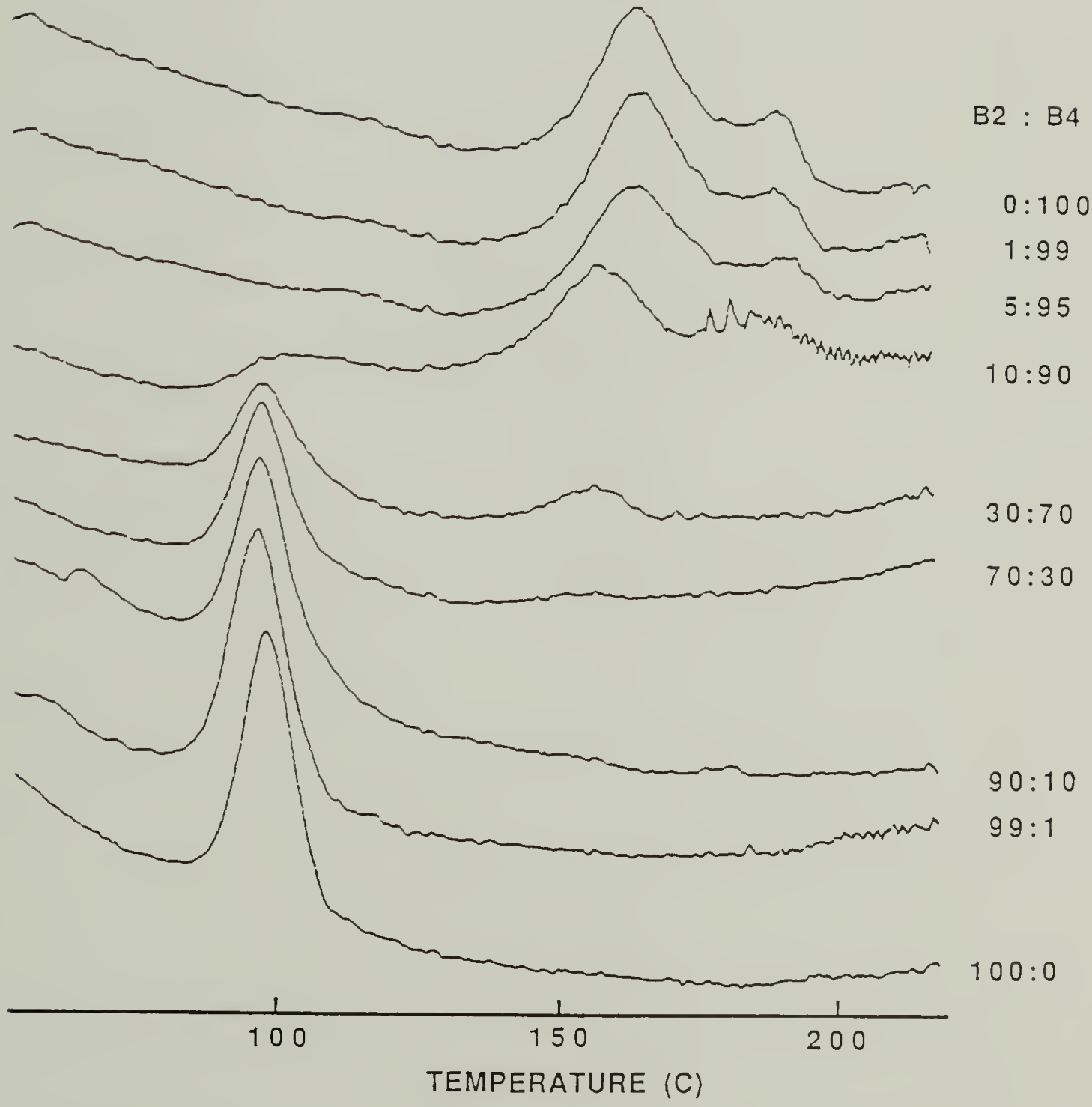

respectively. The B4 hard segments is, therefore, approximately 65% longer than the B2 hard segments.

The size effect on the formation of the solid solution has been carefully studied with the linear paraffins.[32,33] For binary mixtures of two n-alkanes, i.e. n-C_nH_{2n+2}, the empirical relationship for continuous solid solution to exist is

$$C_N^{max} = 1.224\, C_N^{min} - 0.411 \qquad (5.9)$$

where C_N^{max} and C_N^{min} are the number of carbons in the long and short linear chains respectively.[32] Equation 5.9 suggests that continuous solid solubility is assured for binary extended chain polyethylene systems in which the molecular weight differs by less than about 22% of the shorter chain.

Even though the results of linear paraffins cannot be directly applied to the hard segments of the polyurethane, the difference of about 65% in length seems to be the major reason for the limited miscibility of the hard segments. It is to be noted that there is no extensive chain folding in the hard segment of the model polyurethanes with monodisperse segmental length as verified in the previous section. The difference in the hard segment length is, therefore, directly related to the difference in long spacings of the hard domains.

The single transition behavior of the strong asymmetric blend seems to be either due to the dissolution of the small amount of the "guest" hard segments with different segment

length in the "host" hard/soft matrix or due to the instrumental limit to detect the small endothermic signal. It is known that polyurethanes have to contain at least a certain amount of hard segment to become a heterogeneous structure. If the hard segment contents are small, the polyurethanes do not show any thermoplastic elastomeric properties.

The high temperature melting endotherms have a broad shoulder at the higher temperature side. The exact explanation for that shoulder is not available at this moment. It may be due to either the small amount of longer hard segment residue which shows a higher melting endotherm or the difference in the degree of ordering achieved at a high temperature during temperature scanning.

The temperature-composition diagram is shown in Figure 5.10. Samples annealed at 85°C are also included to investigate the annealing effect. The lower transition temperature does not change to any significant extent, whereas the higher transition temperature is depressed by about 8 degrees by changing from the pure B4 polymer to the 50/50 mixture.

Thermodynamics of the polymer mixing behavior have been obtained by differentiating the Flory-Huggins' free energy mixing equation with respect to the crystallizable component as shown in Equation 5.10.[18] Denoting the amorphous and crystallizable unit with subscripts 1 and 2 respectively, the equation is

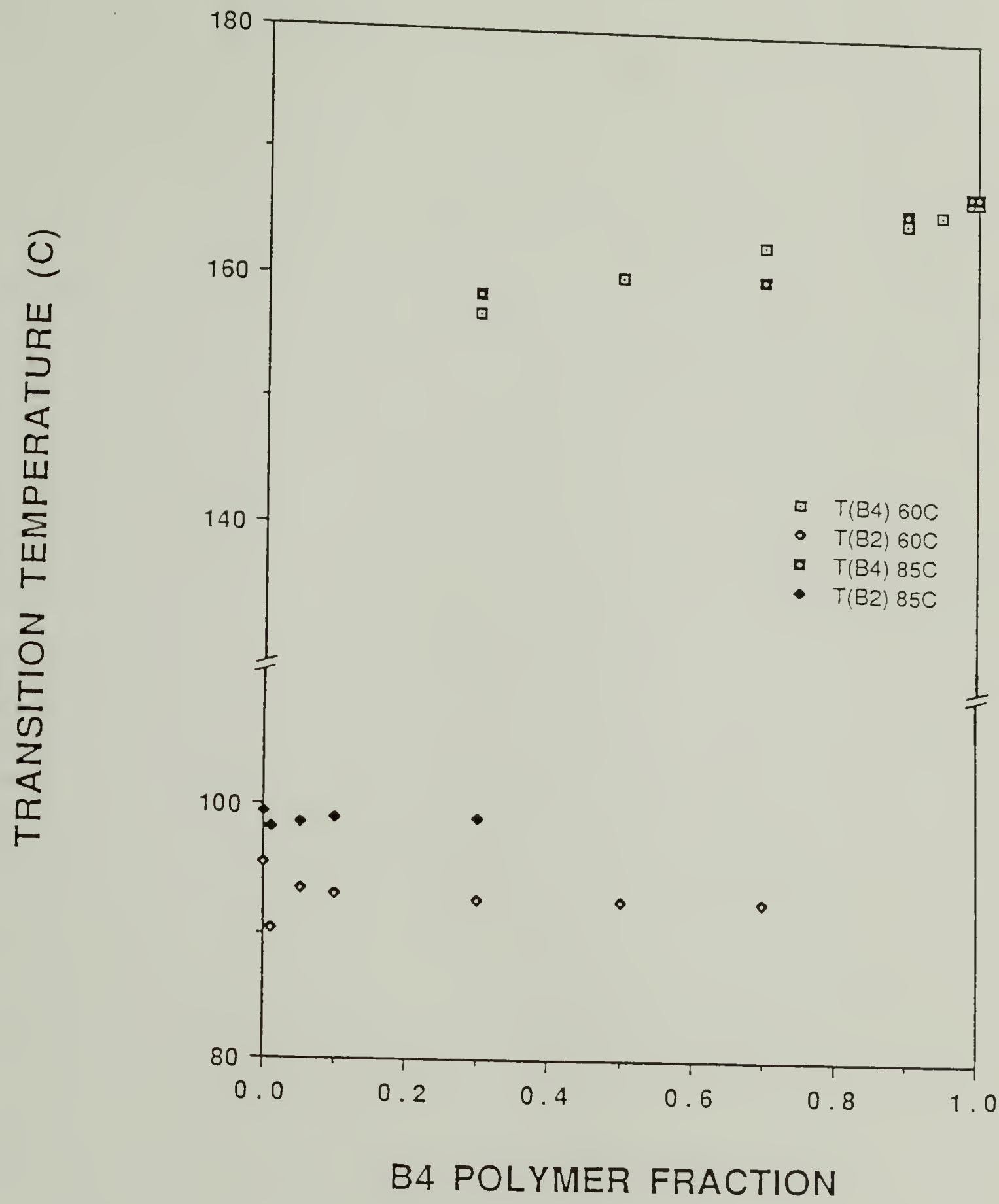

FIGURE 5.10 Composition and transition temperatures diagram; Annealing temperatures are indicated with the legends; T(B2) and T(B4) in the legend indicate the transition temperatures of the corresponding domains.

$$\mu_{2u}^{l} - \mu_{2u}^{\circ} = \frac{RTV_{2u}}{V_{1u}} \left[\frac{\ln\phi_2}{M_2} + \left(\frac{1}{M_2} - \frac{1}{M_1}\right)\phi_1 + \chi_{12}\,\phi_1^2 \right] \qquad (5.10)$$

where $\mu_{2u}{}^{l}$ and $\mu_{2u}{}^{\circ}$ are chemical potentials of the crystallizable unit, 2u, of the liquid polymer blend and of the pure liquid at a standard state respectively, V is the molar volume of the repeating unit, M is the degree of polymerization, ϕ is the volume fraction of the component, χ is the polymer-polymer interaction parameter, R is the gas constant.

Since the chemical potential of the crystalline unit is the same as that of a liquid state at the melting temperature, Equation 5.10 can also be represented as $\mu_{2u}{}^{c} - \mu_{2u}{}^{\circ}$, which is the negative of the free energy of fusion, i.e.,

$$\begin{aligned} \mu_{2u}^{c} - \mu_{2u}^{\circ} = -\Delta G_{2u}^{M} &= -\left(\Delta H_{2u}^{M} - T\Delta S_{2u}^{M}\right) \\ &= -\Delta H_{2u}^{M}\left[1 - \left(\frac{T}{T_m^{\circ}}\right)\right] \end{aligned} \qquad (5.11)$$

where $\Delta G_{2u}{}^{M}$, $\Delta H_{2u}{}^{M}$ and $\Delta S_{2u}{}^{M}$ are the partial molar free energy, enthalpy and entropy of fusion of the repeating unit, respectively, and the ratio $\Delta H_{2u}{}^{M}/\Delta S_{2u}{}^{M}$ is assumed to be independent of the temperature within the range being considered and equal to $T_m{}^{\circ}$, the equilibrium melting temperature of the pure polymer.[17,34] From Equations 5.10 and 5.11, Equation 5.12 can be obtained as

$$\frac{1}{T_m} - \frac{1}{T_m^{\circ}} = -\frac{RV_{2u}}{\Delta H_{2u} V_{1u}} \left[\frac{\ln\phi_2}{M_2} + \left(\frac{1}{M_2} - \frac{1}{M_1}\right)\phi_1 + \chi_{12}\,\phi_1^2 \right] \qquad (5.12)$$

which describes the melting temperature depression of the crystalline unit due to the presence of the diluent component. The first two terms in Equation 5.12 correspond to the configurational entropy and the third term is due to both enthalpic and entropic change upon interaction. In the case of the polymer blend system, the configurational entropic contribution is usually negligible due to the high degree of polymerization.

Since the hard segments of the B2 and B4 polyurethanes have a relatively low degree of polymerization, the entropic terms cannot be neglected in order to explain the melting point depression of the B4 hard domains. It is to be noted that the repeat units of the two hard segments have identical chemical structure or approximately the same intermolecular interactions. The entropic terms, therefore, can affect significantly the melting temperature of the B4 hard domain. This will be further discussed later.

There is a very important point to note for this blend system. As shown from the infrared and thermal data, two hard segments phase separate into the different hard domains. The melting temperature of the B4-rich domain is, therefore, mainly affected by the B2 hard segments dissolved in the B4 hard domain. The B2 hard segments in the B2 hard domain are believed to have little effect on the melting transition behavior of the B4 domain. Thus, the ϕ value in Equations 5.10 and 5.12 for these polyurethane blend systems have to be a "true" volume fraction of the non-crystallizable component

dissolved inside the domains of the crystallizable unit. The blend compositions in Table 5.3 are the "apparent" volume fraction of the polymers.

It is obvious from Equation 5.12 that the direct relationship between T_m and ϕ_1, the "true" volume fraction which is different from the "apparent" volume fraction, can only be analyzed if the χ value and all other parameters are known. Since the exact χ value in this case is hard to obtain, the relationship between T_m and ϕ_1 is plotted for a range of χ values in Figure 5.11 using the experimental data in Table 5.4. The experimental data are also included with the B4 polymer fraction. The abscissas of the two plots are adjusted so that both experimental and calculated values fall on top of each other. The "true" volume fraction of an experimental data point, **A** (50/50 blend) for example, can be readily obtained by reading the value on the corresponding abscissa, **B**. If the χ value is not very different from zero, for example between -0.1 and 0.1, the range of "true" **B** is between **C** and **D** as shown in Figure 5.11. The uncertainty due to the unknown χ value is very small at a low volume fraction. As can be seen in Equation 5.12, the melting temperature is significantly affected by the interaction term only if the volume fraction of the noncrystallizable component is large. According to this analysis, the noncrystalline B4 domain of the sample **A** seems to contain approximately 15% B2 hard segments. The volume fractions of the B2 hard segments in

FIGURE 5.11 Melting temperature depression of the samples annealed at 60°C; Experimental data points are with the lower abscissa (blend composition) and the calculated lines are with the upper abscissa ("true" ϕ_1).

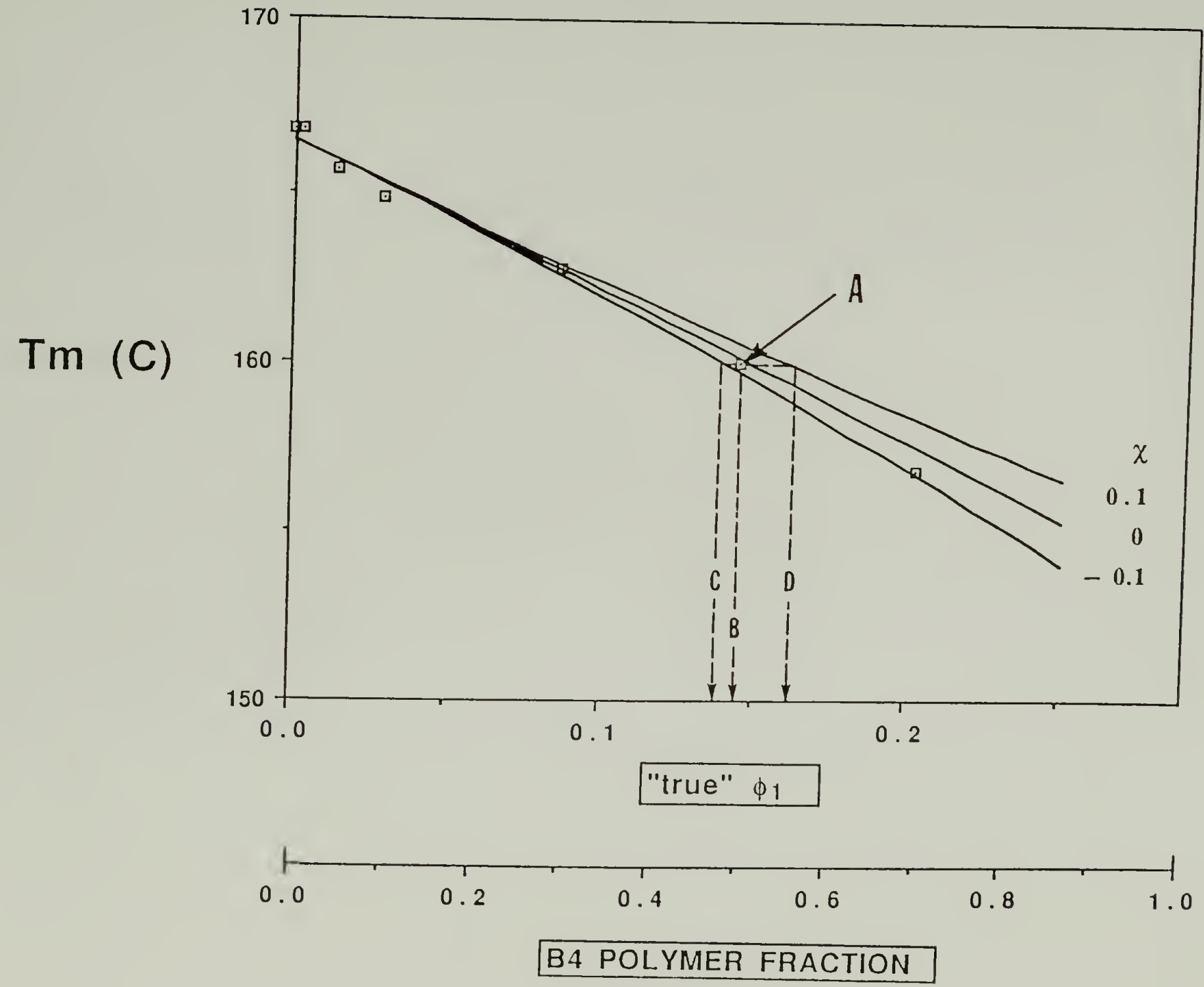
Tm (C)
170
160
150
A
C
B
D
χ
0.1
0
− 0.1
0.0
0.1
0.2
"true" ϕ_1
0.0
0.2
0.4
0.6
0.8
1.0
B4 POLYMER FRACTION

Table 5.4 Parameter Values Used for Equation 5.12.

Parameter	value	comment
T_m^o	166.5 (°C)	Melting Temperature of the B4 crystal (Peak value of the DSC Endotherm)
M_1	5	Degree of Polymerization of the B2 Hard Segment Structural Unit (3 MDI + 2 BD)
M_2	9	Degree of Polymerization of the B4 Hard Segment Structural Unit (5 MDI + 4 BD)
V_{2u}/V_{1u}	~ 1	Molar Volume Ratio of the Structural Unit of two Hard Segments (Same Structural Unit)
ΔH_{2u}	1807[a] (cal/mole)	Heat of Fusion of the Structural Unit

[a]
3.25 (cal/g of B4 Polymer)
45% Hard Segment in B4 Polymer
73% Crystallinity[1]
1644 g/mole of B4 Hard Segment
9 Structural Units in a B4 Hard Segment

1807 (cal/mole of Structural Unit)

the non-crystalline B4 domain of the samples with other blend composition can also be obtained in a similar fashion.

The phase behaviors of the linear paraffin mixtures have been studied widely.[35,36] In the case of the binary blend system $n\text{-}C_{32}H_{66}/n\text{-}C_{36}H_{74}$, it has been shown that this pair forms a continuous solid solution over all compositions as predicted.[37] By changing the blend composition, the melting temperature is changed continuously from the T_m of $n\text{-}C_{32}H_{66}$ to the T_m of $n\text{-}C_{36}H_{74}$. In other words, the incorporation of the long molecule in the matrix of the small molecules results in the increase of the melting temperature.

The transition temperature of the B2 hard domain does not seem to be sensitive to the blend composition as shown in Figure 5.10. Even though the results of the n-paraffins cannot be directly applied to this hard segment blend system, it may be inferred from the data that the B2 hard domain seems to be relatively pure with no evidence indicating the incorporation of B4 segments in B2 domains. More experimental results are required to characterize the smaller hard segment domains.

The annealing effect on the transition temperature can also be observed from Figure 5.10. The 25 degree difference of the annealing temperature results in approximately a 6 degree difference in the transition temperature of the B2 hard domain. In contrast, the B4 hard domain does not seem to be affected by that difference in the annealing temperature. Since the transition temperature of the B2 hard

domain is close to the annealing temperature, the difference in the transition temperature may be due to the increased order of chain packing. The melting temperature of the B4 hard domain is too far from the annealing temperature to be affected.

Conclusion

The conformation of the hard segments inside hard domain has been studied with SAXS studies. Since the main difference between two polyurethanes used is the difference in the hard segment length, the difference in the domain spacing is used to determine the hard segment conformation. According to the calculated and experimental values of difference in the domain spacing, the extended conformation model appears to be the more realistic on these materials. The monodisperse distribution of the hard segment length seems to be a determining factor for the extended chain model in contrast with the folded chain model of the polyurethanes with the broad distribution of hard segments length.

The miscibility behavior of the two hard segments with different segment length has been investigated by the infrared and differential scanning calorimetric methods. Even though two polymers have hard segments with similar chemical structure and identical soft segment, it is clearly shown that the two hard segments form separate hard domains at least for the blends of which composition is not very

skewed, i.e. 30/70 through 70/30 (B2/B4). Since the size similarity is one of the several requirements for the formation of the solid solution crystal,[10] the incompatibility between the two hard segments seems to be due to the difference in the segmental length.

The melting temperature of the B4 hard domain is shown to be sensitive to the blend composition. For the 50/50 blend sample, the melting temperature of the B4 hard domain is lowered by about 10 degrees from that of the pure B4 polymer. From the melting temperature depression analysis, it is estimated that the noncrystalline B4 hard domain of the 50/50 blend contains about 15% B2 hard segments. The contribution of the configurational entropy on the melting temperature depression is shown to be significant due to the low degree of the polymerization of the hard segments. The effect of the interaction term becomes significant at the higher volume fractions. Since the transition temperature of the B2 hard domain is shown to be insensitive to the blend composition, it seems to indicate that the B2 hard domain is relatively free of the B4 hard segments.

From the results obtained in this study, the schematic model of the internal structure of the polyurethane blend is suggested in Figure 5.12. There are two different hard domains with different hard segments. The hard domains with the longer hard segments contain small amounts of the short hard segments ("A" in the figure), whereas the domain with the short hard segments is relatively pure. Furthermore, the

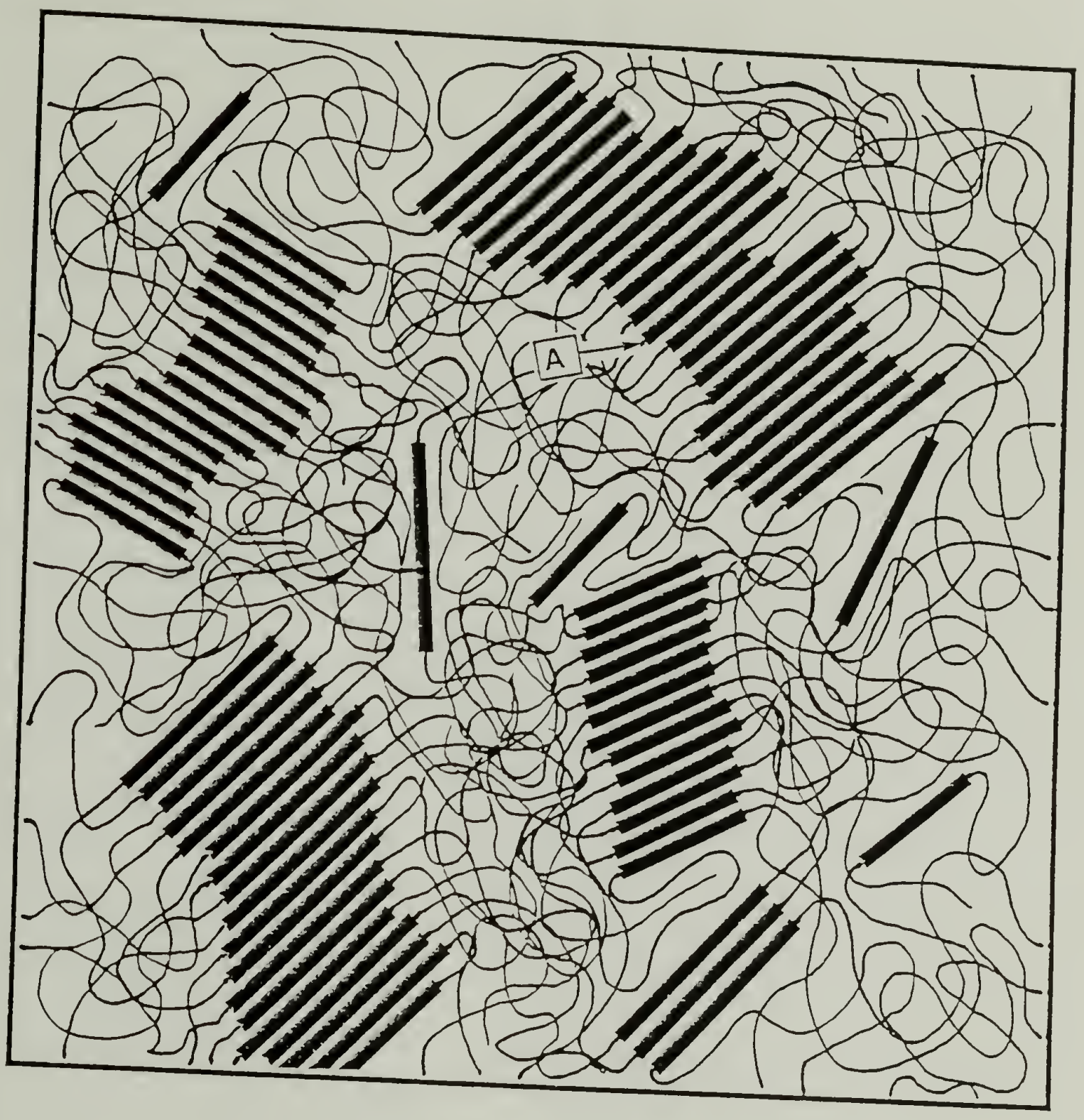

FIGURE 5.12 Schematic picture of the internal phase structure of the B2/B4 blend; Two types of hard domains containing the different hard segments are shown; "A" denotes the short hard segments dissolved in the hard domains of the long hard segments.

main conformation of hard segments are an extended conformation as shown in Figure 5.12. The soft segment matrix is expected to contain a small amount of the hard segments due to the incomplete phase separation. The dependence of the soft matrix on the blend composition can be characterized at the low temperature (< 0°C) region of the DSC thermograms.

This study is useful for understanding the phase separated structures of commercial polyurethanes with a broad hard segment length distribution. Since the hard segments phase separate into different domains according to their segmental length, the hard domains of the commercial polyurethane may not be all the same but roughly divided into the different domains according to their segmental length. Similar behavior has been claimed in literature.[15]

The phase separation of the hard segments according to their segmental length can be also applied to the fractionation of the hard segments. By annealing at the high temperature, only those hard domains that are stable at that temperature can be formed. By lowering the temperature slowly, the hard segments will, therefore, form separate hard domains according to their segmental length. The commercial material will have, of course, much more complicated structure due to the random sequence of the hard segment length and the connectivity between them. However, the results obtained here can be applied, at least qualitatively,

to understand the phase behavior of commercially important polyurethane materials.

References

1. Cooper,S.L.; Tobolsky,A.V. *J.Appl.Polym.Sci.* **1966**, 10, 1837.

2. Miller,J.A.; Lin,S.B.; Hwang,K.K.S.; Wu,K.S.; Gibson,P.E.; Cooper,S.L. *Macromolecules* **1985**, 18, 32.

3. Christenson,C.P.; Harthcock,M.A.; Meadow,M.D.; Spell,H.L.; Howard,W.L.; Creswick,M.W.; Guerra,R.E.; Turner,R.B. *J.Polym.Sci.-Phys.* **1986**, 24, 1401.

4. Eisenbach,C.D. *Polymer Preprint* **1985**, 26, 7.

5. Qin,Z.Y.; Macosko,C.W.; Wellinghoff,S.T. *Proc.Div.Polym.Mat. Sci.Eng.* **1983**, 49, 475.

6. Harrell,L.L. *Macromolecules* **1969**, 2, 607.

7. Eisenbach,C.D.; Guenter,Cl. *Proc.Div.Polym.Mat.Sci.Eng.* **1983**, 49, 239.

8. Hwang,K.K.S.; Hemker,D.J.; Cooper,S.L. *Macromolecules* **1984**, 17, 307.

9. Hwang,K.K.S.; Lin,S.B.; Tsay,S.Y.; Cooper,S.L. *Polymer* **1984**, 25, 947.

10. Kitaigorodsky,A.I. "Molecular Crystals and Molecules" Academic Press, New York, **1973**.

11. Gardner,K.H.; Blackwell,J. *Acta Crystallogr.* **1980**, B36, 1975.

12. Blackwell,J.; Nagarajan,M.R.; Hoitnik,T.B. *Polymer* **1982**, 23, 950.

13. Blackwell.J.; Lee,C.D. *J.Polym.Sci.-Polym.Phys.Ed.* **1983**, 21, 2169.

14. Van Bogart,J.W.C.; Gibson,P.E., Cooper,S.L. *J.Polym.Sci.-Polym.Phys.Ed.* **1983**, 21, 65.

15. Koberstein,J.T.; Stein,R.S. *J.Polym.Sci.-Polym.Phys.Ed.* **1983**, 21, 1439.

16. Leung,L.; Koberstein,J.T. *J.Polym.Sci.-Polym.Phys.Ed.* **1985**, 23, 1883.

17. Flory,P.J. "Principles of Polymer Chemistry" Cornell Univ. Press, Ithaca, **1953**.

18. Scott,R.L. *J.Chem.Phys.* **1949**, 17, 279.

19. Lee,H.S.; Wang,Y.K.; Hsu,S.L. *Macromolecules* **1987**, 20, 2089.

20. Debye,P.; Bueche,A.M. *J.Appl.Phys.* **1949**, 20, 518.

21. Blackwell,J.; Gardner,K.H. *Polymer* **1979**, 20, 13.

22. Born,L.; Crone,J.; Hespe,H., Mueller,E.H.; Wolf,K.H. *J.Polym.Sci.-Polym.Phys.Ed.* **1984**, 22, 163.

23. Briber,R.M.; Thomas,E.L. *J.Polym.Sci.-Polym.Phys.Ed.* **1985**, 23, 1915.

24. Bonart,R.; Morbitzer,L.; Hentze,G. *J.Macromol.Sci.(B)* **1969**, 3, 337.

25. Seymour,R.W.; Estes,G.M.; Cooper,S.L. *Macromolecules* **1970**, 3, 579.

26. Lee,H.S.; Wang,Y.K.; MacKnight,W.J.; Hsu,S.L. *Macromolecules* **1988**, 21, 270.

27. Lee,H.S.; Hsu,S.L. *Macromolecules* **1989**, 22, 1100.

28. Coleman,M.M.; Lee,K.H.; Skrovanek,D.J.; Painter,P.C. *Macromolecules* **1986**, 19, 2149.

29. Trifan,D.S.; Terenzi,J.F. *J.Polym.Sci.* **1958**, 28, 443.

30. Tsubomura,H. *J.Chem.Phys.* **1956**, 24, 927.

31. Skrovanek,D.J.; Howe,S.E.; Painter,P.C.; Coleman,M.M. *Macromolelcules* **1985**, 18, 1676.

32. Matheson,R.R.Jr.; Smith,P. *Polymer* **1985**, 26, 288.

33. Asbach,G.I.; Kilian,H.G.; Stracke,Fr. *Colloid & Polymer Sci.* **1982**, 260, 151.

34. Nishi,T.; Wang,T.T. *Macromolecules* **1975**, 8, 909.

35. Dorset,D.L. *Macromolecules* **1986**, 19, 2965.

36. Lueth,H.; Nyburg,S.C.; Robinson,P.M.; Scott,H.G. *Mol.Cryst. Liq.Cryst.* **1974**, 27, 337.

37. Dorset,D.L. *Macromolecules* **1985**, 18, 2158.

CHAPTER VI

INVESTIGATION OF THE MOLECULAR ORIENTATION BY THE METHOD OF INFRARED DICHROISM

Introduction

Considerable amount of studies have been carried out to comprehend the structure property relationship of thermoplastic elastomers. It is generally accepted that the elastic properties of the segmented polyurethanes are mainly due to the phase separated heterogeneous structure.[1,2] The two components, hard and soft segments, undergo microphase separation due to the incompatibility between the two structural units.

It has been shown that there is a close relationship between the mechanical properties of the polyurethanes and their morphology. Sample morphology is affected by many factors such as the chemical nature of the components,[3-5] stoichiometric ratio between the two segments,[6] molecular weight and distribution of the segments[7,8] and also the synthetic method used in making the polymer.[9,10] It is, therefore, extremely important to study the well defined polymers from which several factors affecting the physical properties have been excluded.

The effect of the morphology on the physical properties has been demonstrated by studying a series of polyurethanes

with similar chemical composition but different relative amount of individual component.[11] By increasing the hard segment content to slightly above the certain critical value, there is abrupt change in the deformation behavior. The morphology change from the isolated hard domains to the interconnected hard domain is well correlated to that abrupt change in the deformation behavior.

The crystallinity of the hard domain has also been found to have a significant effect on orientational behavior.[12] For a crystalline hard segment, a peculiar negative orientation has been observed for small strain value, whereas a noncrystalline hard domain shows an increasing orientation function for all strain levels.[13] The negative orientation function of vibratios has been observed in many cases for a variety of polymers such as polyethylene,[14-17] polyester,[18] nylon,[19] polyvinyl chloride[20] and polyurethane[11,21] even though the exact explanation has still to be given; particularly in the case of the polyurethanes.

As stated above, the deformation behavior of the heterogeneous material is extremely complicated. The information on the orientational behavior of all parts of the molecule has to be combined in order to understand the overall response of the material upon deformation. Since infrared spectroscopy can be used to study the orientation behavior of each of the individual functional groups, it has been extensively used in the study of the orientational properties of polyurethanes.

In this chapter, the molecular orientation of the hard and soft domains will be analyzed to study the characteristic responses when stressed. Infrared dichroism is extensively used to monitor the local segmental orientation. The stress and orientation relaxation behavior of selected vibrational modes is expected to reveal the time variation of the domain change upon deformation.

Overview of the Orientation Theory

Orientation Function Measurements by Infrared Dichroism

Infrared activity in organic molecules occurs when a vibrational mode produces a changing electric dipole moment **M**, which is a transition moment vector of the normal mode.[22,23] Absorption occurs when the electric field vector of the incident radiation, **E**, has a component parallel to the direction of **M**. The absorption of infrared radiation can be given in terms of the absorbance, A, defined by

$$A = \mathrm{Log}_{10}\frac{I_o}{I} \tag{6.1}$$

where I_o is the incident intensity and I is the transmitted intensity. For a given normal mode of vibration, the transition moment vector has a definite orientation in the molecule. If the angle between **M** and **E** is β, then the absorbance is proportional to $\cos^2\beta$.

For non-oriented materials, the absorbance is independent of the polarization of the incident radiation

because of the random orientation of the molecules. In a drawn polymer, the molecular chains are preferentially oriented along the deformation direction. With the polarization parallel and perpendicular to the deformation direction, the two separate absorbances can, therefore, be obtained. From the ratio of the two absorbances, a dichroic ratio, R, is defined as

$$R = \frac{A_{\parallel}}{A_{\perp}} \tag{6.2}$$

where $A_{\parallel}$ is the absorbance for linearly polarized light parallel to the chain direction and $A_{\perp}$ perpendicular to the chain axis.

In the case of uniaxial orientation, the dichroic ratio for perfectly oriented material, R_o, has been obtained as[24]

$$R_o = 2 \cot^2\alpha \tag{6.3}$$

where α is the angle between the transition moment vector **M** and the chain axis as shown in Figure 6.1. For perfectly oriented materials, the angle α can be, therefore, calculated by measuring the dichroic value. In general, the orientation of the molecule is incomplete. The molecular chain axis is generally distributed around the deformation direction. If only a certain fraction, f, of the total molecules are perfectly oriented and the remaining molecules are randomly oriented in the three dimensional space, the relationship between f and the dichroic ratio is then expressed as follows[25]

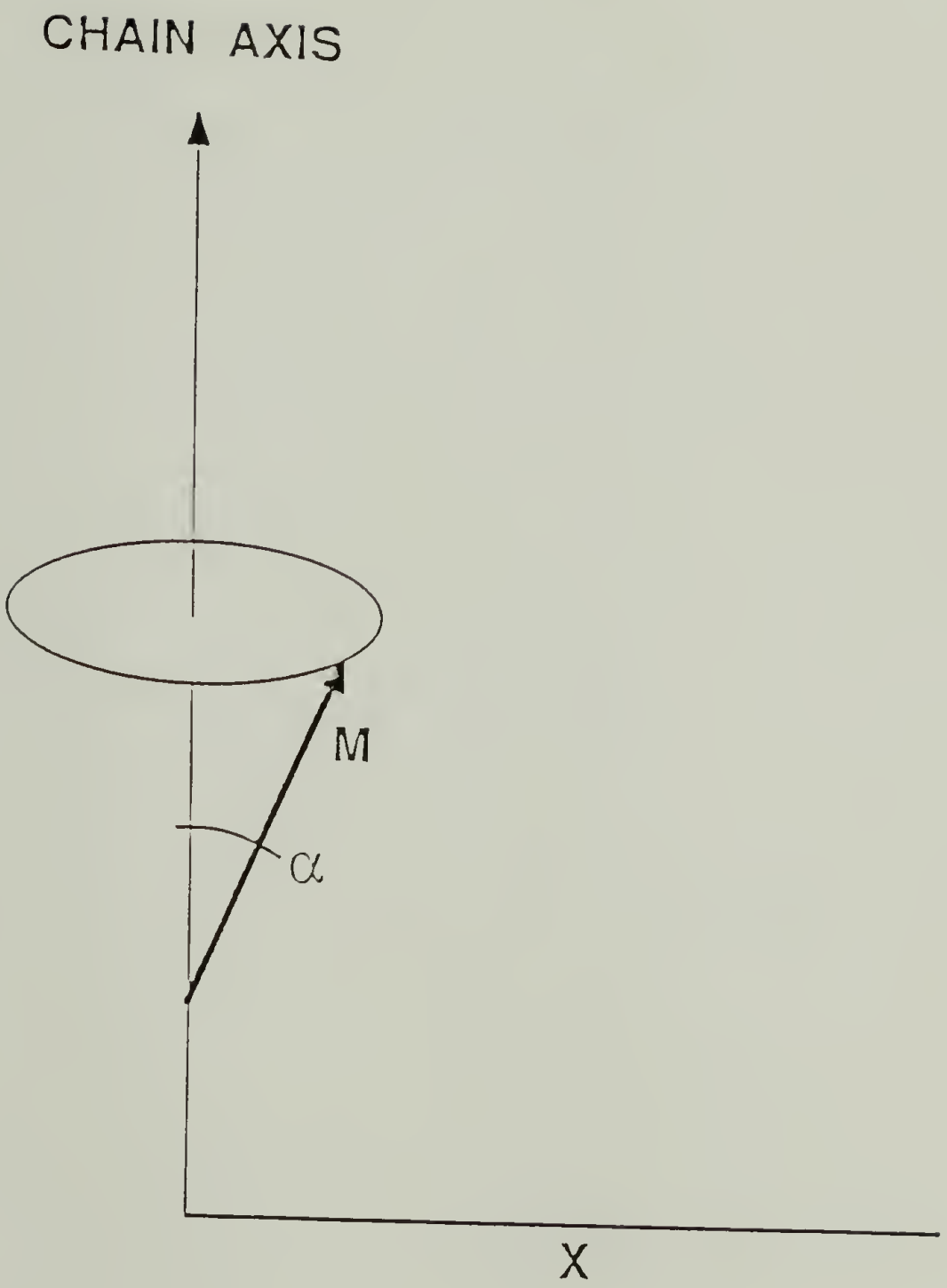

FIGURE 6.1 Schematic representation of relationship between transition moment (**M**) and chain axis of perfectly ordered sample.

$$f = \frac{(R_o + 2)}{(R_o - 1)} \frac{(R - 1)}{(R + 2)} \tag{6.4}$$

The incomplete orientation can also be treated by assuming that all the molecules have the average angle, θ, with the deformation direction as shown in Figure 6.2. The relationship between the average angle, θ, and the fraction, f, of the perfectly oriented molecule have been obtained as

$$f = \frac{3\cos^2\theta - 1}{2} \tag{6.5}$$

The concepts of a fraction, f, of perfectly oriented material and an average angle of disorientation θ were used by Hermans treatment, f is called Herman's orientation function.

Deformation Theory of Elastic Network

Extensive theoretical developments for the deformation of a polymer network have been made.[27] Since the physical crosslinks of polyurethanes acts as crosslinks, the network deformation theory can be applied to polyurethanes with appropriate modification.

Several assumptions usually made during the derivation of the orientation distribution function are as follows.[27]

1. It is assumed that each chain consists of N freely jointed statistical segments.
2. The end-to-end vector distance r_o of a chain in the unstrained state is equal to the root-mean-square vector distance of the free chain, i.e.,

$$r_o = N^{1/2} l_s \tag{6.6}$$

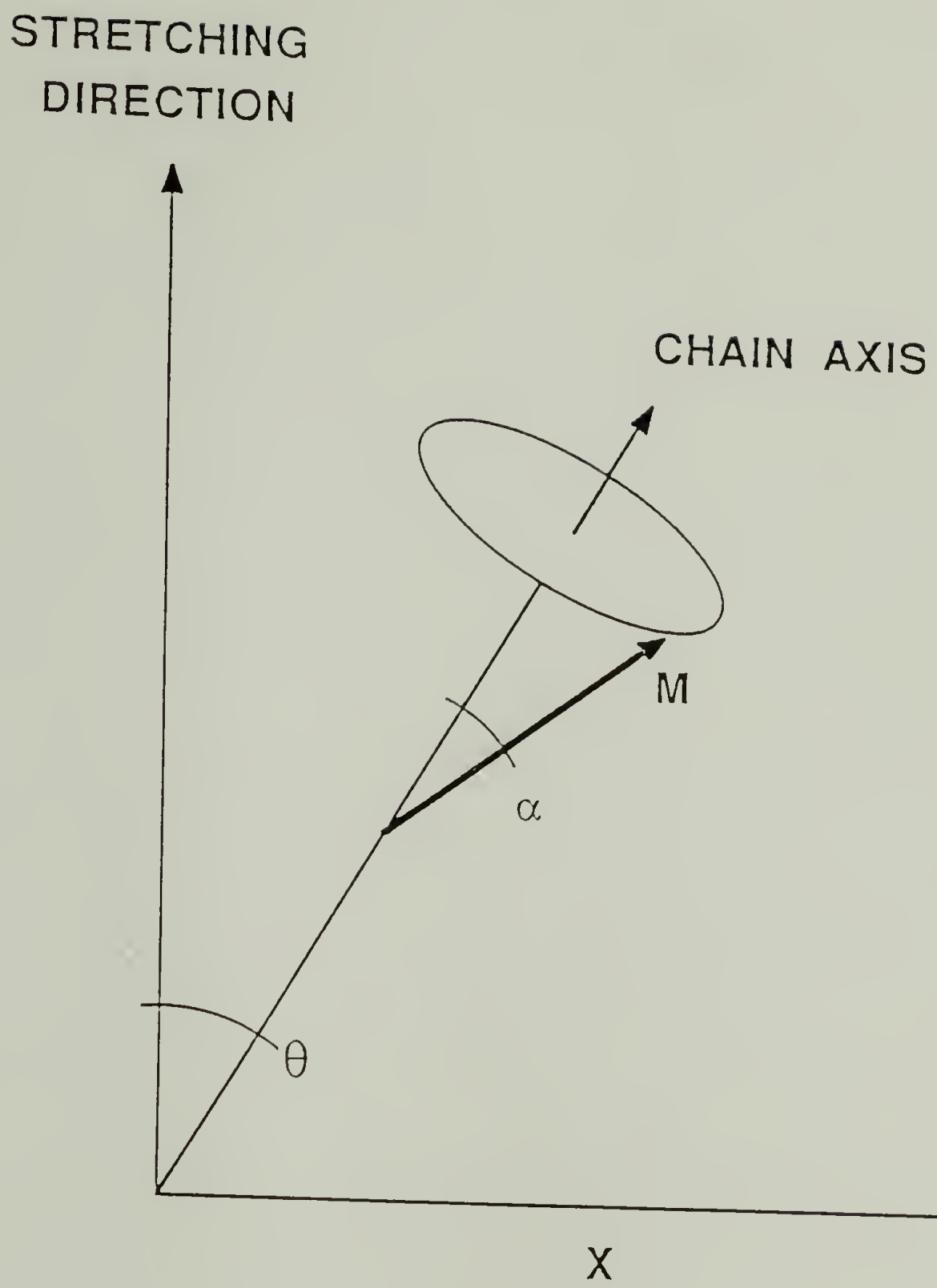

FIGURE 6.2 Schematic representation of relationship between transition moment (**M**), chain axis and stretching direction.

where l_s is the length of a statistical segment.

3. On deformation, the end-to-end vectors undergo an affine deformation.
4. There is no volume change on deformation.

The orientation function of the statistical segments in a collection of chains can be obtained by combining the two orientation distribution functions, i.e. the distribution function of the end-to-end vectors of the chains in the deformed state with respect to the laboratory axis, $g_c(\theta_c)$ and the angular distribution function of the statistical segments with respect to the end-to-end vector direction, $g_s(\theta_s)$.

Kratky introduced a pseudo affine model where orientation is treated as occurring with the angular rotation of the microstructural units, for example crystalline units, without any dimensional change.[28] Applying this model to the deformation of the polymeric chain, the end-to-end vector of a chain is assumed to be a rigid structural unit that undergoes rotation to the deformation direction without stretching.

The distribution function of the end-to-end vectors of the chains with respect to the stretch direction is[28]

$$g_c(\theta_c) = \frac{1}{2} \cdot \frac{\lambda^3 \sin\theta_c}{[\cos^2\theta_c + \lambda^3 \sin^2\theta_c]^{3/2}} \qquad (6.7)$$

where λ is the draw ratio and θ_c is the angle between the end-to-end vector, $\mathbf{r}$, and the stretch direction.

The orientation distribution function, $g_s(\theta_s)$, of the segments along the end-to-end vector direction of a single chain has been obtained by Kuhn & Grun.[29] If θ_s is the angle specifying the orientation of a segment with respect to the end-to-end vector, **r**, of the chain, then it is given as

$$g_s(\theta_s) = \frac{1}{2} \cdot \frac{N\beta}{\sinh\beta} e^{-\beta\cos\theta_s} \sin\theta_s \tag{6.8}$$

where $\beta = L^{-1}(r/Nl_s)$. L is the Langevin function defined as

$$L(\beta) = r/Nl_s = \coth\beta - 1/\beta \tag{6.9}$$

It is to be noted that the inverse Langevin function, $L^{-1}(r/Nl_s)$, approaches infinity as the magnitude of the end-to-end vector becomes fully extended length, i.e. Nl_s.

Several optical properties of the network which depend on the orientation can be calculated with the two distribution functions. The polarizability difference, $P_{\parallel} - P_{\perp}$, of the network can be calculated with Equations 6.7 and 6.8 as[27]

$$\Delta P = P_{\parallel} - P_{\perp} = \frac{1}{5} \cdot N_c (b_1 - b_2)\left[\lambda^2 - \frac{1}{\lambda}\right] \tag{6.10}$$

where b_1, b_2 are segment polarizabilities in the parallel and perpendicular direction, respectively. By applying Equation 6.10 to the differentiated Lorenz-Lorentz equation, the birefringence can be expressed as[27]

$$\Delta n = \frac{2\pi}{45} \cdot N_c (b_1 - b_2) \frac{(n^2 + 2)^2}{n}\left[\lambda^2 - \frac{1}{\lambda}\right] \tag{6.11}$$

For the network of the elastomeric polymer chains, the theoretical value of the infrared dichroism can be calculated

with Equations 6.7 and 6.8.[30,31] Integration over all the segments in a single chain has to be obtained with Equation 6.13 and over all chains with Equation 6.12. The resulting dichroism, R, is

$$R = \frac{N + \frac{2}{5}\left(\cos^2\alpha - \frac{1}{2}\sin^2\alpha\right)\left(\lambda^2 - \frac{1}{\lambda}\right)}{N - \frac{1}{5}\left(\cos^2\alpha - \frac{1}{2}\sin^2\alpha\right)\left(\lambda^2 - \frac{1}{\lambda}\right)} \qquad (6.12)$$

where α is the angle between statistical segment direction and transition moment. Since the dichroic and extension ratio can be measured relatively easily, the number of statistical chain segments, N, can be obtained by comparing the experimental data with Equation 6.12 for the infrared band, for which the transition moment direction is known.

Experimental

The one model polyurethane extensively used in this deformation experiment is the B4 polyurethane. Each hard segment of the B4 polyurethane contains five MDI and four BD units. The chemical structure is shown in Figure 2.2. The butadiene based polyurethane (T3MI), which was synthesized in solution to ensure the homogeneous state during polymerization, has also been used to compare the experimental dichroic ratio with the theoretical values predicted from the elastomeric network theory. The chemical structure of the butadiene based polyurethane is shown in

Figure 4.1. The information about the hard segments of the butadiene based polyurethane is given in the Experimental section of Chapter IV.

The polymers were dissolved in THF solvent to make about a 2%(w/v) solution. A thin film was then obtained by casting the solution on a Teflon coated glass slide or a Teflon mold. The film was dried initially under the hood for several hours, followed by vacuum drying for a few days at about 60 degrees.

The sample mounted on the stretcher was strained from both directions so that the identical position of the sample could be characterized during the deformation process. For stress relaxation measurements, the load cell, which was connected to the sample holder, was used to monitor the stress relaxation as a function of time.

The polarization of the incident infrared light was achieved with a gold wire polarizer on a KRS-5 substrate. Infrared spectra were obtained with the Bruker model IFS 113v vacuum Fourier transform infrared spectrometer.

The infrared spectra of the B4 polyurethane with two different polarizations at a 300% strain are shown in Figure 6.3. The spectrum with no strain is also shown in a dotted line as a reference. The thickness change due to the deformation is compensated by equating the integrated area of the C-H stretching peaks. The dichroic behavior of the many peaks is obvious from Figure 6.3.

FIGURE 6.3 Survey spectra of B4 polyurethanes with two polarizations at 300% strain; Spectra without strain are shown in dotted line; Thickness change due to stretching is corrected; Stretching direction is vertical and polarizations of each peak are shown in the figure.
(a) 3600-2600cm^{-1}
(b) 1900-900cm^{-1}

(a)

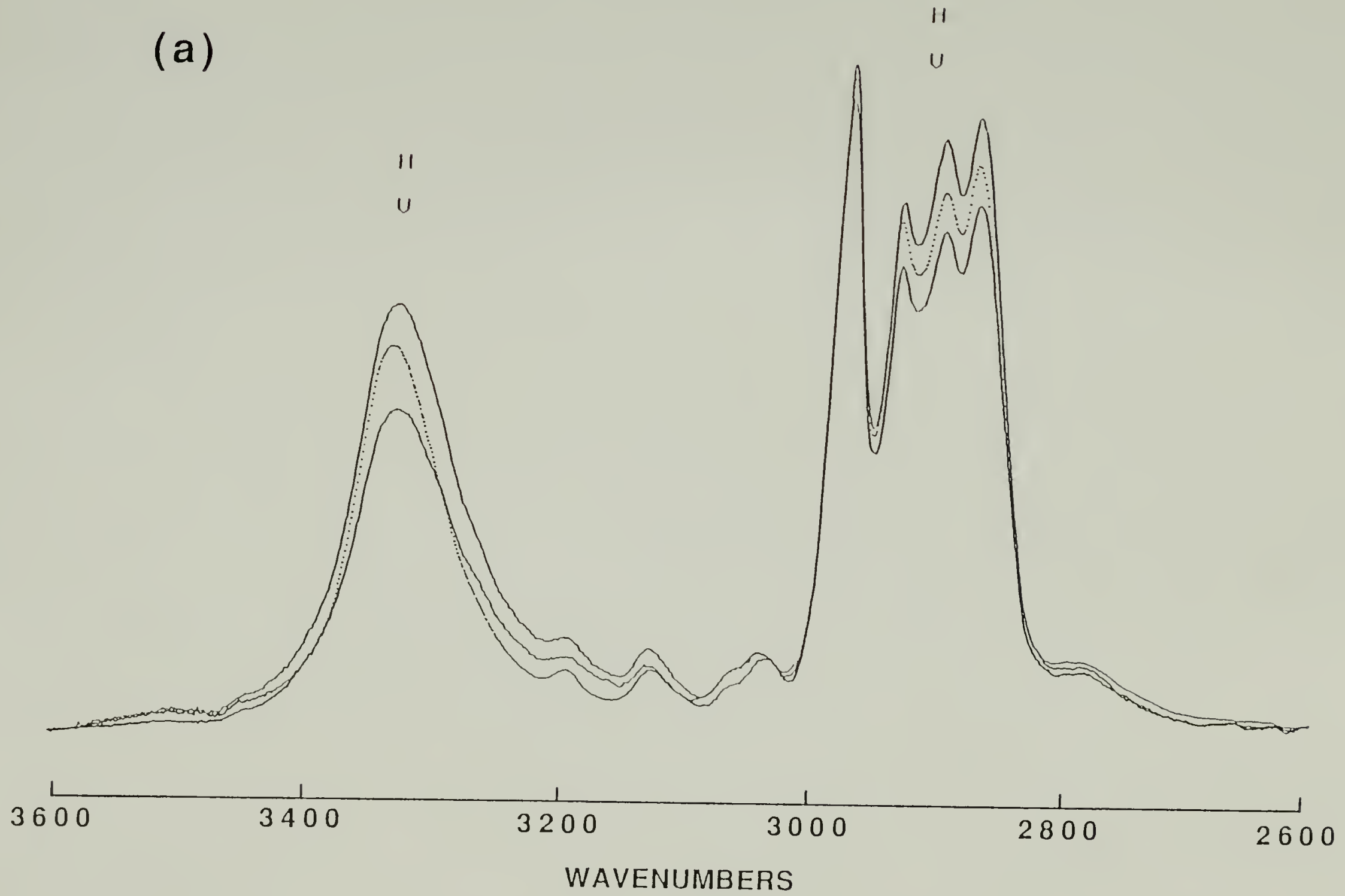

(b)

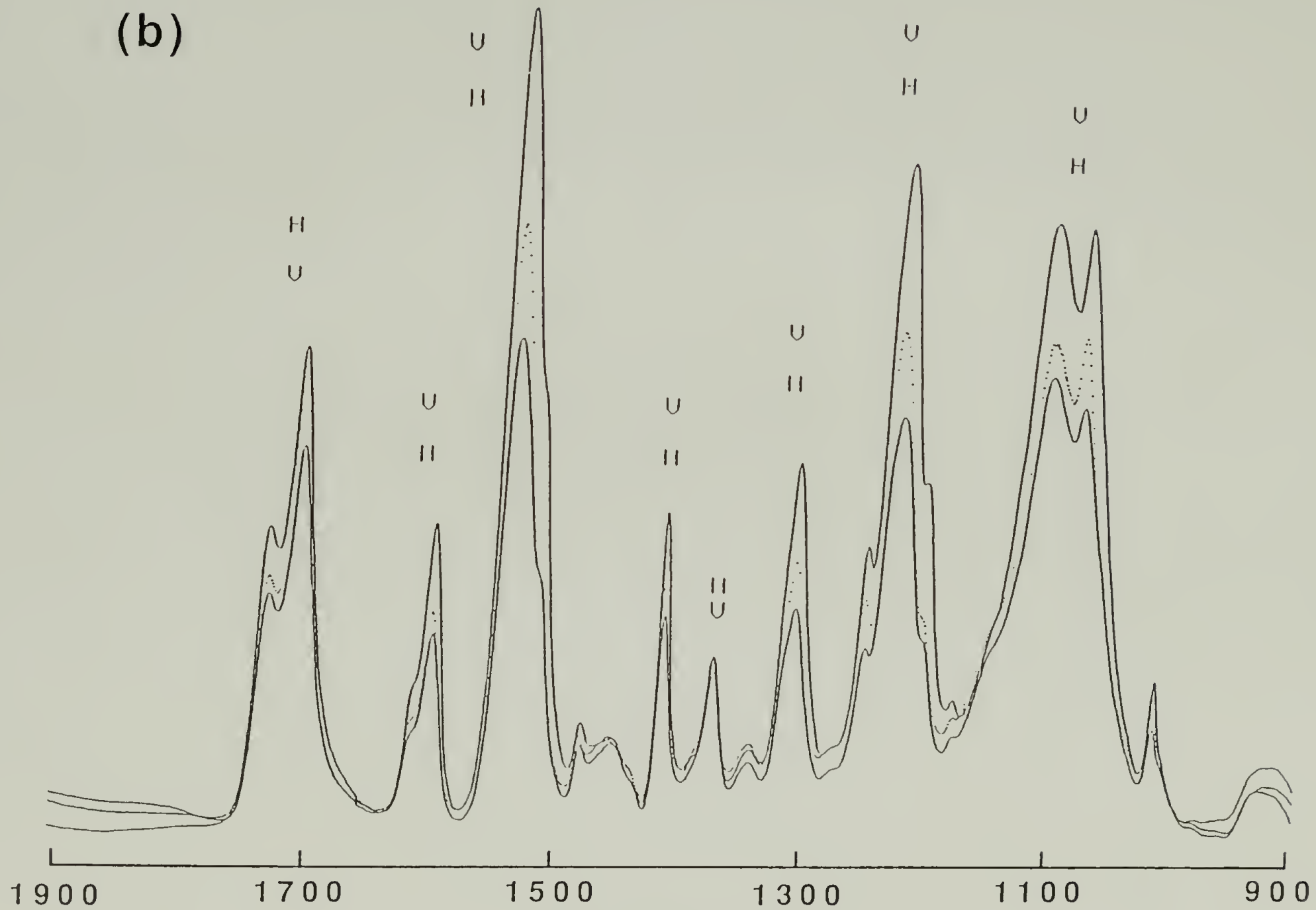

The deformation during a tensile experiment was carried out by a step-wise process. After each deformation, the sample was relaxed for about five minutes to achieve the equilibrium state. Unless stated otherwise, the intensity was obtained from the peak height due to the ambiguity of band overlap. The sample temperature was controlled by nitrogen gas blown into the purge box. The experimental set-up is shown schematically in Figure 3.2.

The stress relaxation experiment was done at a 100% strain. After a step strain, the two spectra with perpendicular and parallel polarization were obtained consecutively as a function of time. The orientation functions were calculated with the two spectra obtained consecutively, even though the exact collection time could be slightly different. This difference is assumed to be negligible.

Results and Discussion

Orientation Behavior of Each Segment

The deformation behavior of each domain in the phase separated polyurethanes is expected to be different. Since the modulus of the soft segment is lower than that of the hard segment, initial deformation has to occur mainly through the soft segment. The soft domain stress is then transferred into the hard segment deformation. The final orientation behavior is further affected by the different relaxation

behavior. Due to the low glass transition temperature of the soft segment, the orientation of the soft segment after step strain is applied is expected to relax rapidly. Since the hard segment is in its glassy state, the orientation of the hard domain as a whole may occur simultaneously with the hard segment orientation.

The carbonyl stretching bands at several different strains are shown in Figure 6.4. The dotted spectra are obtained with parallel polarization. The intensity change due to a thickness change during deformation has been corrected as explained in the Experimental section. The relative intensity change can be compared directly. Since the angle of the transition moment vector of the C=O stretching component is known to be close to 90°, most of the perpendicular components show higher absorbance than the corresponding parallel parts.

For the C=O stretching peak at 1730cm^{-1} which is free of hydrogen bonding, the dichroic ratio decreases continuously by increasing the strain from 50% to 300%. At the 50% strain, there is an appreciable amount of dichroism already developed. As the strain increases, the polymeric chains tend to better align to the stretch direction. Since the C=O group is approximately perpendicular to the chain direction, the dichroic change of the free C=O peak is easily understood by the orientation of the chain along the stretch direction. It has been shown that the free C=O peak is mainly due to the hard segment dissolved in the soft matrix.[32,33] The

FIGURE 6.4 Carbonyl stretching region at different strain; Relative orientations of the polarizer to the stretching direction are indicated in the figure.

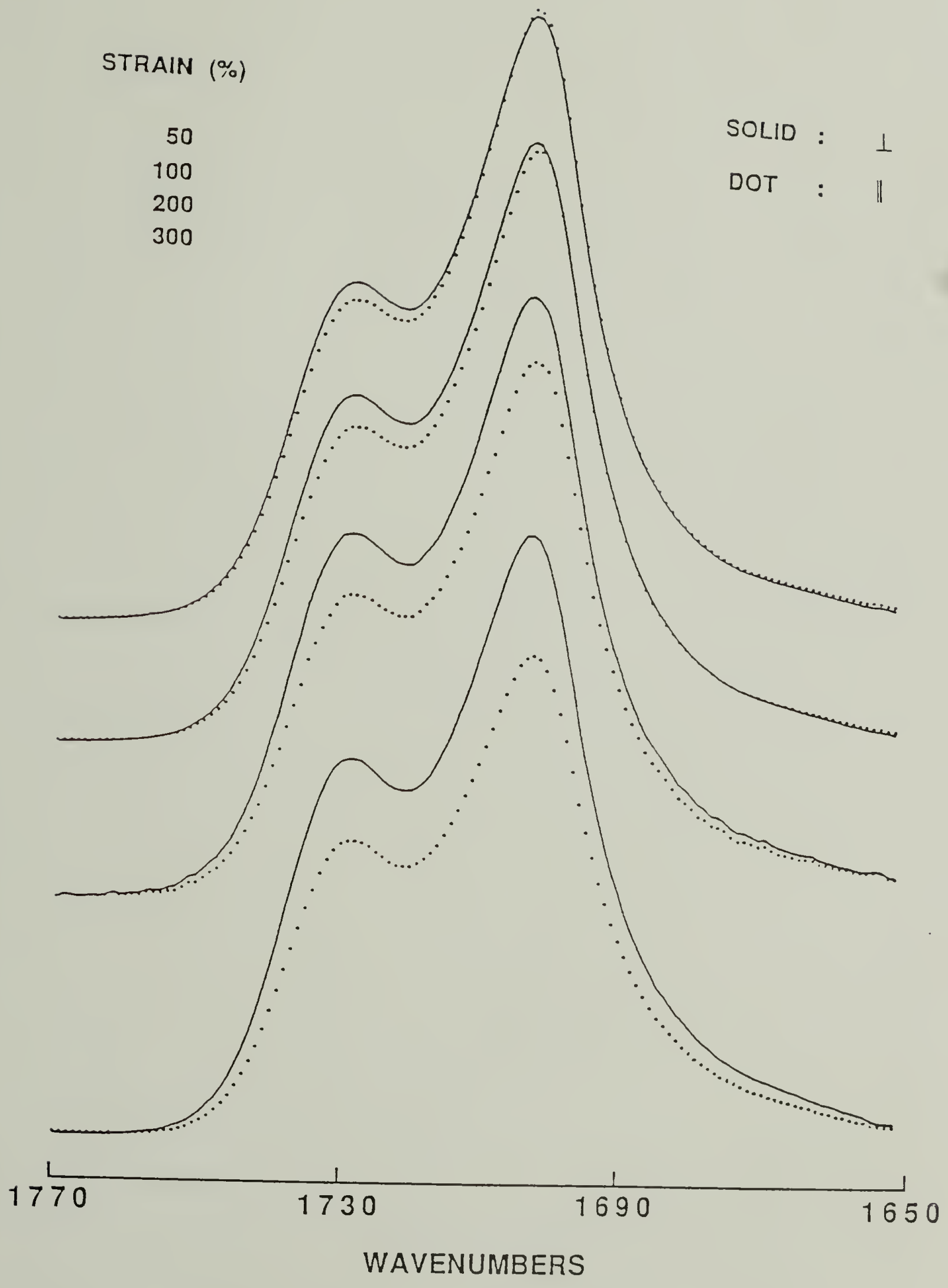
STRAIN (%)
50
100
200
300
SOLID : ⊥
DOT : ∥
1770
1730
1690
1650
WAVENUMBERS

deformation behavior of the free C=O peak is, therefore, expected to represent the deformation behavior of the chains in the soft matrix.

The deformation behavior of the hydrogen bonded C=O stretching peak at 1700cm^{-1} is different from that of free component. The dichroism of this peak at the 50% strain is opposite to that of the corresponding free component. At the 100% strain, only a small amount of dichroism has been observed compared with the free component. This different dichroic behavior indicates that the deformation behavior of the hard segments in the hard domain, which is represented by the hydrogen bonded C=O component, is distinctively different from that of the hard segments in the soft matrix.

The orientation functions of the two components, i.e. free and hydrogen bonded C=O stretching components, are calculated according to Equation 6.4 and shown in Figure 6.5 as a function of strain. The transition moment direction of that peak is assumed to be 78° with respect to the chain direction.[34] The orientation functions are obtained during the full cycle of deformation. The different orientation behavior has been clearly observed. The free component which represents the chains in the soft matrix exhibits the highly elastic behavior, whereas the hydrogen bonded component shows significant hysteresis behavior. The orientation function of the bonded component becomes negative initially before it increases to a positive value at high strain. This negative

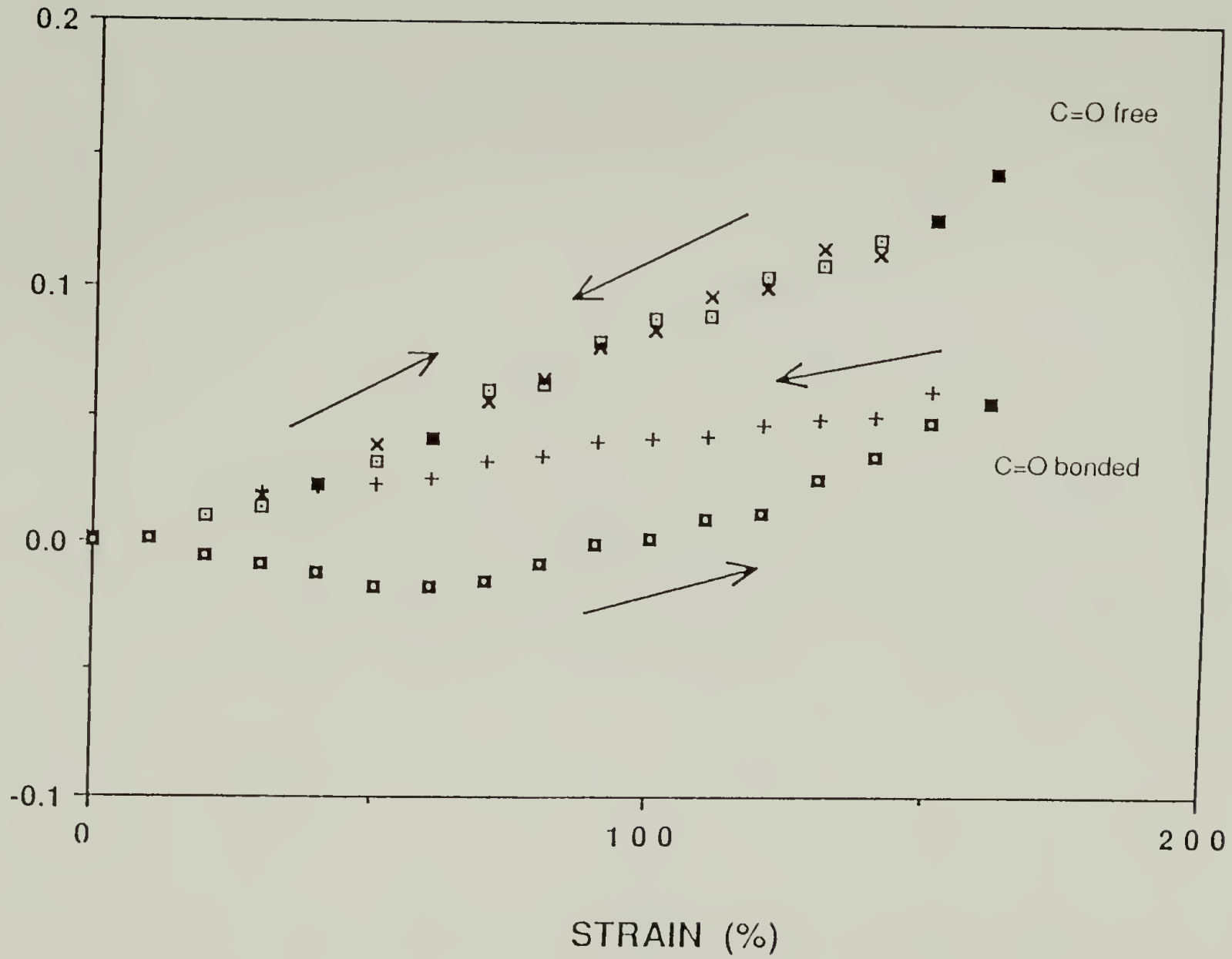

FIGURE 6.5 Orientation function of two carbonyl peaks plotted as a function of full cycle of strain.

orientation function is already predicted from the peculiar dichroic behavior of this component observed in Figure 6.4.

The inversion of the orientation function, that is a negative value at a small strain and a positive value at a high strain, has been generally attributed to the initial orientation of the long lamellar hard domains into the deformation direction and the subsequent disruption of the hard domain resulting in a positive orientation function.[11] Since the explanation given above could not account for the non-negative orientation function of the different vibrational modes in the same segment, other interpretations based on the conformational transition model are also suggested.[35] In the case of the polyether urethane urea elastomers, the conformational transition model seems to explain fully the peculiar orientation phenomenon of all vibrational modes in the same hard segment. Even though the orientation of the hard domain, rather that hard segments itself, is generally believed to cause the negative orientation function at a small strain, the complete explanation has to be given due to the inability of that model to account for the non-negative orientation behavior of other infrared bands pertaining to the same hard segment.

The hysteresis seems to be due to the restructuring of the hard domain. At a high strain, the hard domain starts to break and new hard domains are formed upon the release of the stain. The area of the hysteresis curve is, therefore, related to the amount of work needed to restructure the hard

domain during deformation. The elastic behavior of the free C=O peak indicates that the elastic energy stored in the soft matrix is mainly entropic in nature.

The orientation function of the C-H stretching region at 3000-2800cm^{-1} is shown in Figure 6.6. The integrated area of the C-H stretching peak is assumed to represent the soft segments even though the hard segments contain a small amount of the C-H functional group. The degree of orientation of the soft segments is found to be smaller than that of the hard segments. It is due to the fast relaxation of the flexible soft segments. The soft segment seems to transfer the orientation to the hard segment to undergo the relaxation process. The resultant orientation remains, therefore, mainly on the hard segments resulting in the small orientation for the soft segment.[36]

The orientational relaxation of the soft segments can also be observed from the deformation experiments at different temperatures. The tensile experiments were carried out at three different temperatures and the orientation functions of the free and hydrogen bonded C=O stretching peaks are plotted in Figures 6.7a and b. Orientation function of the free C=O component is found higher at a low temperature (4°C) than at a high temperature (44°C). The temperature effect on the orientation behavior of the hydrogen bonded component is not significant as shown in Figure 6.7b.

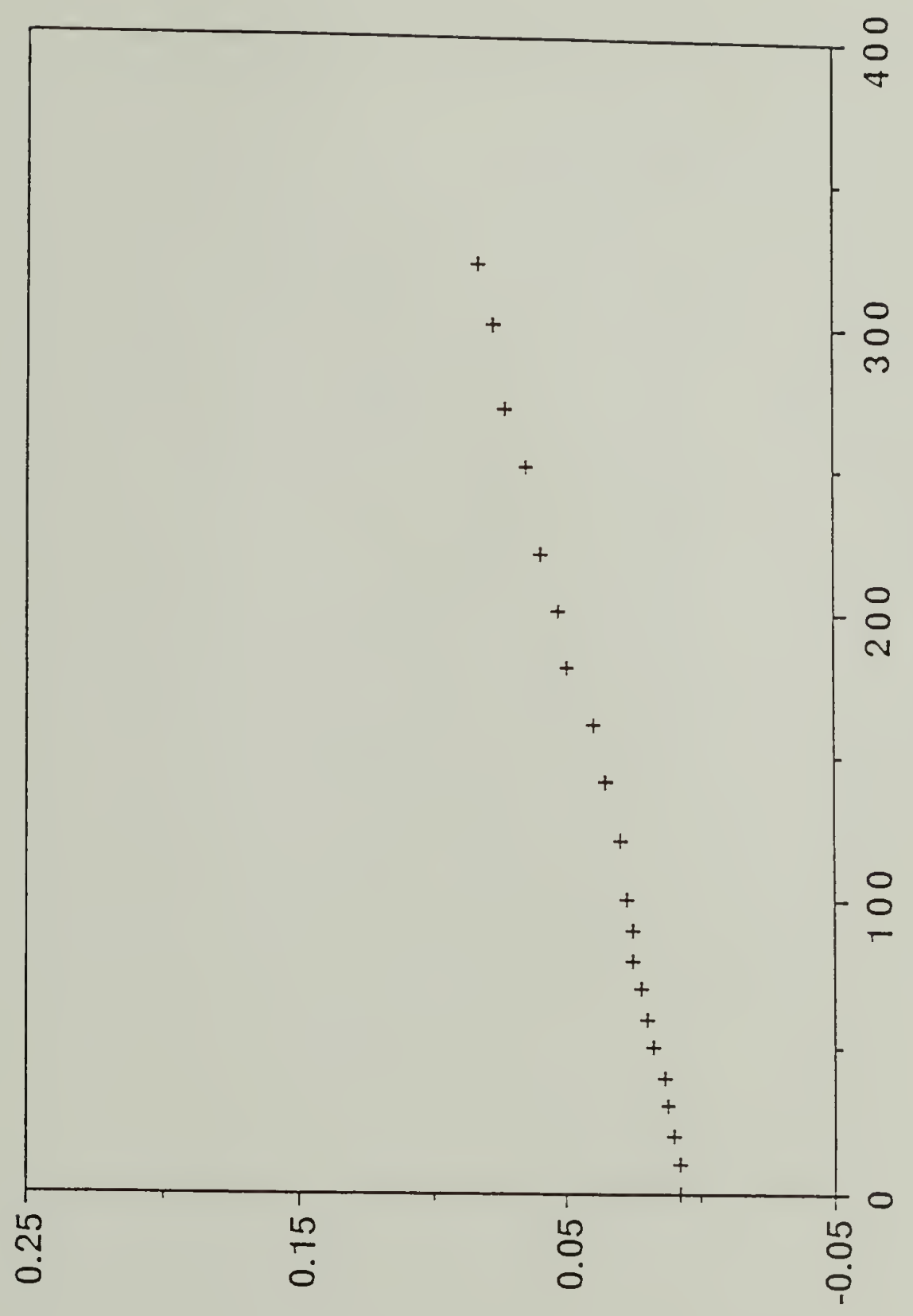

FIGURE 6.6 Orientation function of integrated C-H stretching region plotted as a function of strain.

FIGURE 6.7 Orientation function of carbonyl peaks at three different temperatures plotted as a function of strain. (a) free peak (b) hydrogen bonded peak

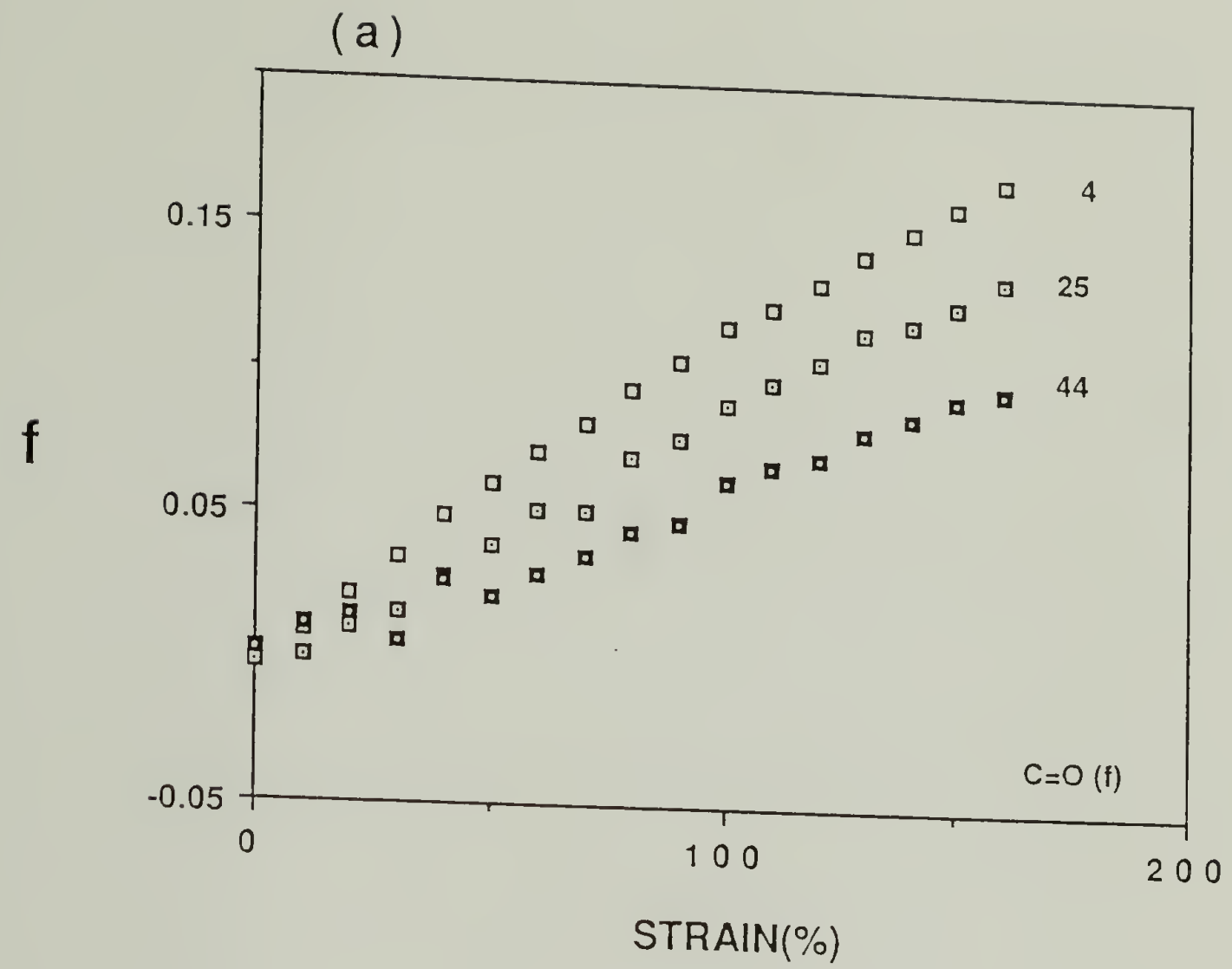
(a)
f
0.15
0.05
-0.05
0
100
200
STRAIN(%)
4
25
44
C=O (f)

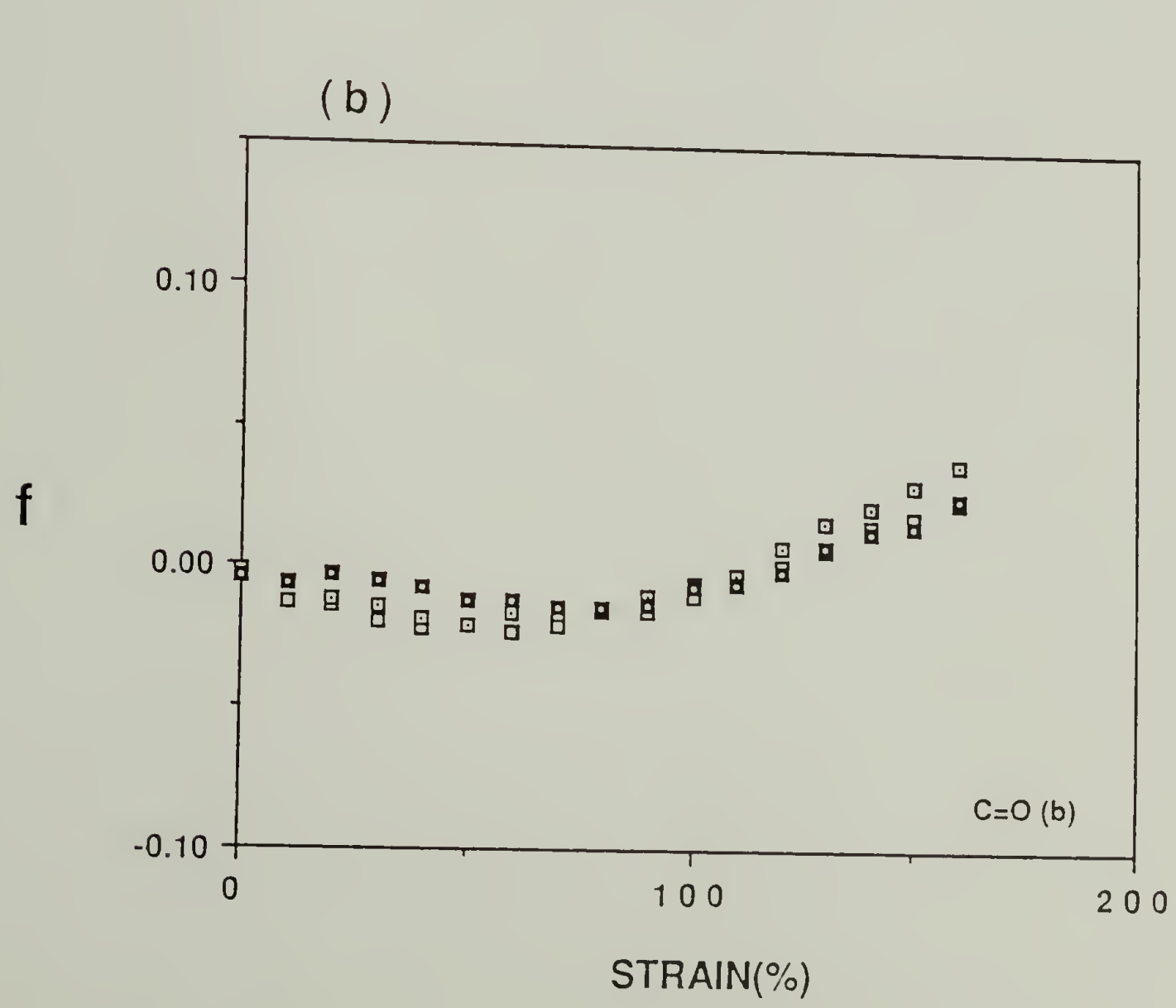
(b)
f
0.10
0.00
-0.10
0
100
200
STRAIN(%)
C=O (b)

The difference in the orientation behavior of the two C=O stretching components appears to be due to the different relaxation properties. Since the three temperatures are well above the glass transition temperature of the soft segment,[37] the chain mobility is increased by increasing the temperature resulting in the fast relaxation. The glass transition temperature of the hard segments is known to be about 80°C. The hard segments are at the glassy state for all three temperatures. It is, therefore, expected that the orientational behavior of the hard segments is independent of the temperature as long as the temperature is below the glass transition temperature of the hard segments.

Domain Change during Deformation

From the orientation changes of the hydrogen bonded C=O stretching component, it has been suggested that the hard domain undergoes structural reorganization at a high strain. The effect of the deformation on the domain can be further analyzed by studying the C=O and N-H stretching components.

The C=O stretching spectra obtained with the two polarization directions are shown in Figure 6.8 at three strain values. The thickness change has again been corrected as explained before. The reference spectrum with no strain is plotted in a dotted line. For parallel spectra shown at the top, the intensity of the two C=O peaks decreases as strain increases. Since the strain is well above the strain value at which the negative orientation function can be

FIGURE 6.8 Carbonyl stretching region at different strain; Relative orientations of polarization directions to stretching direction are shown in the figure.

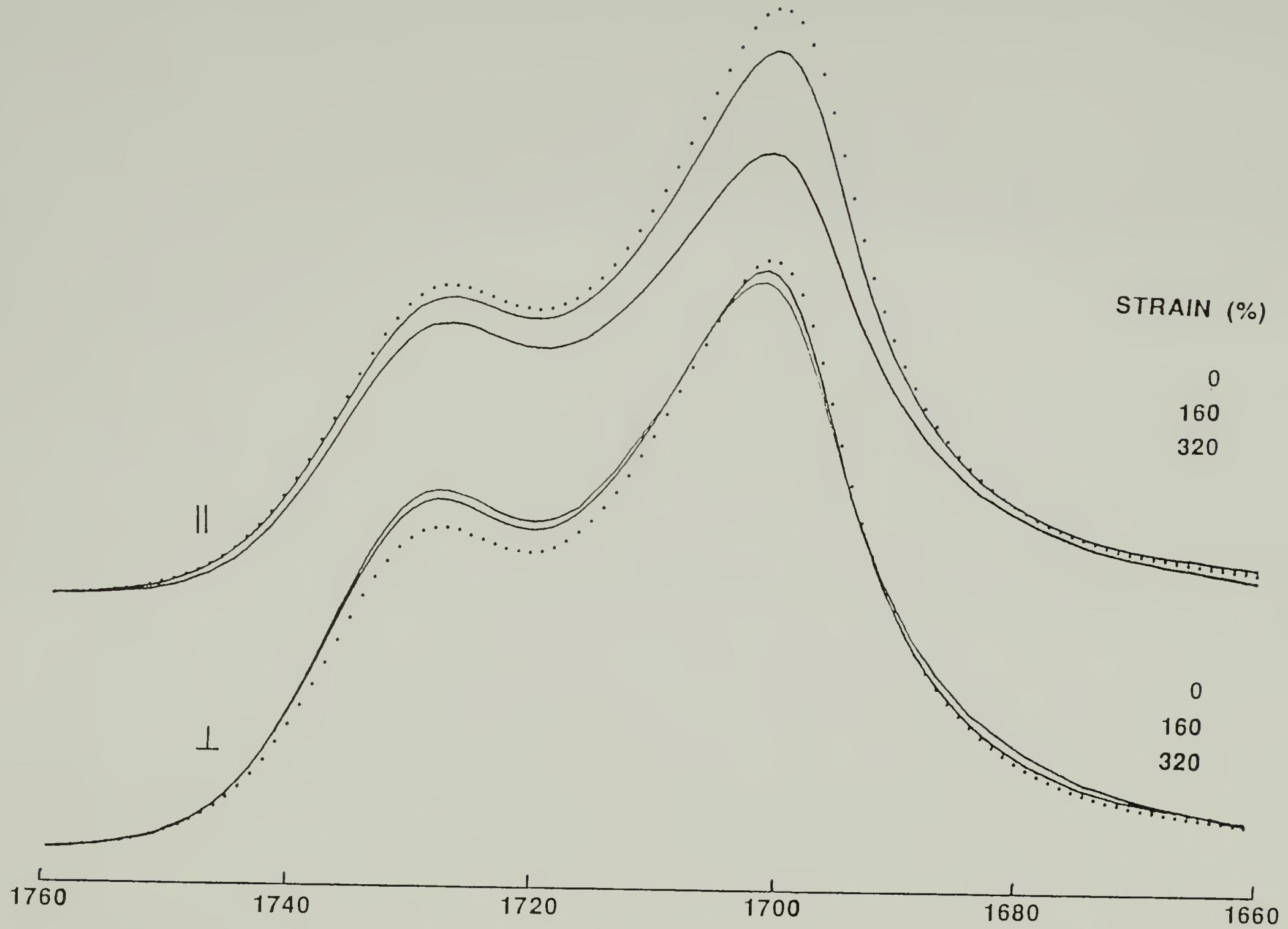
STRAIN (%)
0
160
320
0
160
320
∥
⊥
1760
1740
1720
1700
1680
1660
WAVENUMBERS

observed, the changing intensity is easily understood in terms of the chain orientation along the stretching direction. As the chain orients better, the parallel intensity is expected to decrease due to the perpendicular transition moment direction of the C=O stretching vibrational mode.

For the perpendicular spectra of the free C=O peak, the intensity is increased with the strain as expected. However, the intensity of the hydrogen bonded C=O component decreases with strain. Its intensity is expected to increase at a higher strain if the intensity change is solely due to the chain orientation along the stretching direction. The decreased intensity of this component at a higher strain seems to be mainly due to the decreased amount of the hydrogen bonded C=O functional groups. It indicates that the amount of the hard segments in the hard domain is decreased upon large deformation. Some of the hard segments in the hard domain seem to be pulled out into the soft matrix during the restructuring of the hard domain.

The total absorbance, A_T, can be obtained from the polarized spectra as $A_{\parallel} + 2A_{\perp}$. The ratio of $A_T(b)$ of the hydrogen bonded C=O to $A_T(f)$ of the free C=O is plotted as a function of strain in Figure 6.9. One of the samples was annealed at 150°C for 24 hours under vacuum to investigate the annealing effect on the structural reorganization and also included in Figure 6.9.

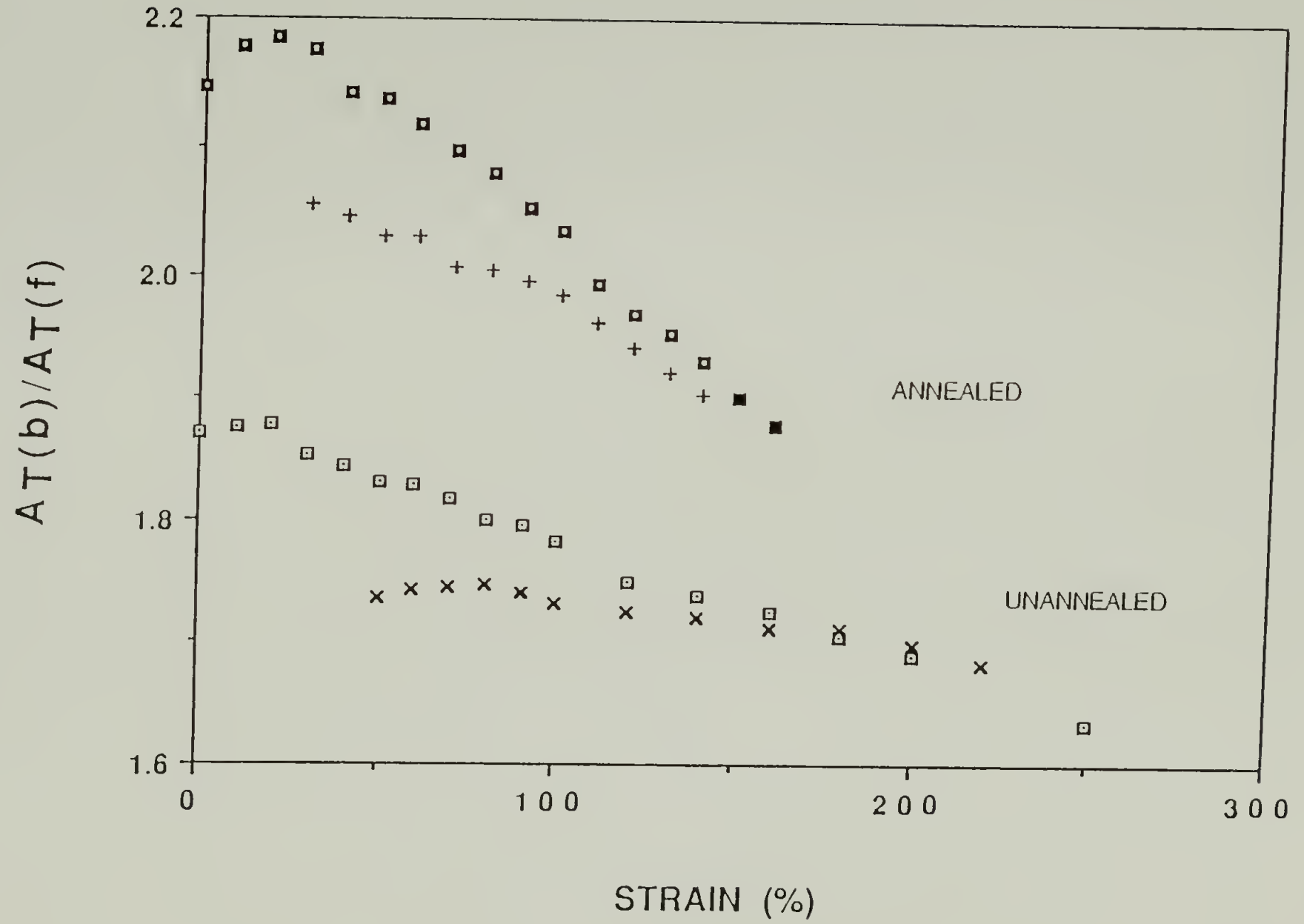

FIGURE 6.9 Intensity ratio of bonded to free C=O peak, $A_T(b)/A_T(f)$, plotted as a function of strain; One sample has been annealed at 150°C for a day.

The ratio is not expected to change as function of strain if the amount of each functional group, i.e. free and hydrogen bonded C=O groups, is constant. However, if some of the hard segments are pulled out of the hard domain into the soft matrix, the ratio, $A_T(b)/A_T(f)$, will decrease as observed in Figure 6.9. The decreasing ratio, therefore, confirms that there is a hard domain structural reorganization during deformation and some of the hydrogen bonded C=O groups are transformed into the free C=O group by being dissolved into the soft matrix.

The annealing effect on the domain restructuring can be observed by comparing the two samples shown in Figure 6.9. For the well annealed sample, the ratio decreases more rapidly as the strain increases. Annealing seems to decrease the amount of the hard segment dissolved in the soft matrix. It can also increase the degree of order inside the hard domain. In the case of the annealed sample, the strain applied initially to the soft segment can be easily transferred to the hard segment, since hard domains are well developed and most of the hard segments are inside the hard domain. Furthermore, the soft segment is expected to have a more extended conformation when both hard segments at the end of the soft segment are incorporated in the hard domain as in the well annealed sample.[38-40] The more extended chains are less likely to undergo higher deformation without applying severe entropic contractile force on the hard segments at the ends. The annealing effect shown in Figure 6.9 can,

therefore, be understood in terms of the differences in the morphology developed by the annealing.

The hard segment transfer from the hard domain to the soft matrix upon deformation can also be observed from the N-H stretching peak. For the hard segments transferred into the soft matrix, the hydrogen bonded N-H functional group changes its proton acceptor from the carbonyl group to the ether group as shown in Figure 6.10.[32] As explained in Chapter II, the N-H stretching frequency changes from 3330 to 3295cm^{-1} by changing its proton acceptor from the C=O group to the ether group.[32]

The N-H stretching peaks obtained with two polarizations at 300% strain are shown in Figure 6.11. The reference spectrum with no strain is plotted in a dotted line. The two spectra in solid lines show an increased band width. The spectra at a 300% strain has actually increased the shoulder at the low frequency shoulder around 3290cm^{-1}. This is due to the increased hard segments dissolved in the soft matrix at a high strain. Those hard segments are expected to form hydrogen bonds with the ether groups of the soft segments resulting in the increased intensity at 3295cm^{-1}. Due to the relatively small amount of the hard segments transferred, the increased contribution at 3295cm^{-1} is only observed from the increased shoulder.

The full-width at half-height (FWHH) of the N-H stretching peaks are plotted in Figure 6.12 as a function of the strain. Even though the data are relatively scattered,

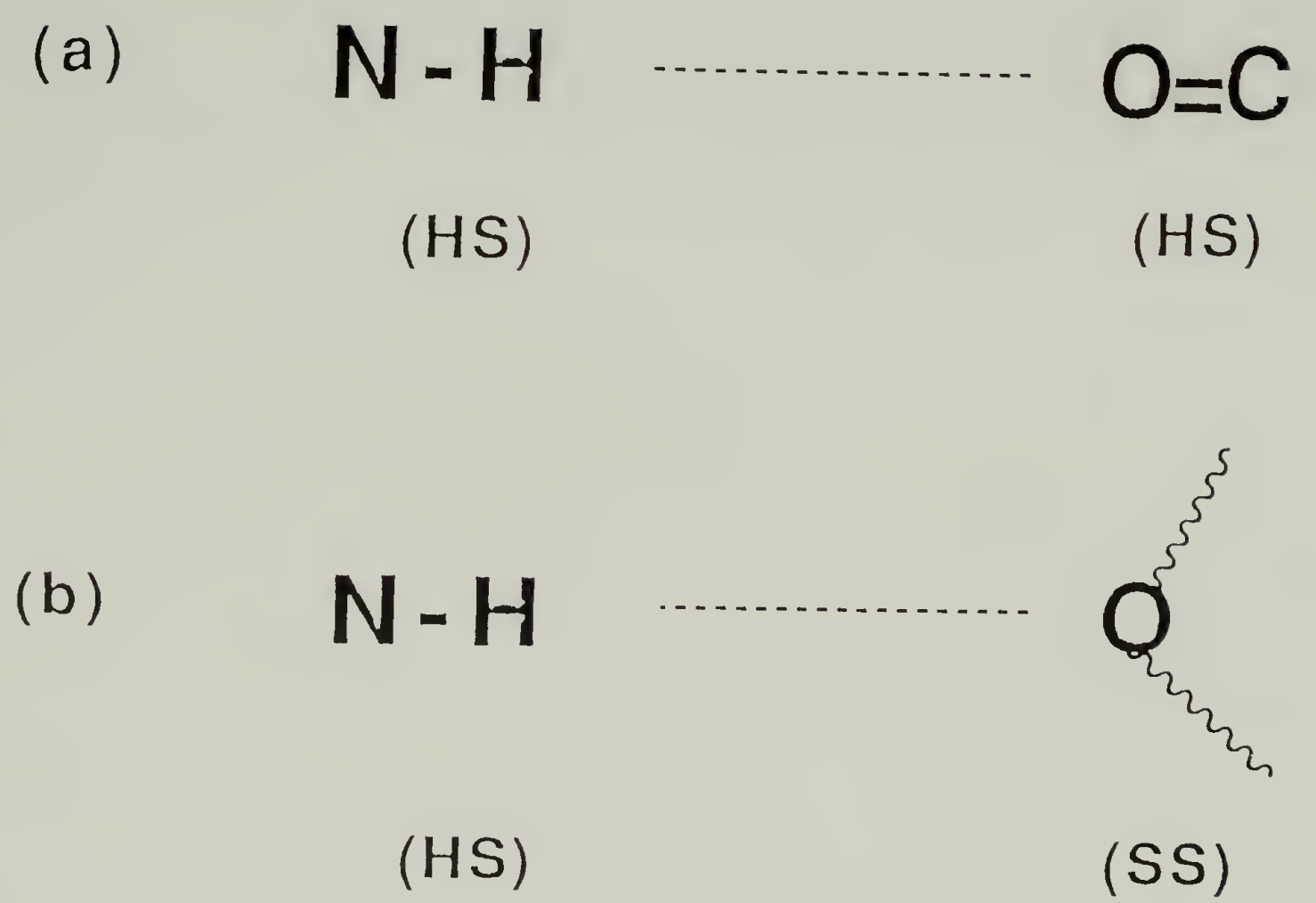

FIGURE 6.10 Schematic representation of two possible modes of hydrogen bonding; (a) between hard segments (b) between hard and soft segment.

FIGURE 6.11 Expanded scale spectra of N-H stretching region at 300% strain; Relative polarization directions to stretching direction are indicated on the spectra; Spectrum without strain is in dotted line; Intensity change due to strain has been corrected.

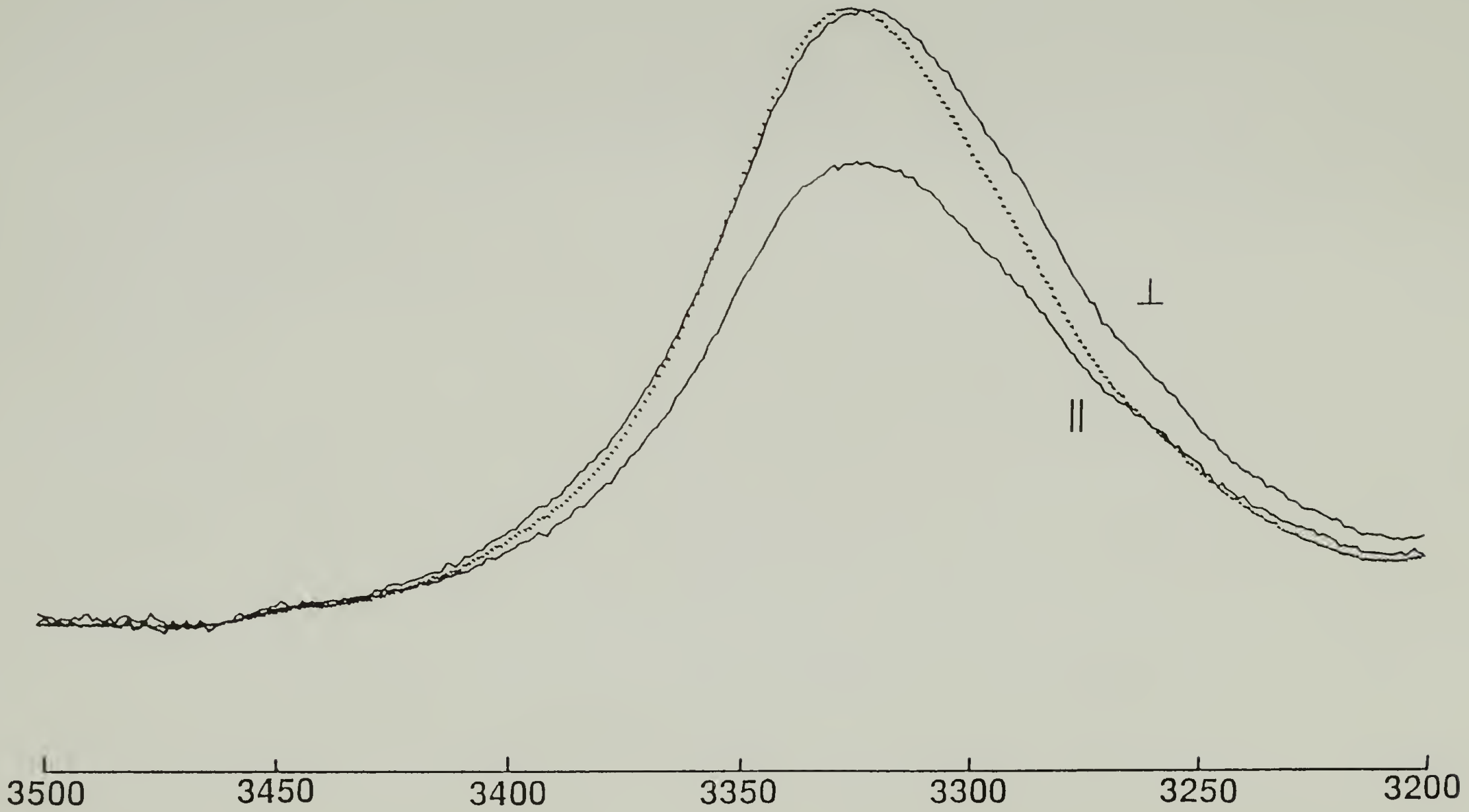
⊥
∥
3500
3450
3400
3350
3300
3250
3200
WAVENUMBERS(CM-1)

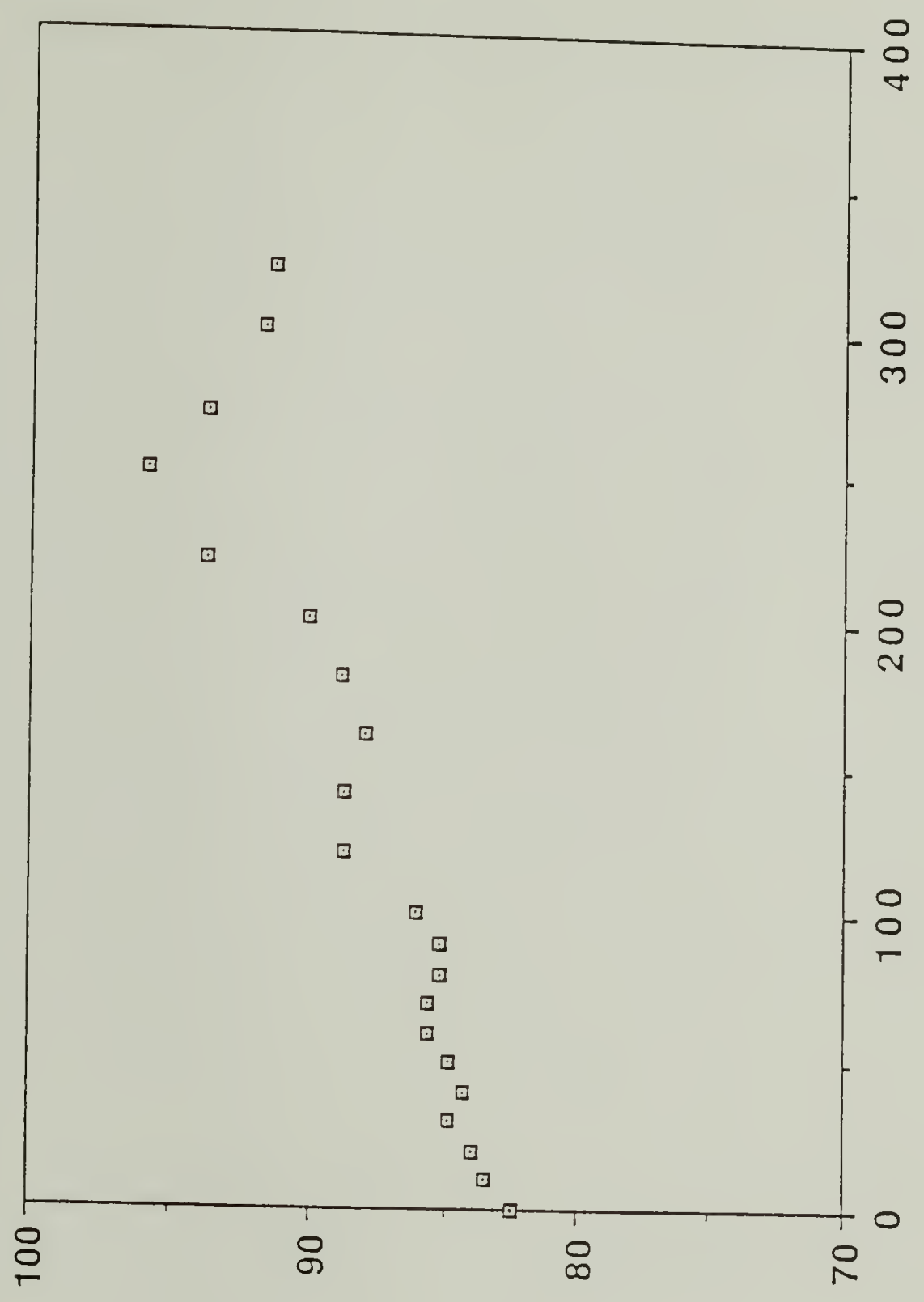

FIGURE 6.12 Band width of N-H stretching peak plotted as a function of strain.

the FWHH seems to increase with the strain. Since the increased shoulder at 3295cm^{-1} can be observed from the increased FWHH, the results in Figure 6.12 confirm that more hard segments form hydrogen bonding with the ether group of the soft segment at the increased strain.

The temperature effect on the domain restructuring is shown in Figure 6.13. The ratio, i.e. $A_T(b)/A_T(f)$, of the C=O stretching component are plotted at three different temperatures. The decreasing tendency of the ratio observed at the low temperature becomes less obvious at the increased temperature. The chains at the high temperature may have increased flexibility that enables the soft chains to undergo more deformation without transferring the stress to the hard segments. In the low temperature region, the stress of the soft segment seems to be easily transferred to the hard segments in the hard domain resulting in the more extensive domain restructuring. For the sample at 44°C, the second half of the deformation cycle, which is the strain releasing period, shows a slightly increased value of the ratio. At this temperature, the chains appear to have enough mobility to form a better phase separated morphology upon releasing of the strain.

Orientation and Stress Relaxation

The deformation behavior of the viscoelastic material is fairly complicated. Depending on the time scale of the experiment, material's response can be changed widely from

FIGURE 6.13 Intensity ratio of bonded to free C=O peak, $A_T(b)/A_T(f)$, at three different temperatures plotted as a function of full cycle of strain; Squares obtained during increasing strain and crosses obtained during decreasing strain.

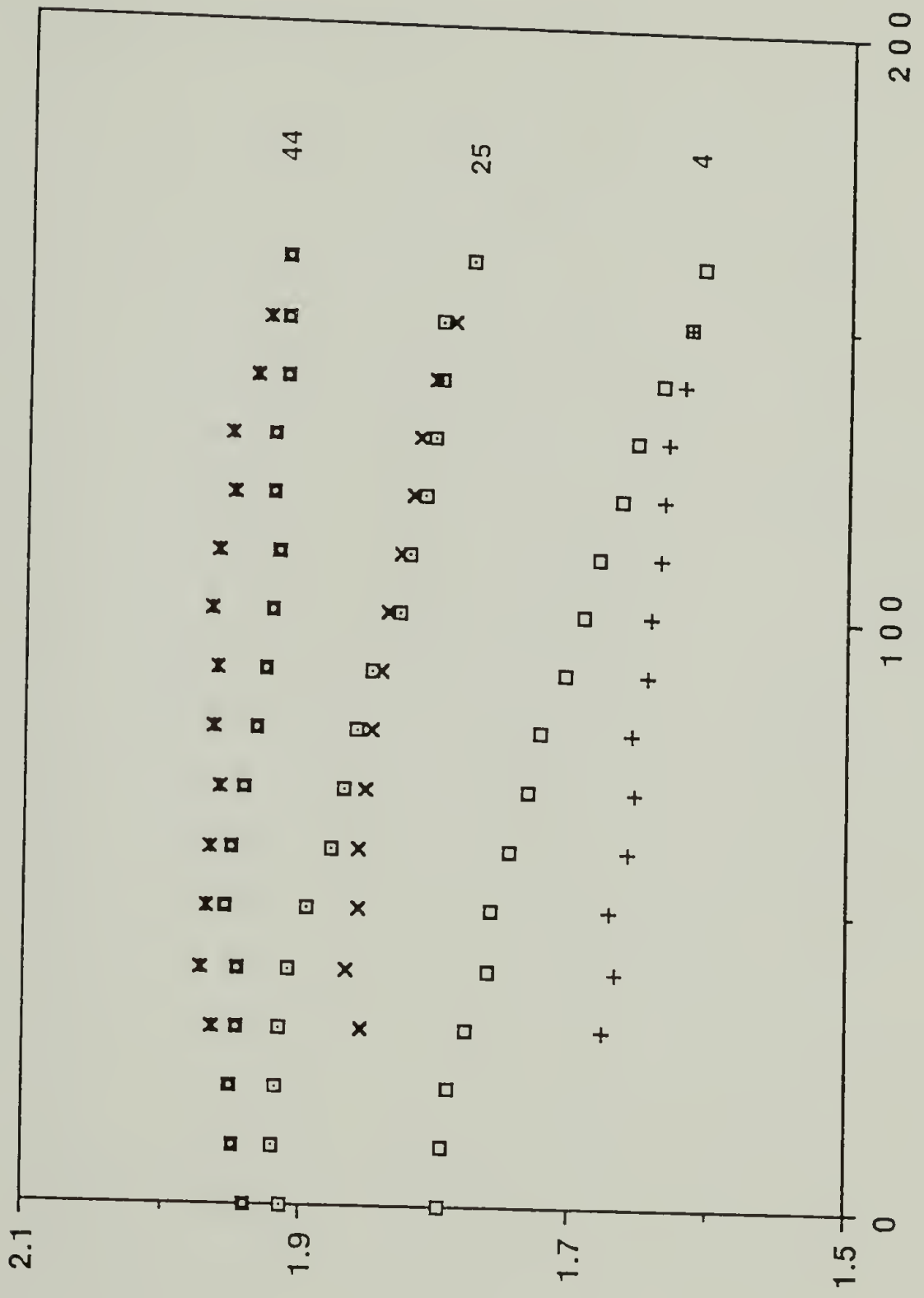
44
25
4
200
100
0
STRAIN (%)
2.1
1.9
1.7
1.5
ΔT(b)/ΔT(f)

elastic to fluid properties.[41] In the case of heterogeneous materials, the deformation behavior is even more complex. The segments in the different domains may have different observable response times to the applied deformation. Since it takes a certain amount of time to reach the equilibrium structure, the time variation of the structure can be analyzed through the orientation function change as a function of time.

The stress change during the stress relaxation experiment is shown in Figure 6.14. It was obtained for the B4 polyurethane which was step strained by 100%. The initial period of stress build-up corresponds to the stretching period up to a 100% strain. The stress relaxation is found to be extremely fast initially, followed by the slow relaxation. The final stress value is approached asymptotically.

The carbonyl stretching peaks obtained with the two polarizations are shown in Figure 6.15. The lower spectra are obtained just after step strain and the upper spectra are obtained after 220.5 minutes relaxation time. The most interesting phenomenon is that the negative orientation of the hydrogen bonded C=O stretching peak shown at time zero becomes positive after relaxation. According to Figure 6.5, the orientation function of the hydrogen bonded C=O stretching peak was not negative at 100%. The negative orientation function of the same sample used in this experiment may be due to no relaxation time after the strain.

FIGURE 6.14 Stress relaxation of the B4 polyurethane; Sample has been step strained for 100%.

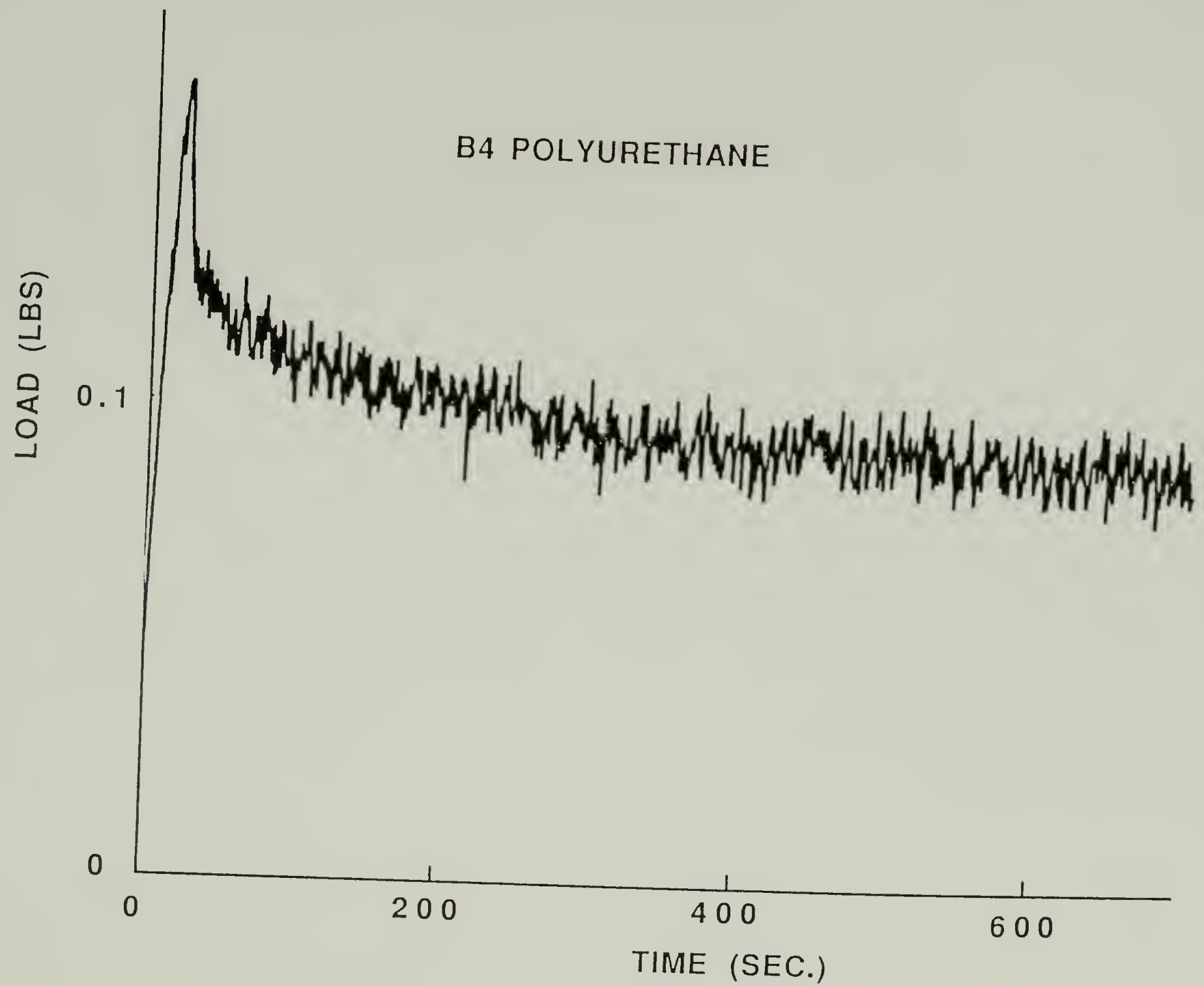
B4 POLYURETHANE
LOAD (LBS)
0.1
0
0
200
400
600
TIME (SEC.)

FIGURE 6.15 Carbonyl stretching region before and after relaxation; Solid and dotted spectra are obtained with perpendicular and parallel polarization, respectively.

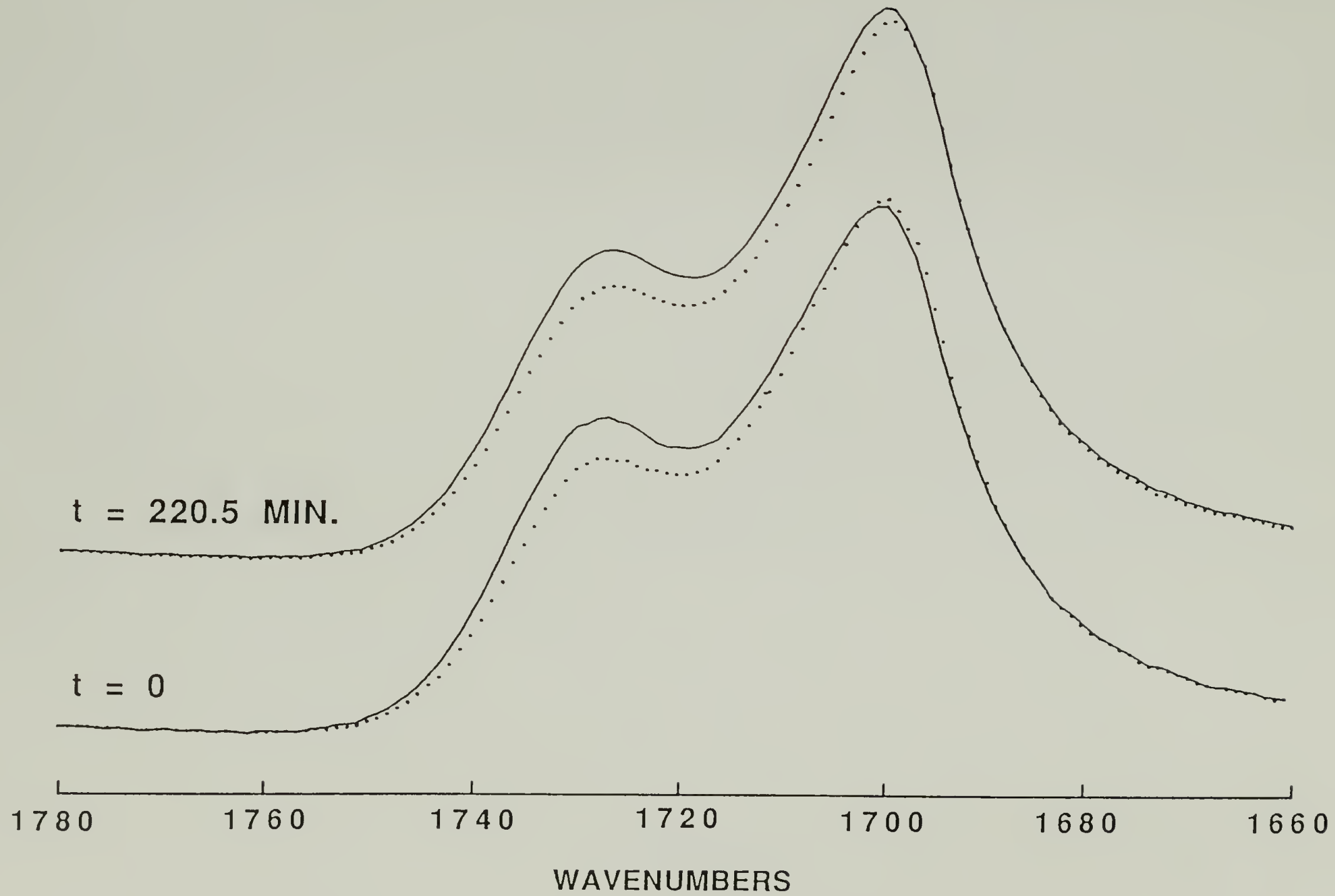
t = 220.5 MIN.
t = 0
1780
1760
1740
1720
1700
1680
1660
WAVENUMBERS

The data in Figure 6.5 was obtained about 5 minutes after applying the strain.

The orientation functions of the two C=O components are plotted as a function of the strain at two different temperatures in Figures 6.16a and b. According to the stress relaxation behavior shown in Figure 6.14, the magnitude of the relaxation is very small especially after the the initial fast relaxation. The orientation relaxation is, therefore, expected to be small. Even though the data are widely scattered, there seems to be a consistent tendency of the orientation function. The orientation relaxation behavior of the two functional groups appear to be exactly opposite to each other. The orientation function of the free C=O peaks seems to decrease with the strain, whereas that of the hydrogen bonded component increases. The orientation function of the hydrogen bonded component changes from the initial negative value to the positive value at a higher strain. Since this inversion of the orientation function is already observed from Figure 6.15, the tendency observed in Figure 6.16 appears to be generally true.

The relaxation behavior is expected to be sensitive to various temperatures. Temperature effects on the relaxation process for different functional groups will be helpful in understanding the segmental mobility at different temperatures. Unfortunately, the temperature effect on the relaxation process is not clearly observed from Figure 6.16 due to the small changes of the orientation function during

FIGURE 6.16 Orientation function relaxation of two carbonyl peaks plotted as a function of relaxation time at
(a) 25°C
(b) 0°C

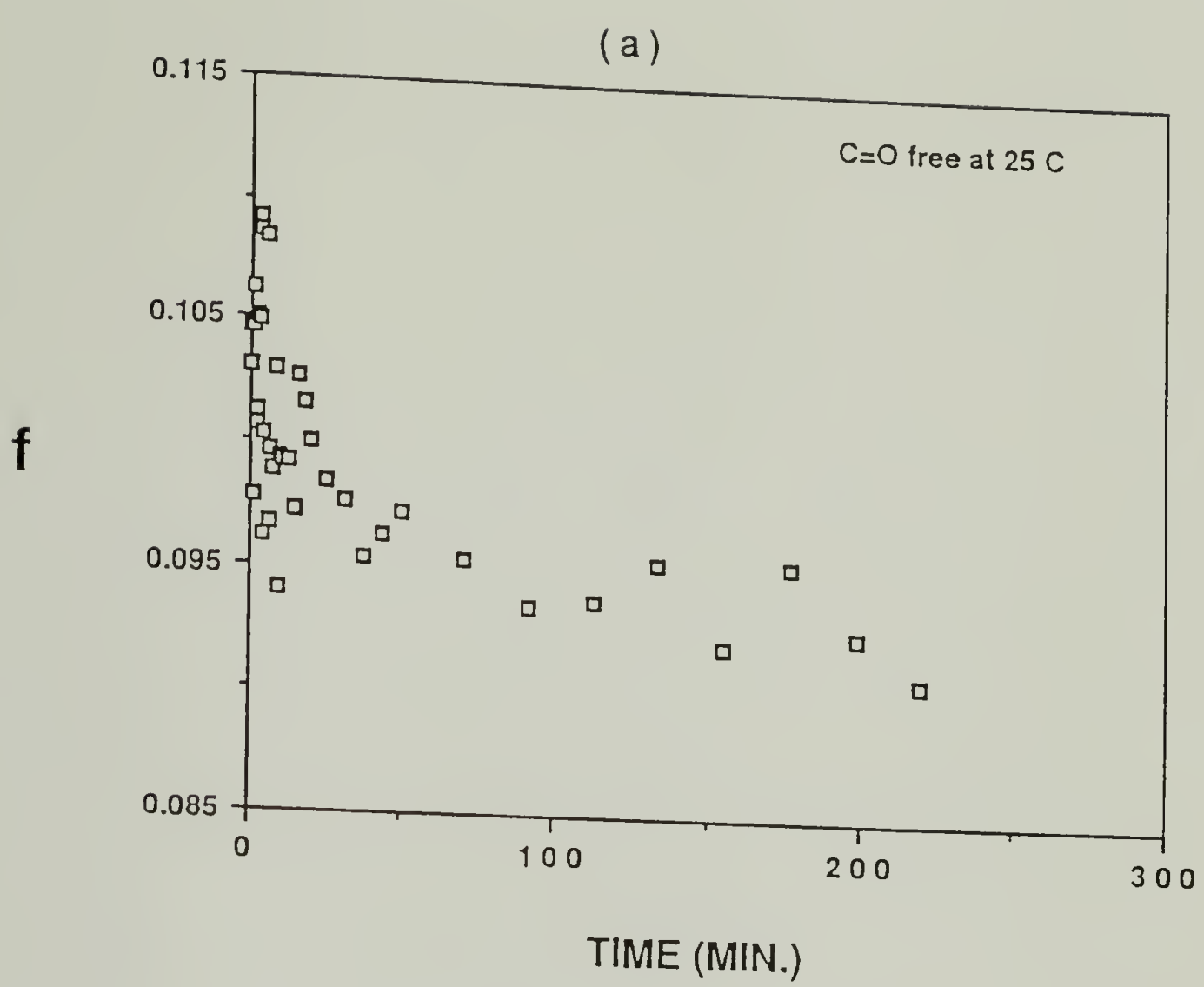
(a)
0.115
0.105
0.095
0.085
f
C=O free at 25 C
0
100
200
300
TIME (MIN.)

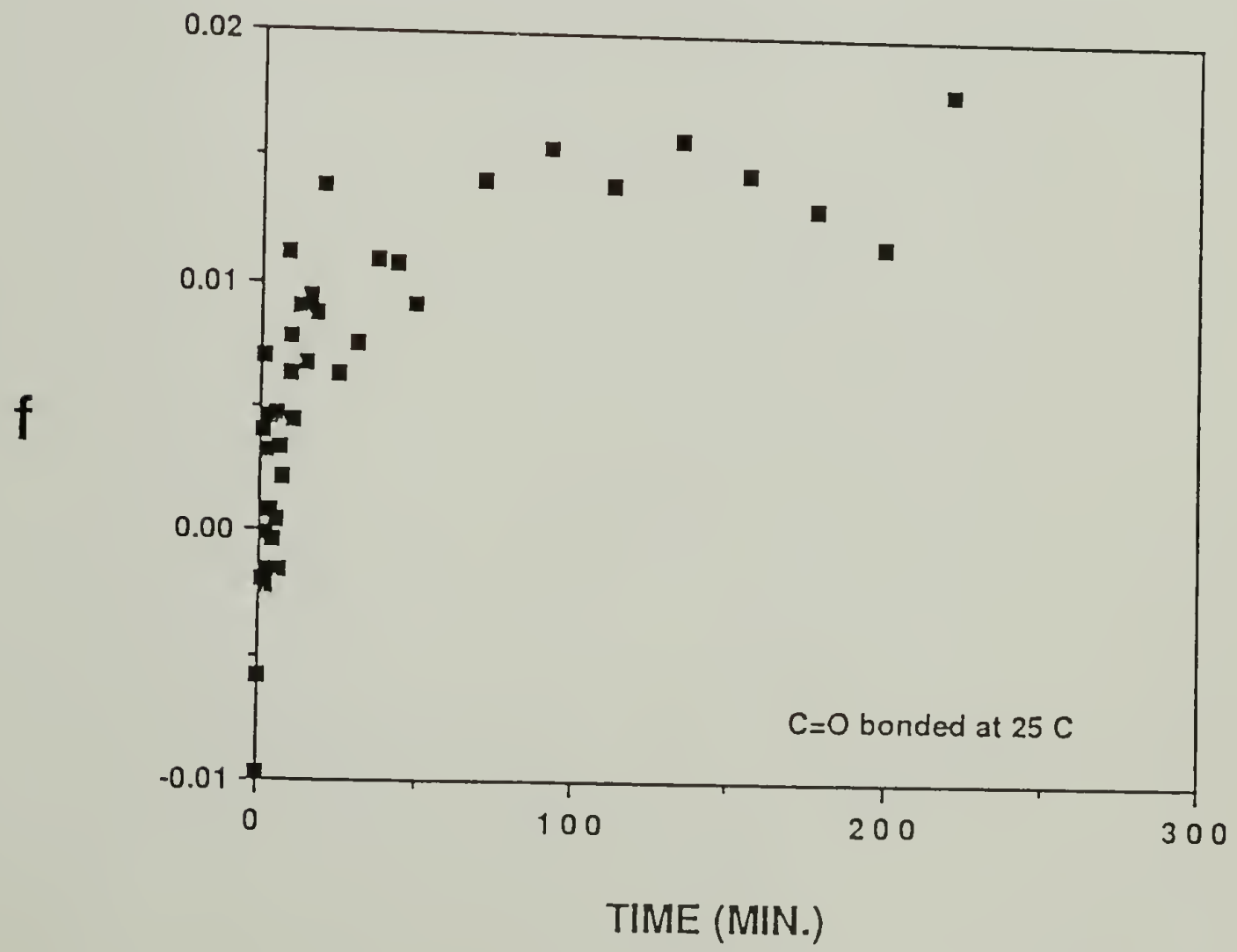
0.02
0.01
0.00
-0.01
f
C=O bonded at 25 C
0
100
200
300
TIME (MIN.)

(b)

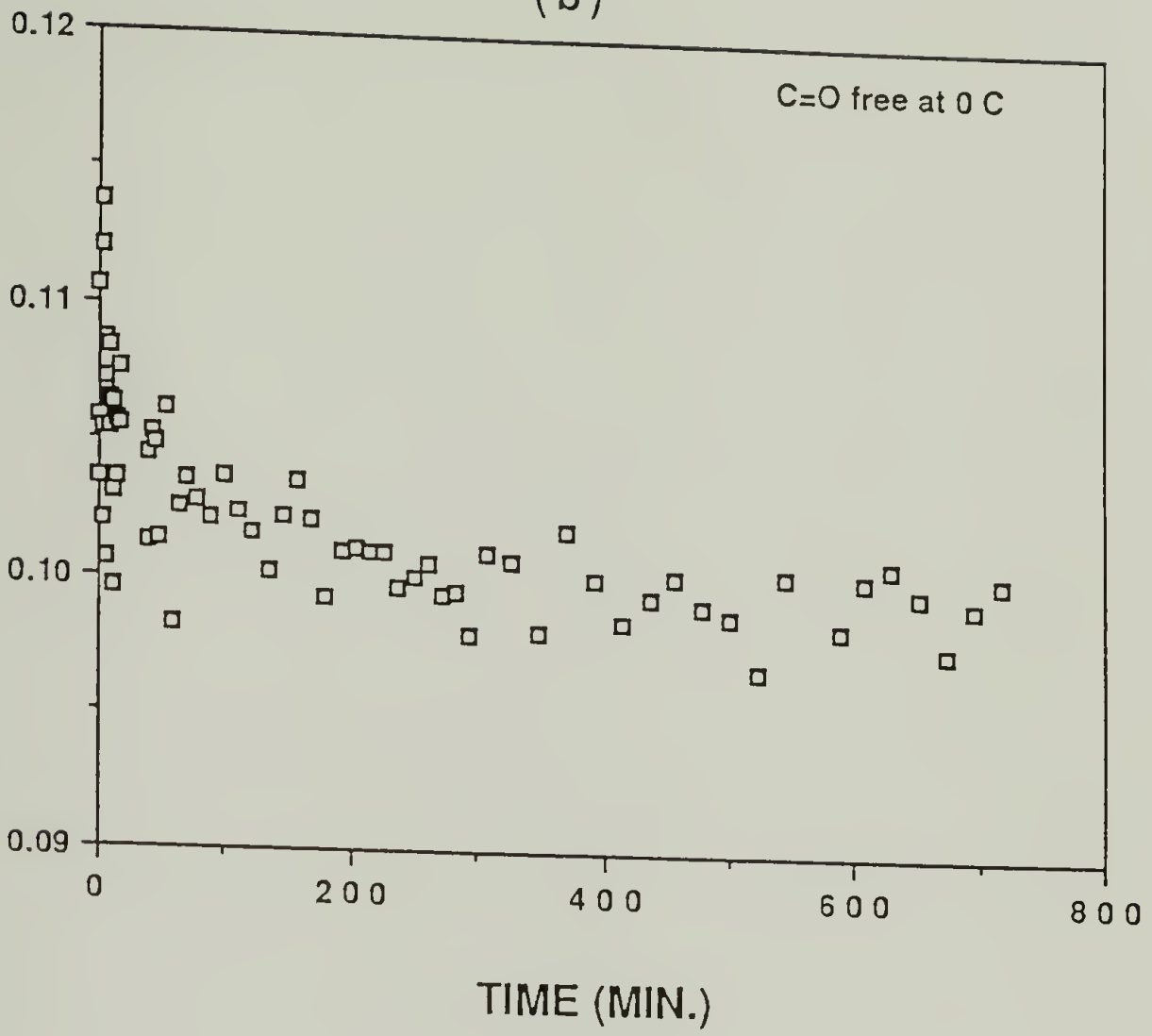
0.12
0.11
0.10
0.09
f
C=O free at 0 C
0
200
400
600
800
TIME (MIN.)

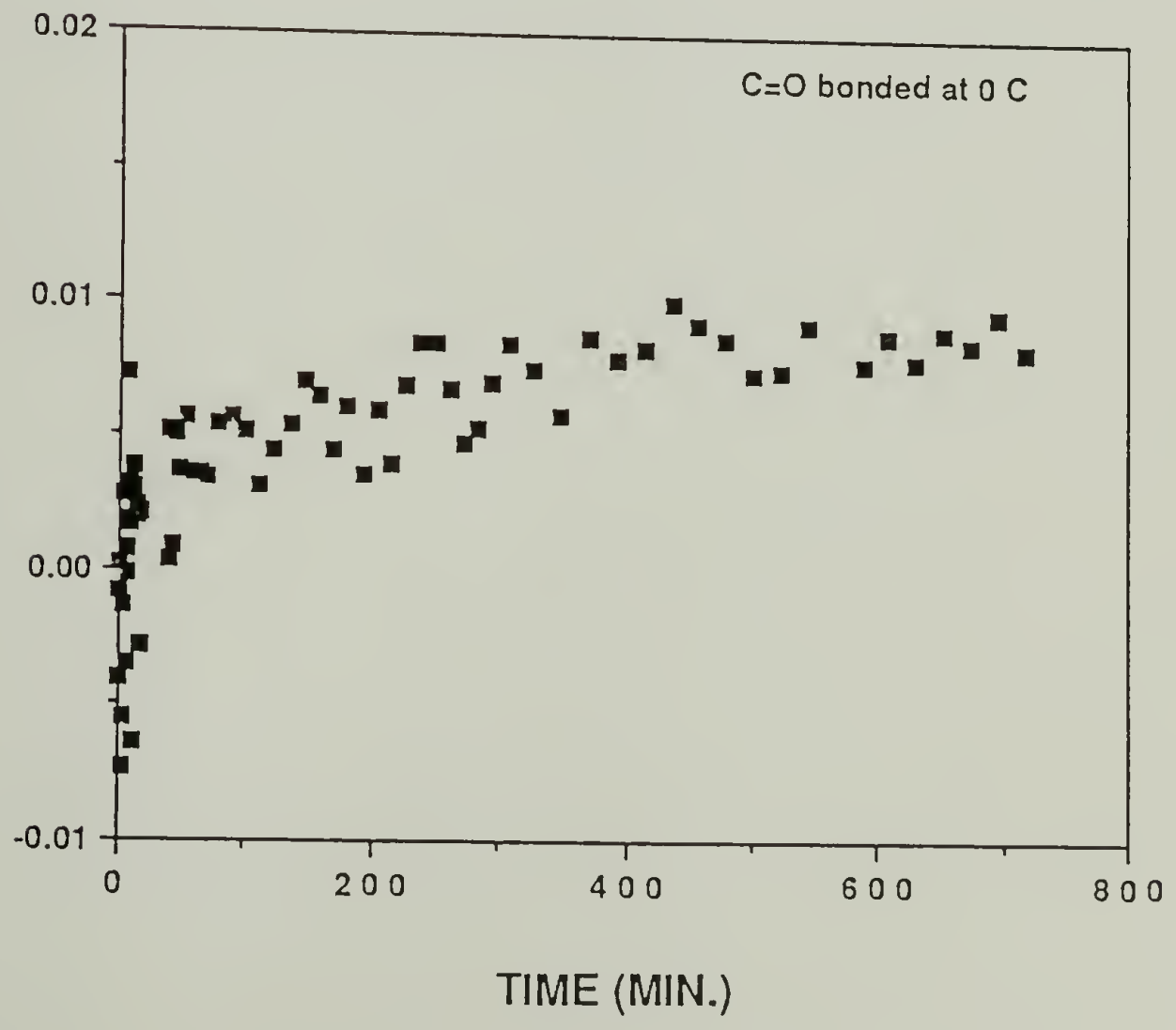
0.02
0.01
0.00
-0.01
f
C=O bonded at 0 C
0
200
400
600
800
TIME (MIN.)

the relaxation process. However, the relaxation process at two temperatures shows a consistent tendency rendering the explanation given above.

Theoretical Dichroism for Morphology Characterization

It has been shown in Equation 6.12 that the theoretical dichroic ratio, R, can be expressed in terms of the draw ratio λ, transition moment angle α and the number of the statistical chain segments N. By comparing the experimental dichroic data with the theoretical prediction, the number of statistical segments N can be obtained. Since the flexibility of the chain will be dependent on many factors such as temperature, soft segment chain length, hard domain orderness and the degree of phase separation, the calculated number of statistical segments can be used to estimate the morphology of the material.[30]

The infrared spectrum of the butadiene based polyurethane (T3MI) is shown in Figure 6.17. The characteristic bands for the soft segment are those that are C-H deformation related to the double bond at $995cm^{-1}$ (cis-1,4), $965cm^{-1}$(trans-1,4) and $910cm^{-1}$ (1,2-vinyl).[42,43] As with MDI based polyurethane, characteristic bands for the hard segments are $3310cm^{-1}$ (N-H stretching), $1710cm^{-1}$ (C=O stretching) and $1537cm^{-1}$ (amide II, N-H bending and C-N stretching).

Dichroic changes of the two peaks pertaining to the soft segment are plotted in Figure 6.18 as a function of strain.

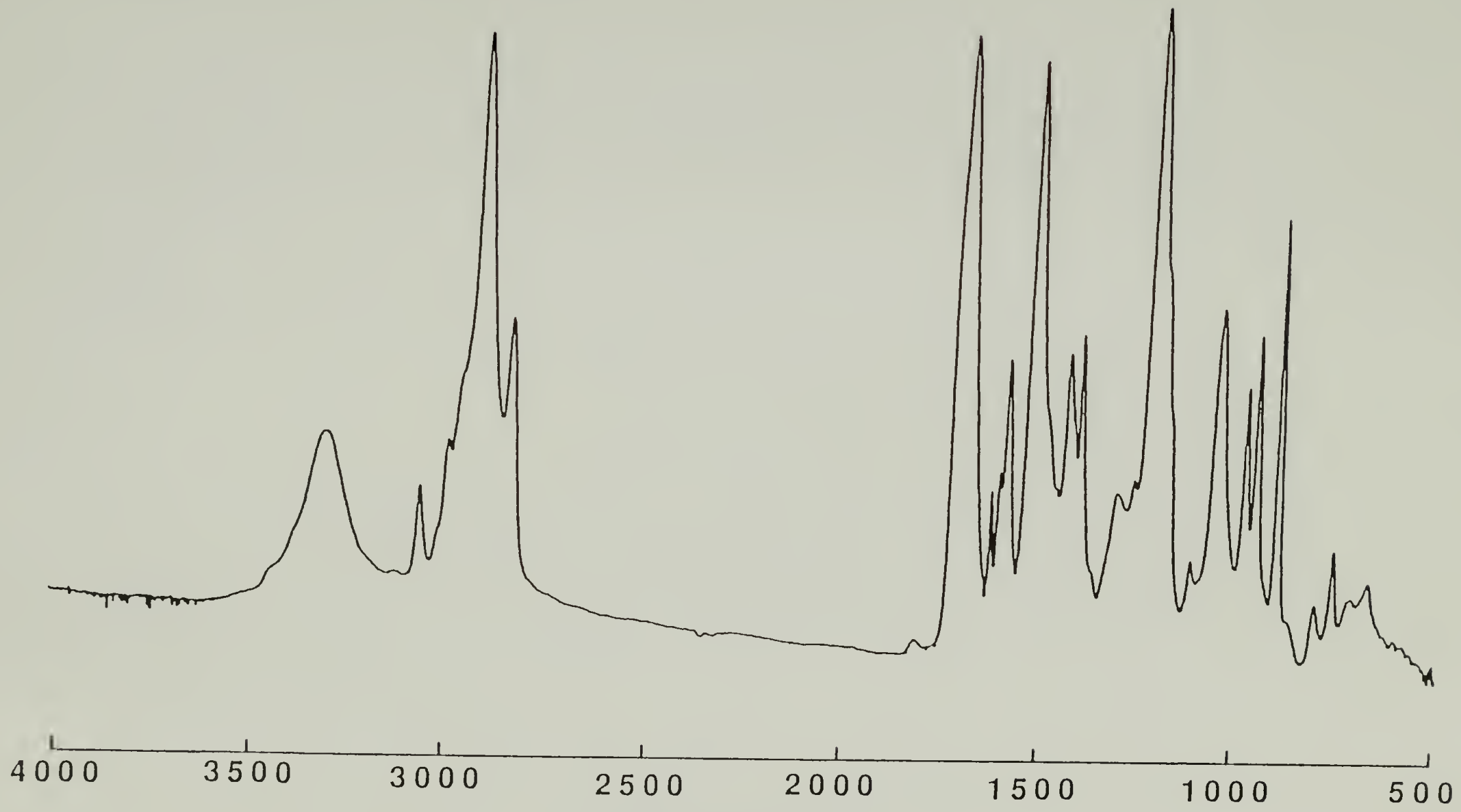

FIGURE 6.17 Survey spectrum of polybutadiene based polyurethane.

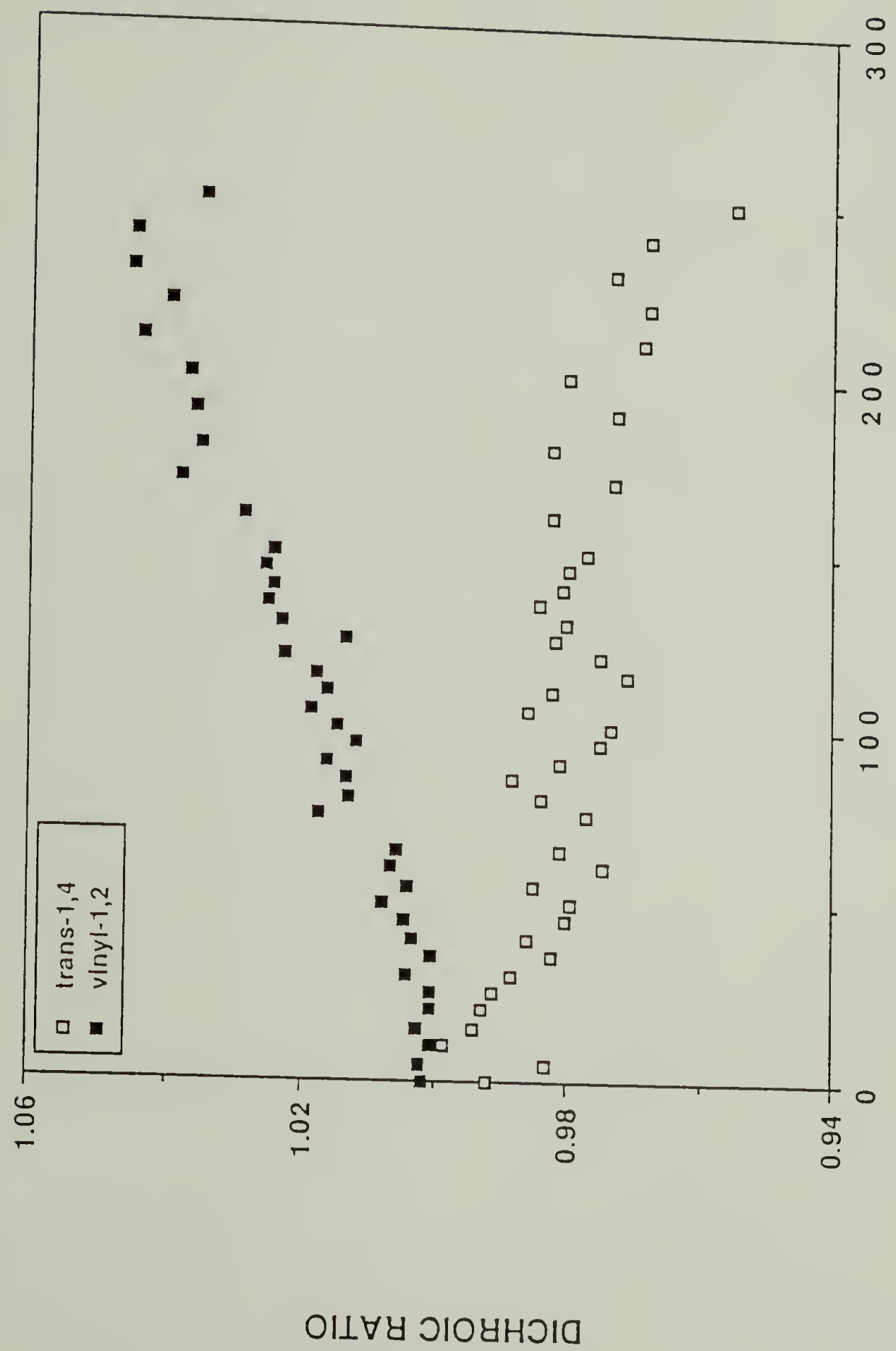

FIGURE 6.18 Dichroic ratio of two peaks plotted as a function of strain; Vinyl-1,2 and trans-1,4 are at 910cm^{-1} and 965cm^{-1}, respectively.

The transition moment direction of the 1,2-vinyl C-H deformation peak at 910cm^{-1} is found to be parallel, whereas the trans-1,4 peak at 965cm^{-1} is perpendicular. Since the dichroic data of the 965cm^{-1} band are somewhat scattered, the peak at 910cm^{-1} is more likely to give better results. The transition moment direction of the trans-1,4 peak is expected to be close to 90°, whereas that of 1,2-vinyl peak is unclear due to the rotational freedom around the C-C bond; which connects the vinyl group to the main chain.

The transition moment direction of the one component can be calculated from the known transition moment direction of the other component as far as the two bands are related to the same segment.[44] Since the orientation function of the two bands is the same, the following relationship can be obtained from Equation 6.4.

$$\left(\frac{R_o+2}{R_o-1}\cdot\frac{R-1}{R+2}\right)_{965} = f_{965} = f_{910} = \left(\frac{R_o+2}{R_o-1}\cdot\frac{R-1}{R+2}\right)_{910} \qquad (6.13)$$

By rearranging the first and last parts in Equation 6.13, it can be obtained as

$$\left(\frac{R-1}{R+2}\right)_{965}\left(\frac{R+2}{R-1}\right)_{910} = \left(\frac{R_o+2}{R_o-1}\right)_{965}\left(\frac{R_o-1}{R_o+2}\right)_{910} \qquad (6.14)$$

Since the R_o is constant, the right hand side of Equation 6.14 is also constant. The experimental data of the left hand side is plotted in Figure 6.19. Even though there is a deviation from the constant value at the small strain value, it is mainly due to the small value at the denominator, the

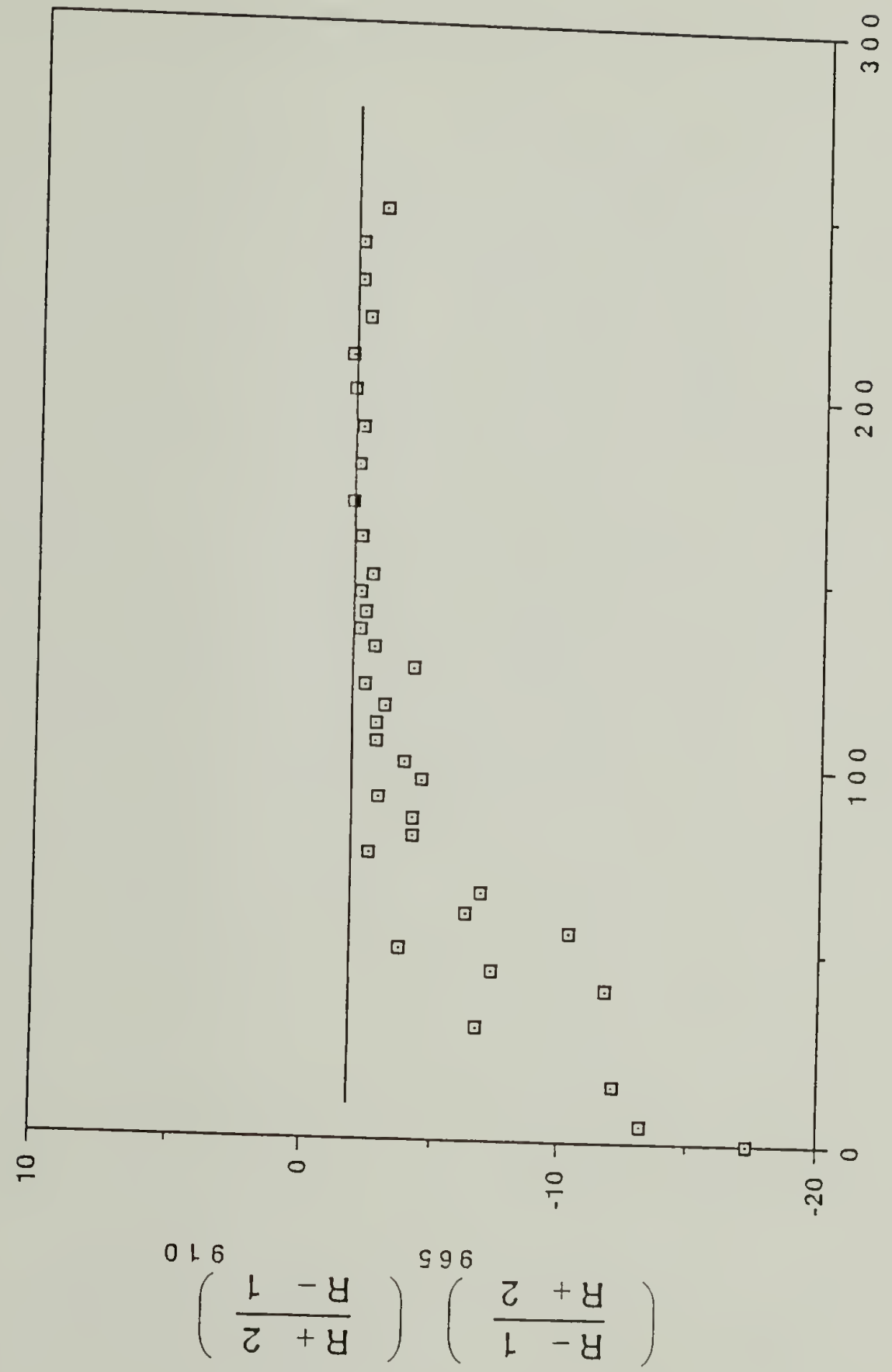

FIGURE 6.19 Ratio of Equation 6.14 plotted as a function of strain.

overall data seems to approach the constant value fairly well. From the constant value and Equation 6.3, the angle of the transition moment direction of the vinyl-1,2 peak at $910cm^{-1}$ is found to be about 45°. It has been suggested that the rotation of the vinyl group about the C-C bond, which connects the vinyl group to the main chain, is sterically hindered.[44]

The network deformation theory developed for the network comprised of the elastic chains cannot be directly applied to the results of the polyurethane deformation work. Even though the hard domains act as junction points preventing permanent deformation, its volume percent cannot be neglected as in a conventional network. Furthermore, the possible deformation and orientation of the hard domain has to be characterized before Equation 6.12 is applied to the dichroic data of the segmented polyurethanes.

The orientation functions of the hard and soft segment functional groups are plotted in Figure 6.20 as a function of the strain. As a hard segment deformation, the C=O stretching band is used. The orientation function of the vinyl-1,2 peak is again included for comparison. As shown in Figure 6.20, the hard segment orientation seems to be negligible compared with the soft segment orientation. During the following analysis it is, therefore, approximated that most of the deformation occurs to the soft matrix.

The draw ratio λ in Equation 6.12 is the real draw ratio to which the soft segments are actually subjected. Since it

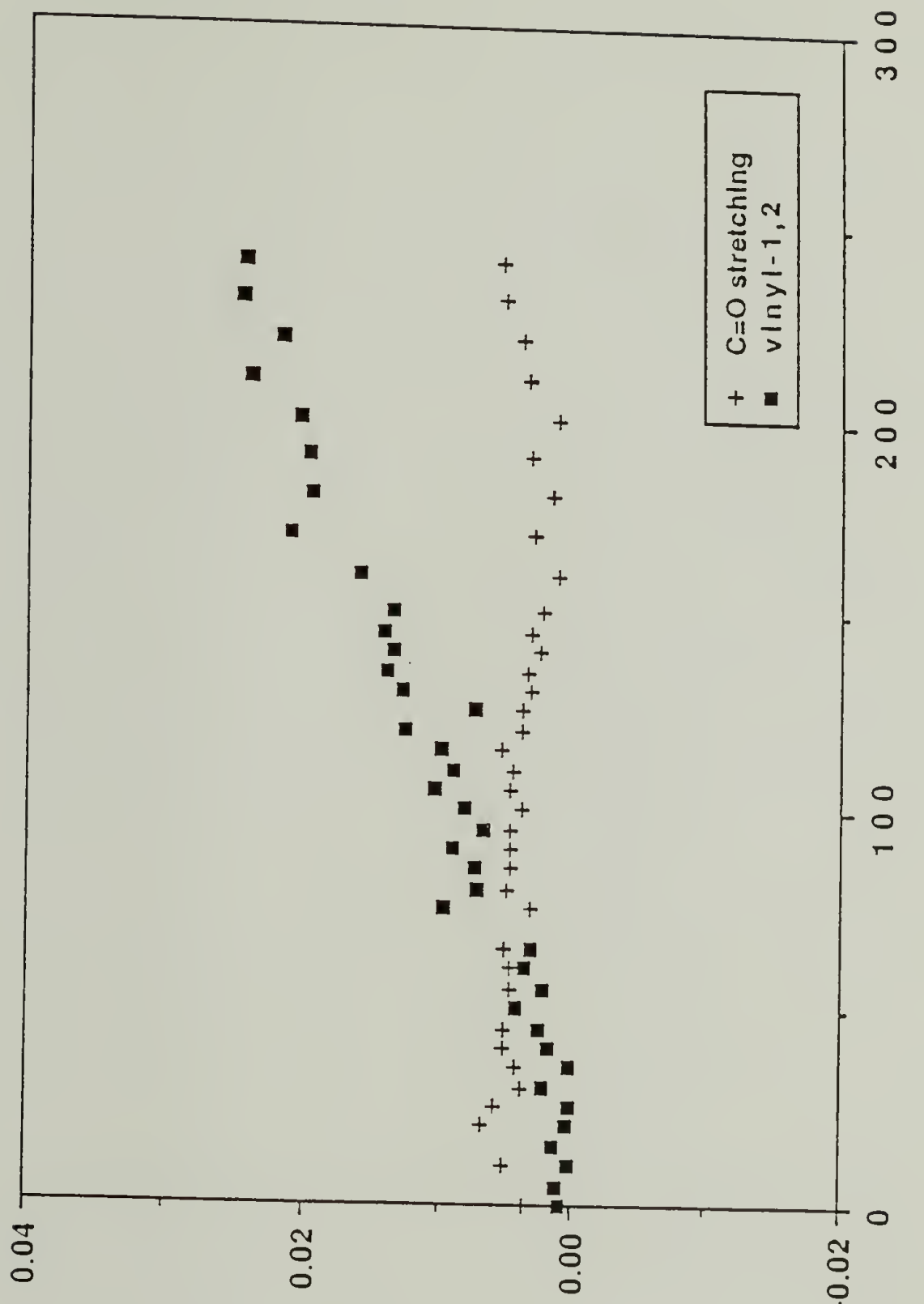

FIGURE 6.20 Orientation function of two peaks plotted as a function of strain.

is assumed that most of the deformation occurs in the soft matrix, the experimental λ value has to be modified according to the amount of the volume fraction of the hard domain. The polyurethane investigated in this analysis has a hard segment volume fraction of 0.20. It has been calculated by Smallwood[45] and extended by Guth[46] that for systems with spherical filler particles, the matrix strain ε may be interpreted in terms of the sample strain ε_o by Equation 6.15,

$$\varepsilon = \varepsilon_o (1 + 0.25C + 14.1C^2) \qquad (6.15)$$

where C is the volume fraction of filler.

In Figure 6.21, the dichroic ratio R is plotted as a function of the corrected draw ratio. The theoretical values are plotted according to Equation 6.12 in the solid lines for a few N values, i.e. number of statistical chain segments. The experimental data points seem to indicate that the average soft segment contains about 90 statistical chain segments. Since the single soft segment with a 2200 molecular weight has about 110 backbone bonds, the obtained N value appears to be greater than expected. The hard domain of this mixed TDI based polyurethane is not crystalline. Therefore, the treatment of the hard domain as a solid junction point seems to be a crude approximation. If there is a hard domain relaxation during deformation, the flexibility of the soft chains is expected to be increased resulting in the increased number of statistical chain segments.

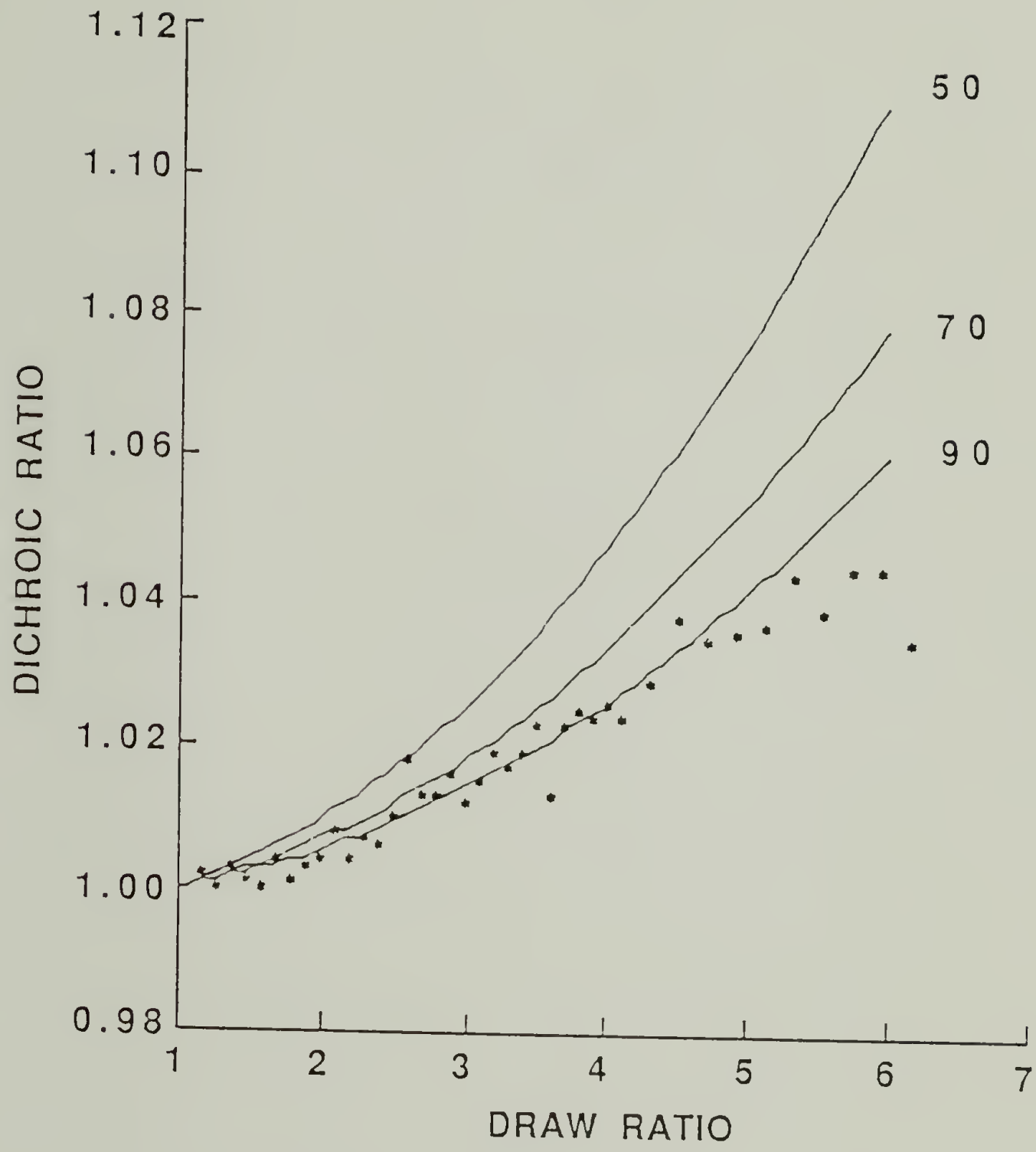

FIGURE 6.21 Dichroic ratio for vinyl-1,2 peak as a function estimated soft segment strain; Three lines obtained with Equation 6.12 are included; Numbers on each line are N values of Equation 6.12.

Conclusion

The deformation behavior of the two different polyurethanes has been characterized with the infrared spectroscopic method. For the MDI based polyurethane, the orientation behavior of the hard segments is found to be very different from that of the soft segments. The hard segments show significant hysteresis behavior, whereas the soft chains appear to be highly elastic. The orientation inversion has been observed for the hard segments. Even though the inversion phenomenon has been explained in terms of the orientation of the long lamellar hard domain along the stretching direction, an exact explanation has to be made due to the inability of the previous model to account for the non-negative orientation behavior of the other vibrational mode pertaining to the same hard segment. The conformational transition model used for the polyurethane urea seems to explain the general orientation behavior fairly well.

Domain change due to deformation is also characterized. At high strain (approximately above 100%) some of the hard segments, which were initially inside the hard domain, appear to be pulled out into the soft matrix. The increased interaction between the hard segments newly dissolved in the soft matrix, and the soft segments, has been observed from the decreased hydrogen bonded C=O component as well as the increased N-H functional group hydrogen bonded with the ether group. The hard segment pull out appears to be significant

only at low temperatures (close to 0 degree). The effect becomes negligible at the elevated temperature (44°C).

It has been observed that for the polyurethane step strained to 100%, the stress relaxation is extremely fast. The subsequent slow relaxation persists over a long period. The orientation relaxation of the two C=O components shows the characteristics of each domain. The soft segments, which were initially oriented along the stretch direction, lose their orientation during slow relaxation. It is shown that very slow orientational relaxation can be observed by the infrared method. The orientation inversion is also observed from the relaxation process. For the hard segments in the hard domain, the initial negative orientation turns into the positive orientation during relaxation. It is believed that the initial strain mainly applied to the soft segment is transferred to the hard segments as soft chains relax. The deformation of the hard segment itself is, therefore, observed after soft segment relaxation resulting in the positive orientation function at the later stage of the relaxation.

The dichroic value obtained with the butadiene based polyurethane is analyzed by a prediction given by the network deformation theory. The soft segment with 2200 molecular weight is found to have about 90 statistical chain segments. The higher number of segments compared to the average chain length may be due to the noncrystalline nature of the hard domain. The treatment of the hard domains as solid junction

points seems to be a crude approximation. However, it has been demonstrated that the information obtained about the number of statistical chain segments can be used to estimate the degree of phase separation at the hard domain state.

References

1. Cooper,S.L.; Tobolsky,A.V. *J.Appl.Polym.Sci.* **1966**, 10, 1837.

2. Cooper,S.L.; West,J.C.; Seymour,R.W. "Encyclopedia of Polymer Science and Technology" Suppl.Vol.1, N.M.Bikales, M.Bickford Eds., Interscience Pub., New York, **1976**.

3. Pigott,K.A.; Frye,B.F.; Allen,K.R.; Steigiser,S.; Darr,W.C.; Saunders,J.H.; Hardy,E.E. *J.Chem.Eng.Data* **1960**, 5, 391.

4. MacKnight,W.J.; Yang,M. *J.Polym.Sci. Part C* **1973**, 42, 817.

5. Bayer,O.; Mueller,E.; Petersen,S.; Piepenbrink,H.F.; Windemuth,E. *Rubber Chem.Tech.* **1950**, 23, 812 and *Angew.Chem.* **1950**, 62, 57.

6. Abouzahr,S.; Wilkes,G.L.; Ophir,Z. *Polymer* **1982**, 23, 1077.

7. Ng,H.N.; Allegrezza,A.E.; Seymour,R.W.; Cooper,S.L. *Polymer* **1973**, 14, 255.

8. Miller,J.A.; Lin,S.B.; Hwang,K.K.S.; Wu,K.S.; Gibson,P.E.; Cooper,S.L. *Macromolecules* **1985**, 18, 32.

9. Abouzahr,S.; Wilkes,G.L. *J.Appl.Polym.Sci.* **1984**, 29, 2695.

10. Camargo,R.E.; Macosko,C.W.; Tirrell,M.; Wellinghoff,S.T. *Polymer* **1985**, 26, 1145.

11. Lin,S.B.; Hwang,K.S.; Tsay,S.Y.; Cooper,S.L. *Colloid & Polym. Sci.* **1985**, 263, 128.

12. Allegrezza,A.E.Jr.; Seymour,R.W.; Ng,H.N.; Cooper,S.L. *Polymer* **1974**, 15, 433.

13. Laptij,S.V.; Lipatov,Y.S.; Kercha,Y.Y.; Kosenko,L.A.; Vatulev,V.N.; Gaiduk,R.L. *Polymer* **1982**, 23, 1917.

14. Holmes,D.R.; Miller,R.G.; Palmer,R.P.; Bunn,C.W. *Nature* **1953**, 171, 1104.

15. Keller,A.; Sandeman,I. *J.Polym.Sci.* **1955**, 15, 133.

16. Aggarwal,S.L.; Tilley,G.P.; Sweeting,O.J. *J.Polym.Sci.* **1959**, 1, 91.

17. Hoshino,S.; Powers,J.; Legrand,D.J.; Kawai,H.; Stein,R.S. *J.Polym.Sci.* **1962**, 58, 185.

18. Quynn,R.G.; Steele,R. *Nature* **1954**, 173, 1240.

19. Caroti,G.; Dusenbury,J.H. *J.Polym.Sci.* **1956**, 22, 399.

20. Tasumi,M.; Shimanouchi,T. *Spectrochimia Acta* **1961**, 17, 731.

21. Seymour,R.W.; Allegrezza,A.E.Jr.; Cooper,S.L. *Macromolecules* **1973**, 6, 896.

22. Wilkes,G.L. *J.Macromol.Sci. -Rev.Macromol.Chem.* **1974**, C10, 149.

23. Jasse,B.; Koenig,J.L. *J.Macromol.Sci. - Rev.Macromol.Chem.* **1979**, C17, 61.

24. Fraser,R.D.B. *J.Chem.Phys.* **1953**, 21, 1511.

25. Fraser,R.D.B. *J.Chem.Phys.* **1956**, 24, 89.

26. Hermans,P.H. "Contributions to the Physics of Cellulose Fibers" Elsevier, Amsterdam, **1946**.

27. Treloar,L.R.G. "The Physics of Rubber Elasticity" Oxford Univ. Press, London, **1949**.

28. Kratky,V.O. *Kolloid Z.* **1933**, 64, 21.

29. Kuhn,V.W.; Grun,F. *Kolloid Z.* **1942**, 101, 248.

30. Stein,R.S. *J.Polym.Sci.* **1968**, 28, 83.

31. Marrinan,H.J. *J.Polym.Sci.* **1959**, 39, 461.

32. Lee,H.S.; Wang,Y.K.; Hsu,S.L. *Macromolecules* **1987**, 20, 2089.

33. Yokoyama,T. "Adv. in Urethane Sci.Technol." **1975**, 6, 1; Frisch,K.C., Reegen,S.L. Eds., Technomic Pub., USA.

34. Zbinden,R. "Infrared Spectroscopy of High Polymers" Academic Press, New York, **1964**.

35. Khranovskii,V.A. *Akad.Nauk* SSSR **1979**, 244, 408.

36. Estes,G.M.; Seymour,R.W.; Cooper,S.L. *Macromolecules* **1971**, 4, 452.

37. Christenson,G.P.; Harthcock,M.A.; Meadows,M.D.; Spell,H.L.; Howard,W.L.; Creswick,M.W.; Guerra,R.E.; Turner,P.B. *J.Polym.Sci.-Phys.* **1986**, 24, 1401.

38. Hashimoto,T.; Shibayama,M.; Kawai,H. *Macromolecules* **1983**, 16, 1093.

39. Miller,J.A.; Pruckmayr,G.; Epperson,E.; Cooper,S.L. *Polymer* **1985**, 26, 1915.

40. Miller,J.A.; Cooper,S.L.; Han,C.C.; Pruckmayr,G. *Macromolecules* **1984**, 17, 1063.

41. Aklonis,J.J.; MacKnight,W.J. "Introduction to Polymer Viscoelasticity" John Wiley and Sons, **1983**.

42. Hsu,S.L.; Moore,W.H.; Krimm,S. *J.Appl.Phys.* **1975**, 46, 4185.

43. Xu,M.; MacKnight,W.J.; Chen,C.H.Y.; Thomas,E.L. *Polymer* **1983**, 24, 1327.

44. Molis,S.E. Ph.D. Thesis, University of Massachusetts, **1986**.

45. Smallwood,H.M. *J.Appl.Phys.* **1944**, 15, 758.

46. Guth,E. *J.Appl.Phys.* **1945**, 16, 20.

CHAPTER VII

RECOMMENDATIONS FOR FUTURE WORK

The results obtained with the polyurethanes based on the monodisperse hard and soft segments used in this study have led to an increased understanding of the phase separation, miscibility behavior, and the structural reorganization phenomenon of the model polyurethanes. It has been proven that infrared spectroscopy is a very powerful technique for the investigation of the molecular properties of the heterogeneous materials. Since the information obtained with the infrared method is fairly characteristic to the environment at the segmental level, the behavior of the different segments should be analyzed independently. In this chapter, the main achievements of this work and the new questions which have been subsequently suggested, will be presented in three sections.

Phase Separation of Polyurethanes

In Chapter II, the direct observation for the hydrogen bonding between the N-H and the ether functional group has been made. The new results are expected to facilitate the interpretation of the infrared spectra, and thus understanding of the phase separation behavior of

polyurethanes, particularly polyester based polyurethanes. Even though N-H ··· -O- hydrogen bonding is, at room temperature, found to be stronger than the interurethane hydrogen bonding, the former becomes less stable at a high temperature than the latter. The exact explanation is still in question. It may be answered by measuring the thermodynamic parameters of the two hydrogen bonds. The conformational entropy loss of the N-H···-O- bond, which is only obvious at high temperature, appears to be the main reason. The temperature dependence of the infrared spectra of the small model compounds will determine the relative stability of the two hydrogen bonds.

The phase separation kinetics of the segmented polyurethanes have been characterized by infrared and thermal methods in Chapter III. Direct observation of the kinetic phenomena contributes to the understanding of the structural reorganization during the phase separation process. Since infrared spectroscopy has not been previously utilized for phase separation kinetic studies of segmented polyurethanes, more experimental studies have to be carried out. The information on the kinetic behavior of the polyurethanes with different hard segment length, will be useful to determine the effect of segment length on phase separation.

The theoretical development of the phase separation of the segmented copolymer will be particularly useful to determine the mechanism. The theory available for diblock/triblock copolymers seems to be inadequate to apply

to the segmented polyurethane due to the multiple connectivity of the segments. The effect of the extended nature of the soft segment upon phase separation, to the phase separation mechanism, has to be carefully evaluated. The initial result indicates that at a 50% phase separation, more than 85% of the soft segments are locked to at least a single hard domain if all the hard segments participate to the hard domain formation randomly. The effect of the conformational entropy loss on the phase separation will then be obvious, well before the completion of phase separation. The thermal analysis on the kinetics has only been done at a high temperature due to technical difficulties. The temperature drop to a low temperature can be done out of the DSC sample cell, and then transferred to the cell where the temperature is preadjusted to the isothermal phase separation temperature.

Compatibility of the Hard Segments

The compatibility of the hard segments with different segmental length has not been carefully studied due to the lack of the model polyurethane having a monodisperse segmental length. Since the commercial polyurethane has a hard segment with a broad segmental length distribution, the characterization of the miscibility behavior between those hard segments will provide extremely valuable information. The results in Chapter VI suggest that the two hard segments,

with different segmental length, can phase separate into separate hard domains even though the two hard segments have very similar chemical structures, thus similar interaction. The effect of the various parameters such as soft segment length, temperature, difference in segmental length and the miscibility of the hard segments has also to be determined. The low temperature DSC experiment, which has not been done in Chapter VI, can also provide information relevant to the high temperature. The characterization of the soft domain can be done at low temperatures. DSC studies will show the concentration dependence of the hard segment solubility in the soft matrix.

The solid solution formation of the two hard segments can be studied with the model hard segments without using soft segments. The dependence of the crystal structure on the concentration of the foreign material can be studied with the wide angle x-ray scattering technique. However, the effect of the segment connectivity in the copolymer appears to be dominant enough to significantly change the hard segment packing structure.

Molecular Orientation Behavior

The understanding of the hard domain orientation behavior at a small strain is incomplete. The explanation for the negative orientation in terms of hard domain lamellar orientation along the stretch direction, instead of chain

orientation, could not completely satisfy the orientation behavior of the various other infrared bands pertaining to the same hard segment. A conformational analysis during the deformation of a single hard segment would help to better understand the small deformation behavior. The deformation studies in this investigation have been carried out mainly with the B4 polyurethane. Further studies with the polyurethanes having different hard segment length would be quite useful to comprehend the effect of the segmental length on the negative orientation behavior.

The relaxation of the polyurethane has been observed to be an extremely fast process. In order to characterize the initial relaxation behavior, increased time resolution is required. Double modulation infrared spectroscopy in which the D.C. and A.C. switching is performed electronically, could be used to follow the rapid changes which occur in the molecular structure during the relaxation process.

The elastic network deformation theory could not be applied directly to the deformation of the soft segment of the butadiene based polyurethane due to the nonrigid nature of the hard domain. Studies with the MDI hard segment and butadiene soft segment based polyurethane would determine the effect of the hard domain rigidity on the deformation behavior of the soft chains. The effect of annealing on the number of the statistical chain segments could be studied, and the results would be very useful to evaluate the approximation which treats the deformation of the soft

segment of the heterogeneous polyurethane as that of an elastic network.